UNIVERSITÀ DEGLI STUDI DI MILANO

Doctoral Program in Industrial Chemistry

Chemistry Department

New adipic acid production process starting from hydrolyzed lignin and cellulose, experimental and modelling study

Supervisor: Prof. Carlo PIROLA

Co-supervisor: Prof. Laura PRATI

Program Coordinator: Prof. Maddalena PIZZOTTI

Doctoral dissertation of: Sofia Capelli

Identification Number: R11391

A.Y. 2017/2018

“You must grant you the time to understand what you like and make mistake. Your success will not define from what you have taken from the world, but from what you have given to it. You have the abilities and the necessary determination to solve every problem that will arise in front of you and us. The obstacles will be great, but they will not prevail on a so ambitious, smart, and knowledgeable generation, like you. We make important things happen. You must leave to the discovery of this world, have confidence in your talent and make it better compared to how you inherited it from your parents.”

“Dovete concedervi il tempo per capire cosa vi appassiona, per fare errori. Il vostro successo non sarà definito da ciò che avrete preso dal mondo, ma da ciò che avrete dato. Avete le capacità e la determinazione necessaria per risolvere ogni problema che si porrà di fronte a voi e a noi. Gli ostacoli saranno grandi, ma non avranno la meglio su una generazione così ambiziosa, brillante e preparata come la vostra. Possiamo far succedere cose importanti. Partite alla scoperta di questo mondo, abbiate fiducia nelle vostre capacità e rendetelo migliore di come lo avete ereditato dai vostri genitori.”

Justin Trudeau (Canadian Prime Minister)
University of Ottawa, 19th June 2017

Summary

List of figures

List of tables

List of papers

F. Galli, L. Bonfanti, S. Capelli, F. Manenti, C. L. Bianchi, G. S. Patience, C. Pirola *Heterogeneous Oil Transesterification in a Single-Phase Liquid Mixture using a Co-Solvent for Improved Biofuels Production, (2015),* **Energy Technology**, 3 (12), 1170-1173.

C. L. Bianchi, B. Sacchi, S. Capelli, C. Pirola, G. Cerrato, S. Morandi, V. Capucci *Micro-sized TiO2 as photoactive catalyst coated on industrial porcelain grès tiles to photodegrade drugs in water, (2017),* **Environ. Sci. Pollut. Res.** doi:10.1007/s11356-017-9066-6.

A. Rosengart, S. Capelli, C. Pirola, A. Citterio, C. L. Bianchi, L. Prati, A. Villa *Renewable Adipic Acid From the Hydrogenation of trans,trans-Muconic Acid: Selection of a Three Phases Kinetic Model,* (2017) **Chemical engineering transaction,** 57, 931-936.

S. Capelli, A. Rosengart, A. Villa, A. Citterio, A. Di Michele, C.L. Bianchi, L. Prati, C. Pirola *Bio-adipic acid production by catalysed hydrogenation of muconic acid in mild operating conditions (2017),* **Appl. Cat. B,** 218, 220–229.

S. Campisi, S. Capelli, D. Motta, F. J. Sanchez, Trujilo, T. E. Davies, L. Prati, N. Dimitratos, A. Villa *Catalytic performance of AuPt nanoparticles on phosphorous functionalized carbon nanofibers towards HMF oxidation, (2018),* **C,** 4(3), 48.

Abstract

The awareness of the negative impacts of human activities against environment and public health have pushed western governments to support long-term programs aimed at mitigating pollution and reducing resource consumptions.[1] In this spirit, both industry and academia are searching for new solutions towards a “green” manufacturing practice, and the concept of “biorefinery” is taking place, as a renewable counterpart of the ill-famed oil industry. Biorefineries are supposed to produce entire classes of chemicals and fuels just as a real refinery.[2] The great difference is that the carbon source derives from renewable resources, following the natural cycle of CO_2, which is captured from atmosphere and fixed into living organisms (plants, algae, bacteria).[3] Adipic acid (AdA) production was chosen as base case due to the continuous increasing demand and the lack of some experimental data necessary for further developments.[4] The current AdA production covers a market of 3.7 million tons per year (with a 4.1% of yearly growth)[5] and increasing applications of AdA in various end-use industries, automobiles, textiles, consumer goods, electrical and electronics, wires and cables and food and packaging industry is expected to boost the AdA production during the forecast period (2017-2025).[6] Despite 70 years of technological maturity, the traditional benzene-based processes still raise serious safety and environmental concerns.[7] For these reasons, both private and public research institutions have pursued alternative bio (and chemical) routes for AdA production.[8] However, none of these processes has reached industrialization yet, also due to the oil-price fall in 2014. This event evidenced the main weakness of drop-in biorefineries: the need to compete in costs with a well-established and optimized technology. A novel approach to process development is therefore required for the case of bulk bio-derived chemical with low added value. Conceptual design acquires particular importance from the early stage of process development, to produce reliable cost estimates and projections, and to define a strategy for R&D. Due to the extensive and interdisciplinary literature available, the first task was to collect and reorganize the accessible knowledge, identifying the current alternative processes. A two steps biological-chemical process was considered worth of more detailed investigation for its good yields and sustainability potential.[9] This process consists in a first fermentation to produce muconic acid (MA), starting from either glucose (from cellulose)[10] or benzoic acid (from lignin).[11] In the second step the so produced MA is catalytically hydrogenated to AdA.

This doctoral thesis deals with the study of the hydrogenation of MA (a double unsaturated dicarboxylic acid) to AdA with particular attention to understand the reaction mechanism. Moreover, thanks to the collaboration with Politecnico di Milano, a first estimate of the kinetic parameters was performed, and a process superstructure was designed. This lead to a first economic and environmental feasibility analysis that allowed to highlight the bottle neck of this new process.

Chapter 1 introduces the subject of the thesis including a discussion on the application of AdA. Chapter 2 describes the aim of the thesis. Chapter 3 illustrates the analytical instrument used during the experimental work. Chapter 4 accurately describes the analytical method developed for the evaluation of conversion and selectivity. Chapter 5 talks about the experimental details and the results obtained using noble metals (Pt and Pd) supported commercial catalysts. After the collection of the first experimental data, a regression of the kinetic parameter and a modelling of the reaction pathway was performed as reported in Chapter 6. Chapter 7 describes the experimental details for the preparation of home-made catalysts and their characterization. Moreover, the results obtained from the hydrogenation of muconic acid and sodium muconate are reported. Finally, Chapter 8 provides a first study about the environmental and economic feasibility analysis of the new purposed process.

The first experimental chapter describes the development of the analytical method used for the evaluation of the conversion and products yield.

The conversion of the reaction was evaluated by UV-Vis analysis. A sample, collected after the catalyst filtration, was analysed in a spectrophotometer T60 UV-Visible Spectrophotometer PRIXMA from 400 to 190 nm. The maximum absorption was at 264 nm (Figure 0-1 A). The calibration of the analysis was done with sodium muconate (Na-Muc) prepared starting from commercial *t,t*-muconic acid (*t,t*-MA). The selectivity was estimated by gas-chromatographic analyses. The aqueous collected sample was dried in oven at 70 °C. The obtained white solid was then esterified with methanol in large excess and sulphuric acid (50 µL) under blind stirring condition at 70 °C for 48 h. Derivatized methyl esters were analysed by GC (Master GC Fast Gas Chromatograph Dani Instrument) equipped with TCD (or FID) detector operating in split mode (1:3). Two different chromatographic columns were used during the PhD period working at different operating conditions and detectors.

Supelcowax 10 column. The GC was outfitted with an Aldrich Supelcowax 10 (60 m, 0.53 mm, film thickness 1 µm), and helium (15 mL·min^{-1} column flow) was used as carrier gas. The GC-TCD method consisted of an inlet temperature of 210 °C and TCD transfer line at 240 °C. A starting temperature of 60 °C was set and then ramped at 18 °C min^{-1} to a temperature of 120 °C. Then from 120 °C to 160 °C ramped at 20 °C·min^{-1}. From 160 °C to 260 °C the temperature increases at 15 °C·min^{-1} and held from 1 minute to purge the column. Butanol was used as internal standard.

SP-2380 column. The GC was outfitted with an Aldrich SP-2380 column (60 m, 0.53 mm 0.20 µm). Helium, air and hydrogen was used to feed the column and the FID detector. The analysis was performed using an isothermal analysis at 180 °C (Figure 0-1 B).

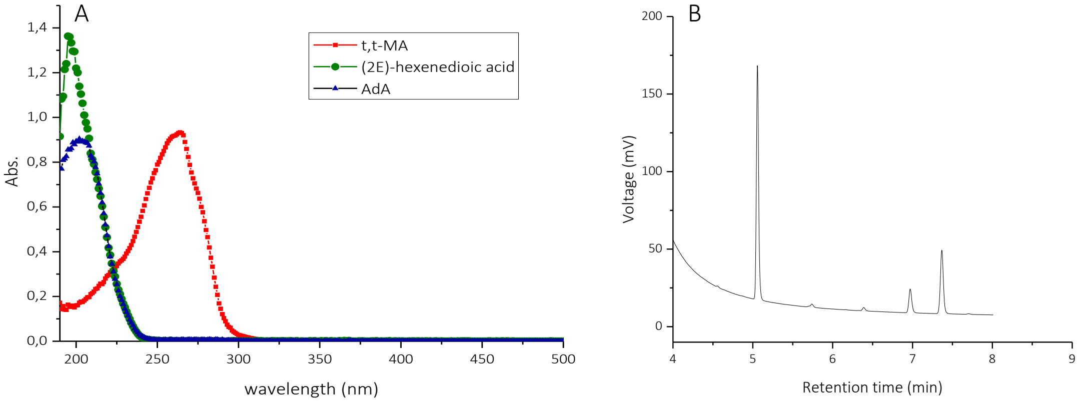

Figure 0-1: UV-Vis analysis (A) and GC-FID chromatogram (B)

The second experimental chapter describes the results obtained during the hydrogenation reaction of muconic acid and sodium muconate using noble metal supported commercial catalyst.

Hydrogenation reactions were conducted in a stainless-steel autoclave (at medium pressure of static hydrogen) or in a glass reactor (at 1-1.2 bar of static hydrogen) equipped with an external jacket that allowed to keep the reaction temperature constant. After the reaction (or after the collection of the sample during the catalytic test) the catalyst was filtered, and the reactant solution was recovered for the evaluation of conversion and selectivity. The conversion of the reaction was evaluated by UV-Vis analysis. A sample, collected after the catalyst filtration, was analysed in a spectrophotometer from 400 to 190 nm. The maximum absorption was at 264 nm. The selectivity was estimated by gas-chromatographic analyses after a derivatization of the reaction products.

Pt/AC 5% commercial catalyst (Sigma Aldrich) was used after a pre-activation step made in the autoclave at 200 °C for 3 h at 6 bar of hydrogen. Exploring different temperatures, hydrogen pressures and amount of catalyst the most interesting results were obtained varying the temperature. Increasing the temperature from 50 °C to 70 °C both Na-Muc conversion and AdA yield increase. After 60 min of reaction at 70 °C full conversion and yield to AdA was obtained (Figure 0-2).

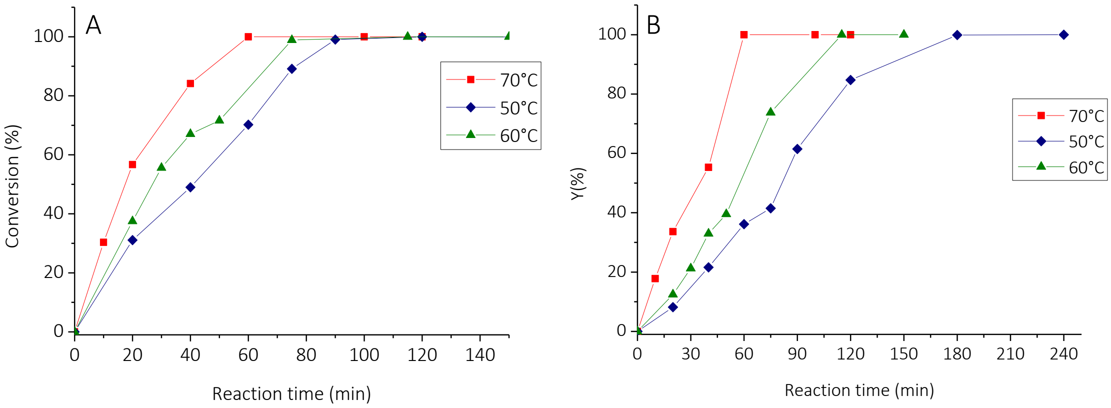

Figure 0-2: Na-Muc conversion (A) and AdA yield (B) at 50, 60 and 70 °C. Operating parameter: P(H_2)= 4 bar, stirring= 700 rpm, sub/cat=10/1 (wt/wt)

Recycling test showed the possibility to reuse the catalyst up to 10 times without loss in activity and selectivity. Moreover, hydrogenation reaction was performed on Na-Muc using a synthetic fermentation broth as reaction media. The minimal salt medium (M9) contains essential salts and nitrogen suitable for recombinant *E. Coli* strains with the presence of large amount of NaOH.

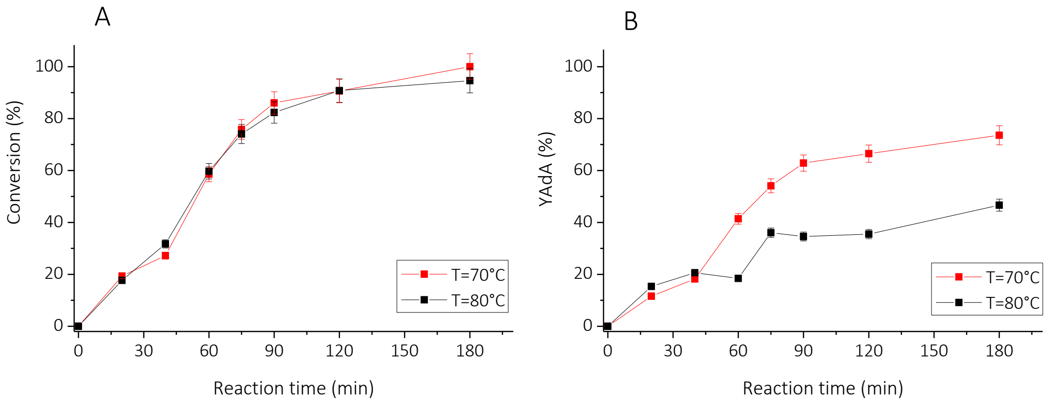

Figure 0-3: Na-Muc conversion (A) and AdA yield (B) in M9 fermentation broth at 70 and 80 °C. Operating parameter: P(H_2)= 3 bar, stirring= 700 rpm, sub/cat=10/1 (wt/wt)

The results showed that the conversion was not affected by temperature variation, but AdA yield was higher increasing the temperature. The washings of the catalyst with water revealed that the salts contained in the fermentation broth were absorbed on the catalyst surface blocking the active site to the substrate. In fact, the reaction was slower than the one conducted in distilled water and the maximum yield was about 80% after 3 hours of reaction (Figure 0-3).

Due to the good performance of Pt/AC 5% commercial catalyst we decided to change the noble Pt with another noble metal but cheaper than platinum. Therefore, ***Pd/AC 5% commercial catalyst*** was chosen due to its lower cost and the possibility to directly use it without any pre-activation step. Fresh catalyst was characterized, and the most important feature was the presence of both Pd and Pd(II)

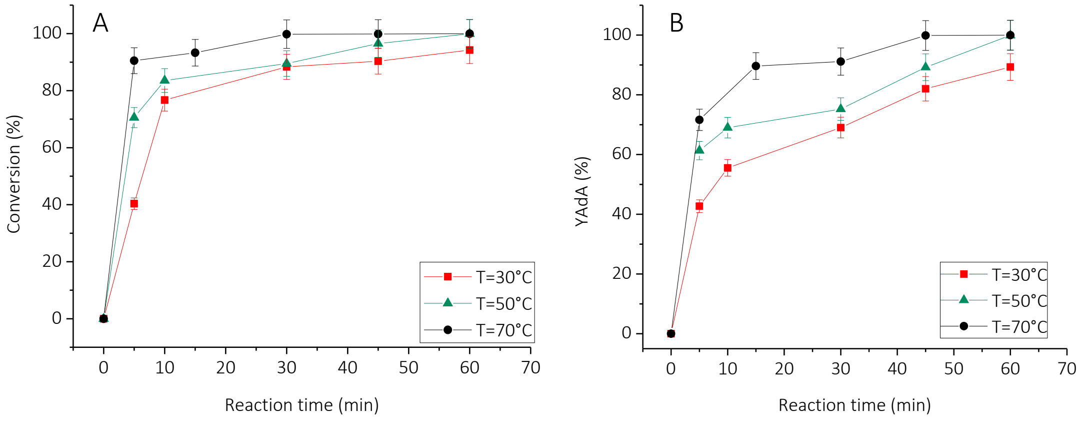

Figure 0-4: conversion (A) and AdA yield (B) obtained from the hydrogenation reaction of t,t-MA at 30, 50 and 70 °C. Operating parameters: P(H2)= 1 bar, cat/sub=1/200 (mol_{Pd}/mol_{sub})

species on the catalyst surface in a ratio of about 1:1. Hydrogenation reactions were made with *t,t*-MA and Na-Muc as substrates varying the pressure, the temperature and the amount of catalyst, keeping constant the substrate concentration to 1.42E-02 M. Hydrogen pressure was varied from 1 to 3 bar, but the initial activity was not largely affected to this parameters as well as AdA yield.

Different results were obtained increasing the temperature from 30 °C to 70 °C. *t,t*-MA conversion did not depend from the temperature except for short reaction time (Figure 0-4 A). On the other hand, AdA yield was higher increasing the temperature (Figure 0-4 B).

Performing the reaction using the same operating parameters with Na-Muc the results were quite different. In particular the conversion of Na-Muc at 30 °C was very slow and the yield to AdA reached a maximum value of 90% at 70 °C (Figure 0-5). Therefore, the hydrogenation reaction differently occurs on Na-Muc and *t,t*-MA. The evaluation of the initial activity confirmed this behaviour. The calculated activation energy was: 3685 kJ/mol for the reduction of *t,t*-MA and 36170 kJ/mol for the hydrogenation of Na-Muc. Apparent activation energy for Na-Muc is one order of magnitude greater than the one related to the hydrogenation of *t,t*-MA. The characterization of used catalyst at different reaction times revealed that during the reaction the Pd(II) specie was reduced to metal Pd and this change in the oxidation state was faster using *t,t*-MA as substrate. Therefore, it was possible to hypothesize that the hydrogenation of *t,t*-MA was faster due to the presence of higher amount of metal Pd.

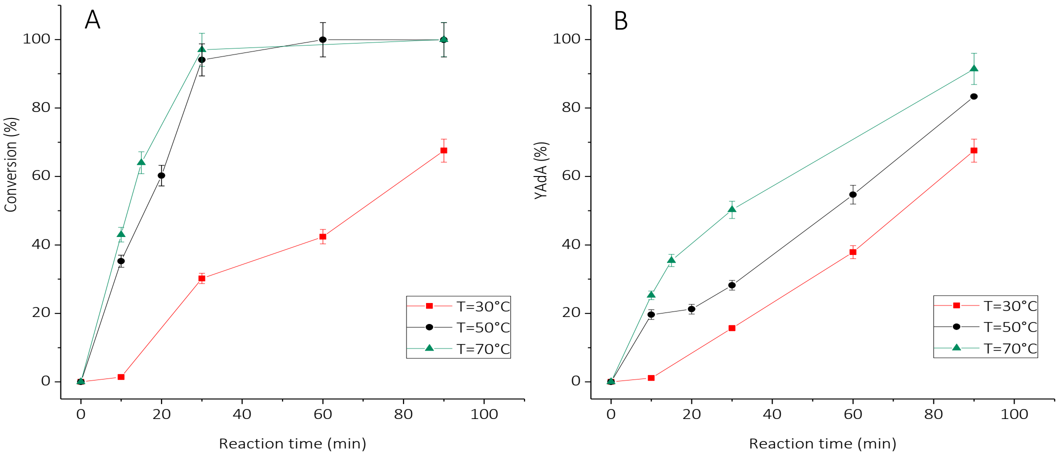

Figure 0-5: conversion (A) and AdA yield (B) obtained from the hydrogenation reaction of Na-Muc at 30, 50 and 70 °C. Operating parameters: $P(H_2)$= 1 bar, cat/sub=1/200 (mol_{Pd}/mol_{sub})

Starting from the collected data, a ***kinetic model was proposed as described in the chapter 6***. We considered the equations representing the absorption/desorption processes of all the species, including hydrogen. It was not possible to establish the mechanism of H_2 absorption process, so both dissociated and un-dissociated hydrogen absorption was considered. Moreover, the kinetic equations were proposed on the basis of the ones reported in the work of Yang e Hougen.[12] Hence, different

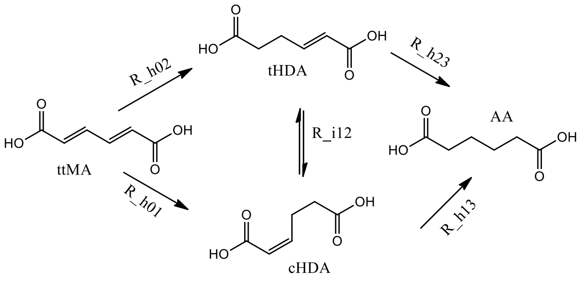

Figure 0-6: hypothesized reaction pathway

kinetic models were written considering reversible or not the *cis-trans* isomerization of the intermediate in the adsorption/desorption process. The models that were used to obtain the kinetic parameters of the equations by data fitting were all modifications of LHHW scheme according to Yang Hougen tables.[12] The reaction mechanism identified in the preliminary tests is presented in Figure 0-6. The first step of MA hydrogenation yields two isomers, namely (2Z)-2-hexenedioic acid (tHDA) and (2E)-2-hexenedioic acid (cHDA), in a single irreversible step. The concentration of the intermediates is regulated by an equilibrium isomerization reaction. The second step of hydrogenation yields AdA from both the intermediates. The results were achieved using the experimental data obtained from the hydrogenation reaction of Na-Muc in water at different temperatures using Pt/AC 5% commercial catalyst. The empirical study allowed identifying a catalyst with optimal performances in very mild conditions, providing the data points for a kinetic study on the mechanism of MA hydrogenation. At the beginning of the study a kinetic data modelling and regression at fixed temperature was performed but the model showed an overestimation of the reactant and the intermediates concentrations due to the group of the different intermediates. Dividing the intermediates and introducing the different reaction temperatures the model was able to predict the concentration of the different species during the reaction. The best kinetic model involves 4 hydrogenations reactions and 1 isomerization reaction (Figure 6). Therefore, the adsorption/desorption of the species, the hydrogen dissociation on the catalyst surface and the chemical reactions were considered and a model containing 11 parameters (activations and adsorption energy, kinetic constants...) was obtained. This model was able to represent the kinetic data as reported in Figure 0-7.

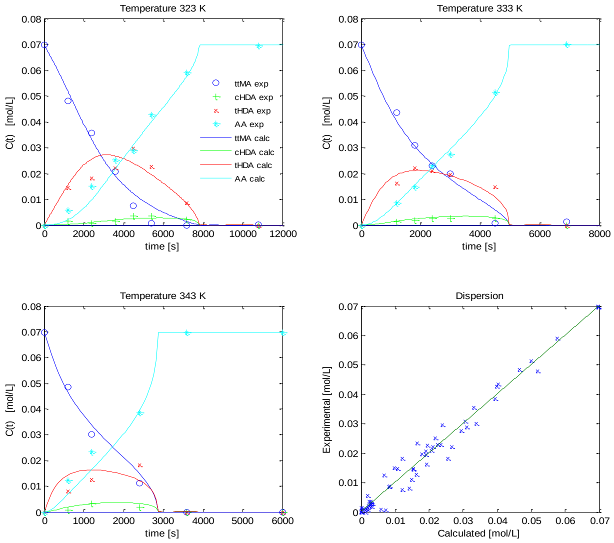

Figure 0-7: 11 parameters regression model results

Due to the good performance of the Pd based catalyst, 7 catalysts were synthesized using the sol-immobilization method. The method allows to synthesize supported NPs of noble metal controlling the shape and the surface properties. Pd NPs were synthesized staring from the potassium chloride precursor and using PVA an $NaBH_4$ as stabilizing and reducing agent, respectively. 3 activated carbon supports having different surface area were used as support***. The detailed about the synthesis of the home-made catalysts is described in chapter 7***. Using *t,t*-MA as substrate no significant differences among the catalysts were observed: full conversion of MA was obtained after 30 minutes of reaction, while complete yield toward AdA was achieved after 60 minutes only with KB 0.65PVA (Figure 0-8). Due to the good performance of the KB activated carbon support in the hydrogenation of *t,t*-MA and Na-Muc (Figure 0-9 A and B) the influence of the amount of PVA used during the catalyst preparation was studied. Therefore, different Pd/AC 1% using this carbon support were prepared varying the weight ratio between the stabilizer and the metal (polyvinyl alcohol_PVA) from 0 to 1.2. The most significant results were obtained using Na-Muc. Considering the YAdA all the curves showed an induction period due to the production of a high amount of monounsaturated intermediate (Figure 0-9 D). Finally, the initial activity at 10 minutes of reaction was calculated dividing the reacted amount of Na-Muc (mol) for the amount of Pd (mol) used for the reaction and the reaction time (sec). The results reported in Table 1 shows that increasing the amount of PVA, the initial activity increases. This behaviour might be explained considering that a larger amount of PVA helps the stabilization of small nanoparticles which are more active than larger ones.

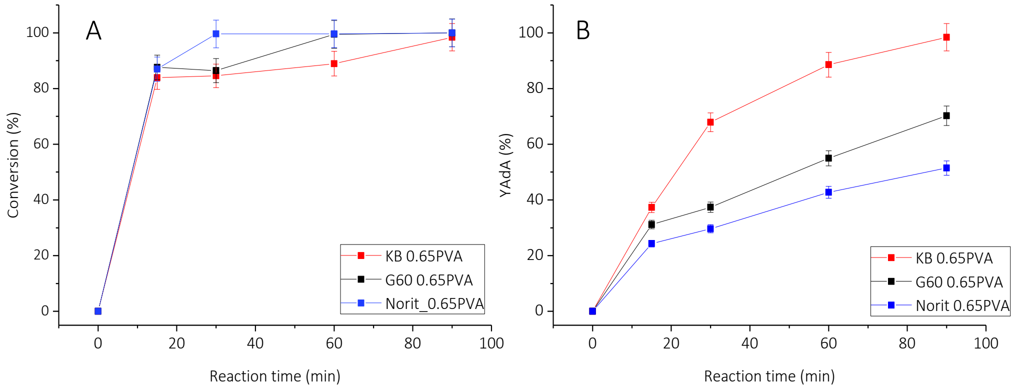

Figure 0-8: conversion (A) and AdA yield (B) for t,t-MA hydrogenation. Operating parameters: $P(H_2)$= 1 bar, cat/sub=1/200 (mol_{Pd}/mol_{sub}), temperature= 50 °C

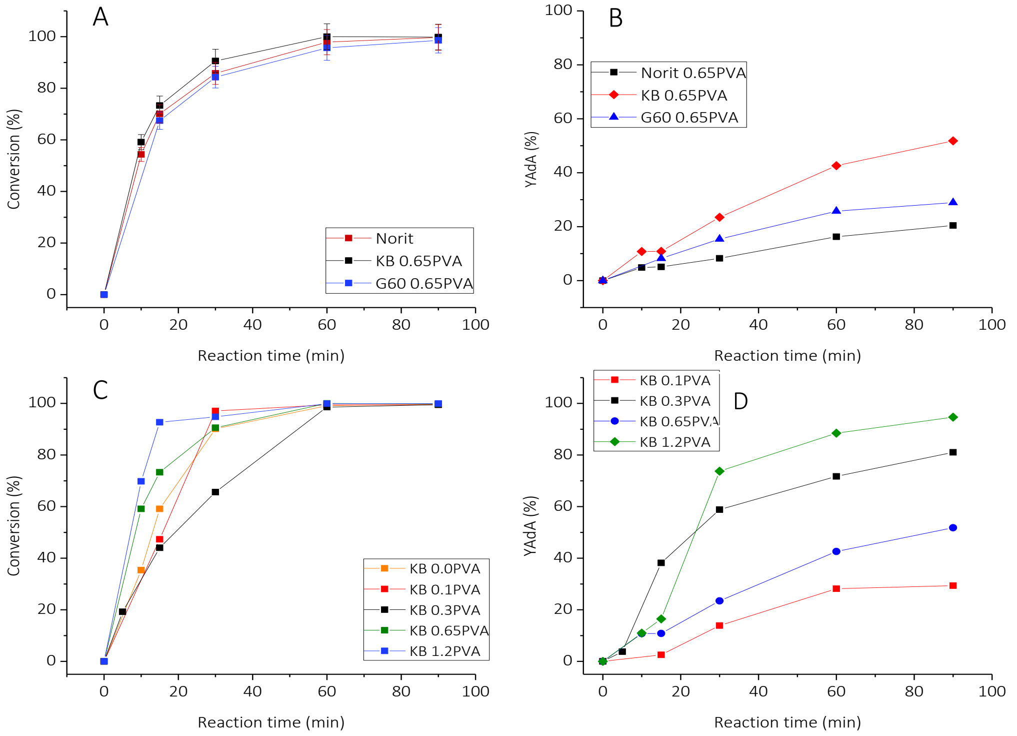

Figure 0-9: conversion (A) and AdA yield (B) for Na-Muc hydrogenation. Operating parameters: P(H_2)= 1 bar, cat/sub=1/200 (mol_{Pd}/mol_{sub}), temperature= 50 °C

Table 0-1: initial activity after 10 minutes of reaction on Pd/AC 1% home-made catalyst

Sample	Initial activity (s^{-1})
KB_0.0PVA	0.11
KB_0.1PVA	0.10
KB_0.3PVA	0.13
KB_0.65PVA	0.19
KB_1.2PVA	0.25

Finally, an ***environmental and economic analysis*** compared the traditional petrochemical process with two purposed bio processes for the production of AdA from glucose. The first bio process started from the production of starch from maize culture, while the second used wood biomass as glucose source. Detailed analysis of the results (Figure 0-10) revealed the advantages and weaknesses of the innovative bio-processed. ReCiPe method was adopted for the evaluation of 18 environmental impact categories. The results show that the traditional petrochemical process has a lower environmental impact in all the categories except for the global warming. Firstly, industrial process for the production of glucose from starch was considered and the results were largely affected by the cultivation, the production of maize starch and all the respective waste treatments. Since the purpose is to produce glucose from waste wood, a second study was performed starting from the hydrolysis of wood and its further conversion to glucose.

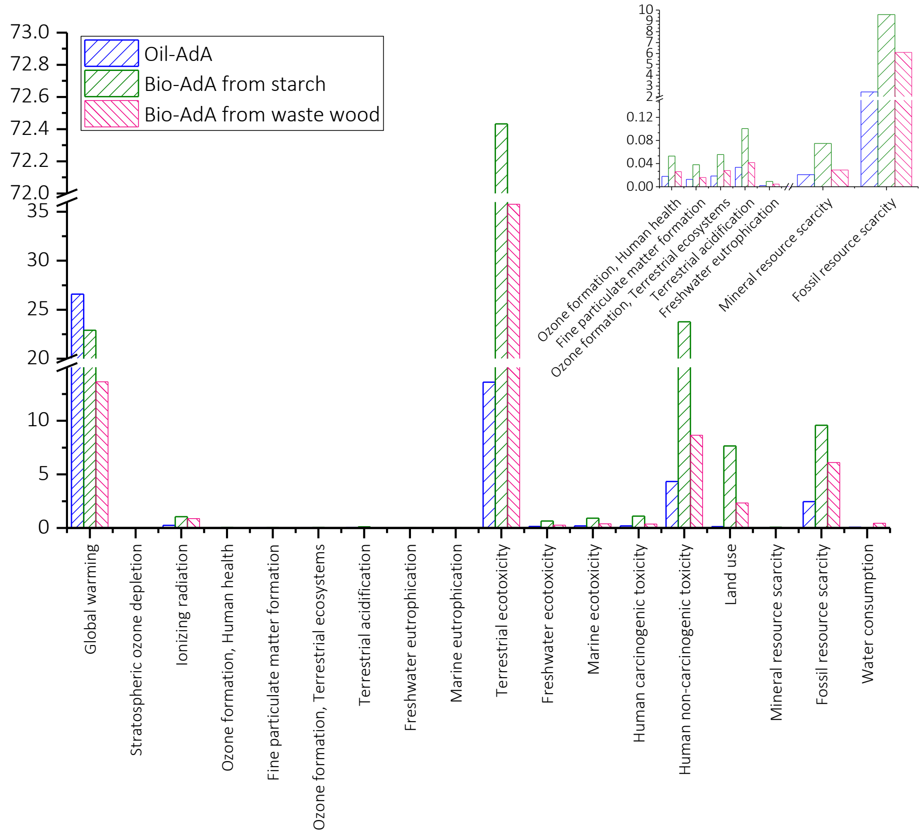

Figure 0-10: results of the environmental impact analysis

In this case the study started from the production process of bio-ethanol since no hydrolysis plant was present in the software. Moreover, an average wood humidity was considered using literature data for the yield of the process. Despite these limitations, the results obtained without considering cooling water recycle and steam production from the process water were extremely different from the first study. The global warming decreases from 22.9 to 13.6 Kg CO_2 eq. that is the half of the value obtained from the oil-derived process. All the results can be further improved introducing recycles of chemicals and water, which will lead to a process capable of quasi- self-sustaining from energy demand point of view and the purification products demand.

The economic study considered a base case scenario for a plant for 10000 metric ton/year of AdA, located in America, with an annual productivity of 8150 h. The utilities and the cost of the chemicals were referred to a plant located in America. From the base case scenario 4 other scenarios were hypothesized considering the variation of glucose and AdA price, the variation of plant size and strain yield and product concentration. The economic analysis in different scenarios confirmed that a bio-AdA production is affected by the availability of cheap feedstock. In this specific case, the AdA process

can be profitable if it is located in Brazil, using first generation glucose at a price not higher than 0.21 $/kg. Finally, since the data used in this work are derived from early-stage and lab-scale investigations, the estimates can be further refined, as soon as new insights are provided by the ongoing R&D. The indications on the current technological bottlenecks, the main assumptions done while defining the superstructure and the sensitivity analysis are useful to indicate the priority aspects to be further investigated. Moreover, the lack of data did not allow to perform the economic analysis within the European market, but due to the increment of the price of oil, the bio-route could be competitive in a few years. due to the instability price of AdA in Europe and the continuous increment of incentives bio-AdA could find in a few years a piece of market.

Riassunto

I governi occidentali, consapevoli dell'impatto negativo delle attività umane sulla salute dell'ambiente e il benessere delle persone, hanno elargito programmi a lungo termine, atti a mitigare l'inquinamento e a ridurre il consumo di risorse energetiche e materiali.[1] Contestualmente, sia l'industria che il mondo accademico stanno incanalando i loro sforzi verso la ricerca di nuove soluzioni "green". Un esempio concreto sono le bio-raffinerie, sviluppate come controparte delle nocive industrie petrolchimiche, che sono in grado di produrre intere classi di composti chimici e combustibili come una vera e propria raffineria.[2] La differenza sostanziale tra una raffineria e una bio-raffineria è la fonte di carbonio che, nel caso di quest'ultima, deriva da risorse rinnovabili: l'anidride carbonica viene catturata dall'atmosfera e fissata all'interno di alcuni microorganismi e piante, seguendo così il suo ciclo naturale.[3] L'acido adipico (AdA) è stato scelto come caso base, data la sua continua crescente domanda e la mancanza di alcuni dati importanti per un ulteriore sviluppo in campo bio.[4] La domanda attuale di AdA copre un mercato di 3.7 milioni di tonnellate all'anno con una domanda che cresce del circa 4.1%[5] a causa delle prosperanti industrie automobilistiche, di vernici, tessili, dei beni di consumo, elettriche ed elettroniche, di cablaggio e di imballaggio che continueranno a stimolarne la domanda nel periodo 2017-2025.[6] Nonostante i 70 anni di maturità tecnologica, il processo tradizionale di produzione dell'AdA basato sull'utilizzo di benzene è tutt'ora al centro di controversie riguardanti la sicurezza e l'impatto ambientale.[7] Per tali ragioni sia le istituzioni di ricerca private che pubbliche hanno perseguito strade alternative bio (e chimiche)[8] per la produzione di tale composto chimico, ma sfortunatamente, nessuno di tali processi ha raggiunto l'industrializzazione a causa della caduta del prezzo del greggio nel 2014. Questo evento mise in luce la principale debolezza delle bio-raffinerie, ovvero la necessità di competere in termini di costo con le tecnologie oramai consolidate e ottimizzate. Nel caso di prodotti chimici di massa derivanti da processi bio si rende necessario lo sviluppo di un approccio nuovo e innovativo: il design concettuale acquisisce quindi un ruolo di fondamentale importanza nella fase iniziale di sviluppo di processo e le capacità di stimare consistentemente costi e proiezioni e definire saldamente le strategie di ricerca e sviluppo sono i punti chiave della buona riuscita del progetto. Data l'enorme quantità di letteratura disponibile e l'interdisciplinarietà del progetto, il primo passo è stato la raccolta e l'organizzazione di tutta la conoscenza accessibile e l'identificazione delle alternative di processo attuali e attuabili. A tale riguardo si è deciso di scegliere un processo a due step che prevede un passaggio biotecnologico seguito da uno puramente chimico in grado di dare buone rese e una potenziale sostenibilità

ambientale ed economica.[9] Più nel dettaglio il processo scelto consiste in una prima fermentazione per la produzione di acido muconico (MA) partendo da glucosio (derivante dal trattamento della cellulosa)[10] o da acida benzoico (derivante dalla lignina).[11] Successivamente l'MA così prodotto viene idrogenato tramite processi catalitici ad AdA. La Tesi di Dottorato riguarda lo studio della reazione di idrogenazione dell'acido muconico (un acido dicarbossilico di-insaturo) ad acido adipico con particolare attenzione al meccanismo di reazione. Inoltre, grazie alla collaborazione con un gruppo di ricerca del Politecnico di Milano è stata eseguita un prima stima dei parametri cinetici di reazione ed è stata sviluppata la superstruttura dell'intero nuovo processo. Questo ha permesso di poter effettuare una prima stima di fattibilità economica e di evidenziare i colli di bottiglia del nuovo processo. Il Capitolo 1 fornisce un'introduzione all'oggetto della ricerca e la discussione dei principali utilizzi e processi di produzione dell'AdA. Nel Capitolo 2 viene descritto lo scopo della tesi, mentre all'interno del Capitolo 3 sono introdotti e descritti gli strumenti utilizzati durante la parte sperimentale del lavoro. Il Capitolo 4 descrive accuratamente il metodo analitico sviluppato per la valutazione della conversione e della resa dei prodotti e la sua consistenza. Nel Capitolo 5 vengono riportate le procedure sperimentali e i risultati ottenuti utilizzando catalizzatori commerciali a base di metalli nobili (Pt e Pd). Dopo la raccolta dei primi dati sperimentali si è proceduto alla regressione cinetica dei parametri di reazione e alla modellizzazione del meccanismo di reazione (Capitolo 6). Nel Capitolo 7 viene descritta la procedura di sintesi di catalizzatori a base di nanoparticelle di Pd supportate su carboni attivi e i risultati ottenuti riguardo l'idrogenazione dell'MA e del sodio muconato in ambiente acquoso. Infine, il Capitolo 8 riguarda lo studio di sostenibilità ambientale ed economica del nuovo processo.

Il primo capitolo sperimentale descrive lo sviluppo del metodo analitico utilizzato per la valutazione della conversione e delle rese di reazione.

La conversione della reazione è stata valutata utilizzando un'analisi UV-Vis; nel dettaglio un campione prelevato dopo la filtrazione del catalizzatore eterogeneo è stato analizzato in uno spettrofotometro T60 PRIXMA tra i 400 e i 190 nm. L'assorbimento massimo ottenuto si trova alla lunghezza d'onda di 264 nm ed è imputabile solamente all'MA (Figura 1 A). La calibrazione dell'analisi è stata eseguita con sodio muconato (Na-Muc) preparata partendo da acido *t,t*-muconico (*t,t*-MA) e con acido *t,t*-MA puro. La selettività dei prodotti di reazione è stata determinata servendosi di un'analisi gas cromatografica. Il campione filtrato è stato essiccato in forno a 70 °C e il solido bianco così ottenuto è stato esterificato in metanolo utilizzando un eccesso di acido solforico a 70 °C per 48 ore. I metilesteri così prodotti sono stati analizzati tramite l'utilizzo di un gas cromatografo (Master Dani GC) fornito sia di rivelatore

TCD che FID ed operante in modalità split. Durante il periodo di ricerca sono state utilizzate due diverse colonne.

Colonna Supelcowax 10. All'interno del GC è stata montata una colonna Supelcowax 10 della casa Aldrich (60 m x 0.53 mm di diametro ed uno spessore interno del film pare a 1 µm) e l'elio (con flusso in colonna di 15 mL/min) è stato usato come gas carrier. Il metodo prevede l'utilizzo di un iniettore ad una temperatura pari a 210 °C, mentre il detector TCD ad una temperatura di 240 °C. L'analisi è stata effettuata in rampa di temperatura partendo da 60 °C con un incremento di 18 °C/min fino a 120 °C. Dopodiché la rampa viene aumentata a 20 °C/min da 120 a 160 °C e successivamente ridotta a 15 °C/min fino a 260 °C. Raggiunta la massima temperatura di 260 °C questa viene mantenuta costante per 1 min in modo da spurgare eventuali residui rimasti all'interno della colonna. Come standard interno è stata utilizzata una soluzione di butanolo in metanolo.

Colonna SP-2380. Il GC è stato munito di una colonna Sigma Aldrich (60 m x 0.53 mm, spessore del film interno 0.2 µm). Elio, aria ed idrogeno sono stati utilizzato come gas carrier per alimentare la colonna e il detector a ionizzazione di fiamma (FID). L'analisi in questo caso è stata condotta in isoterma a 180 °C (Figura 1 B).

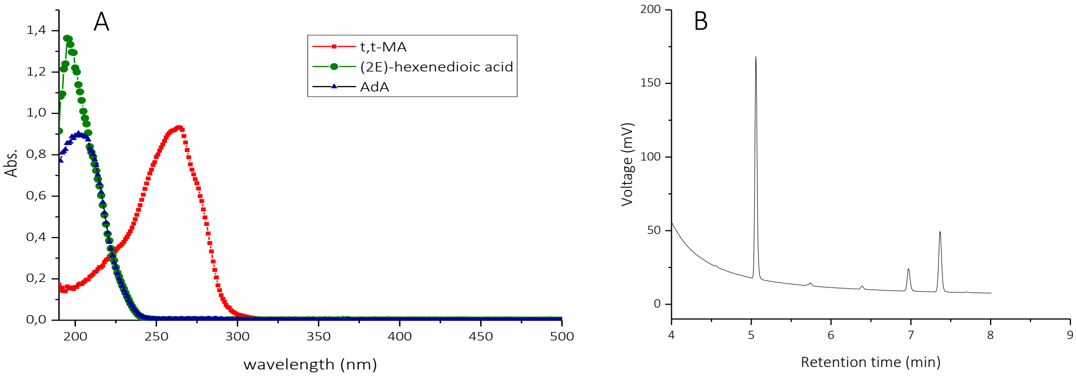

Figura 1: spettro di analisi UV-Vis (A) e cromatogramma da analisi GC (B)

Il secondo capitolo sperimentale descrive i risultati ottenuti dalle reazioni di idrogenazioni condotte su acido muconico e muconato di sodio utilizzando catalizzatori commerciali a base di metalli nobili supportati.

Le reazioni di idrogenazione sono state effettuate in un'autoclave d'acciaio (per medie pressioni e atmosfera statica di idrogeno), o in un reattore di vetro (per pressioni di 1-1.2 bar in atmosfera statica di idrogeno), dotati di una camicia esterna riscaldante che permetteva di mantenere costante la temperatura della reazione. A reazione conclusa (o dopo il prelievo dei campioni di reazione durante lo svolgimento della prova) il catalizzatore è stato separato dalla soluzione mediante filtrazione e la fase acquosa così ottenuta è stata recuperata per poter effettuare la valutazione della conversione e della selettività. Una parte del campione acquoso è stato analizzato (dopo diluizione) allo spettrofotometro, mentre la selettività e stata determinata dopo una derivatizzazione dei prodotti di reazione.

Il catalizzatore commerciale Pt/AC 5% (Sigma Aldrich) è stato utilizzato dopo un a pre-attivazione in situ condotta a 200 °C per 3 ore a 6 bar di idrogeno. Le reazioni sono state effettuate variando la temperatura, la pressione di idrogeno e la quantità di catalizzatore; i risultati più interessanti sono stati ottenuti variando la temperatura di reazione. Aumentando la temperatura da 50 a 70 °C sia la conversione del muconato di sodio che la resa in acido adipico aumentano. Dopo 1 ora di reazione a 70 °C si è ottenuta una completa conversione del substrato e una resa totale ad acido adipico (Figura 2).

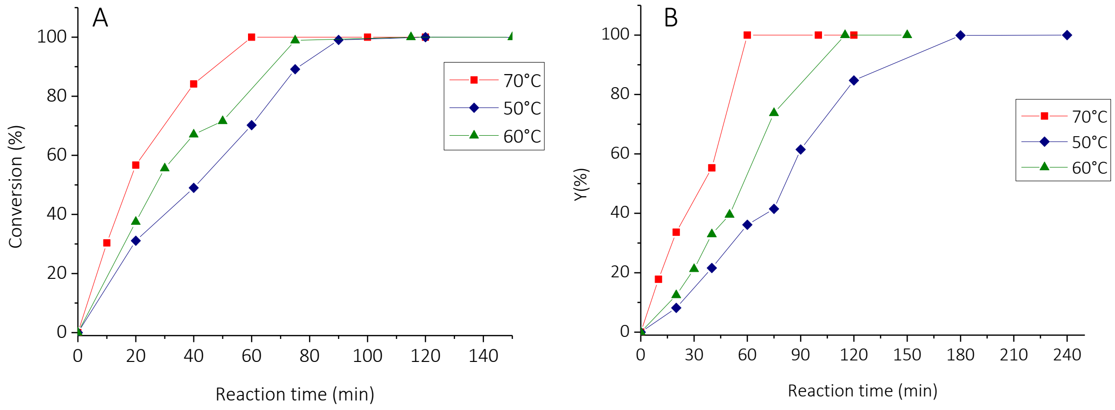

Figura 2: conversione Na-Muc (A) e resa in AdA (B) a 50, 60, 70 °C. Parametri operativi: P(H_2)= 4 bar, agitazione= 700 rpm, sub /cat=10/1 (massa/massa)

Dai test di riciclo del catalizzatore si è evinto che è possibile utilizzare il catalizzatore per almeno 10 volte senza perdere in conversione e resa. Inoltre, per non escludere completamente la possibilità di poter effettuare la reazione di idrogenazione direttamente all'interno del brodo di fermentazione, è stato effettuato un test catalitico su un brodo sintetico composto dal cosiddetto "minimal salt media M9", un insieme di sali essenziali e composti azotati adatti a ceppi batterici ricombinanti del tipo *E. Coli*, e da una grande quantità di idrossido di sodio. I risultati ottenuti hanno mostrato che la

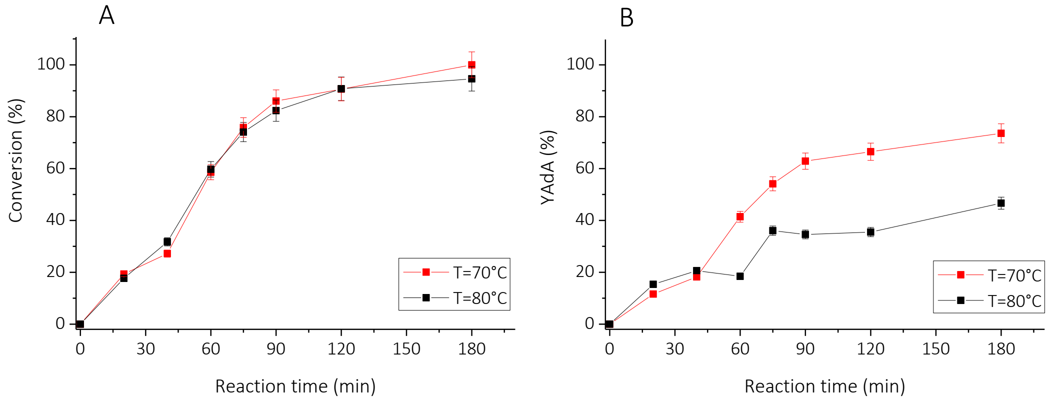

Figura 3: conversione Na-Muc (A) e resa in AdA (B) all'interno del brodo di fermentazione a 70 e 80 °C. Parametri ooperativi: P(H_2)= 3 bar, agitazione= 700 rpm, sub/cat= 10/1 (massa/massa)

conversione sembra non dipendere dalla temperatura del brodo di fermentazione, ma la resa in AdA aumenta all'aumentare della temperatura. La reazione si è rivelata più lenta rispetto a quella condotta in acqua distillata e la massima resa ottenuta è stata dell'80% circa dopo 3 ore di reazione.

Visti i buoni risultati ottenuti utilizzando il catalizzatore commerciale Pt/AC 5% si è optato per cambiare il costoso catalizzatore a base di platino con un più economico ***catalizzatore commerciale di palladio (Pd/AC 5%)*** che, oltretutto, non necessita di pre-attivazione. Il catalizzatore fresco è stato caratterizzato utilizzando le principali tecniche e, grazie all'analisi XPS, si è dedotta la presenza di Pd(0) e Pd(II) in superficie in equa quantità. La reazione di idrogenazione è stata condotta sia su *t,t*-MA che sul Na-Muc variando la pressione, la temperatura e la quantità di catalizzatore, e tenendo costante la concentrazione di partenza dei substrati a 1.42E-02 M. La pressione dell'idrogeno è stata variata da 1 a 3 bar; in tali condizioni l'attività iniziale resta pressoché costante così come la resa in AdA. Risultati differenti sono stati ottenuti variando la temperatura da 30 °C a 70 °C. La conversione di *t,t*-MA non dipende dalla temperatura, fatta eccezione per tempi brevi di reazione (Figura 4 A), mentre la resa in AdA aumenta all'aumentare della temperatura (Figura 4 B).

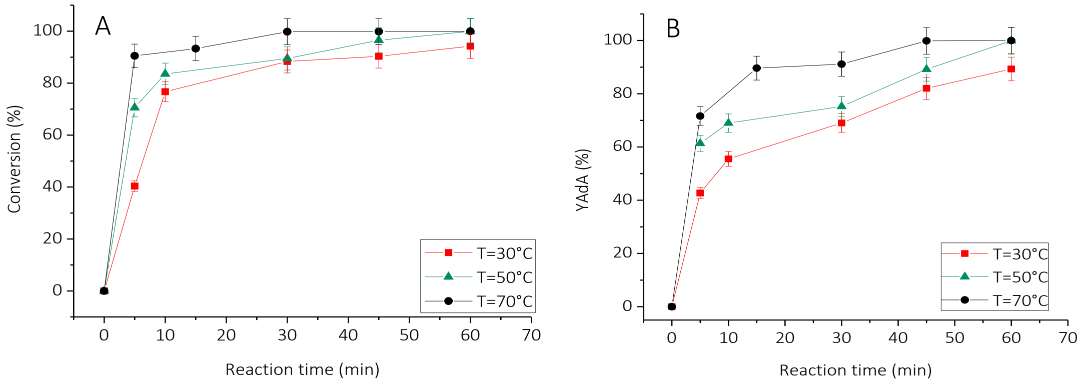

Figura 5: conversione (A) e resa in AdA (B) ottenute dall'idrogenazione di t,t-MA a 30, 50 e 70 °C. Parametri operativi:$P(H_2)$= 1 bar, cat/sub= 1/200 (mol_{Pd}/mol_{sub})

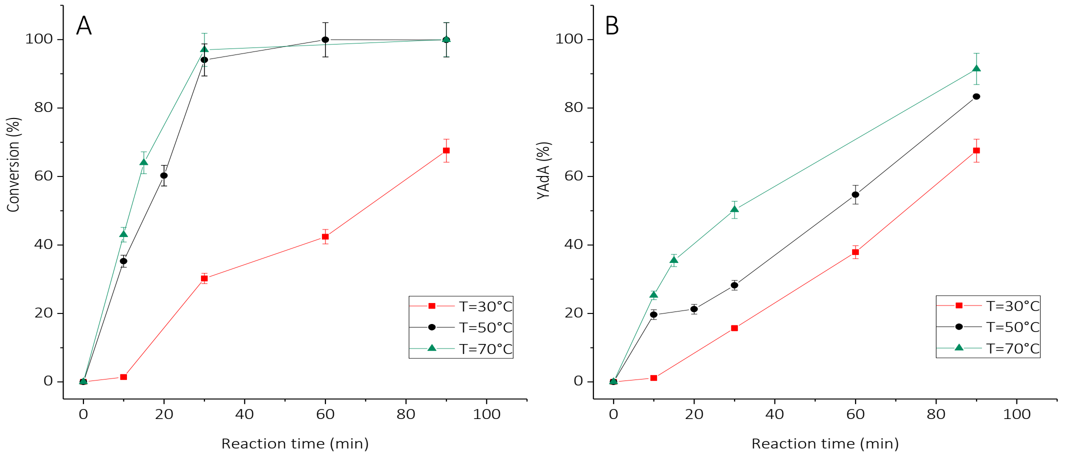

Figura 4: conversione (A) e resa in AdA (B) ottenuti dall'idrogenazione di Na-Muc a 30, 50 e 70 °C. Parametri operativi: $P(H_2)$= 1 bar, cat/sub= 1/200 (mol_{Pd}/mol_{sub})

Utilizzando invece Na-Muc come substrato i risultati ottenuti sono differenti. La conversione di Na-Muc a 30 °C procede lentamente e la resa in AdA raggiunge il suo massimo valore operando a 70 °C (Figura 5 A). L'idrogenazione dei due substrati sembra avvenire in modo diverso e, valutando i valori di attività iniziale, si sono trovati due numeri diversi tra loro di un ordine di grandezza: la riduzione di *t,t*-MA avviene con un'attività iniziale pari a 3685 kJ/mol, mentre quella di Na-Muc a 36170 kJ/mol. Dalle caratterizzazioni effettuate sui catalizzatori a diversi tempi di reazione è emerso che il Pd(II) viene ridotto a Pd(0) durante la reazione e che tale riduzione avviene più velocemente se nell'ambiente di reazione è presente *t,t*-MA. Quindi è possibile ipotizzare che l'idrogenazione di *t,t*-MA è più rapida a causa della presenza di maggiori quantità di Pd(0) presenti sulla superficie del catalizzatore.

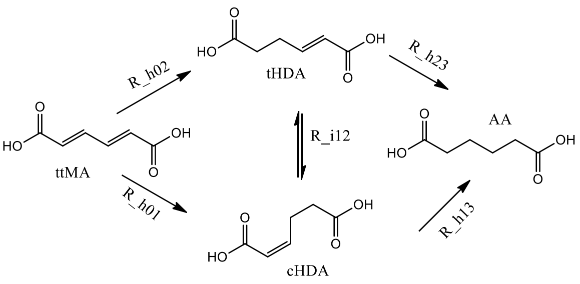

Figura 7: cammino di reazione ipotizzato

Partendo dai dati raccolti precedentemente con il catalizzatore a base di Pt è stato quindi proposto ***un modello cinetico, come descritto nel capitolo 6.*** Per lo sviluppo del modello sono state considerate le equazioni che rappresentano i modelli di adsorbimento /desorbimento di tutte le specie chimiche presenti nell'ambiente di reazione, entrambi i meccanismi di adsorbimento dell'idrogeno (dissociativo e non) e le velocità delle reazioni, come riportato nel lavoro di Yang e Hougen.[12] Inoltre, sono stati scritti diversi modelli che tenevano in considerazione l'isomerizzazione *cis-trans* degli intermedi e del substrato. L'ottenimento dei parametri cinetici presenti nelle equazioni è stato ottenuto modificando le equazioni LHHW in accordo con le tabelle riportate da Yang e Hougen.[12] Il cammino di reazione conseguito dallo studio cinetico mostra come *t,t*-MA venga dapprima idrogenato agli intermedi monoinsaturi (2Z)-2-acido esenedioico (tHDA) e (2E)-2-acido esenedioico (cHDA) attraverso un passaggio irreversibile. I due intermedi vengono poi successivamente idrogenati ad AdA (Figura 6). Tale studio empirico ha permesso l'identificazione e la valutazione preliminare dei parametri cinetici della reazione condotta in condizioni blande. Inizialmente lo studio è stato

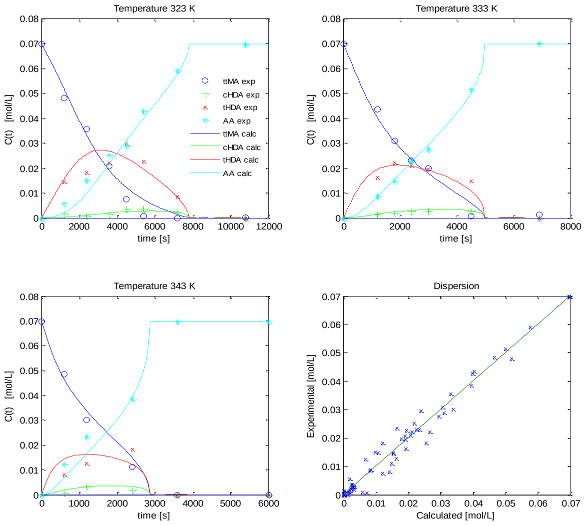

Figura 6: risultati della regressione

effettuato su dati raccolti a temperatura costante, ma il modello sovrastimava la concentrazione degli intermedi a causa del raggruppamento di questi ultimi in una sola specie. Dividendo gli intermedi e introducendo anche i dati ottenuti a diverse temperature il modello è in grado di predire la concentrazione di tutte le specie. Il miglior modello cinetico sviluppato prevede 4 reazioni di idrogenazione ed una di isomerizzazione. Considerando tutti gli step di reazione è quindi stato scritto un modello contenente 11 parametri (energie di attivazione, energie di adsorbimento, costanti cinetiche…) e che riesce a sovrapporsi ai dati sperimentali (Figura 7).

Considerando gli ottimi risultati ottenuti utilizzando il catalizzatore a base di Pd si è deciso di sintetizzare 7 catalizzatori utilizzando il metodo del “sol-immobilization”; tale metodo permette di sintetizzare nanoparticelle di Pd supportate su un materiale controllandone le dimensioni e le proprietà superficiali. Le nanoparticelle di Pd sono state sintetizzate partendo dal precursore K_2PdCl_4, utilizzando polivinilalcol (PVA) come agente stabilizzante e $NaBH_4$ come agente riducente. Per la sintesi di questi catalizzatori sono stati utilizzati 3 diversi carboni attivi aventi aree superficiali molto diverse. ***I dettagli sulla sintesi dei catalizzatori sono descritti all’interno del capitolo 7.*** Conducendo la reazione di idrogenazione su *t,t*-MA non si sono riscontrate grandi differenze in termini di conversione, mentre una completa resa ad AdA è stata ottenuta solo per il catalizzatore preparato utilizzando KB come carbone attivo di supporto (Figura 8 A e B). Anche nel caso di idrogenazione del Na-Muc il carbone attivo KB è risultato quello in grado di produrre una maggiore quantità di AdA (Figura 9 A e B). Considerati i buoni risultati ottenuti con il carbone KB, si è deciso di investigare come la quantità di PVA utilizzato durante la sintesi possa inficiare sulla conversione e sulla resa in AdA; per tale motivo si sono sintetizzati 5 diversi catalizzatori variando il rapporto in peso PVA/metallo tra 0 e 1.2. I risultati migliori sono stati ottenuti utilizzando come substrato Na-Muc. Tutte le curve di conversione mostrano un periodo di induzione nella produzione di AdA tra gli 0 e i 15 minuti dovuta all’iniziale produzione di grandi quantità di intermedio monoinsaturo (Figura 9 D). Infine, l’attività iniziale valutata dopo 10 minuti di reazione mostra come, al crescere della quantità di PVA utilizzato durante la sintesi, aumenti anche il suo valore. Questo andamento può essere spiegato considerando che un’elevata quantità di PVA aiuta il processo di stabilizzazione di nanoparticelle più piccole che sono più attive rispetto a quelle più grandi.

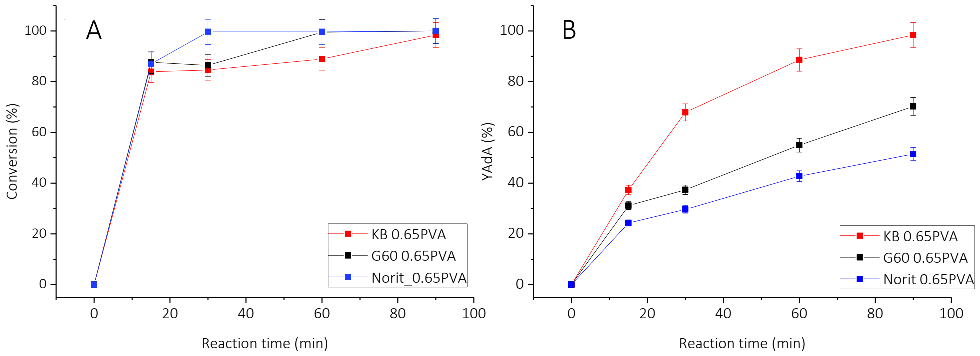

Figura 8: conversione (A) e resa in AdA (B) durante l'idrogenazione di t,t-MA. Parametri operativi: P(H_2)= 1 bar, cat/sub= 1/200 (mol_{Pd}/mol_{sub}), temperatura= 50 °C

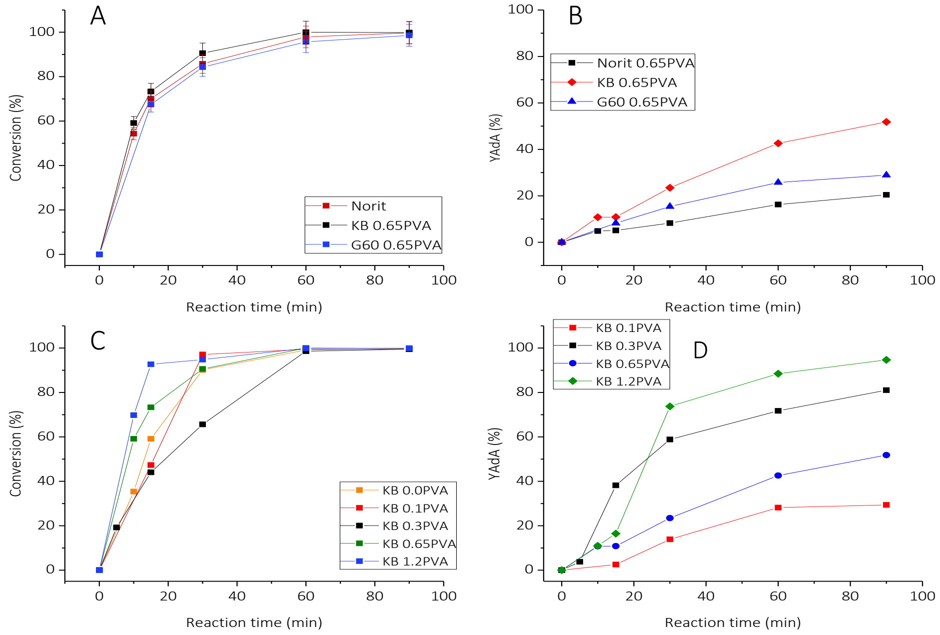

Figura 9: conversione (A) e resa in AdA (B) durante l'idrogenazione di Na-Muc. Parametri operativi: P(H_2)= 1 bar, cat/sub= 1/200 (mol_{Pd}/mol_{sub}), temperatura= 50 °C

Tabella 1: attività iniziale dopo 10 minuti di reazione con Pd/AC 1% sintetizzati

Sample	Initial activity (s^{-1})
KB_0.0PVA	0.11
KB_0.1PVA	0.10
KB_0.3PVA	0.13
KB_0.65PVA	0.19
KB_1.2PVA	0.25

Infine, è stata effettuata ***un'analisi ambientale ed economica*** per confrontare il processo tradizionale petrolchimico di produzione di AdA con quello bio (partendo da glucosio) da noi proposto. Si è deciso di considerare due processi bio che si differenziano solamente per la parte di produzione del glucosio: il primo (in verde) parte dalla piantagione mais, mentre il secondo (in rosa) converte il legno di scarto. Per la valutazione degli impatti ambientali è stato utilizzato il metodo ReCiPe che considera 18 diverse categorie di impatto: i risultati dettagliati mostrati in Figura 10 rivelano i vantaggi e le debolezze del nuovo processo bio. Innanzitutto, bisogna premettere che i risultati ottenuti partendo dalla piantagione di mais sono ampiamente influenzati da tutte le utenze, l'acqua e i fertilizzanti utilizzati durante la coltivazione e, di conseguenza, dal trattamento di tutte le acque di scarto derivanti dalla conversione del mais in amido. Siccome l'idea principale è quella di produrre AdA da glucosio derivante dagli scarti del legno, nel secondo processo bio si è considerata invece l'idrolisi del legno e la sua successiva trasformazione in glucosio. Nell'ultimo caso, data l'assenza all'interno del software del processo specifico di idrolisi, si è partiti da un impianto di produzione di bio-etanolo considerando un'umidità media del legno e utilizzando rese di processo riportate in letteratura. Nonostante tali limitazioni, i risultati ottenuti senza considerare ricicli delle acque di raffreddamento e di generazione del vapore d'acqua dalle acque di processo, sono molto diversi rispetto a quelli ottenuti nel primo caso. Per esempio, il riscaldamento globale decresce da 22.9 a 13.6 Kg CO_2 eq., che è la metà del valore ottenuto per il processo tradizionale. Tutti i risultati ottenuti sono ampiamente migliorabili introducendo ricicli di alcuni composti chimici e dell'acqua; tali accorgimenti potrebbero rendere il nuovo processo bio completamente auto sostiene sia dal punto di vista energetico che nella purificazione dei prodotti di reazione. Lo studio di fattibilità economica parte da uno scenario di base che prevede un impianto con capacità produttiva di 10000 ton/anno di acido adipico situato in nord America con una produttività annua di 8150 ore. Il costo delle utenze e dei composti chimici necessari fa riferimento ai prezzi americani. Partendo dallo scenario di base sono stati ipotizzati ulteriori 4 scenari considerando la variazione del prezzo del glucosio e del AdA, la modifica delle dimensioni dell'impianto, della concentrazione dei prodotti e della resa dei ceppi batterici. L'analisi economica su tali scenari ha confermato che la produzione del bio-AdA è influenzata dalla disponibilità di materie prime economiche; nel caso specifico l'impianto potrebbe portare profitto se situato in Brasile ed utilizza glucosio di prima generazione avente un prezzo non superiore a 0.21 \$/kg. Siccome i risultati derivano da uno studio che si trova ancora nella fase inziale di investigazione in laboratorio, i risultati potranno essere ulteriormente ottimizzati durante le future fasi della ricerca. Tale studio ha permesso di valutare i punti deboli di questa tecnologia e l'analisi di sensitività ha fornito indicazioni sugli aspetti prioritari da investigare. Inoltre, data la mancanza di alcuni dati fondamentali riguardanti il continente europeo, non è stato possibile effettuare un'analisi economica dettagliata riguardo alla possibilità di applicare tecnologia nel nuovo continente. Dato però il graduale aumento e l'instabilità del prezzo dell'AdA il processo biotecnologico potrebbe risultare competitivo tra qualche anno.

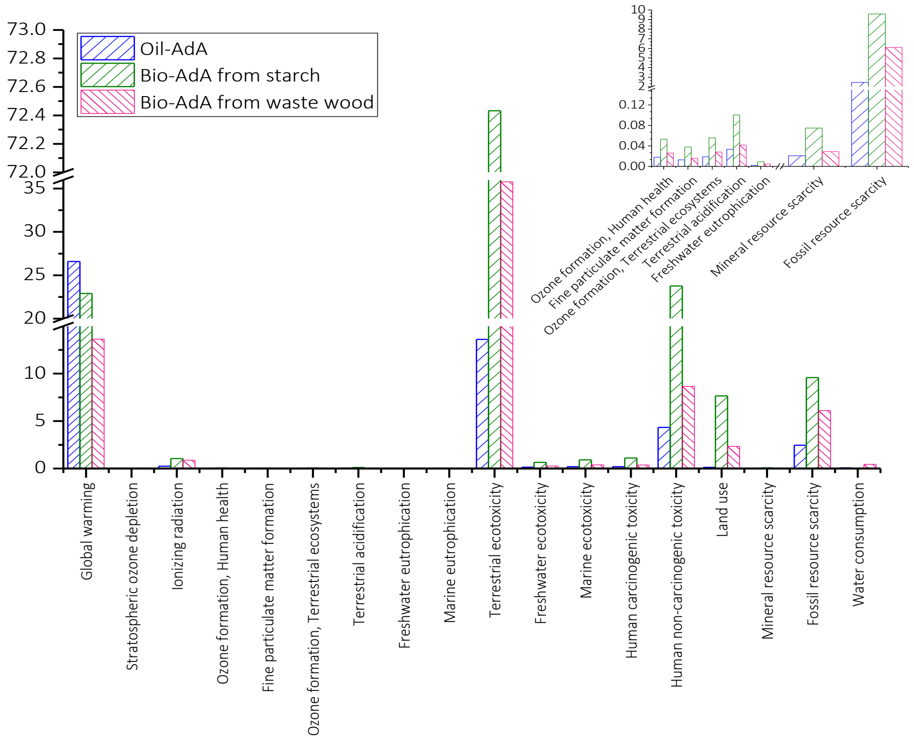

Figura 10: risultati dello studio di impatto ambientale

1. European_commission. Environment & Climate Action_ Horizon 2020 programmes.
2. Wright, M. & Brown, R. C. Establishing the optimal sizes of different kinds of biorefineries. *Biofuels, Bioprod. Biorefining* **1,** 191–200 (2007).
3. MacDowell, N. *et al.* An overview of CO2 capture technologies. *Energy Environ. Sci.* (2010). doi:10.1039/c004106h
4. Pyne, M. E. *et al.* An engineered Aro1 protein degradation approach for increased cis,cis -muconic acid biosynthesis in Saccharomyces cerevisiae. *Appl. Environ. Microbiol.* (2018). doi:10.1128/AEM.01095-18
5. Marketsandmarkets. Adipic Acid Market- Global Trends & Forecast to 2019. (2014). Available at: http://www.marketsandmarkets.com/Market-Reports/adipic-acid-269.html.
6. Adipic acid prices, markets & analysis. Available at: https://www.icis.com/chemicals/adipic-acid/.
7. Mainhardt, H. & Kruger, D. N2O emissions from adipic acid and nitric acid production. *Good Pract. Guid. Uncertain. Manag. Natl. Greenh. Gas Invent.* 183–195
8. Bart, J. C. J. & Cavallaro, S. Transiting from Adipic Acid to Bioadipic Acid. 1, Petroleum-Based Processes. *Ind. Eng. Chem. Res.* **54,** 1–46 (2015).
9. Vardon, D. R. *et al.* cis,cis-Muconic acid: separation and catalysis to bio-adipic acid for nylon-6,6 polymerization. *Green Chem.* **18,** 3397–3413 (2016).
10. Johnson, C. W. *et al.* Enhancing muconic acid production from glucose and lignin-derived aromatic compounds via increased protocatechuate decarboxylase activity. *Metab. Eng. Commun.* **3,** 111–119 (2016).
11. Mizuno, S., Yoshikaw, N., Seki, M., Mikawa, T. & Imada, Y. *Microbial production of cis,cis-muconic acid from benzoic acid*. *Appl. Microbiol. Biotechnol* **28,** (1988).
12. Yang, K. H. & Hougen, O. A. Determination of mechanism of catalyzed gaseous reactions. *Chem. Eng. Prog.* **46,** 146–157 (1950).

General overview

Our environment is constantly changing

Our environment is constantly changing. There is no denying that. This is the sentence that inspire this PhD research project.

In the last few years several natural disasters occurred, warming and cooling periods are becoming more and more frequent and different types of weather patterns and much more are affecting our daily life. All across the world, people are facing a wealth of new and challenging environmental problems every day. Some of them are quite small and only affect a few ecosystems, but others are greatly changing the landscape of what we already know. Currently many environmental processes must be considered, and they are briefly described below.

1. *Climate Change*: problem that occurs due to rise in global warming which causes the increment of atmosphere temperature by realising harmful gases by industry and burning fossil fuels. The effects of the climate change are different such as modification in seasons, melting of polar ice and frequent occurrence of floods and new diseases.
2. *Global Warming*: is the result of human practices like emission of greenhouse gases (CO_2, NOx, CO...). Global warming leads to rising temperatures of the oceans and the earth's surface causing excessive snow or desertification and other unpleasant weather phenomena.

3. *Pollution*: water and air pollution are one of the main topics discussed during several conferences and congresses. Water pollution is caused by acid rain, oil spill and urban runoff, while air pollution is manly related to gas emission by industries and factories and the combustion of fossil fuel.
4. *Natural resource depletion*: fossil fuel consumption results in greenhouse gasses emission. In the las few years people are taking efforts to shift to renewable sources (solar energy, wind or biomass energy…) but the cost for their installation are often non-competitive.
5. *Deforestation*: our forests are natural sinks of carbon dioxide and produce fresh oxygen. Deforestation simply means clearing of green cover and make that land available for residential, industrial or commercial purpose.
6. *Ocean acidification*: it is a direct impact of excessive production of CO_2. 25% of the total CO_2 is produced by humans.[1] The ocean acidity has increased by the last 250 years but by 2100, it may shoot up by 150%.[2]
7. *Water pollution*: water is becoming an economic and political issue as the human population fights for this resource. Desalting processes are becoming more and more important.
8. *Overpopulation*: population of the planet is increasing a lot due to the presence of more and more specific disease treatments. This caused the depletion of sources like fuel, food and water and the consequence increment of intensive agricultures productions.
9. *Ozone layer depletion*: it is attributed to pollution caused by chlorine and bromide found in Chloro-floro carbons (CFC’s). The CFC’s are banned in many industries and consumer products. Ozone layer is valuable because it prevents harmful UV radiation from reaching the earth.
10. *Acid rains*: occurs due to the presence of pollutants in the atmosphere. Acid rain is a known environmental problem that can have serious effect on human health, wildlife and aquatic species
11. *Waste disposal*: the over consumption of resources and creation of plastics are creating a global crisis of waste disposal. Plastic, fast food, packaging and cheap electronic wastes threaten the well-being of humans. Waste disposal is one of urgent current environmental problem.

All these described problems must be considered during the development of new industrial processes and might be taken in to account also to improve the existing ones.

One of the most important rules to design a sustainable process are defined by Anastas and Warner.[3] They identified 12 principles to follow to make a new process as greener as possible. Among these principles the use of renewable feedstocks and less hazardous compounds, that means safer process and pollution prevention, are the key points for the development of environmental friendly processes.

Green Chemistry

The slogan "benign by design" summarizes the ethos of green chemistry, and 12 principles guide its implementation.[4] Green chemistry involves different and interdisciplinary knowledges about chemical engineering, chemistry, ecology and toxicology.

For example, it has been shown that solvents account for 50-80% of the mass in a standard batch chemical operation, depending on whether you include water, or you do not. Solvents account for about 75% of the cumulative life cycle environmental impacts of a standard batch chemical operation.[5]

Moreover, the principle #7 is about the use of renewable feedstocks. Nature produces about 170 billion tons of plant biomass annually, of which we currently use about 3.5% for human needs. It is estimated that about 40 billion tons of biomass, or about 25% of the annual production, would be required to completely generate a bio-based economy. The technical challenge in the use of such renewable feedstocks is to develop low energy, non-toxic pathways to convert the biomass to useful chemicals in a manner that does not generate more carbon than is being removed from "thin air"; the difference between C(in) from the air, and C(out) from the energy used, is the carbon footprint ΔC. Ideally, when using principal #7, all carbon footprints by design should be positive such that $C_{in} >> C_{out}$. This leads in a natural way to the reduction of global warming gasses impacting our current climate change. We should also insure that the new chemicals and materials derived from renewable resources are non-toxic or injurious to human health and the biosphere. (Dr. Richard Wool)[1]

---

[1] Dr. Richard Wool, Professor of Chemical and Biomolecular Engineering and Director of the Affordable Composites from Renewable Materials program, University of Delaware. Green Chemistry Pirnciple #7 https://www.acs.org/content/acs/en/greenchemistry/what-is-green-chemistry/principles/green-chemistry-principle--7.html

General purpose of the PhD research project

To develop new and greener chemical ***processes different approaches can be used.*** Biotechnologist, chemists and chemical engineers are involved in different part of the research, *but the key point is* ***to group all the results*** *of the different approaches trying to find the* ***best compromise*** *in terms of human health, environmental health and economic return.*

This multidisciplinary thesis tries to put together different chemical scientific disciplines: physical chemistry, theoretical chemistry, engineering chemistry, environmental chemical study and biochemistry/biotechnology. It is not always simple to be on the same page. Often the results considered good for a chemist, are not so good for the engineer and are completely unsuitable and useless for a theoretical chemist. However, the key of the success is the common starting point: improve the knowledge about the production of bio adipic acid starting from renewable sources. This implies that the final aim is to develop an industrial process, so all the efforts are funneled to reach this goal. This work starts from the basic research (i.e. catalytic study, development of analytical method, characterization of the different catalysts, variation of the operating conditions...) and ends with the development of an ideal bio adipic acid industrial process.

All this work is the results of a constructive collaboration with different professional figures and I want to thank:

Alessandro ROSENGART, Ph.D., M.Sci in Chemical and Industrial Process Engineering (Politecnico di Milano);

Alberto VILLA, Assistant professor, Chemistry Department, Università degli Studi di Milano;

Luca BRAMBILLA, Assistant Professor, Department of biotechnology and bioscience (Università degli Studi di Milano Bicocca);

Nikolaos DIMITRATOS, Research Fellow, School of Chemistry (Cardiff University).

1. McMichael, A. J. & Woodruff, R. E. Climate Change and Human Health. in *Encyclopedia of World Climatology* (ed. Oliver, J. E.) 209–213 (Springer Netherlands, 2005). doi:10.1007/1-4020-3266-8_41
2. Kerr, R. A. Ocean Acidification Unprecedented, Unsettling. *Science* **328,** 1500–1501 (2010).
3. Anastas, P. T. & Warner, J. C. *Green chemistry: theory and practice*. (New York: Oxford University Press, 1998).
4. Anastas, P. T. & Zimmerman, J. B. Peer Reviewed: Design Through the 12 Principles of Green Engineering. *Environ. Sci. Technol.* **37,** 94A–101A (2003).
5. Rani, B., Singh, U. & Maheshwari, R. K. Role of emerging green chemistry for human comfort and economic intensification. *Unique Res. J. Chem.* **1,** 1–15 (2013).

Chapter 1

Introduction

Climate change, limited oil reserves and geopolitical concerns combine to motivate an urgent quest for alternatives to fossil derived fuels and commodity chemicals (the Grand Challenges).[1] In this sense, industrial innovation has already accepted the responsible practice of low energy use and minimal waste generation, to align economic and environmental sustainability.[2] As a further step, a growing number of chemical industries are developing alternative processes that are based on renewable sources.[3] Much effort has been done in this direction for the development of a bio-based and environmental friendly adipic acid (AdA) production.[4] AdA is a strategic commodity chemical, widely used as monomer in the synthesis of polyamides (PA-6,6), polyesters and other specialty products: PA-6,6 accounts for about 85.4% of the total AdA demand, while other relevant applications are polyurethanes (5%), and adipic esters (4%).[5] In the geographical side, Asia-Pacific (APAC) accounted for 36.5% of the overall the global adipic acid market.[6]

AdA is a crystalline powder, odorless and with a lethal dose concentration (LD_{50}) of 3600 mg/kg. The main physico-chemical properties are reported in Table 1-1.

Table 1-1: Physico-chemical properties of AdA

Physico-chemical properties	
CAS number	124-04-9*
Chemical formula	HOOC(CH2)4COOH*
Molar mass	146.14 g/mol*
Odour	Odourless*
Melting point	152 °C*
Boiling point	337.5 °C*
Solubility in water	23 g/L at 25 °C§
$\log P_{ow}$	0.081#
Flash point	196 °C§
Hazard statements	H319§
Precautionary statements	P305+P351+P338§

*http://www.sciencelab.com/msds.php?msdsId=9927423

§Sigma Aldrich

#Fisher chemical

Global AdA annual demand was estimated at 3750.8 metric tons in 2021 with a growth rate of 3–5% per year.[6,7] and its world consumption is reported in Figure 1-1.[8]

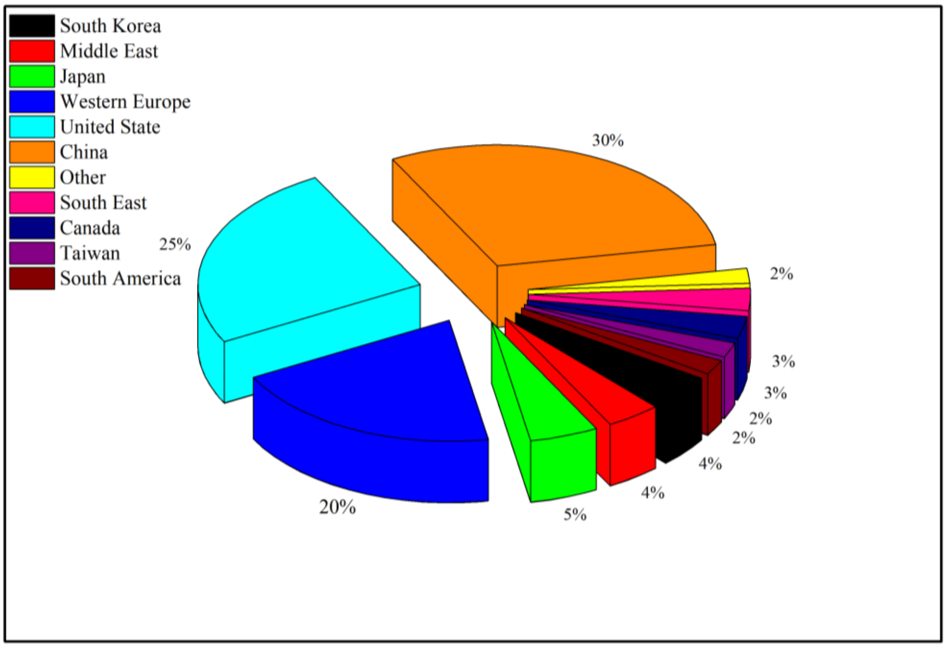

Figure 1-1: world consumption of AdA-2016

So far, the totality of the commercialized AdA derives from oil, mostly from the relatively expensive benzene fraction.[9] In Figure 1-2 the total amount of AdA and the value of import is reported.[10]

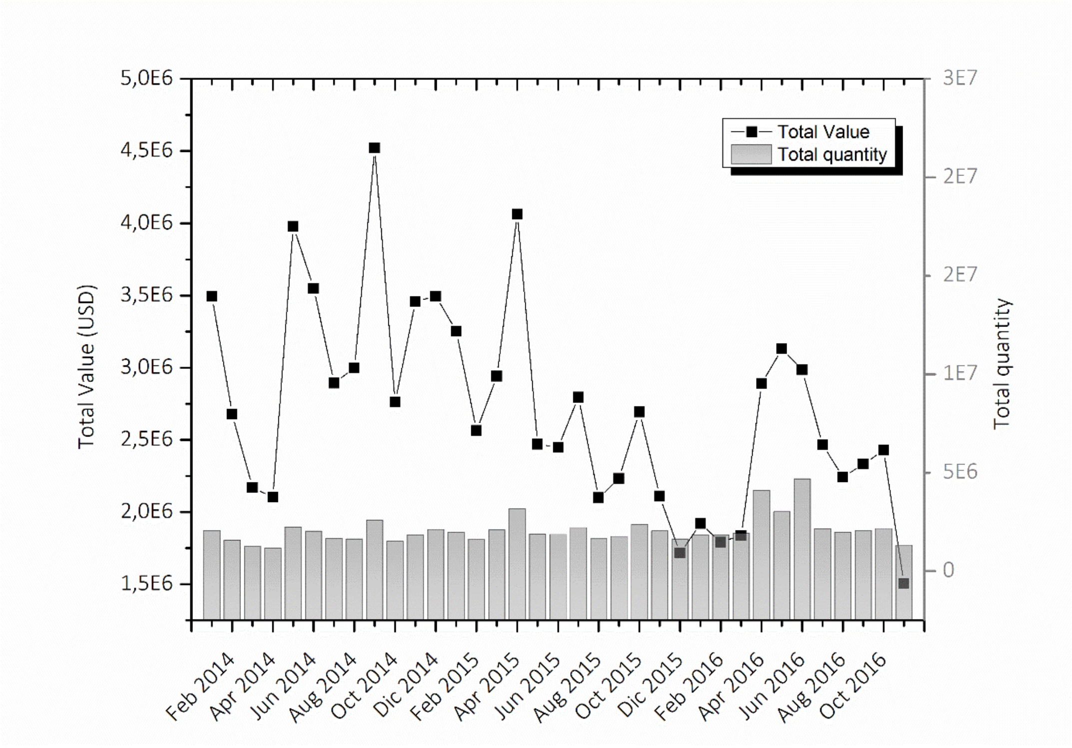

Figure 1-2: total volume and value of import of AdA

Worldwide, there are very few AdA plants. The U.S. is a major producer with three companies in four locations accounting for approximately forty percent of world production. Other producing countries include Brazil, Canada, China, France, Germany, Italy, Japan, Korea, Singapore, Ukraine, and United Kingdom. Most of these countries have only one adipic acid plant except China (3), Germany (2), Japan (2), and U.S. (4).

1.1 Adipic acid production from traditional petrochemical process

In commercial use, two approaches predominate the air oxidation of cyclohexane process: cobalt-catalyzed oxidation and borate-promoted oxidation. A third method, the high-peroxide process, has found limited commercial use.[11]

Cobalt-catalyzed air oxidation of cyclohexane is the most widely used method for producing AdA. Cyclohexane is oxidized with air at 150 °C to 160 °C and 810 to 8-10 atm in the presence of the cobalt catalyst in a sparged reactor or multi-staged column contactor. Several oxidation stages are usually necessary to avoid over-oxidizing the KA mixture. Oxidizer effluent is distilled to recover unconverted cyclohexane then recycled to the reactor feed. The resultant KA-mixture may then be distilled for improved quality before being sent to the nitric acid oxidation stage. This process yields 75 to 80 mole percent KA, with a ketone to alcohol ratio of 1:2.[5]

The schematic plant is reported in Figure 1-3.

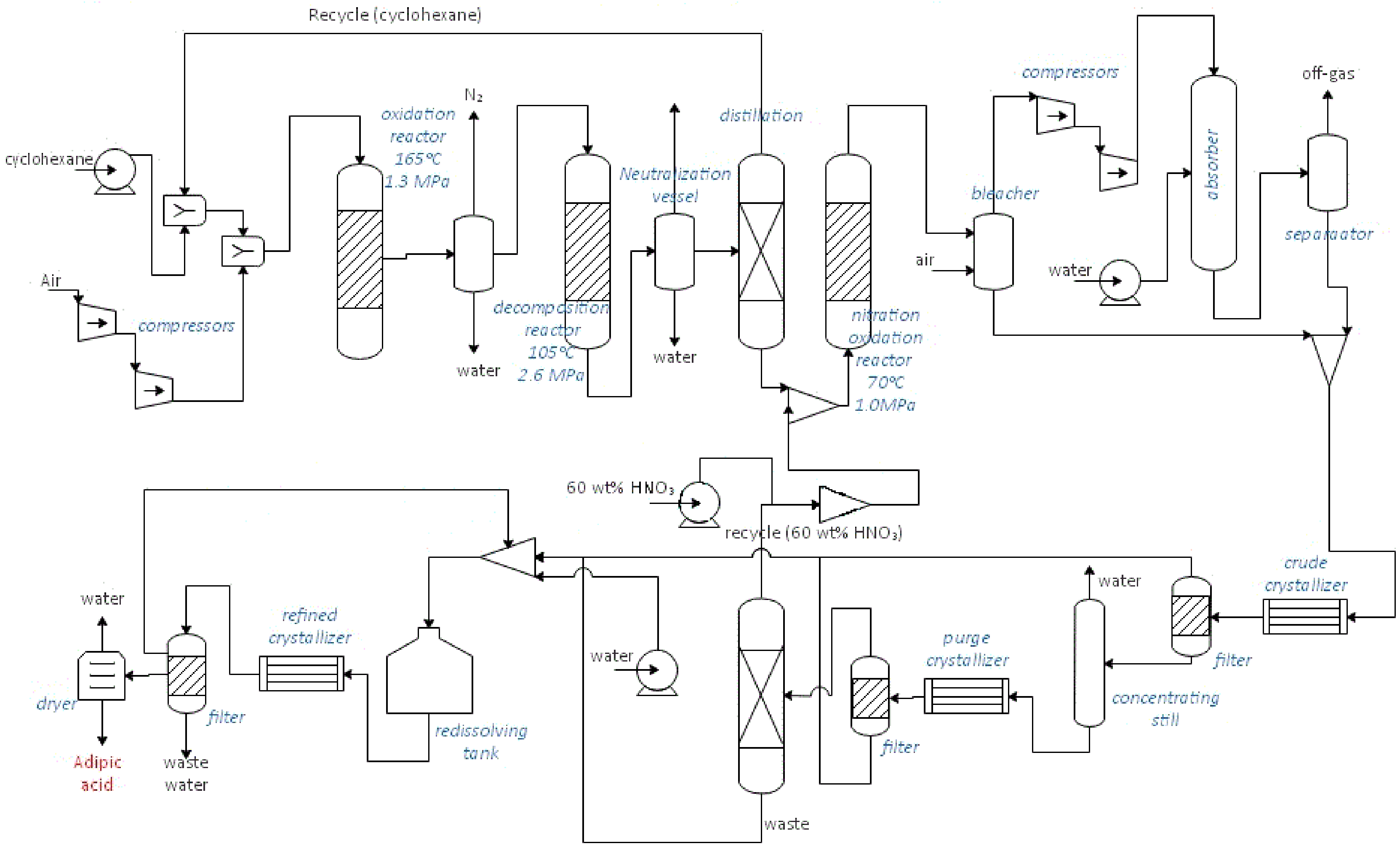

Figure 1-3: flow diagram of the traditional petrochemical process

The second step in commercial production of AdA is nitric acid oxidation of the cyclohexanol-cyclohexanone mixture.[12] Figure 1-4 shows the main reactions which occurs during the AdA synthesis process.

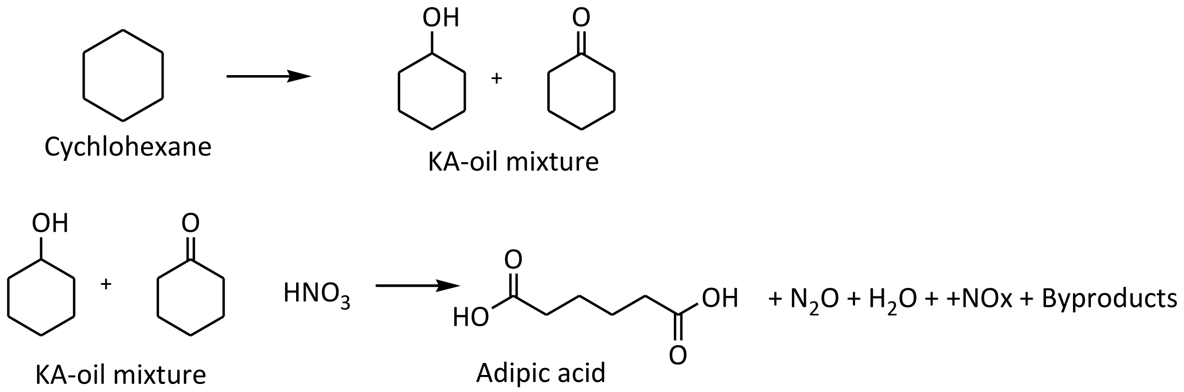

Figure 1-4: reactions involved in the production of AdA from KA-oil oxidation

As the reaction is highly exothermic, heat of reaction is usually dissipated by maintaining a high ratio (40:1) of nitric acid to KA-mixture.[13] Nitric acid (50% to 60%) and a copper-vanadium catalyst are added to the KA-mixture in a reactor vessel at 60 °C- 80 °C and 0.1- 0.4 MPa. Conversion yields of 92%-96% are attainable when using high-purity KA feedstock. Upon reaction, nitric acid is reduced to nitrogen oxides: NO_2, NO, N_2O, and N_2. The dissolved oxides are stripped from the reaction product using air in a bleaching column and subsequently recovered as nitric acid in an absorption tower.[13,14] The stripped AdA/nitric acid solution is chilled and sent to a crystallizer, where crystals of AdA are formed. The crystals are separated from the mother liquor in a centrifuge and transported to the AdA drying and/or melting facilities. The mother liquor is separated from the remaining uncrystallised AdA in the product still and recycled to the reactors.

During the reaction many intermediates are formed such as succinic and glutaric acid.[15]

The hazards related to this process mainly derives from the use of nitric acid, as it is a strong acid and a powerful oxidant, so the plant must be constructed of durable materials, more expensive than normal steels. Moreover, a large amount of nitrogen oxides and nitrous oxide are produced during the oxidation process. The real emission coefficient of nitrous oxide measured at the Nobeoka Works of Asahi Chemical is 0.25 kg_{N2O}/kg_{AdA} (survey by Myiazaki Prefecture in 1994) because part of nitric acid becomes N_2 and NOx.[16] The mixture of nitrogen oxides (reactions by-products) can be re-oxidized to HNO_3, except nitrous oxide (N_2O), which, for environmental protection reasons, had to be eliminated in catalytic or thermal processes.[17] The nitrogen oxides (NO, NO_2) are the main causes of acid rain and under suitable atmospheric conditions favour the photochemical smog that leads to the formation of ozone in the troposphere resulting harmful to living beings. NOx can be almost completely recovered by water adsorption in a multistage column, yielding a nitric acid solution.[18] The main reactions are reported below.

$$2\ NO + O_2 \rightarrow 2\ NO_2$$

$$3\ NO_2 + H_2O \rightarrow 2HNO_3 + NO$$

This route allows the recovery of nitric acid which can be reused within the process itself. The greater cost is in the low temperatures and high pressures needed to maximize the efficiency of the process. Nitrous oxide is a greenhouse gas due to its strong IR absorption and relatively non-toxic, but it has a number of recognized ill effects on human health, whether through breathing it in or by contact of the liquid with skin or eyes.[19,20] In the troposphere it also acts as a catalyst in the cycles of ozone destruction, contributing to its decline. Before the introduction of the most recent N_2O abatement technology, AdA plants alone were the responsible of the 10% of anthropogenic nitrous pollution worldwide.[16] The most important N_2O abatement technologies in order to decrease its emission in the AdA plants are thermal destruction of N_2O, conversion of N_2O into recoverable NO and catalytic dissociation of N_2O to N_2 and O_2 (most common).[17] The catalytic abatement involves highly exothermic reactions:[21,22]

$$2\ O^* \leftrightarrow O_2 + 2^*$$

$$N_2O + {}^* \rightarrow N_2O\ {}^* \rightarrow N_2 + O^*$$

$$N_2O + O^* \rightarrow N_2 + O_2 + {}^*$$

The simplified flow sheet of the catalytic bed reactor is reported in Figure 1-5

There are several classes of catalysts that can be used in this process.[23] Since the reaction is highly exothermic, there are several problems to deal with, as the sintering of the catalyst, the need for special heat-resistant expensive materials for reactors and troubles regarding the environmental regulation. However, the development and the optimization of N_2O abatement technology allows to fully convert nitrous oxide (i.e. using copper/ceria based catalyst) at 550 °C.[24]

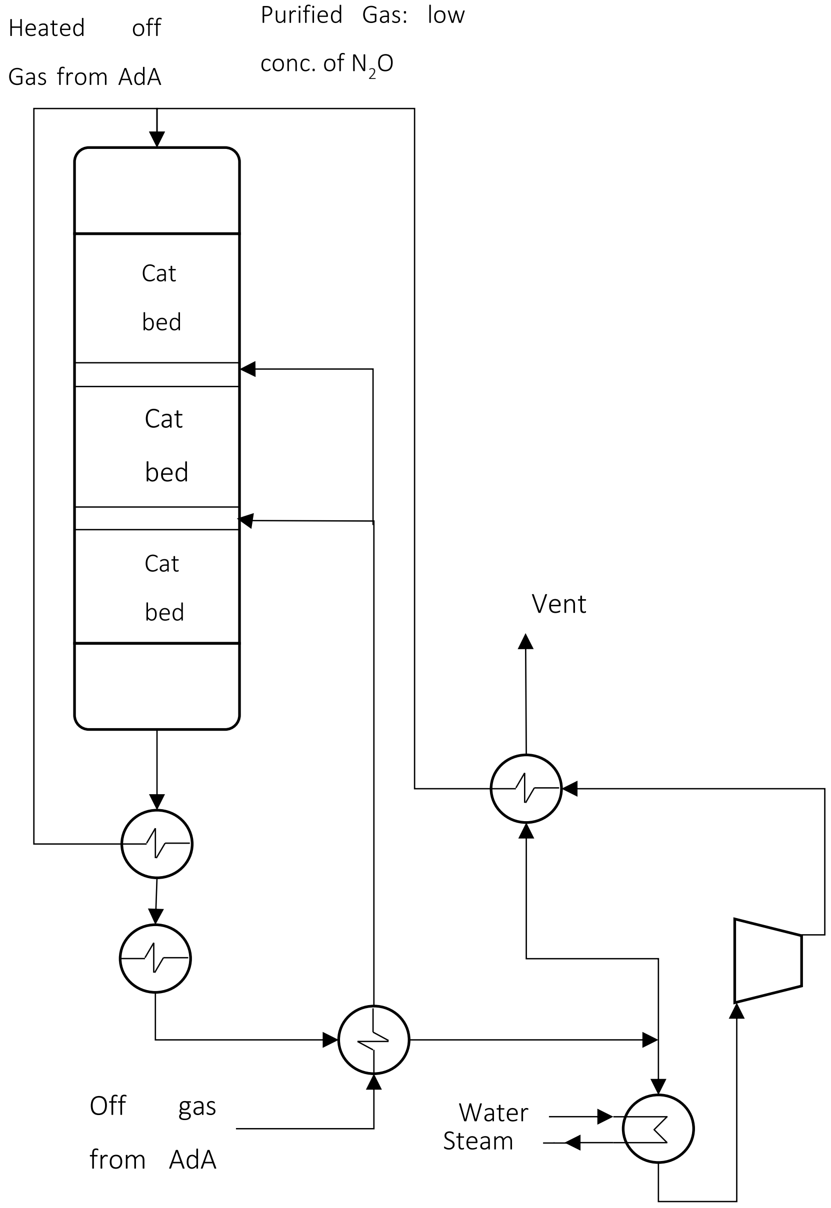

Figure 1-5: simplified scheme of N_2O abatement

1.2 Adipic acid from renewable resources

1.2.1 Overview

Bio adipic acid (bio-AdA) market size is likely to see significant growth as planned capacities come online over the next few years. The bio-AdA market is still at the infancy stage as few companies have focused on research to commercialize production. Companies such as Verdezyne, DSM, BioAmeber, Ameris, Aemethis, Genomatica and Rennovia have successfully designed production technology to develop 100% bio-AdA and would be commercializing the product over the coming years. AdA market price trend is expected to remain stable between 1.6 $ to 1.9 $ per kilo. Increasing nylon 6,6 demand for durable application such as automobiles, textile, carpets, tire-cod and technical fibers is likely to drive bio-AdA market. Industry participants are vying to manufacture 100% bio-based nylon for industrial applications owing to stringent government policies over environmental concerns. Global nylon 6,6 market was estimated at over 1.3 million tons in 2013 and is likely to grow at a CAGR of over 4% from 2016 to 2023. In 2013, Rennovia announced successful completion of 100% bio-based nylon 6,6. It is based on combination of Rennovia's RENNLON bio based AdA and hexamethylene diamine (HMD). Rennovia is able to manufacture both the products through its patented chemical catalytic process technology. Rennovia bio-AdA production is carried out through anaerobic oxidation of glucose to obtain glucaric acid which further goes hydro-oxygenation. Rennovia products are estimated to be cost competitive in comparison to petrochemical based products. The company is targeting to commercialize bio-based AdA market with an initial capacity of 135 kilo tons per year by the end of 2018.

Verdezyne is invested in research to develop bio-AdA through fermentation technique using yeast microorganism which can utilize plant-based oil, alkanes or sugar as feedstock. In 2013, the company announced collaboration with Malaysia's biotechnology investment group, Biotechcorp (Malaysian Biotechnology Corporation). This would help the company to access Malaysia as the prime location to set up biotechnological production facility and it is likely to procure local feedstock such as palm fatty acids and palm kernel oil distillates for manufacturing the end product. Companies are focusing on green alternative routes to mitigate the risks as this could prove to be more beneficial in terms of cost and also would be entitled for government incentives in the form of subsidies and loan guarantees. Technologies developed from Rennovia and Verdezyne can prove to be cost effective as both the process requires glucose as feedstock, available at competitive market rates in comparison to cyclohexane. However, there are significant challenges to be met in terms of high yield and catalyst productivity. Growing preference of bio polyurethane market in applications such as construction, electronics and automotive is likely to drive bio-AdA market growth. It also finds applications in food and medical industries. It is used as flavour and gelling aid for food preparations. Stringent norms by Food and Drug Administration (FDA) over nitrogen dioxide emission from conventional adipic acid are likely to favour bio based adipic acid market growth. Its polymeric coatings are used in hydrophilic drugs and other controlled drug release formulations for medical applications. With established companies such as Invista, BASF, Honeywell and PetroChina in the conventional space and several innovative start-ups developing sustainable technology, adipic acid market share may fragment over the next five years.

1.2.2 Different approaches for the production of bio-adipic acid

Bio-AdA productions strategies can be summarized as reported in Figure 1-6.

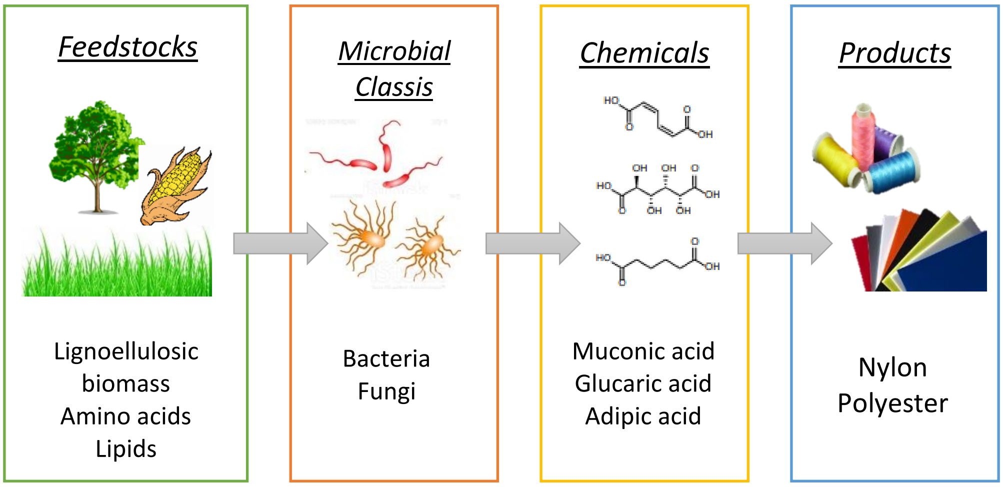

Figure 1-6: simplified representation of the strategies for the production of bio-AdA

Lignocellulosic biomass or lipids-amino acids reach compounds can be converted to muconic acid (MA), glucaric acid and other acids thanks to biotechnology approaches that use modified bacteria and fungi. These intermediates can be further converted to AdA using chemical approaches. Among the many green routes proposed for new “bio-derived building blocks”, the ones that allow AdA production are the most interesting from an economical point of view. These syntheses, though appealing from an economic base, present a series of difficulties that still hinder the diffusion of sugar derived AdA. Several patents and scientific publications have shown the feasibility of the synthesis, exploring a wide range of different technologies to perform the transformations.

1.2.3 Production of bio-adipic acid via glucaric acid

Little scientific research has yet been carried out to explain catalytic routes to selectively oxidise glucose to glucaric acid and most of the available literature efforts on the much easier selective oxidation towards gluconic acid.[25–28] Glucaric acid itself has a widely market potential with uses ranging from detergents,[29] to food and polymers.[30] Very importantly, the dicarboxylic acid functionalisation also makes it an attractive bio-derived precursor to AdA, which could be used as a more sustainable alternative to fossil-fuel derived AdA in nylon production plants. A wide range of other biodegradable polymers are also possible including methacrylates[31] and other ester/amide polymers.[32]

A large market opportunity has presented glucaric acid with the increase in governmental taxes on phosphates in detergents in Europe and more regulation can be expected in the future to fully eradicate the use of phosphates in detergent.[33] Since the 1970s, significant amounts of scientific evidence have linked these phosphates to eutrophication and subsequent decrease in water quality.[34] This realization led to the economic disincentive policies in the EU and outright bans in the U.S. on phosphates in detergents.[35] Glucaric acid is a fascinating drop-in substitute for these banned substances due to its chelating properties in sequestering metal ions in building detergents.[36] The current supply of glucaric acid is very limited and not sufficient for such large market, however, if glucaric acid could be produced at large scale and with competitive cost, this multi-billion-dollar market would be available soon. Table 1-2 outlines the catalytic oxidation studies of glucose to glucaric acid from scientific literature, while in Figure 1-7 are shown the main catalytic reactions.

Table 1-2:Overview of the results achieved in oxidation of glucose (conversion (X) to glucaric acid and yield (Y))

Authors	Year	Catalyst	P (bar)	T (°C)	X (%)	Y (%)
Smith et al.[14]	2012	$NaNO_2$ (HNO_3)	1.25-1.5 (O_2)	25-30	NA	45
Lee et al.[37]	2016	5%Pt/C	13.8 (O_2)	80	100	74
Jin et al.[38]	2016	0.91%Pt 0.95%Pd/TiO_2	1 (O_2)	45	100	40
Solmi et al.[39]	2017	0.71%Au 0.2%Bi/C	10 (O_2)	60	100	31
Thaburet et al.[40]	2001	TEMPO	(NaOCl)	5	NA	90

Figure 1-8 gives an overview of the patent literature involved in the main synthesis glucose/bio-AdA. In the upper part the reactive transformations are reported, while the lower part lists the separation equipment proposed for glucaric acid.

Despite the presence of many patents regarding the bio-AdA production via glucaric acid, some general considerations about the process are mandatory.

i. As for the variety of reaction conditions and of separation processes, a conceptual design approach is necessary to explore all the possible combinations. More information about the economic feasibility and the sustainability of the process are required, also to drive research in the direction of the more promising solutions.
ii. None of the patents reported have any medium-large scale application.
iii. The actual bottlenecks of this technology are the purifications
iv. When glucaric acid is targeted, overoxidation and C-C breaking become a real problem. Despite of this, the oxidative selective oxidation of glucose to glucaric acid continues to attract important industrial interest aligned with the ultimate production of bio-derived adipic acid or for its direct use and the development of very selective systems is still the key.

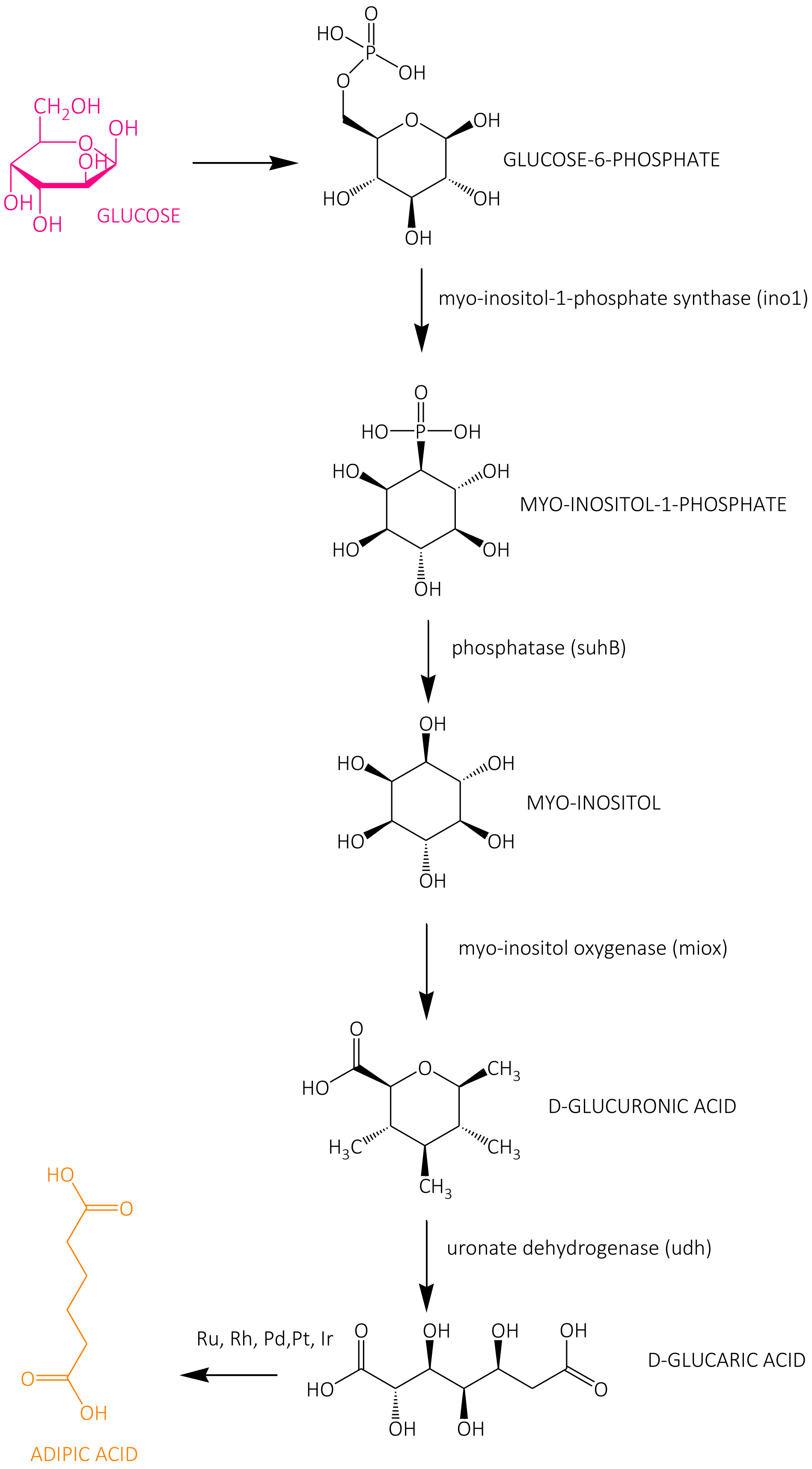

Figure 1-7: reaction pathway from glucose to bio-AdA via glucaric acid

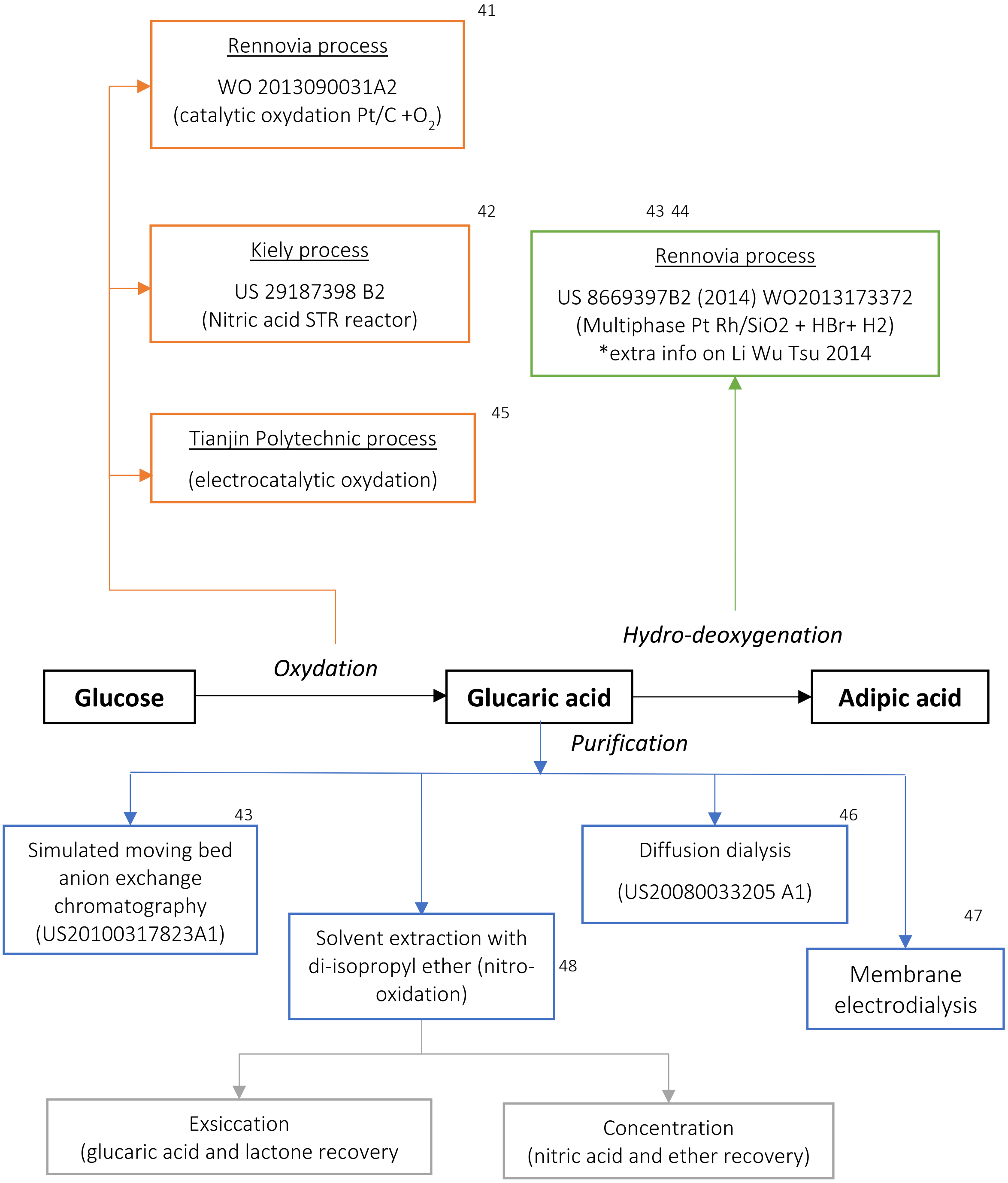

Figure 1-8: overview of patents and literature regarding glucose conversion to AdA via glucaric acid

1.2.3.1 Production of muconic acid as di-unsaturated precursor of adipic acid

The production of AdA through the catalytic hydrogenation of muconic acid (MA) obtained by fermentation of various organic substances is of particular interest. In literature various MA synthesis studies using bio-fermentative pathways where different bacteria strains are used end engineered to increase the yield of the process. Three different substrates are often used to produce MA, i.e. benzoate/benzoic acid, glucose and catechol.

Figure 1-9 represents the main reactions involved in the conversion of these substrates into MA, while In Table 1-3 the most important research and results about the production of MA are reported.

Table 1-3: overview of the literature data about the production of muconic acid

Authors	Year	Bacteria strain	Substrate	MA concentration
Mizuno et al.[49]	1988	*Arthrobacter*	Benzoic acid	44.1 g/L
Yoshikawa et al.[50]	1990	*Arthrobacter* (mutant strain)	Benzoic acid	2.5 g/L
Chue and Hsieh[51]	1990	*Pseudomonas putida* (mutant strain)	Toluene	45.0 g/L
Draths et al.[52]	1994	*Escherichia coli*	Benzoate	7.2 g/L
Niu et al.[9]	2002	*Escherichia coli* (mutant strain)	Glucose	36.9 g/L
Wu et al.[53]	2004	*Sphingobacterium*	Benzoic/succinic acid	90.0 mg/L
Kaneko et al.[54]	2011	*Pseudomonas putida*	Catechol	59.0 g/L
Van Duuren et al.[55]	2011	*Pseudomonas putida KT2440 JD1*	Aromatic feedstock	-
Bui et al.[56,57]	2011/2013	Engineered *Escherichia coli*	Glucose	59.2 g/L
Weber et al.[58]	2012	*Saccharomyces cerevisiae*	Catechol	1.6 mg/L
Curran et al.[59]	2013	*Saccharomyces cerevisiae*	Terephthalic acid	141 mg/L
Yocum et al.[60]	2013	Engineered *Escherichia coli*	Glucose	16.0 g/L
Xie et al.[61]	2014	Pseudomonas putida (mutant strain)	Benzoic acid	7.2 g/L
Sengupta et al.[62]	2015	*Escherichia coli*	Benzoic acid	170.0 mg/L
Zhang et al.[63]	2015	Engineering *Escherichia coli*	Glycerol	2.0 g/L
Vardon et al.[64]	2015	*Pseudomonas putida KT2440*	Benzoate	13.5 g/L
Wang et al.[65]	2015	*Escherichia coli*	Benzoate	0.6 g/L
Johnson et al.[66]	2016	*Pseudomonas putida* (mutant strain)	Glucose	4.9 g/L
			p-coumarate	15.6 g/L

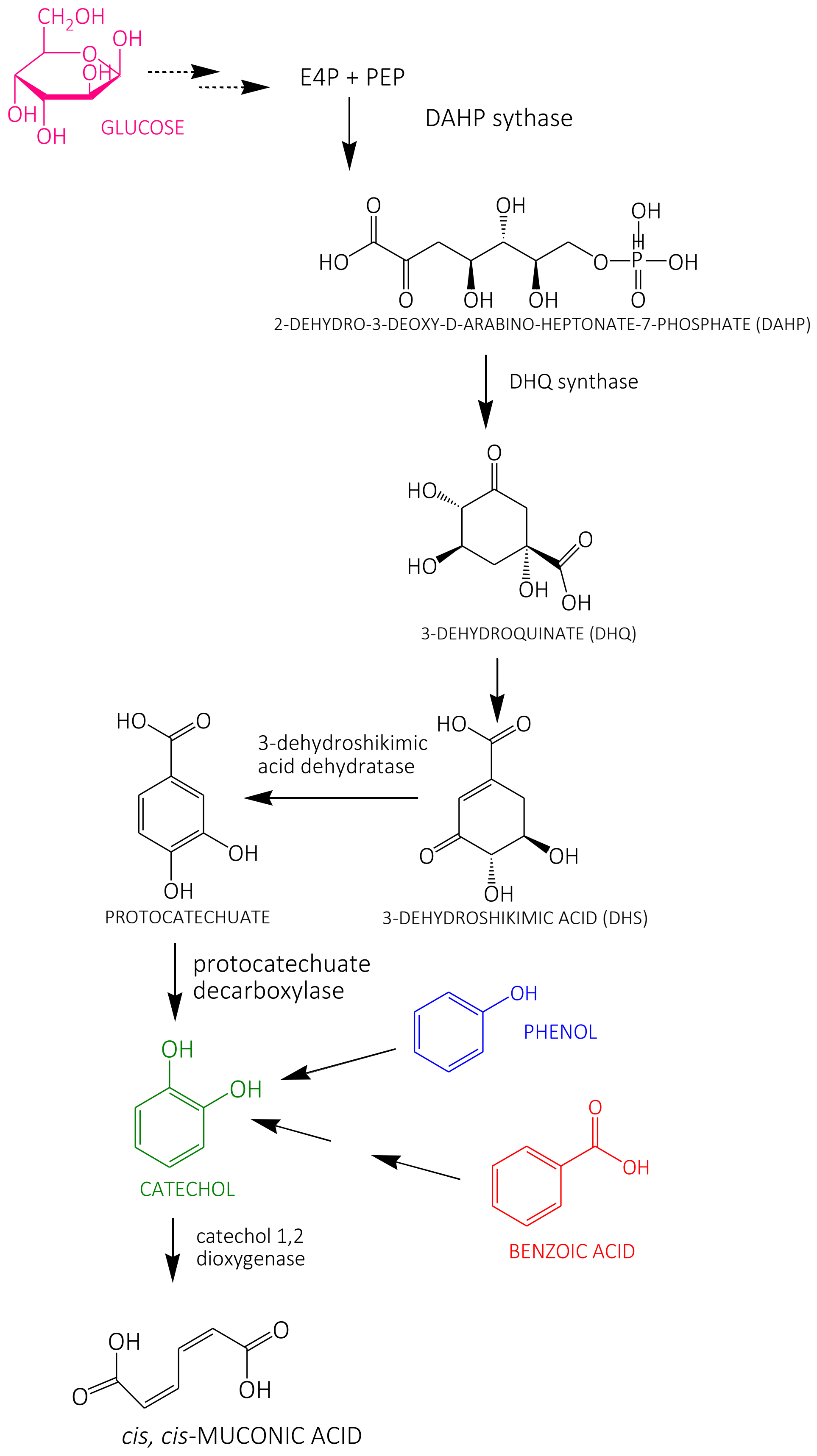

Figure 1-9:conversion of glucose into cis,cis-MA

Despite the literature deeply describes the different ways for the production of MA, only few patents reported its production on medium scale.[67–69] These patents are already expired and applied old purification technology. With the development of new and more sustainable technology for the recovery of chemicals from fermentation broth, the production of MA from glucose might be the best choice for bio-AdA production.

In a recent paper Vardon et al. reported the steps for the recovery of MA achieving a purification yield of 81.4% with a MA final purity of 99.8%.[70]

In Figure 1-10 are schematically reported the main steps of the purification process used to obtain MA having a high purity.

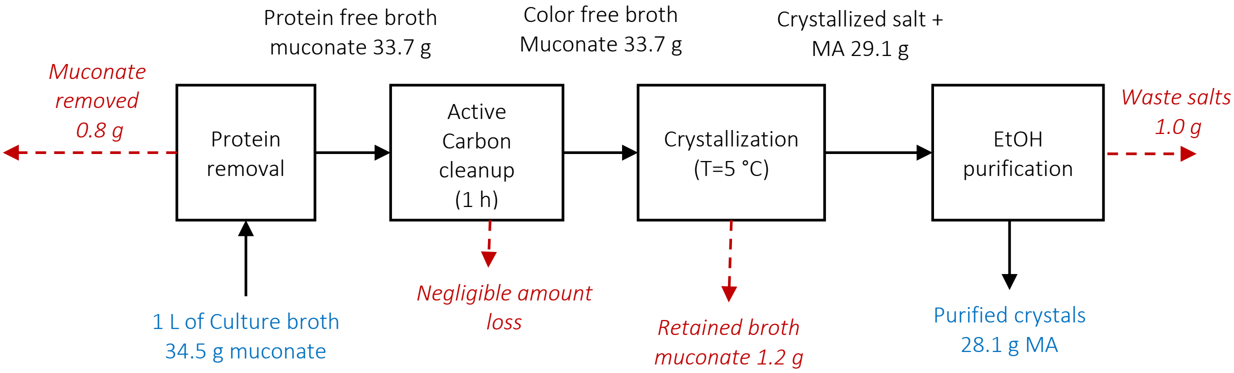

Figure 1-10: diagram of the main purification for the recovery of muconic acid

1.2.3.2 Catalytic hydrogenation of muconic acid to bio-adipic acid

The hydrogenation reaction involving double bonds needs a catalyst and a reducing agent to occur. It is well known that noble metal based catalysts are the most common materials for hydrogenation reactions[71] while molecular gaseous hydrogen is the most common used reducing agent. Heterogeneous catalysis is more common in industry due to the easy recovery of the solid powder after the reaction (i.e. simple filtration is often applied to achieve this purpose). The noble-metal catalysts are prepared depositing a metal precursor on a fine inactive powder, called support. The support is a cheap, porous, bulky, usually granular material, such as alumina, titanium dioxide, activated carbon (AC), and calcium carbonate. For example, platinum on carbon is produced by reduction of chloroplatinic acid *in situ* carbon.[72] In many cases, highly surface modifications involve selective "poisons". Thus, a wisely chosen catalyst can be used to hydrogenate only some functional groups without affecting others (selective hydrogenation reactions). For example it is possible to hydrogenate maleic acid to succinic acid without touching the carboxylic groups.[73] The addition of hydrogen to double or triple bonds in hydrocarbons is a redox reaction that is thermodynamically favourable. The addition of hydrogen to alkenes has a Gibbs free energy change of -101 kJ/mol.[74] However, the reaction rate for most hydrogenation reactions is null without using a catalyst. The mechanism of metal-catalysed hydrogenation of double and triple bonds has been widely studied.[75] On a solid surface, the accepted mechanism for hydrogenation reaction is the Horiuti-Polanyi mechanism[71,76] that occurs in three different steps:

i. binding of the unsaturated bond, and hydrogen dissociation into atomic hydrogen onto the catalyst surface;
ii. addition of one atom of hydrogen (reversible step);
iii. addition of the second atom of hydrogen (irreversible step under hydrogenating conditions).

During the second step, the metal-intermediate formed is a saturated compound that is free to rotate and then break down, detaching the alkene from the catalyst. Consequently, the contact with a hydrogenation catalyst inevitably causes *cis*-*trans* isomerization, because it is thermodynamically favourable. This might be a problem in partial hydrogenation reaction, while in complete one the produces *trans*-alkene is eventually hydrogenated.

The second reagent in this kind of reaction is obviously hydrogen gas. The hydrogenation process often occurs under pressure, usually transported from the cylinders and sometimes improved by "booster pumps". Gaseous hydrogen is mainly produced industrially from hydrocarbons by steam reforming (SR) process.[77] SR method involves a catalytic conversion of steam and hydrocarbons to hydrogen and carbon oxides. The reactions reported below describe the syngas generation (mixture of CO and H_2), CO_2 and H_2 production from water-gas shift reaction (WGS) and H_2 consumption by methanation reactions.

Syngas generation	$C_nH_m + nH_2O \rightarrow nCO + (n+1/2m)H_2$ (non catalytic)
WGS reaction	$CO + H_2O \rightarrow CO_2 + H_2$
Methanation reaction	$CO + 3H_2 \rightarrow CH_4 + H_2O$

To prevent cooking formation on the surface of the catalyst, the operating parameters of this reaction are high temperature, pressure up to 3.5 MPa and steam-to-carbon ratios of 3.5.[78]

After the reformer, the gas mixture passes through a heat recovery step and is fed into a WGS reactor where additional hydrogen is produced. Then the mixture passes either through a CO_2 removal and methanation leaving hydrogen with a purity near 100%.[79] The CO_2 emissions can be strongly reduced using appropriate CO_2 capture and storage (CCS) techniques, through which carbon dioxide is captured and injected in geological reservoirs or the ocean.[80] It is estimated that the hydrogen production cost, corresponding to plants with a design capacity of 379.4 kg/day, at 90% capacity factor and a natural gas cost of 10.00 \$/MMBtu, are 2.27 \$/kg and 2.08 \$/kg with and without carbon capture and sequestration, respectively.[78]

Although hydrocarbons are currently the main feedstock used for hydrogen production, the need to increase the integration of renewable technologies will become inevitable. As the fossil fuels are deteriorating and greenhouse effect is creating greater attention, the share of renewable technologies will rise in the near future while in long term, is expected to dominate over conventional technologies.[81–83] There are many processes for H_2 production from renewable resources such as biomass process and biological process. Biomass is a renewable source of primary energy derived from animals and plants materials crop residues, wood from forests and forest residues, grass, industrial residues, and a host of other materials.[84] Biomass stems from plants is organic matter in which the energy of sunlight is stored in chemical bonds via photosynthesis.[85] Although, CO_2 is released when biomass is used for energy production, this amount of gaseous emission is equal to the amount absorbed by organisms when they were still living.[86] Biological and thermochemical methods are the two hydrogen production processes from biomass. Although biological processes are more environmentally friend and less energy intensive (as they operate under mild conditions), they provide low rates and yields of H_2 depending on the raw materials used.[87] On the other hand, thermochemical processes are much faster and offer higher stoichiometric yield of hydrogen with gasification being a promising option based on economic and environmental considerations.[88] Thermochemical processes are the method through which biomass can be transformed into hydrogen and hydrogen-rich gases.[89,90] Thermochemical technology mainly includes gasification and pyrolysis. Both conversion processes produce, among other gaseous products, CH_4 and CO which can be further treated for more hydrogen production through SR and WGS reaction. Biomass pyrolysis occurs at a range temperature of 377-527 °C at 10.5 MPa and liquid oils, solid charcoal and gaseous compounds are produced by heating the biomass.[88] Biomass pyrolysis takes place in anaerobic conditions except in cases where partial combustion allows to provide the thermal energy needed for the process.[91] CH_4 and other hydrocarbon gases produced can be converted to hydrogen applying WGS reaction. After CO is converted into CO_2 and H_2, the desired purified H_2 is obtained by pressure swing adsorption (PSA).[92] The flow diagram of the pyrolysis process is shown in Figure 1-11.

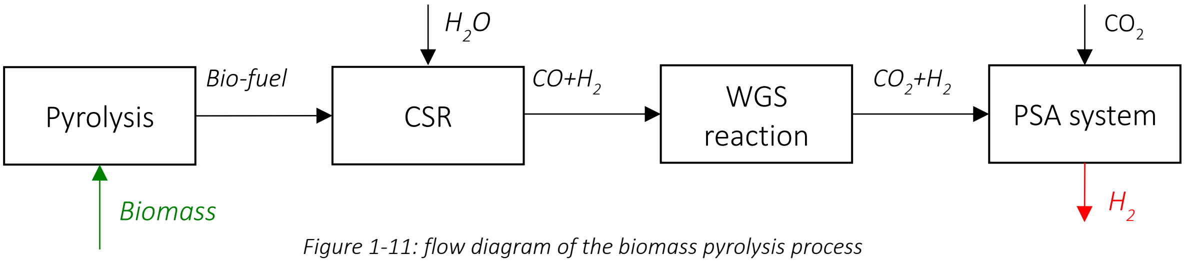

Figure 1-11: flow diagram of the biomass pyrolysis process

The yield of H_2 production from biomass pyrolysis depends on the type of raw materials, the type of the catalyst used, time of residence, and the working temperature.[88,93] The H_2 production cost using biomass pyrolysis technique is expected to be in the range of 1.25 $/kg to 2.20 $/kg, depending on the facility size and biomass type.[94] Biomass gasification is the thermochemical conversion of biomass into syngas in a gasifier where air, oxygen and/or steam are used as medium. It takes place at temperatures between 500 °C and 1400 °C and working pressures from atmospheric to 33 bar.[92] After the transformation of biomass into syngas, the gas mixture is further treated in the same way as the product gas of the pyrolysis process, as shown in Figure 1-12. The H_2 yield is mainly affect by biomass type, particle size, temperature, steam-to-biomass ratio, and type of catalyst used.[89,95] In steam

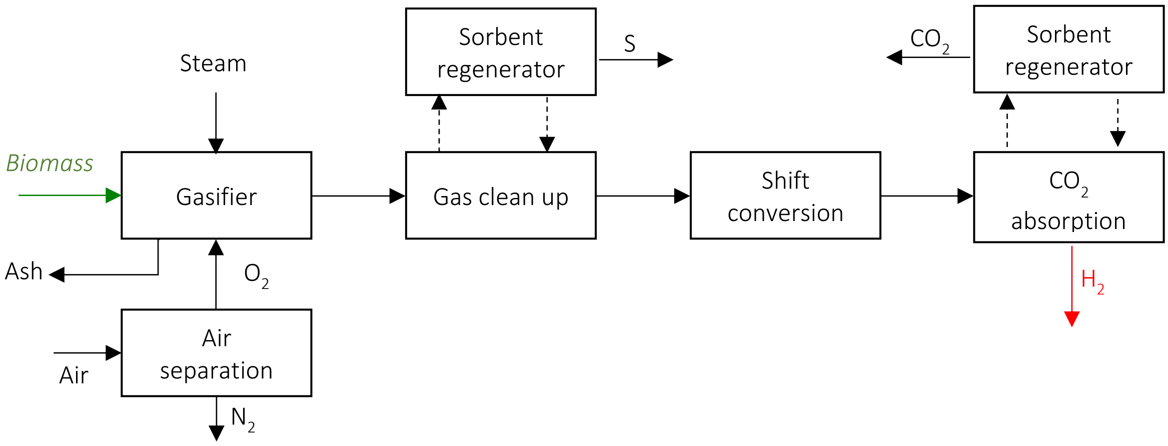

Figure 1-12: flow diagram of the biomass gasification process

gasification, the yield of H_2 is far better than pyrolysis technique while the overall efficiency (thermal-to-hydrogen) can reach up to 52% providing an effective resources of renewable hydrogen production.[91,96] It is estimated that the cost for hydrogen production is 1.77-2.05 $/kg for a plant with an H_2 output of 139700 kg/day and cost of biomass in of 46–80 $/dry-ton.

Although the presence of several papers, only few of them reported the conditions of the hydrogenation of MA to AdA and **no detailed study about the kinetic of this reaction is described until 2002.** The hydrogenation reaction can occur in two consecutive steps and it might suppose that all the possible stereoisomers existing (Figure 1-13).

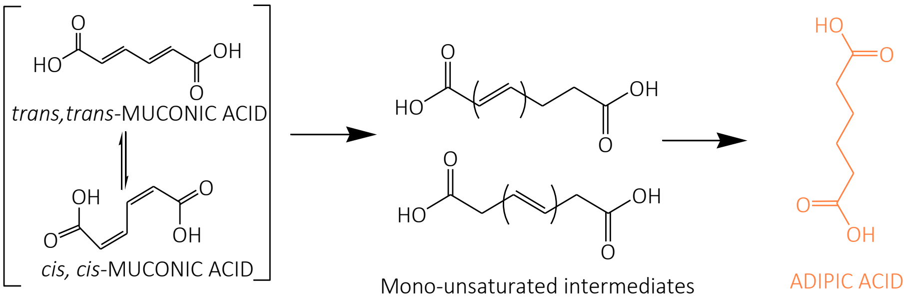

Figure 1-13: hydrogenation reaction of MA to AdA

The scientific literature is widely increased in the last five years due to the more and more attention about the development of sustainable and environmental friendly industrial processes. The main and most important literature about hydrogenation reaction of MA to AdA is reported in Table 1-4.

Table 1-4:overview on the scientific literature about MA hydrogenation to bio-AdA

Authors	Catalyst	Metal loading (%)	Temperature (°C)	H_2 pressure (bar)	MA conversion (%)	AdA yield (%)	solvent
Draths and Frost 1994[52]	Pt/C	10%	25	3.5	100	90	water
Niu et al. 2002[97]	Pt/C	10%	25	34	100	97	water
Thomas et al. 2003[98]	$Ru_{10}Pt_2/SiO_2$	-	80	30	91	96	ethanol
She et al. 2011[99]	Re/TiO_2	-	210	-	-	88	methanol
Li et al. 2014[100]	Pt/C	5%	160	-	-	99	pentanol
Shiramizu and Toste 2013	Pd/C	10%	25	7	-	62	n-butanol
Sirasani et al. 2014[101]	2.44%Pd on PEI/SiO_2	8%	37	-	-	75	-
Vardon et al. 2015[64]	Pd/C 5%	-	-	24	-	97	ethanol
Scelfo et al. 2016[102]	-	-	60	10	-	-	-

Among all these scientific publications, only few of them reported the possibility to recycle the catalyst or cite the possibility of a non-negligible deactivation of the catalyst. Therefore, a detailed kinetic study starting from the basis is needed to better understand and go insight this reaction. Moreover, a modelling and data regression study is mandatory to evaluate all the kinetic parameters (activation energy, adsorption energy…) allowing the optimization of the reaction and the sizing of the reactor.

1.3 The importance of the "at early-stage" life cycle impact assessment (LCIA) for the evaluation of the environmental impact

1.3.1 What is LCIA?

LCIA is a method to evaluate environmental impacts related with all the stages of a product's life from raw material extraction through materials processing, assembly, distribution, use, repair and maintenance, and disposal or recycling. Designers use this technique to help critique their old and new industrial processes and/or products. LCIAs can help avoid a narrow outlook on environmental concerns by:

i. collecting an inventory of relevant material and energy inputs (without forgetting the material and all the stuffs required for the construction of the plant) and environmental releases;
ii. estimating the potential impacts related with identified inputs and releases;
iii. interpreting and understanding the results to help make a more informed decision.

The main aim of the life cycle assessment (LCA) is to compare the full range of environmental effects assignable to products and services by quantifying all inputs and outputs of material flows and calculating how these material flows affect the environment. This information is used to improve processes, provide a sound basis for informed decisions and support policy.

The procedures of LCA is included in ISO 14000 environmental management standards, in ISO 14040:2006, and 14044:2006. (ISO 14044 replaced earlier versions of ISO 14041 to ISO 14043).[103,104]

Although LCA is a global method for assessing impacts of a product on the environment, there are some limitations to consider. First, it is only to evaluate the potential impacts (and not real or measured) of a product or service. Moreover, the results are strictly dependent on data availability, the complexity of the study and the quality of the information. Therefore, achieving this kind of study requires an important level of knowledge and skills.

LCA is becoming more and more important for industry. Like the economic impact the environmental impact is mainly determined in the early stage of development. The challenge in this context is that the ecological impact is hard to predict, if the product has not been fully designed yet and if the production processes are not well known. For the economic impact many empirical formulas exist, whereas for the ecological impact such equations are still missing. Therefore, a life cycle impact assessment tool has been developed which supports the developer during all stages of development.

1.3.2 The four main steps of LCA study

According to the ISO 14040 and 14044 standards, a LCA is carried out in four distinct phases as shown in Figure 1-14. The phases are often interdependent in that the results of one phase will inform how other phases are completed.

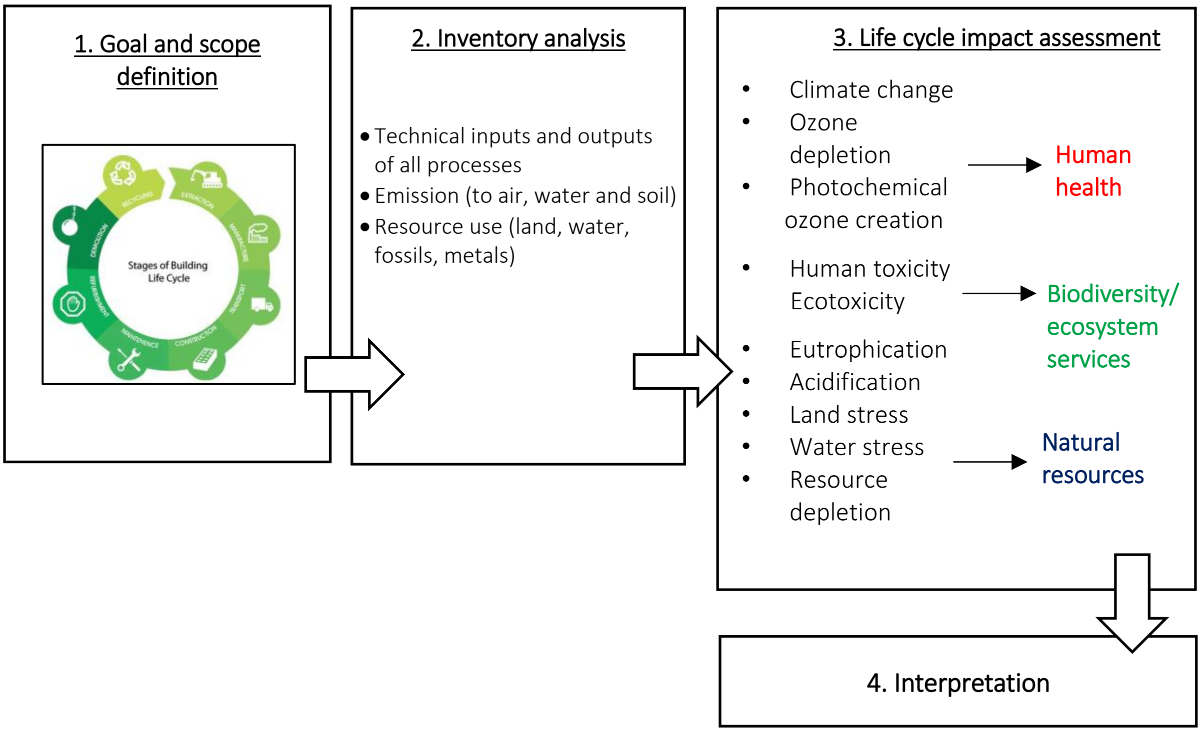

Figure 1-14: four main step of the LCA study

1. Goal and scope definition

The LCA study starts with an explicit declaration of the aim and scope of the study, which includes the context of the study and reported how the results are to be communicated. The goal must be clearly defined and consistent with the selected application.

In this sense the goal and scope document would include technical details such as:

i. *the functional unit*: it defines what exactly is being studied and quantifies the service delivered by the product system, providing a reference to which the inputs and outputs can be related.

Further, the functional unit is a central basis that enables alternative goods, or services, to be compared and analyzed.[105] Therefore, if we want to compare the environmental impact of two different processes to produce AdA, the functional unit will be 1 kg of AdA. The functional flow would be all the different items required for that function. For example, considering the traditional petrochemical process, reactors, N_2O absorber, decanter and concentrator will be taken in to account, while for the bio process fermenter, activated carbon washing, ultrafiltration and other operations will be considered;

ii. *the system boundaries*: they are delimitations of which processes that should be included in the analysis of a product system;[106]

iii. *any assumptions and limitations*;

iv. *the allocation methods:* it is used to partition the environmental load of a process when several products or functions share the same process. The choice of the allocation is a key point of the study because different methods may give different results;

v. *the impact categories* chosen for example human toxicity, smog, global warming, eutrophication…

2. Inventory analysis

Life Cycle Inventory (LCI) analysis involves creating an inventory of flows from and to nature for a product system. The inventory flows must include raw materials, water and energy and all the products that are released in air, water and land. To build this type of document, a flow chart diagram of all unit processes is mandatory where all the inputs and outputs and their amount within the system boundaries are clearly defined. The data must be related to the functional unit defined in the goal and scope definition. All unit processes are linked through intermediate product flows, which makes the process system model linear with respect to the quantity of function it provides. The environmental exchanges are typically assumed to be linearly related to one of the product flows of the unit process.[105] The choices and assumptions made during system modelling, especially with respect to the system boundaries and what processes to include within these boundaries, are often decisive for the result of the LCA study.[107]

3. Life cycle-impact assessment

Inventory analysis is followed by impact assessment. This phase of LCA is aimed at evaluating the significance of potential environmental impacts based on the LCI flow results. Classical life cycle impact assessment (LCIA) consists of the following mandatory elements:

i. selection of impact categories, characterization models, and category indicators;

ii. the classification stage, where the inventory parameters are organized and allocated to specific impact categories;
iii. impact measurement, where the categorized LCI flows are characterized, using one of many possible LCIA methodologies.

Several different LCIA elements may be considered depending on the scope and final aim of the LCA study:

i. *normalization*: the results of the different impact categories are usually compared with the total impacts in the region of interest, the Europe for example;
ii. *grouping*: where the impact categories are sorted and possibly ranked;
iii. *weighting*: all the different environmental impacts are summed up to obtain a single score for the total environmental impact.

LCI can also be considered the different phases of the development, production, use, and disposal of a product. For example it is possible to consider the “first impacts” that includes the extraction of raw material, the conversion of raw materials into a product, the transportation... Therefore the “use impact” may be quantify considering the facilities (water, energy…), the maintenance, repairs and renovations. Finally, the “end of life impact” may include the demolition and processing of waste and recyclable materials.

4. Interpretation

The interpretation allows identifying, quantifying and evaluating all the information obtained during the LCI and/or LCIA process. The result of the interpretation phase is a set of recommendations and conclusions.

According to ISO 14040:2006 the interpretation should include:

- the identification of all the significant topics based on the results of the LCI and LCIA phases;
- evaluation of the study considering sensitivity and consistency checks;
- conclusions, limitations and recommendations.

A key purpose of performing life cycle interpretation is to determine the level of confidence in the final results and communicate them in a fair, complete, and accurate manner. Understanding the results of an LCA is not as simple. The evaluation of the single contribution for each impact category must be clear and complete. Moreover, a consistency estimation of the study is recommended, and the conclusions should be based on a clear understanding of how the LCA was conducted and the results were developed.

Bibliography

1. Peñuelas, J. & Carnicer, J. Climate Change and Peak Oil: The Urgent Need for a Transition to a Non-Carbon-Emitting Society. *Ambio* **39,** 85–90 (2010).
2. Bocken, N. M. P., Short, S. W., Rana, P. & Evans, S. A literature and practice review to develop sustainable business model archetypes. *J. Clean. Prod.* **65,** 42–56 (2014).
3. Clark, J. H., Farmer, T. J., Hunt, A. J. & Sherwood, J. Opportunities for Bio-Based Solvents Created as Petrochemical and Fuel Products Transition towards Renewable Resources. *Int. J. Mol. Sci.* **16,** 17101–17159 (2015).
4. Vardon, D. R. *et al.* Adipic acid production from lignin. *Energy Environ. Sci.* **8,** 617–628 (2015).
5. Oppenheim, J. P., Dickerson, G. L. & Staff, U. B. Adipic Acid. in *Encyclopedia of Chemical Technology* (ed. Kirk-Othmer) 1–27 (Jhon Wiley & Sons, 2014). doi:10.1002/0471238961.0104091604012209.a01.pub2
6. Technavio. Global Adipic Acid Market - Drivers and Forecasts by Technavio. (2017). Available at: https://www.businesswire.com/news/home/20170516006527/en/Global-Adipic-Acid-Market---Drivers-Forecasts.
7. Bart, J. C. J. & Cavallaro, S. Transiting from adipic acid to bioadipic acid. Part II. Biosynthetic pathways. *Ind. Eng. Chem. Res.* **54,** 567–576 (2015).
8. IHS Markit. *Adipic acid*. (2017).
9. Niu, W., Draths, K. M. & Frost, J. W. Benzene-Free Synthesis of Adipic Acid. *Biotechnol. Prog.* **18,** 201–211 (2002).
10. Zauba technology and data. Total volume and value of imports. (2017). Available at: https://www.zauba.com/importanalysis-adipic+acid-report.html.
11. Castellan, A., Bart, J. C. J. & Cavallaro, S. Industrial production and use of adipic acid. *Catal. Today* **9,** 237–254 (1991).
12. Castellan, A. Industrial production and use of adipic acid. *Catal. Today* **9,** 237–254 (1991).
13. Luedeke, V. D. Adipic acid. in *Encyclopedia of Chemical Processing and Design* (ed. J. J. McKetta and W. A. Cunningham) 128–146 (Marcel Dekker, Inc., 1977).
14. Smith, T. N. *et al.* Modifications in the nitric acid oxidation of d-glucose. *Carbohydr. Res.* **350,** 6–13 (2012).
15. Zhou, W. Y., Hu, B. C., Zhao, L. R. & Liu, Z. L. Qualitative and Quantitative Analysis of the By-Products in the Course of Cyclohexanone Production by HPLC-MS/MS. *J, Chin Mass Spectr. Soc* **30,** 31 (2009).
16. Thiemens, M. H. & Trogler, W. C. Nylon Production: An Unknown Source of Atmospheric Nitrous Oxide. *Science (80-.).* **251,** 932 LP-934 (1991).
17. Shimizu, A., Tanaka, K. & Fujimori, M. Abatement technologies for N2O emissions in the adipic acid industry. *Chemosph. - Glob. Chang. Sci.* **2,** 425–434 (2000).
18. Suchak, N. J. & Joshi, J. B. Simulation and optimization of NOx absorption system in nitric acid manufacture. *AIChE J.* **40,** 944–956 (1994).
19. Jay, M. Nitrous oxide: recreational use, regulation and harm reduction. *Drugs and Alcohol Today* **8,** 22–25 (2008).
20. Jevtovic-Todorovic, V., Beals, J., Benshoff, N. & Olney, J. W. Prolonged exposure to inhalational anesthetic nitrous oxide kills neurons in adult rat brain. *Neuroscience* **122,** 609–616 (2003).

21. Reimer, R. A., Slaten, C. S., Seapan, M., Lower, M. W. & Tomlinson, P. E. Abatement of N2O emissions produced in the adipic acid industry. *Environ. Prog.* **13,** 134–137 (1994).

22. Kapteijn, F., Rodriguez-Mirasol, J. & Moulijn, J. A. Heterogeneous catalytic decomposition of nitrous oxide. *Appl. Catal. B Environ.* **9,** 25–64 (1996).

23. Santiago, M., Hevia, M. A. G. & Pérez-Ramírez, J. Evaluation of catalysts for N2O abatement in fluidized-bed combustion. *Appl. Catal. B Environ.* **90,** 83–88 (2009).

24. Liu, Z., He, C., Chen, B. & Liu, H. CuO-CeO2 mixed oxide catalyst for the catalytic decomposition of N2O in the presence of oxygen. *Catal. Today* **297,** 78–83 (2017).

25. Dimitratos, N., Lopez-Sanchez, J. A. & Hutchings, G. J. Selective liquid phase oxidation with supported metal nanoparticles. *Chem. Sci.* **3,** 20–44 (2012).

26. Besson, M., Gallezot, P. & Pinel, C. Conversion of Biomass into Chemicals over Metal Catalysts. *Chem. Rev.* **114,** 1827–1870 (2014).

27. Corma, A. & Garcia, H. Supported gold nanoparticles as catalysts for organic reactions. *Chem. Soc. Rev.* **37,** 2096–2126 (2008).

28. Sheldon, R. A. Green and sustainable manufacture of chemicals from biomass: state of the art. *Green Chem.* **16,** 950–963 (2014).

29. Bessemer, A. C. & van Bekkum, H. Calcium sequestering agents based on carbohydrates. in *Carbohydrates as Organic Raw Materials III* (ed. H.van Bekkum, H. Roper, F. V.) (Wiley-VCH Verlag GmbH, 2007).

30. Mehtiö, T. *et al.* Production and applications of carbohydrate-derived sugar acids as generic biobased chemicals. *Crit. Rev. Biotechnol.* **36,** 904–916 (2016).

31. Gallagher, J. J., Hillmyer, M. A. & Reineke, T. M. Degradable Thermosets from Sugar-Derived Dilactones. *Macromolecules* **47,** 498–505 (2014).

32. Wu, Y., Enomoto-Rogers, Y., Masaki, H. & Iwata, T. Synthesis of Crystalline and Amphiphilic Polymers from d-Glucaric Acid. *ACS Sustain. Chem. Eng.* **4,** 3812–3819 (2016).

33. Köhler, J. Detergent Phosphates: An EU Policy Assessment. *J. Bus. Chem.* **3,** 15–30 (2006).

34. Mitchell, D. Eutrophication of Lake Water Microcosms: Phosphate versus Nonphosphate Detergents. *Science (80-.).* **174,** 827 LP-829 (1971).

35. Litke, D. W. Review of phosphorus control measures in the United States and their effects on water quality. Available at: http://agris.fao.org/agris-search/search.do?recordID=US201300035749.

36. Saeed, K., Priecel, P. & Lopez-Sanchez, J. *Catalytic routes towards bio-renewable glucaric acid*. *Chimica oggi* **35,** (2017).

37. Lee, J., Saha, B. & Vlachos, D. G. Pt catalysts for efficient aerobic oxidation of glucose to glucaric acid in water. *Green Chem.* **18,** 3815–3822 (2016).

38. Jin, X. *et al.* Synergistic Effects of Bimetallic PtPd/TiO2 Nanocatalysts in Oxidation of Glucose to Glucaric Acid: Structure Dependent Activity and Selectivity. *Ind. Eng. Chem. Res.* **55,** 2932–2945 (2016).

39. Solmi, S., Morreale, C., Ospitali, F., Agnoli, S. & Cavani, F. Oxidation of d -Glucose to Glucaric Acid Using Au/C Catalysts. *ChemCatChem* **9,** 2797–2806 (2017).

40. Thaburet, J.-F., Merbouh, N., Ibert, M., Marsais, F. & Queguiner, G. TEMPO-mediated oxidation of maltodextrins and d-glucose: effect of pH on the selectivity and sequestering ability of the resulting polycarboxylates. *Carbohydr. Res.* **330,** 21–29 (2001).

41. Archer, R. *et al.* Processes for the production of adipic acid from D-glucose via hydro-deoxygenation and water concentration reduction in synthesis of hexamethylene diamine and caprolactam (2013).

42. Donen, S., Hash, K., Smith, T. & Jensen, K. Nitric acid oxidation processes. (2013).

43. Boussie, T. R. *et al.* Production of adipic acid and derivatives from carbohydrate-containing materials. (2009).

44. Salem, G. F., Zhu, G., Hagmeyer, A. G. & Dias, E. L. Reduction catalysts. (2012).

45. Bin, D. *et al.* Controllable oxidation of glucose to gluconic acid and glucaric acid using an electrocatalytic reactor. *Electrochim. Acta* **130,** 170–178 (2014).

46. Kiely, D. E. & Hash, K. R. Method of oxidization using nitric acid. (2006).

47. Koter, S. *Ion-Exchange Membranes for Electrodialysis. A Patents Review*. *Recent Patents on Chemical Engineering* **4,** (2011).

48. Reeves, J. B. Use of Nitrobenzene Oxidation for Study of Lignin Composition with an Improved Method for Product Extraction1,2. *J. Dairy Sci.* **69,** 71–76 (1986).

49. Mizuno, S., Yoshikaw, N., Seki, M., Mikawa, T. & Imada, Y. *Microbial production of cis,cis-muconic acid from benzoic acid*. *Appl. Microbiol. Biotechnol* **28,** (1988).

50. Yoshikawa, N., Mizuno, S., Ohta, K. & Suzuki, M. Microbial production of cis,cis-muconic acid. *J. Biotechnol.* **14,** 203–210 (1990).

51. Chua, J. W. & Hsieh, J.-H. Oxidative bioconversion of toluene to 1,3-butadiene-1,4-dicarboxylic acid (cis,cis-muconic acid). *World J. Microbiol. Biotechnol.* **6,** 127–143 (1990).

52. Draths, K. M. & Frost, J. W. Environmentally compatible synthesis of adipic acid from D-glucose. *J. Am. Chem. Soc.* **116,** 399–400 (1994).

53. Wu, C.-M., Lee, T.-H., Lee, S.-N., Lee, Y.-A. & Wu, J.-Y. Microbial synthesis of cis,cis-muconic acid by Sphingobacterium sp. GCG generated from effluent of a styrene monomer (SM) production plant. *Enzyme Microb. Technol.* **35,** 598–604 (2004).

54. Kaneko, A., Ishii, Y. & Kirimura, K. High-yield Production of *cis* , *cis* -Muconic Acid from Catechol in Aqueous Solution by Biocatalyst. *Chem. Lett.* **40,** 381–383 (2011).

55. van Duuren, J. B. J. H. *et al.* Generation of a catR deficient mutant of P. putida KT2440 that produces cis, cis-muconate from benzoate at high rate and yield. *J. Biotechnol.* **156,** 163–172 (2011).

56. Bui, V., Lau, M. K. & Macrare, D. Methods for producing isomers of muconic acid and muconate salts. (2011).

57. Bui, V., Lau, M. K., Macrare, D. & Schweitzer, D. Methods for producing isomers of muconic acid and muconate salts. (2013).

58. Weber, C. *et al.* Biosynthesis of cis,cis-Muconic Acid and Its Aromatic Precursors, Catechol and Protocatechuic Acid, from Renewable Feedstocks by Saccharomyces cerevisiae. *Appl Env. Microbiol* **78,** 8421–8430 (2012).

59. Curran, K. A., Leavitt, J. M., Karim, A. S. & Alper, H. S. Metabolic engineering of muconic acid production in Saccharomyces cerevisiae. *Metab. Eng.* **15,** 55–66 (2013).

60. Yocum, R. R. *et al.* Production of muconic acid from genetically engineered microorganisms. (2013).

61. Xie, N.-Z. *et al. Optimization of medium composition for cis,cis-muconic acid production by a Pseudomonas sp. mutant using statistical methods*. *Preparative biochemistry & biotechnology* **44,** (2014).

62. Sengupta, S., Jonnalagadda, S., Goonewardena, L. & Juturu, V. Metabolic engineering of a novel muconic acid biosynthesis pathway via 4-hydroxybenzoic acid in Escherichia coli. *Appl. Environ. Microbiol.* **81,** 8037–43 (2015).

63. Zhang, H., Li, Z., Pereira, B. & Stephanopoulos, G. Engineering E. coli–E. coli cocultures for production of

muconic acid from glycerol. *Microb. Cell Fact.* **14,** 134 (2015).

64. Vardon, D. R. *et al.* Adipic acid production from lignin. *Energy Environ. Sci.* **8,** 617–628 (2015).

65. Wang, J. & Zheng, P. Muconic acid production from glucose using enterobactin precursors in Escherichia coli. *J. Ind. Microbiol. Biotechnol.* **42,** 701–709 (2015).

66. Johnson, C. W. *et al.* Enhancing muconic acid production from glucose and lignin-derived aromatic compounds via increased protocatechuate decarboxylase activity. *Metab. Eng. Commun.* **3,** 111–119 (2016).

67. Frost, J. W. & Draths, K. M. Bacterial cell tranformants for production of cis, cis-muconic acid and catechol, (1993).

68. Imada, Y., Yoshikawa, N., Mizuno, S. & Takashi, M. Process for preparing muconic acid, (1984).

69. Maxwell, P. C. Production of muconic acid, (1982).

70. Vardon, D. R. *et al.* cis,cis-Muconic acid: separation and catalysis to bio-adipic acid for nylon-6,6 polymerization. *Green Chem.* **18,** 3397–3413 (2016).

71. Horiuti, I. & Polanyi, M. Exchange reactions of hydrogen on metallic catalysts. *Trans. Faraday Soc.* **30,** 1164–1172 (1934).

72. Nishimura, S. *Handbook of Heterogeneous Catalytic Hydrogenation for Organic Synthesis*. (2001).

73. Amoa, K. Catalytic Hydrogenation of Maleic Acid at Moderate Pressures. *J. Chem. Educ.* **84,** 1948 (2007).

74. Atkins, P. W. & Atkins, P. W. *Shriver & Atkins' inorganic chemistry*. (Oxford University Press ; W.H. Freeman and Co., 2006).

75. Kubas, G. J. *Metal Dihydrogen and σ-Bond Complexes*. (Springer US, 2001). doi:10.1007/b113929.

76. Gallezot, P. Hydrogenation - Heterogeneous. in *Encyclopedia of Catalysis* (Jhon Wiley & Sons, 2003).

77. Rylander, P. N. Hydrogenation and Dehydrogenation. in *Ullman's Encyclopedia of Industrial Chemistry* (Wiley-VCH, 2005). doi:10.1002/14356007.a13_487.

78. Nikolaidis, P. & Poullikkas, A. A comparative overview of hydrogen production processes. *Renew. Sustain. Energy Rev.* **67,** 597–611 (2017).

79. Steinberg, M. & Cheng, H. C. Modern and prospective technologies for hydrogen production from fossil fuels. *Int. J. Hydrogen Energy* **14,** 797–820 (1989).

80. Damen, K., Troost, M. van, Faaij, A. & Turkenburg, W. A comparison of electricity and hydrogen production systems with CO2 capture and storage. Part A: Review and selection of promising conversion and capture technologies. *Prog. Energy Combust. Sci.* **32,** 215–246 (2006).

81. Hites, R. A. Persistent Organic Pollutants in the Great Lakes: An Overview BT - Persistent Organic Pollutants in the Great Lakes. in (ed. Hites, R. A.) 1–12 (Springer Berlin Heidelberg, 2006). doi:10.1007/698_5_038.

82. Ćosić, B., Krajačić, G. & Duić, N. A 100% renewable energy system in the year 2050: The case of Macedonia. *Energy* **48,** 80–87 (2012).

83. Mathiesen, B. V, Lund, H. & Karlsson, K. 100% Renewable energy systems, climate mitigation and economic growth. *Appl. Energy* **88,** 488–501 (2011).

84. Demirbaş, A. Biomass resource facilities and biomass conversion processing for fuels and chemicals. *Energy Convers. Manag.* **42,** 1357–1378 (2001).

85. McKendry, P. Energy production from biomass (part 1): overview of biomass. *Bioresour. Technol.* **83,** 37–46 (2002).

86. Flamos, A., Georgallis, P. G., Doukas, H. & Psarras, J. Using Biomass to Achieve European Union Energy

Targets—A Review of Biomass Status, Potential, and Supporting Policies. *Int. J. Green Energy* **8,** 411–428 (2011).

87. Balat, H. & Kırtay, E. Hydrogen from biomass – Present scenario and future prospects. *Int. J. Hydrogen Energy* **35,** 7416–7426 (2010).

88. Demirbaş, A. Yields of hydrogen-rich gaseous products via pyrolysis from selected biomass samples. *Fuel* **80,** 1885–1891 (2001).

89. Wang, Z. *et al.* Gasification of biomass with oxygen-enriched air in a pilot scale two-stage gasifier. *Fuel* **150,** 386–393 (2015).

90. Liu, S. *et al.* Hydrogen production via catalytic pyrolysis of biomass in a two-stage fixed bed reactor system. *Int. J. Hydrogen Energy* **39,** 13128–13135 (2014).

91. Parthasarathy, P. & Narayanan, K. S. Hydrogen production from steam gasification of biomass: Influence of process parameters on hydrogen yield – A review. *Renew. Energy* **66,** 570–579 (2014).

92. Iribarren, D., Susmozas, A., Petrakopoulou, F. & Dufour, J. Environmental and exergetic evaluation of hydrogen production via lignocellulosic biomass gasification. *J. Clean. Prod.* **69,** 165–175 (2014).

93. Duman, G., Uddin, M. A. & Yanik, J. Hydrogen production from algal biomass via steam gasification. *Bioresour. Technol.* **166,** 24–30 (2014).

94. Ni, M., Leung, D. Y. C., Leung, M. K. H. & Sumathy, K. An overview of hydrogen production from biomass. *Fuel Process. Technol.* **87,** 461–472 (2006).

95. Fremaux, S., Beheshti, S.-M., Ghassemi, H. & Shahsavan-Markadeh, R. An experimental study on hydrogen-rich gas production via steam gasification of biomass in a research-scale fluidized bed. *Energy Convers. Manag.* **91,** 427–432 (2015).

96. Balat, M. Hydrogen-rich gas production from biomass via pyrolysis and gasification processes and effects of catalyst on hydrogen yield. *Energy Sources, Part A Recover. Util. Environ. Eff.* **30,** 552–564 (2008).

97. Niu, W., Draths, K. M. & Frost, J. W. Benzene-Free synthesis of adipic acid. *Biotechnol. Prog.* **18,** 201–211 (2002).

98. Thomas, J. M. *et al.* Bimetallic nanocatalysts for the conversion of muconic acid to adipic acid. *Chem. Commun. (Camb).* 1126–1127 (2003). doi:10.1039/b300203a.

99. She, X., Brown, H. M., Zhang, X., Ahring, B. K. & Wang, Y. Selective hydrogenation of trans,trans-muconic acid to adipic acid over a titania-supported rhenium catalyst. *ChemSusChem* **4,** 1071–1073 (2011).

100. Li, X. *et al.* Highly efficient chemical process to convert mucic acid into adipic acid and DFT studies of the mechanism of the rhenium-catalyzed deoxydehydration. *Angew. Chemie - Int. Ed.* **53,** 4200–4204 (2014).

101. Sirasani, G., Tong, L. & Balskus, E. P. A biocompatible alkene hydrogenation merges organic synthesis with microbial metabolism. *Angew. Chemie - Int. Ed.* **53,** 7785–7788 (2014).

102. Scelfo, S., Pirone, R. & Russo, N. Highly efficient catalysts for the synthesis of adipic acid from cis,cis-muconic acid. *Catal. Commun.* **84,** 98–102 (2016).

103. ISO, 2006a. ISO 14040 International Standard. In: Environmental Management – Life Cycle Assessment – Principles and Framework. International Organisation for Standardization, Geneva, Switzerland.

104. ISO, 2006b. ISO 14044 International Standard. In: Environmental Management – Life Cycle Assessment – Requirements and Guidelines. International Organisation for Standardisation, Geneva, Switzerland.

105. Rebitzer, G. *et al.* Life cycle assessment: Part 1: Framework, goal and scope definition, inventory analysis, and applications. *Environ. Int.* **30,** 701–720 (2004).

106. Finnveden, G. *et al.* Recent developments in Life Cycle Assessment. *J. Environ. Manage.* **91,** 1–21 (2009).

107. Heijungs, R. *et al. Environmental life cycle assessment of products. Vol. I: Guide and Vol. II: Backgrounds*. (Centre of Environmental Science, 1992).

Chapter 2

Aim of the PhD research project

The aim of this PhD research project is to study, starting from the bottom, the bio-production of AdA from renewable source (i.e. hydrolysed lignin and cellulose). Since the MA production is widely studied and reported in literature (see Chapter 2), we decided to focus the research on the hydrogenation reaction of MA to bio-AdA.

This reaction might occur in several steps and different reaction equilibria could be established among the regent itself and the different intermediates. Observing the compounds shown in Figure 2-1 it is possible to observe the unquestionable similarity among them.

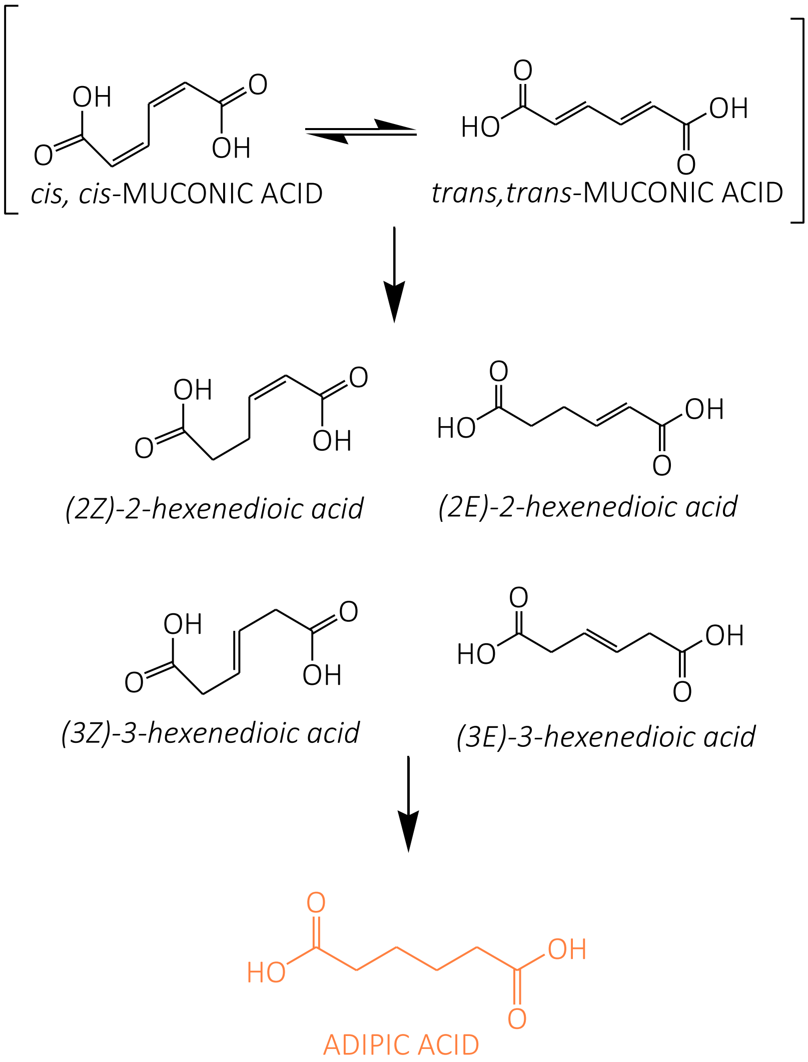

Figure 2-1:hydrogenation reaction of muconic acid to adipic acid

Therefore, the development of a suitable analytical method capable to separate and recognize these compounds is mandatory. The selectivity toward the different intermediates is one of the key step to make possible the optimization and the sizing of a hypothetical industrial reactor.

After the collection of the experimental data, a kinetic regression/modelling study will calculate the kinetic parameters for each step involved in the reaction. Activation energy, absorption/desorption energy for each step will be evaluated using accurate and appropriate equations and regression models.

Due to the more and more awareness of the scientific and industrial community about environmental process, an early-stage environmental impact analysis will be performed on the whole industrial process. To achieved reasonably results, a superstructure of the overall industrial plant with all the feeding/exiting flows and the amount of the different utilities (electricity power, cooling water, steam…) is mandatory.

The research PhD project is divided in main steps:

i. Development of a suitable analytical method able to recognize and quantify the reagent, the products and all the different intermediates. This allow to calculate the conversion, selectivity and yield of the performed reaction;

ii. The research of suitable starting operating conditions in terms of hydrogen pressure, solvent, MA concentration without be in diffusional regime;

iii. The collection of experimental data varying the temperature of the reaction, the substrate-catalyst ratio, type of catalyst and solvent, and hydrogen pressure;

iv. The regression of the experimental data based on adsorption/desorption mechanism of the species on the surface of the catalyst. The work was performed in collaboration with Politecnico di Milano;

v. The preparation and characterization of different catalysts performed in collaboration with Cardiff Catalysis Institute (Cardiff University_UK);

vi. The design of a superstructure model and of the overall plant to estimate the composition of each feed, the utilities required… (this study was performed in collaboration with Politecnico di Milano);

vii. The estimation of the environmental impact of the developed process from the wood biomass.

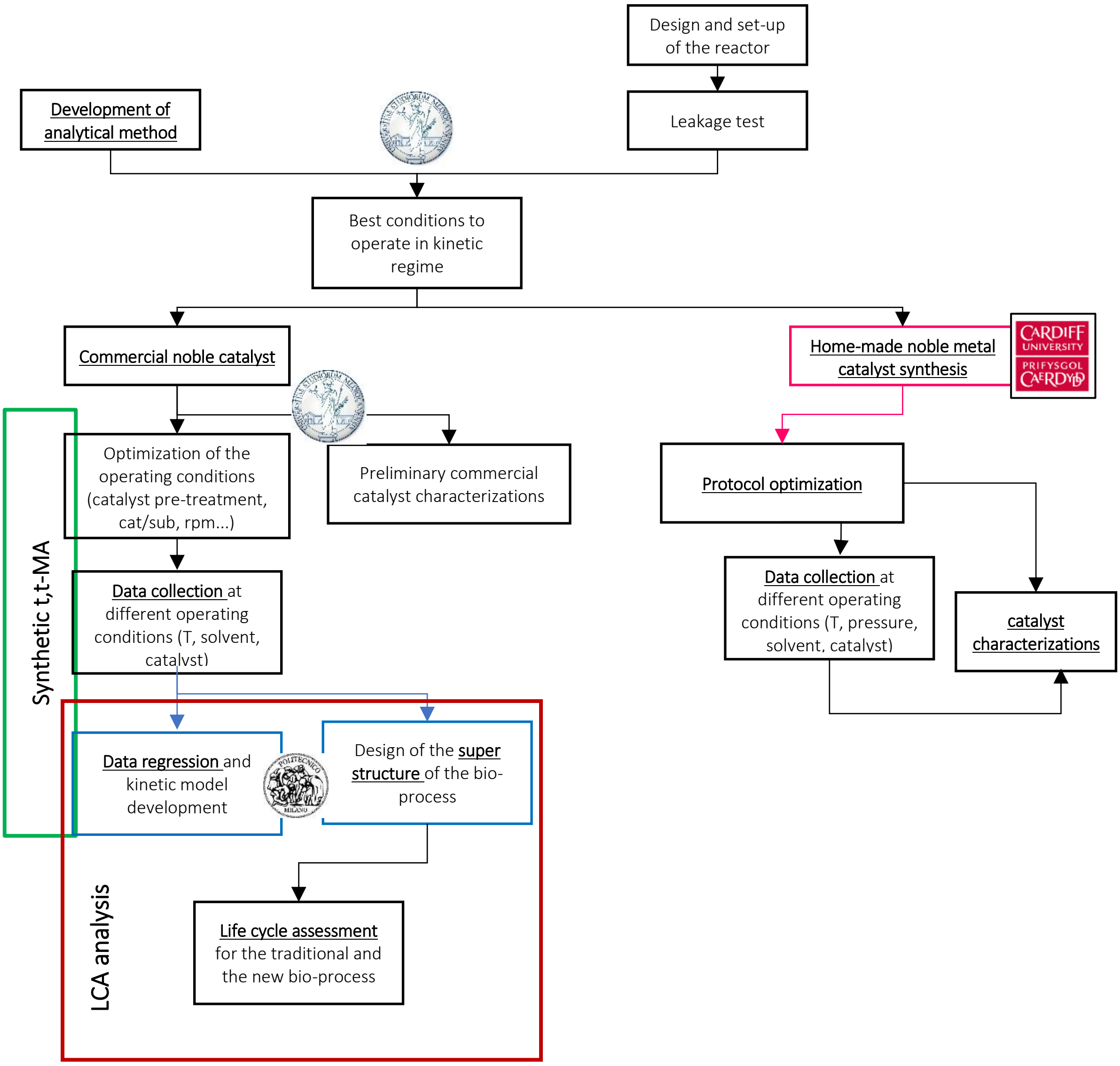

Figure 2-2: representative scheme of the whole project and collaborations

Chapter 3

Description of characterization techniques and analytical instruments

Catalyst characterization, if properly utilized, can be both the cornerstone of the science of catalysis and the "catalyst in its own right for industrial progress". As a long-term research effort, its goal should be an understanding of the catalytic act on a molecular level, a clear explanation of the nature of the individual catalyst sites and of their interdependence and interaction with each other as well as with the reactants. It must also provide an incentive for the development of instrumental capabilities and chemical techniques which are the tools for this research effort. A basic knowledge of catalysis and the ability to conceptualize a working hypothesis is a most desirable prerequisite for such studies.[1] Synthetize a good catalyst and follow/evaluate the reagent conversion and products evolution play a key role in the design of a new industrial process. This chapter describes the techniques used for catalyst characterization and products recognition, the starting point for a robust work.

3.1 Catalyst characterization: introduction and theory

In general, catalyst characterization involves two main steps: the investigation of the porous nature of the catalyst support (physical properties) and the properties of the active sites that are dispersed on the surface of the support (Table 3-1).

Table 3-1: summary of the main techniques used for the characterization of a solid material

Catalyst texture			
Physical properties		Chemical properties	
Result	Technique	Result	Technique
Geometry and shape		Chemical composition	-Electron spectroscopy -Atomic adsorption
Total specific surface area	-Gas physisorption -Mercury porosimetry	Degree of dispersion	-Selective chemisorption -X-ray -Electron microscopy -Magnetisation analysis
True density	-X-ray analysis -Neutron diffraction	Degree of dispersion	-Selective chemisorption -X-Ray -Electron microscopy -Magnetisation analysis
Bulk and apparent density	-Mercury porosimetry -Liquid displacement	Surface Energy	-Thermal analysis test -Temperature programmed desorption and reaction calorimetry
-Pore specific volume -Porosity	-Mercury porosimetry -Gas adsorption	Acid-base sites	-Selective chemisorption -Temperature programmed desorption
Pore size and mean pore size	-Mercury porosimetry -Gas Adsorption	Redox sites	-Spectroscopic methods -Temp. programmed reduction -Temp. Programmed oxidation
Particle size	-Sieves -Laser scattering -Sedimentation -Electrical sensing zone -Etc.	-Catalytic properties -Activity -Selectivity	Reactor tests and simulation
Surface structure	-Optical microscopy -Electron microscopy -X-Ray analysis		
Surface change	Z potential		

The complete and accurate knowledge of the properties of a catalyst is fundamental for evaluating its performances. The catalysts used in this work were characterized using several techniques to investigate their physical and chemical properties.

The techniques used to characterize the catalysts were:

- Physisorption of gas using Brunauer–Emmett–Teller (BET) method: for the evaluation of surface area and pore size distribution;

- Scanning Electron Microscopy (SEM) and Transmission Electron Microscopy (TEM): for the evaluation of nanoparticles morphology;
- RAMAN spectroscopy: observation of vibrational, rotational, and other low-frequency modes in a system;
- Inductively coupled plasma mass spectrometry (ICP-MS): for the detection and quantification of metal inside a solution;
- X-ray Photoelectron Spectroscopy (XPS): metal oxidation state and metal exposure;
- Temperature Programmed Reduction (TPR): evaluation of the reduction temperature of commercial Pt/AC 5% catalyst;
- X-Ray Powder Diffraction (XRPD): evaluation of crystal domain of metal and carbon support.

3.1.1 Surface area evaluation (BET method)

Figure 3-1: BET instrument

Adsorption methods may be used to provide information about the total surface area of a catalyst and the pore size distribution. The interaction between the adsorbate and the adsorbent may be chemical (chemisorption) or physical (physisorption) and ideally should be a surface-specific interaction. Physical adsorption is used in the BET method to determine total surface areas.[2] This technique was developed by Brunauer, Emmett and Teller[3] (the acronyms of their surname is in fact BET) and allows determining the surface area that is commonly expressed as m^2/g. The BET theory is applied to systems of multilayer adsorption and usually uses probing gases that do not chemically react with material surfaces as adsorbates to quantify specific surface area. Nitrogen is the most commonly employed gaseous adsorbate used for surface probing by BET methods. For this reason, standard BET analysis is most often conducted at the boiling temperature of N_2 (77 K). Specific surface area is a scale-dependent property, with no single true value of specific surface area definable, and thus quantities of specific surface area determined through BET theory may depend on the adsorbate molecule utilized and its adsorption cross section. The concept of the theory is an extension of the Langmuir theory,[4] which is a theory for monolayer molecular adsorption, to multilayer adsorption with the following hypotheses:

- gas molecules are physically adsorbed on a solid in layers infinitely;
- there is no interaction between each adsorption layer;
- the Langmuir theory can be applied to each layer.

The resulting BET equation is reported in Eq.1:

$$\frac{V}{V_m} = \frac{c\frac{p}{p^0}}{\left[1-\frac{p}{p^0}\right]\left[1+(c-1)\frac{p}{p^0}\right]} \qquad \text{(Eq.3-1)}$$

where:

V = volume of adsorbed gas at pressure p;

$\mathrm{p}°$ = gas saturation pressure, at temperature T;

$\mathrm{p/p}°$ = relative pressure;

$\mathrm{V_{m=}}$ the monolayer adsorbed gas quantity;

c = BET constant, expressed by Eq.2.

$$c = exp\left(\frac{q_1 - q_L}{RT}\right) \qquad \text{(Eq.3-2)}$$

where:

$\mathrm{q_1}$ = heat of adsorption of the first layer;

$\mathrm{q_L}$ = heat of adsorption of the second and higher layers.

For the $\mathrm{V_m}$ calculation the Eq.3-1 must be linearized and the linear relationship of this equation is maintained only in the range of 0.05 p< p^0 < 0.35.

$$\frac{\frac{p}{p^0}}{V\left[\left(1-\frac{p}{p^0}\right)\right]} = \frac{1}{cV_m} + \frac{\frac{p}{p^0}(c-1)}{cV_m} \qquad \text{(Eq.3-3)}$$

Eq.3-3 is an adsorption isotherm and can be plotted as a straight line with 1 / V[(p°/p) − 1] on the y-axis and p/p^0 on the x-axis according to experimental results. The specific surface area is determined on the V_m basis:

$$Surface\ area\ (S.A.) = \frac{V_m N_{AV} A_{mol}}{V_{mol}} \qquad \text{(Eq.3-4)}$$

where:

$\mathrm{N_{AV}}$ = Avogadro's number;

$\mathrm{A_{mol}}$= adsorption cross section (for N_2 = 16.2 Å^2);

$\mathrm{V_{mol}}$= molar volume of gas (22414 mL/mol);

3.1.2 Scanning Electron Microscopy (SEM)

The scanning electron microscope (SEM) uses a focused beam of high-energy electrons to generate a variety of signals at the surface of solid specimens. The signals that derive from electron-sample interactions reveal information about the sample including external morphology (texture), chemical composition, and crystalline structure and orientation of materials making up the sample. In most applications, data are collected over a selected area of the surface of the sample, and a 2-dimensional image is generated that displays spatial variations in these properties. Areas ranging from approximately 1 cm to 5 microns in width can be imaged in a scanning mode using conventional SEM techniques. The SEM is also capable of performing analyses of selected point locations on the sample; this approach is especially useful in qualitatively or semi-quantitatively determining chemical compositions (using EDS), crystalline structure, and crystal orientations (using EBSD).

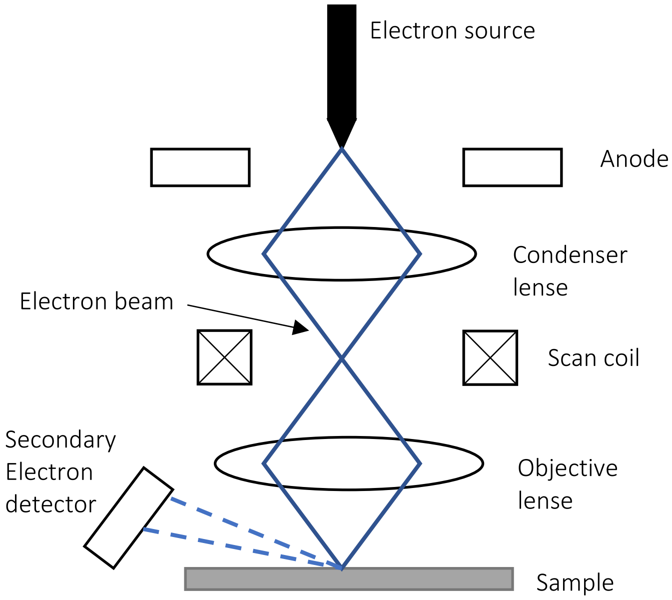

Figure 3-2: SEM internal section and beam pathway

Accelerated electrons in an SEM transmit significant amounts of kinetic energy, and this energy is dissipated as a variety of signals produced by electron-sample interactions when the incident electrons are decelerated in the solid sample. These signals consist of secondary electrons (that produce SEM images), backscattered electrons (BSE), diffracted backscattered electrons (EBSD that are used to determine crystal structures and orientations of minerals), photons (characteristic X-rays that are used for elemental analysis and continuum X-rays), visible light (cathodoluminescence-CL), and heat. Secondary electrons and backscattered electrons are commonly used for imaging samples: secondary electrons are most valuable for showing morphology and topography on samples and backscattered electrons are most valuable for showing contrasts in composition in multiphase samples. Measurement of the energy of photons emitted from the sample is a common method to get analytical capabilities. Examples are the energy-dispersive X-ray spectroscopy (EDS) detectors used in elemental analysis and CL systems that analyses the intensity and spectrum of electron-induced luminescence. In SEM systems using these detectors it is common to colour code these extra signals and superimpose them, so that differences in the distribution of the various components of the sample can be seen clearly and compared. SEM analysis is considered to be "non-destructive"; that is, X-rays generated by electron interactions do not lead to volume loss of the sample, so it is possible to analyse the same material repetitively.

3.1.3 Transmission Electron Microscopy (TEM)

Figure 3-3: TEM instrument

TEM type of electron microscope that has three essential systems:

1. an electron gun, which produces the electron beam, and the condenser system, which focuses the beam onto the object;
2. the image-producing system, consisting of the objective lens, movable specimen stage, and intermediate and projector lenses, which focus the electrons passing through the specimen to form a real, highly magnified image;
3. the image-recording system, which converts the electron image into some form perceptible to the human eye. The image-recording system usually consists of a fluorescent screen for viewing and focusing the image and a digital camera for permanent records. In addition, a vacuum system, consisting of pumps and their associated gauges and valves, and power supplies are required.

The source of electrons, the cathode, is a heated V-shaped tungsten filament or, in high-performance instruments, a sharply pointed rod of a material such as lanthanum hexaboride. The filament is surrounded by a control grid, with a central aperture arranged on the axis of the column; the apex of the cathode is arranged to lie at or just above or below this aperture. The cathode and control grid are at a negative potential equal to the desired accelerating voltage and are insulated from the rest of the instrument. The final electrode of the electron gun is the anode, which takes the form of a disk with an axial hole. Electrons leave the cathode and shield, accelerate toward the anode, and, if the stabilization of the high voltage is adequate, pass through the central aperture at a constant energy. The control and alignment of the electron gun are critical in ensuring satisfactory operation. The intensity and angular aperture of the beam are controlled by the condenser lens system between the gun and the specimen. A single lens may be used to converge the beam onto the object, but, more commonly, a double condenser is employed. In this the first lens is strong and produces a reduced image of the source, which is then imaged by the second lens onto the sample. The use of a small spot size minimizes disturbances in the specimen due to heating and irradiation.

The specimen grid is carried in a small holder in a movable specimen stage. The objective lens is usually of short focal length (1–5 mm) and produces a real intermediate image that is further magnified by the projector lens or lenses. A single projector lens may provide a range of magnification of 5:1, and by the use of interchangeable pole pieces in the projector a wider range of magnifications may be obtained. Modern instruments employ two projector lenses (one called the intermediate lens) to permit a greater range of magnification and to provide a greater overall magnification without a commensurate increase in the physical length of the column of the microscope.

3.1.4 RAMAN spectroscopy

Figure 3-4: RAMAN instrument

Raman spectroscopy is one of the vibrational spectroscopic techniques used to provide information on molecular vibrations and crystal structures. This technique involves a laser light source to irradiate a sample, and generates an infinitesimal amount of Raman scattered light, which is detected as a Raman spectrum using a CCD camera. The characteristic fingerprinting pattern in a Raman spectrum makes it possible to identify substances including polymorphs and evaluate local crystallinity, orientation and stress.

Raman spectroscopy has some unique advantages such as:

- non-contact and non-destructive analysis;
- high spatial resolution up to sub-micron scale;
- in-depth analysis of transparent samples using a confocal optical system;
- no sample preparation needed;
- both organic and inorganic substances can be measured;
- samples in various states such as gas, liquid, solution, solid, crystal, emulsion can be measured;
- samples in a chamber can be measured through a glass window;
- typically, only 10 msec to 1 sec exposure to get a Raman spectrum;
- imaging analysis is possible by scanning the motorized stage or laser beam.

When light is scattered by matter, almost all of the scattering is an elastic process (Rayleigh scattering) and there is no change in energy. However, a very small percentage of scattering is an inelastic process, thus a scattered light has different energy from incident light. This inelastic scattering of light was predicted theoretically by Adolf Smekal in 1923 and first observed experimentally by Chandrasekhara Venkata Raman in 1928, which is why this inelastic scattering is called Raman scattering (Raman effect).[5]

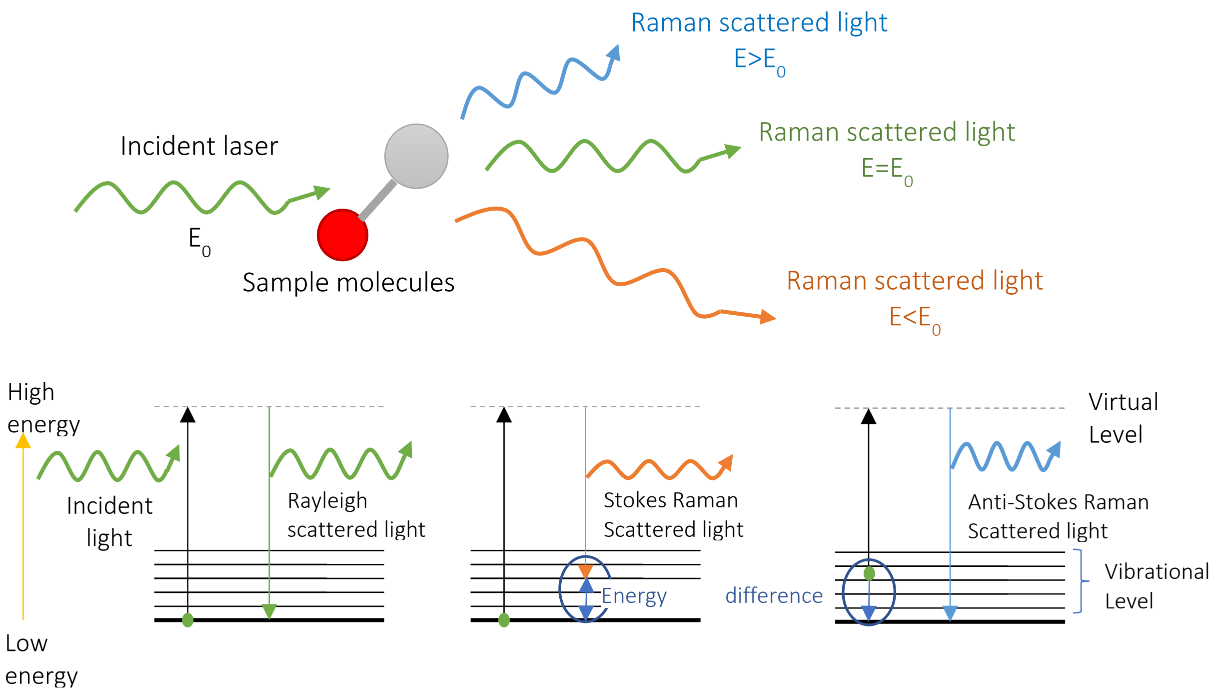

Figure 3-5: diagram of Rayleigh and Raman scattering process

Figure 3-5 shows the energy diagram of Rayleigh and Raman scattering. The incident light interacts with the molecule and distorts the cloud of electrons to form a “virtual state”. This state is not stable, and the photon is immediately re-radiated as scattered light. Rayleigh scattering is a process in which an electron in the ground level is excited and falls to the original ground level. It does not involve any energy change, so Rayleigh scattered light has the same energy as incident light (which means both lights have the same wavelength). Raman scattering can be classified as two types, Stokes Raman scattering and anti-Stokes Raman scattering. Stokes Raman scattering is a process in which an electron is excited from the ground level and falls to a vibrational level. It involves energy absorption by the molecule thus Stokes Raman scattered light has less energy (longer wavelength) than incident light. By contrast, anti-Stokes Raman scattering is a process in which an electron is excited from the vibrational level to the ground level. It involves an energy transfer to the scattered photon thus anti-Stokes Raman scattered light has more energy (shorter wavelength) than incident light.

The dominant process is Rayleigh scattering, and Raman scattering is an extremely weak process in that only one in every 106-108 photons scatters. The ratio of Stokes Raman and anti-Stokes Raman scattering depends on the population of the various states of the molecule. At room temperature, the number of molecules in an excited vibrational level is smaller than that of in the ground level, thus generally the intensity of Stokes Raman light is higher than anti-Stokes Raman light. In standard Raman measurement, Rayleigh scattered light is rejected using a filter and only the Stokes Raman scattering is recorded for simplicity. The intensity of anti-Stokes Raman light increases relative to Stokes scattering as the temperature rises, thus the intensity ratio of anti-Stokes and Stokes light can be used to measure the temperature of a sample.

Raman shifts are typically reported in wavenumbers, which have units of inverse length, as this value is directly related to energy. In order to convert between spectral wavelength and wavenumbers of shift in the Raman spectrum, the following formula can be used:

$$\Delta\omega = \frac{1}{\lambda_0} - \frac{1}{\lambda_1} \qquad \text{(Eq.3-5)}$$

Where:

$\Delta\omega$= Raman shift expressed in wavenumber;

λ_0= excitation wavelength;

λ_1= Raman spectrum wavelength.

Most commonly, the unit chosen for expressing wavenumber in Raman spectra is inverse centimeters (cm^{-1}). Since wavelength is often expressed in units of nanometers (nm), the formula above can scale for this unit conversion explicitly, giving:

$$\Delta\omega(cm^{-1}) = \frac{1}{\lambda_0(nm)} - \frac{1}{\lambda_1(nm)} \cdot \frac{(10^7 nm)}{(cm)} \qquad \text{(Eq.3-6)}$$

Different parameters can be selected during the analysis and they affect the final spectrum. The parameters of the analysis (time of scan, number of scans, wavelength region...) are chosen to highlight a selected region or to enhance the signal.

3.1.5 inductively coupled plasma mass spectrometry (ICP-MS)

Figure 3-6: ICP-MS apparatus

The ICP-MS instrument measures most of the elements in the periodic table. The elements shown in color in Figure 3-7 can be analyzed by ICP-MS with detection limits a at or below the ppt range. Elements that are in white are either not measurable by ICP-MS (the upper right-hand side) or do not have naturally occurring isotopes. Most analyses performed on ICP-MS instrumentation are quantitative; however, it also can work as an excellent semi-quantitative instrument. By using a semi-quantitative software package, an unknown sample can be analyzed for 80 elements in three minutes, providing semi-quantitative data that is typically within ±30% of the quantitative values.

An ICP-MS consists of the following components:

- sample introduction system: composed of a nebulizer and spray chamber and provides the means of getting samples into the instrument;
- ICP torch and RF coil: generates the argon plasma, which serves as the ion source of the ICP-MS;
- Interface: links the atmospheric pressure ICP ion source to the high vacuum mass spectrometer;
- vacuum system: provides high vacuum for ion optics, quadrupole, and detector;
- collision/reaction cell: precedes the mass spectrometer and is used to remove interferences that can degrade the detection limits achieved. It is possible to have a cell that can be used both in the collision cell and reaction cell modes, which is referred to as a universal cell;
- ion optics: guides the desired ions into the quadrupole while assuring that neutral species and photons are discarded from the ion beam;
- mass spectrometer: acts as a mass filter to sort ions by their mass-to-charge ratio (m/z);
- detector: counts individual ions exiting the quadrupole;
- data handling and system controller: controls all aspects of instrument control and data handling to obtain final concentration results.

Samples are introduced into an argon plasma as aerosol droplets. The plasma dries the aerosol, dissociates the molecules, and then removes an electron from the components, thereby forming singly-charged ions, which are directed into a mass filtering device known as the mass spectrometer. Most commercial ICP-MS systems employ a quadrupole mass spectrometer which rapidly scans the mass range. At any given time, only one mass-to-charge ratio will be allowed to pass through the mass spectrometer from the entrance to the exit. If, for example, the quadrupole was set to allow ions with a mass to charge ratio of 23/1 to pass through, we would find that sodium (Na) ions would, while all other singly charged ions would not. Upon exiting the mass spectrometer, ions strike the first dynode of an electron multiplier, which serves as a detector. The impact of the ions releases a cascade of electrons, which are amplified until they become a measurable pulse. The software compares the intensities of the measured pulses to those from standards, which make up the calibration curve, to determine the concentration of the element. For each element measured, it is typically necessary to measure just one isotope, since the ratio of the isotopes, or natural abundance, is fixed in nature. It may be helpful to refer again to Figure 3-7 where you will see a simple bar graph for each element. The bars depict the number and relative abundance of the natural isotopes for that element, which is sometimes referred to as the isotopic fingerprint of the element. ICP-MS can be used to measure the individual isotopes of each element; this capability brings value to laboratories interested in one specific isotope of an element or in the ratio between two isotopes of an element.

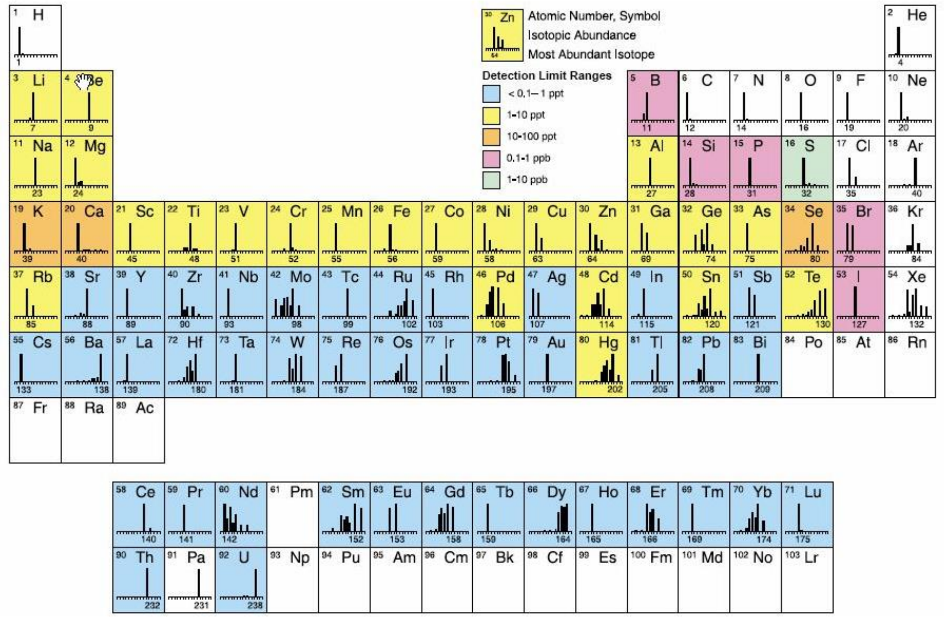

Figure 3-7:ICP detectable chemical element

3.1.6 X-ray photoelectron spectroscopy (XPS)

Figure 3-8: XPS apparatus

XPS is a surface-sensitive quantitative spectroscopic technique that measures the elemental composition at the parts per thousand range, chemical state, empirical formula, and electronic state of the elements that exist within a material. XPS spectra are obtained by irradiating a material with a beam of X-rays while at the same time measuring the kinetic energy and number of electrons that are emitted from the top 0 to 10 nm of the material being analyzed. XPS requires high vacuum (P =10−8 mbar) or ultra-high vacuum (UHV; P< 10−9 mbar) conditions. XPS can be used to analyze the surface chemistry of a material in its initial state, or after some treatment, for example: exposure to heat to study the changes due to heating, exposure to reactive gases or solutions, and exposure to ion beam implant.

XPS is able to detect all elements with an atomic number (Z) between lithium (Z=3) and lawrencium (Z=103). This limitation means that it cannot detect hydrogen (Z=1) or helium (Z=2). Detection limits for most of the elements is 1000 ppm. Detections limits of parts per million (ppm) are possible but require special conditions: concentration at top surface or very long collection time (overnight).

XPS technique is based on the analysis of the kinetic energy distribution of core level photoelectrons emitted as the result of irradiation with monochromatic or narrow band X-rays[2]. Under optimum conditions, the quantitative accuracy of the atomic percent (at%) values calculated from the Major XPS Peaks is 90-95% for each major peak. If a high-level quality control protocol is used, the accuracy can be further improved. Under routine work conditions, where the surface is a mixture of contamination and expected material, the accuracy ranges from 80-90% of the value reported in atomic percent values. The quantitative accuracy for the weaker XPS signals, that have peak intensities 10-20% of the strongest signal, are 60-80% of the true value, and depend upon the amount of effort used to improve the signal-to-noise ratio (for example by signal averaging). The major interest is the study of the "chemical shift" which reflects the oxidation state, and the chemical environment of the emitter. Several problems can be occurred during the application of quantitative analysis to complex systems (such as catalysts): sample charging, the choice of calibration procedures and the collection time can widely affect the measurement. For this reason, XPS is widely used in catalyst research to provide general qualitative analyses, to investigate the depth profile distribution of active species, to obtain estimates of dispersion, clustering and other morphological variations, to study metal-metal and metal-support interactions and to study the chemical states of additives, poisons and transition metal ions in zeolites. Proven measurement techniques and models for interpolation are available.[6,7]

3.1.7 Temperature programmed reduction (TPR)

Figure 3-9: TPR apparatus

The aims of TPR techniques are:

- to find the most efficient reduction conditions;
- to identify the supported precursor phases and their interactions with the support;
- to characterize complex systems, as bimetallic or doped catalyst, to determine the role of the second component ant to establish alloy formation or promotion effects.

In the TPR technique a metal supported catalyst is treated using a programmed temperature ramp while a reducing gas mixture flows into the sample chamber (usually, hydrogen diluted in some inert gas as nitrogen or argon. The reduction rates are continuously measured by monitoring the change in composition of the reactive mixture after the sample chamber. The decrease in H_2 concentration in the effluent gas with respect to the initial one suggests that the reduction process is occurring. An interesting application of this technique is that the TPR analysis may be used to obtain evidence for the interaction between the atoms of two metallic components, in the case of bimetallic system or alloy as already cited. In general, TPR studies are carried out under low partial pressure of the reactive gas. In this way it is possible to observe the intermediate reactions, depending from analytical conditions as temperature rate, flow rate and concentration of reactive gas. The TPR method is used for qualitative and quantitative analysis and the collected spectra are characteristic of a given solid.

3.1.8 X-ray powder diffraction (XRPD)

XRPD is a fast analytical technique mainly used for phase identification of a crystalline material and can provide information on unit cell dimensions. The analyzed material is homogenized, and average bulk composition is determined.

X-ray diffraction is based on constructive interference of monochromatic X-rays and a crystalline sample. These X-rays are generated by a cathode ray tube, filtered to produce monochromatic radiation, collimated to concentrate, and directed toward the sample. When conditions satisfy Bragg's Law[8] (Eq. 3-7)

$$n\lambda = 2d \cdot sin\theta \tag{Eq.3-7}$$

where:

n= is an integer;

λ =wavelength of the radiation (nm);

d= distance between two adjacent planes (nm);

Θ= scattering angle (°).

the interaction of the incident rays with the sample produces constructive interference (and a diffracted ray). This law relates the wavelength of electromagnetic radiation to the diffraction angle and the lattice spacing in a crystalline sample. These diffracted X-rays are then detected, processed and counted. By scanning the sample through a range of 2θ angles, all possible diffraction directions of the lattice should be attained due to the random orientation of the powdered material. Conversion of the diffraction peaks to d-spacings allows identification of the mineral because each mineral has a set of unique d-spacings. Typically, this is achieved by comparison of d-spacings with standard reference patterns. X-ray diffractometers consist of three basic elements: an X-ray tube, a sample holder, and an X-ray detector. X-rays are generated in a cathode ray tube by heating a filament to produce electrons, accelerating the electrons toward a target by applying a voltage, and bombarding the target material with electrons. When electrons have sufficient energy to displace inner shell electrons of the target material, characteristic X-ray spectra are produced. These spectra consist of several components, the most common are K_α and K_β. Filtering, by foils or crystal monochrometers, is required to produce monochromatic X-rays needed for diffraction. $K_{\alpha 1}$and $K_{\alpha 2}$ are sufficiently close in wavelength such that a weighted average of the two is used. Copper is the most common target material for single-crystal diffraction, with Cu-K_{α} radiation = 1.5418 Å. These X-rays are collimated and directed onto the sample. As the sample and detector are rotated, the intensity of the reflected X-rays is recorded. When the geometry of the incident X-rays impacting the sample satisfies the Bragg Equation, constructive interference occurs and a peak in intensity appears. A detector records and processes this X-ray signal and converts the signal to a count rate which is then output to a device such as a printer or computer monitor. The geometry of an X-ray diffractometer is such that the sample rotates in the path of the collimated X-ray beam at an angle θ while the X-ray detector is mounted on an arm to collect the diffracted X-rays and rotates at an angle of 2θ. The instrument used to maintain the angle and rotate the sample is called a goniometer. For typical powder patterns, data is collected at 2θ from ~5° to 70°, angles that are preset in the X-ray scan.

3.2 Analytical techniques

3.2.1 UV-Visible analysis (UV-Vis)

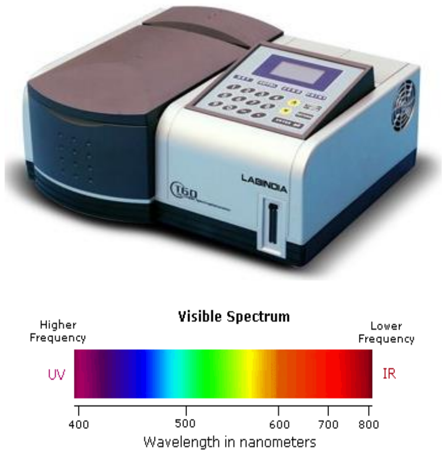

Figure 3-10: UV-Vis instrument and spectrum

Ultraviolet–visible spectroscopy or ultraviolet–visible spectrophotometry (UV–Vis or UV/Vis) refers to absorption spectroscopy or reflectance spectroscopy in the ultraviolet-visible spectral region. The absorption or reflectance in the visible range directly affects the perceived color of the chemicals involved. In this region of the electromagnetic spectrum, atoms and molecules undergo electronic transitions. UV/Vis spectroscopy is routinely used in analytical chemistry for the quantitative determination of different analytes, such as transition metal ions, highly conjugated organic compounds, and biological macromolecules. Spectroscopic analysis is commonly carried out in solution, but solids and gases may also be studied.

Molecules containing π-electrons or non-bonding electrons (n-electrons) can absorb energy in the form of ultraviolet or visible light to excite these electrons to higher anti-bonding molecular orbitals. The more easily excited the electrons (i.e. lower energy gap between the HOMO and the LUMO), the longer the wavelength of light it can absorb. There are four possible types of transitions (π–π*, n–π*, σ–σ*, and n–σ*), and they can be ordered as follows: σ–σ* > n–σ* > π–π* > n–π*.[9]

The reference law is the Lambert-Beer law (Eq.3-8):[10]

$$A = \varepsilon_i \cdot C_i \cdot l \qquad \text{(Eq.3-8)}$$

where:

A= the absorbance of the species;

ε (L·mol^{-1}·cm)= the molar attenuation coefficient or absorptivity of the attenuating species i in the material sample;

C_i (mol/L)= the concentration of the attenuating species *i* in the material sample;

l (cm)= the path length of the beam of light through the material sample.

The path length is normally equal to 1, so the law represents the equation of a centered line in the origin and angular coefficient equal to ε.

The Beer–Lambert Law is useful for characterizing many compounds but does not hold as a universal relationship for the concentration and absorption of all substances

3.2.2 Gas-chromatographic analysis (GC)

Figure 3-11: GC instrument

Gas chromatography is a term used to describe the group of analytical separation techniques used to analyze volatile substances in the gas phase.

A gas chromatograph is based on a gas flow-through narrow tube known as the column, through which different chemical components of a sample pass in a gas stream (carrier gas, mobile phase) at different rates depending on their various chemical and physical properties and their interaction with a specific column filling (stationary phase). As the chemicals exit the end of the column, they are detected and identified electronically by using a detector. The function of the stationary phase in the column is to separate different molecules, affecting the exit time (retention time). Other parameters that can be used to alter the order or time of retention are the carrier gas flow rate, column length and the temperature. In a GC analysis, a known volume of gaseous or liquid analyte is introduced into the injector of the column, usually using a micro syringe. The injector has a temperature of 50 °C above the boiling point of the most low-boiling compound, therefore the injected liquid solution is instantaneously vaporized into the injector. As the carrier gas transports the analyte molecules through the column, this motion is inhibited by the adsorption of the analyte molecules either onto the column walls or onto the stationary phase. The rate at which the molecules progress along the column depends on the strength of adsorption, which depends on the type of molecule and on the solid stationary phase materials. Since each type of molecule has a different rate of progression, the various components of the analyte mixture are separated as they progress along the column and reach the end of the column at different times (retention time). A detector is used to monitor the outlet stream from the column; thus, the time at which each component reaches the outlet and the amount of that component can be determined. Generally, substances are identified (qualitatively) by the order in which they emerge (elute) from the column and by the retention time of the analyte in the column.

Nowadays may different detectors can be coupled with a GC instrument and the most commonly used are:

- Flame ionization detector (FID);
- Thermo conductivity detector (TCD);
- Mass detector (MS).

During this PhD work all these three kinds of detector was used to obtain different information.

FID: in this detector electrodes are placed adjacent to a flame fueled by air/hydrogen mixture near the exit of the column, and when carbon containing compounds exit the column they are pyrolyzed by the flame. This detector works only for organic / hydrocarbon containing compounds due to the ability of the carbons to form cations and electrons upon pyrolysis which generates a current between the electrodes.[11] The increase in current is converted and appears as a peak in a chromatogram. FIDs have low detection limits (a few picograms per second) but they are unable to generate ions from carbonyl containing carbons.[11] FID compatible carrier gasses include helium, hydrogen, nitrogen, and argon.

TCD: compares the thermal conductivity of two gas flows – the pure carrier (reference) gas and the sample. Changes in the temperature of the electrically-heated wires in the detector are affected by the thermal conductivity of the gas which flows around this. The changes in this thermal conductivity are sensed as a change in electrical resistance and are measured. With this detector is possible to detect water (using proper column and filament parameters).

FID and TCD detectors required standards injection to establish which compound is exiting from the column. This recognition is not always simple, especially if new reaction is performed. For the recognition of unknown compound is possible to couple to the GC instrument a mass detector (MS). The compound exiting from the column are fed into the MS analyzer where the compounds are ionized and fragmented. There are several ion sources available; each has advantages and disadvantages for particular applications. For example, electron ionization (EI) gives a high degree of fragmentation, yielding highly detailed mass spectra which when skillfully analyzed can provide important information for structural elucidation/characterization and facilitate identification of unknown compounds by comparison to mass spectral libraries obtained under identical operating conditions.

3.2.3 Nuclear Magnetic Resonance (NMR)

NMR spectroscopy is an analytical chemistry technique used in quality control and research for determining the content and purity of a sample as well as its molecular structure. For example, NMR can quantitatively analyze mixtures containing known compounds. For unknown compounds, NMR can either be used to match against spectral libraries or to infer the basic structure directly. Once the basic structure is known, NMR can be used to determine molecular conformation in solution as well as studying physical properties at the molecular level such as conformational exchange, phase changes, solubility, and diffusion. In order to achieve the desired results, a variety of NMR techniques are available. The principle behind NMR is that many nuclei have spin and all nuclei are electrically charged. If an external magnetic field is applied, an energy transfer is possible between the base energy to a higher energy level (generally a single energy gap). The energy transfer takes place at a wavelength that corresponds to radio frequencies and when the spin returns to its base level, energy is emitted at the same frequency. The signal that matches this transfer is measured in many ways and processed in order to yield an NMR spectrum for the nucleus concerned.

The specific resonant frequency of the energy transition is dependent on the effective magnetic field at the nucleus. This field is affected by electron shielding which is in turn dependent on the chemical environment. As a result, information about the nucleus' chemical environment can be derived from its resonant frequency. In general, the more electronegative the nucleus is, the higher the resonant frequency. Other factors such as ring currents (anisotropy) and bond strain affect the frequency shift. It is customary to adopt tetramethylsilane (TMS) as the proton reference frequency. This is because the precise resonant frequency shift of each nucleus depends on the magnetic field used. The frequency is not easy to describe so it was decided to define chemical shift as follows to yield a more convenient number.

$$Chemical\ shift\ (\delta) = (\nu - \nu_0)/\nu_0 \qquad \text{(Eq.3-9)}$$

The chemical shift, using this equation, is not dependent on the magnetic field and it is convenient to express it in ppm where (for proton) TMS is set to ν_0 thereby giving it a chemical shift of zero.

Bibliography

1. Haensel, V. & Haensel, H. S. The Role of Catalyst Characterization in Process Development. in *Characterization and Catalyst development* 2–11 (1989). doi:10.1021/bk-1989-0411.ch001
2. Haber, J., Block, J. H. & Delmon, B. Manual of method and procedures for catalyst characterization. *Pure Apll. Chem.* **67,** 1257–1306 (1995).
3. Brunauer, S., Emmett, P. H. & Teller, E. Adsorption of Gases in Multimolecular Layers. *J. Am. Chem. Soc.* **60,** 309–319 (1938).
4. Langmuir, I. The adsorption of gases on plane surfaces of glass, mica and platinum. *J. Am. Chem. Soc.* **40,** 1361–1403 (1918).
5. Singh, R. C. V. Raman and the Discovery of the Raman Effect. *Phys. Perspect.* **4,** 399–420 (2002).
6. Bagus, P. S., Ilton, E. S. & Nelin, C. J. The interpretation of XPS spectra: Insights into materials properties. *Surf. Sci. Rep.* **68,** 273–304 (2013).
7. Lascovich, J. C., Giorgi, R. & Scaglione, S. Evaluation of the sp2/sp3 ratio in amorphous carbon structure by XPS and XAES. *Appl. Surf. Sci.* **47,** 17–21 (1991).
8. Bragg, W. H. & Bragg, W. L. The reflection of X-rays by crystals. *Proc. R. Soc. London. Ser. A* **88,** 428 LP-438 (1913).
9. Skoog, D. A., Holler, F. J. & Crouch, S. R. *Principles of Instrumental Analysis*. (Thomson Brooks/Cole, 2007).
10. Buijs, K. & Maurice, M. J. Some considerations on apparent deviations from lambert-beer’s law. *Anal. Chim. Acta* **47,** 469–474 (1969).
11. Harris, D. C. Gas chromatogrphy. in *Quantitative chemical analysis* 657–712 (W.H. freeman and Company, 1999).

Chapter 4

Development of the analytical method

The development of a suitable analytical method able to allow the evaluation of conversion and selectivity is mandatory, even if sometimes different analytical techniques are required to obtain the results. In this chapter the description of the different characterization techniques is reported as well as the analytical methods used to calculate the conversion and the selectivity. Due to laboratory facilities, we have decided to develop a gas chromatographic method able to separate the reaction products (adipic acid, Z and E hexenedioic acids, *cis,cis*-muconic acid). In this chapter the analytical method used for the evaluation of conversion and selectivity is detailly described. The conversion was evaluated by UV-Vis analysis while the selectivity though gas chromatographic analysis after derivatization of the reaction products.

No specific analytical method for the separation and quantification of MA (and its isomers), the monounsaturated intermediates, and AdA is present in literature. Vardon et al[1]. reported a high performance liquid chromatography (HPLC) to separate AdA and the by products utilizing a Phenomenex Rezex RFQ Fast Fruit H^+ column. The system operated at 85 °C with isocratic mobile phase elution t 1.0 ml/min. In this case by-products were identified by co-elution at the same retention time with pure compounds. The spectra obtained with HPLC method is reported in Figure 4-1. MA is very close to ethanol peak and a better resolution is mandatory to correctly evaluate the conversion (key parameter for any industrial application). No mention about (3E)-hexenedioic acid is present. Another research group has mentioned a gas chromatography/mass spectrometry (GC-MS) for the analysis and separation of AdA, dimethyl ester, 2-hexenedioic acid dimethyl ester, and 2, 4-hexadienedioic acid dimethyl ester using a DB-1 MS column.[2] Despite this sentence no operating conditions were reported.

Therefore, a development of a suitable and robust analytical method is mandatory. Due to laboratory facilities, we have decided to develop a gas chromatographic method able to separate the reaction products (adipic acid, Z and E hexenedioic acids, *cis,cis*-muconic acid, and *trans,trans*-muconic acid).

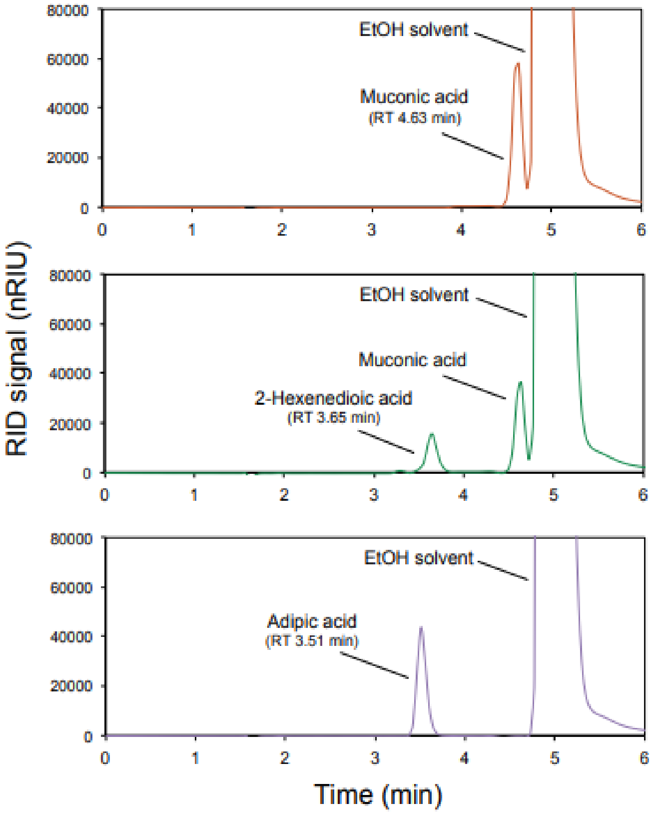

Figure 4-1: chromatogram obtained from HPLC analysis developed by Vardon et al.

4.1 Development and calibration of Ultraviolet-Visible for the evaluation of muconic acid conversion

Firstly, due to the presence of α,β-unsaturated compounds, we tried to design an ultraviolet-visible (UV-Vis) analysis. The instrument used for the spectrophotometric analysis is "T60 UV-Visible Spectrophotometer PRIXMA Spectrophotometer"

The sample is placed inside a quartz cuvette and is irradiated to measure its absorbance at different wavelengths. The instrument has a wavelength range of 190-1100 nm and a spectrophotometric range from -0.3 to 3 Abs. The spectrophotometric accuracy is 0.002/ 0.004 A. The lamp used for the measurement is a monorail "deuterium arc lamp" and the detector is a photodiode with silicon electrodes. The sample is irradiated with a radiation, which provides enough energy for the passage of the electrons from a fundamental state (HOMO) to an excited one (LUMO). The evaluation of this molecular absorption process allows to obtain the absorbance. The wavelength for which the maximum absorbance is recorded is λ_{MAX}.[3]

This property will depend on a number of chemical characteristics, such as the level of aromaticity.

The reference law is the Lambert-Beer law (Eq.4-1):[4]

$$A = \varepsilon_i \cdot C_i \cdot l \qquad \text{(Eq.4-1)}$$

where:

A= the absorbance of the species;

ε (L/mol·cm)= the molar attenuation coefficient or absorptivity of the attenuating species i in the material sample;

C_i (mol/L)= the concentration of the attenuating species *i* in the material sample;

l (cm)= the path length of the beam of light through the material sample.

The path length is normally equal to 1, so the law represents the equation of a centered line in the origin and angular coefficient equal to ε.

A calibration is required for the quantification of muconic acid and sodium muconate. The calibration provides the molar extinction coefficient useful to obtain the concentrations of unknown samples.

Figure 4-2 reported the UV-Vis spectra for the *t,t*-MA, the monounsaturated (2E)-hexenedioic acid and AdA. The maximum absorption for *t,t*-MA compound is at 264 nm, while (2E)-hexenedioic acid ((2E)HxAc) and AdA absorb at the same UV region. That behavior does not allow the possibility to correctly evaluate the selectivity because there is no chance to separate each monounsaturated intermediates.

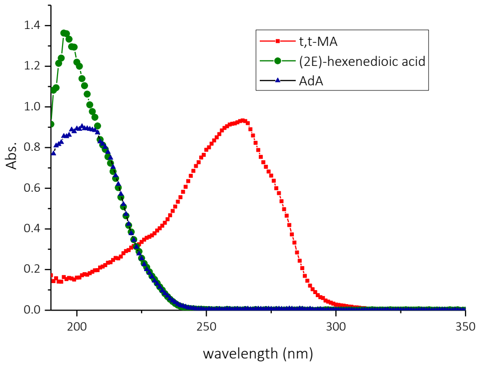

Figure 4-2: UV-Vis spectra of t,t-MA, (2E)-hexenedioic acid and AdA

The calibration of the analysis was then performed as reported in the following paragraph.

4.1.1 Ultraviolet-Visible analysis calibration for sodium muconate acid in water

Sodium muconate (Na-Muc) was prepared starting from *trans,trans*-muconic acid (*t,t*-MA) (Sigma Aldrich, 98%). An amount of *t,t*-MA was dissolved in distilled water and salified using a stoichiometric amount of NaOH (Fluka).

Due to the high absorbance behavior of sodium muconate, very diluted solutions were prepared and analyzed starting from a mother solution with a concentration equal to 4.866E-05 M. The different samples were prepared by weight and due to the very diluted conditions the density of the solution was considered equal to the density of the water (1 mg/L). The concentration of the derived solutions was calculated using Eq.4-2.

$$C_i = \frac{C_{mother\ solution} \times W_{mother\ solution}}{W_{tot}} \qquad \text{(Eq 4-2)}$$

where:

C_i*(mol/L)*= concentration of the sample;

$C_{mother\ solution}$ *(mol/L)*= concentration of the mother solution prepared starting from pure *t,t*-MA and NaOH;

$W_{mother\ solution}$ *(g)*= weight of the mother solution used to preparer the sample;

W_{tot}*(g)*= total weight of the sample ($W_{mother\ solution}$+$W_{added\ water}$).

The absorbance of each sample is reported in Table 4-1.

Table 4-1: Calibration data of Na-Muc in water

# STD	$W_{\text{mother solution}}$ (g)	W_{tot} (g)	$C_{\textit{Na-Muc}}$ (M)	Abs_{264nm}
1	0.00	0.00	0.00E+00	0.000
2	1.00	1.00	4.87E-05	1.284
3	5.00	10.03	2.43E-05	0.648
4	3.03	10.07	1.46E-05	0.382
5	2.51	10.00	1.22E-05	0.323
6	1.26	9.99	6.15E-06	0.172
7	0.64	10.09	3.08E-06	0.089
8	0.52	25.04	1.00E-06	0.032
9	0.52	50.01	5.08E-07	0.017
10	2.01	10.06	9.70E-06	0.258
11	3.51	10.32	1.66E-05	0.443
12	4.01	10.07	1.94E-05	0.528
13	6.01	10.09	2.90E-05	0.765
14	0.00	0.00	0.00E+00	0.000

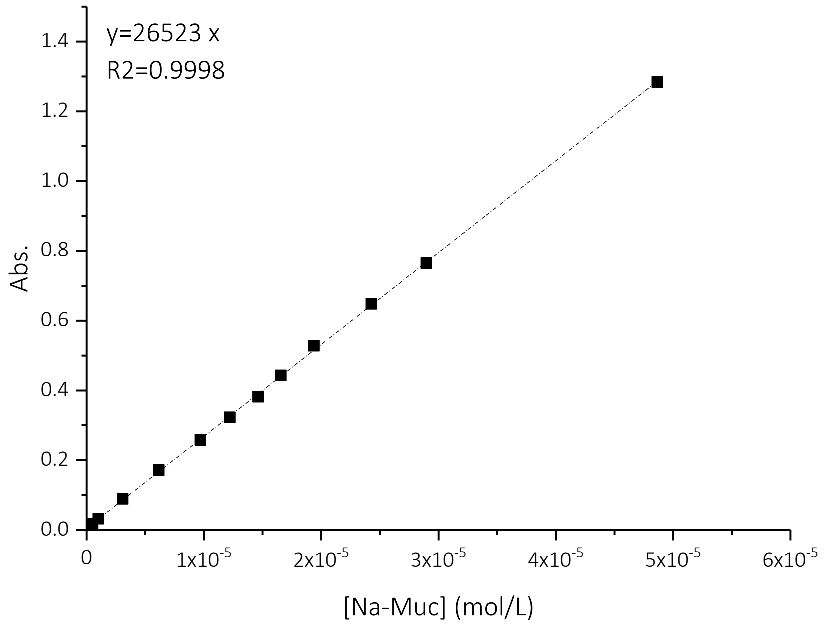

Figure 4-3: Na-Muc calibration in water

A linear correlation was established up to 1.284 value of absorbance. The calculated linear regression resulted is $Abs = 26523 \cdot [t,t-MA]$ with R^2= 0.9998. During the period of research different analysis calibrations were performed obtaining different linear regressions equations.

4.1.2 Ultraviolet-Visible analysis calibration for *t,t*-muconic acid in water

UV-Vis analysis was calibrated using *t,t*-MA provided by Sigma-Aldrich (98% purity).

Two different mother solutions of *t,t*-MA were prepared, (0.0051 M and 1.13E-04 M) using distilled water as solvent. Then, different samples were prepared starting from these mother solutions as reported in Table 4-2.

Table 4-2: Calibration data of t,t-MA in water

# STD	$C_{mother\ solution}$ (M)	$W_{mother\ solution}$ (g)	W_{tot} (g)	$C_{t,t\text{-MA}}$ (M)	Abs_{264nm}
1	0.00	0.000	0.000	0.00E+00	0.000
2	1.13E-04	0.516	25.553	2.282E-06	0.106
3	1.13E-04	1.226	16.023	8.649-06	0.234
4	1.13E-04	2.528	27.655	1.033E-05	0.317
5	1.13E-04	5.033	30.033	1.895E-05	0.542
6	0.0051	10.000	35.000	3.230-05	1.003
7	0.0051	7.081	30.401	2.471-05	0.801

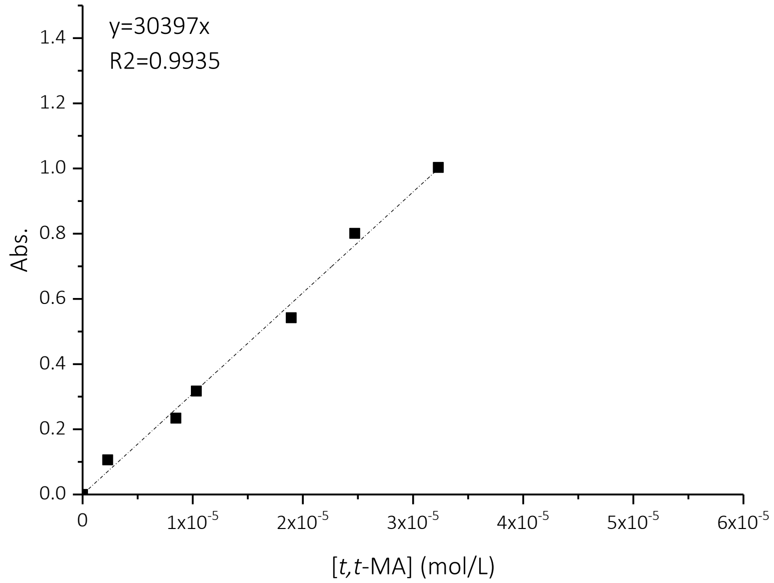

Figure 4-4: calibration of t,t-MA in water

A linear correlation was established until 1.003 value of absorbance. The calculated linear regression resulted is $Abs = 30937 \cdot [t,t - MA]$ with R^2= 0.9935. During the period of research different analysis calibrations were performed obtaining different linear regressions equations.

4.1.3 Ultraviolet-Visible analysis calibration for *t,t*-muconic acid in ethanol

The mother solution was prepared with a *t,t*-MA concentration equal to 2.272E-05 M using ethanol as solvent (GC analytical grade, Sigma Aldrich). Ethanol density was considered equal to 0.79 g/L.

Table 4-3: Calibration data of t,t-MA in ethanol

# STD	W mother solution (g)	W_{tot} (g)	$C_{t,t\text{-MA}}$ (M)	Abs_{264nm}
1	0.000	0.000	0.000E+00	0.000
2	-	-	2.272E-05	0.756
3	1.149	8.070	3.234E-06	0.154
4	1.995	3.984	1.138E-05	0.317
5	0.122	8.167	6.498E-06	0.542

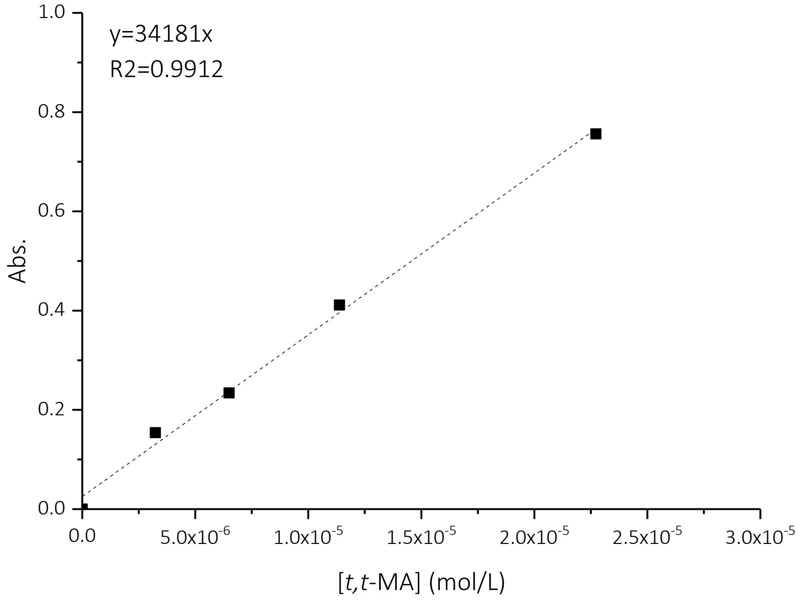

Figure 4-5: calibration of t,t-MA in ethanol

A linear correlation was established until 0.756 value of absorbance. The calculated linear regression resulted is $Abs = 34181 \cdot [t,t - MA]$ with R^2= 0.9912. During the period of research different analysis calibrations were performed obtaining different linear regressions equations.

4.2 Development and calibration of gas-chromatographic method (GC) using different columns and detectors for the evaluation of selectivity.

In general, the quantification of dicarboxylic acids is a critical challenge due to the low instrument sensitivity toward these compounds. Moreover, the separation of stereoisomers and chemical compounds that differ only for the presence or not of a double bond is not always a simple goal to achieve. On this way, the application of Fischer's esterification to dicarboxylic acid could increase the volatility of these chemicals during the GC analysis, allowing a good quantification and analysis reproducibility. For this reason, a Fischer's esterification was performed on each dicarboxylic acid. The general reaction scheme and the mechanism is reported in

Figure *4-6*. The Lewis or Brønstedt acid-catalyzed esterification of carboxylic acids with alcohols to give esters is a typical reaction in which the products and reactants are in equilibrium.

The equilibrium may be influenced by either removing one product from the reaction mixture (for example. removal of the water by azeotropic distillation or absorption by molecular sieves) or by employing an excess of one reactant. Addition of a proton (e.g.: p-TsOH. H_2SO_4) or a Lewis acid leads to a more reactive electrophile. Nucleophilic attack of the alcohol gives a tetrahedral intermediate in which there are two equivalent hydroxyl groups. One of these hydroxyl groups is eliminated after a proton shift (tautomerism) to give water and ester.

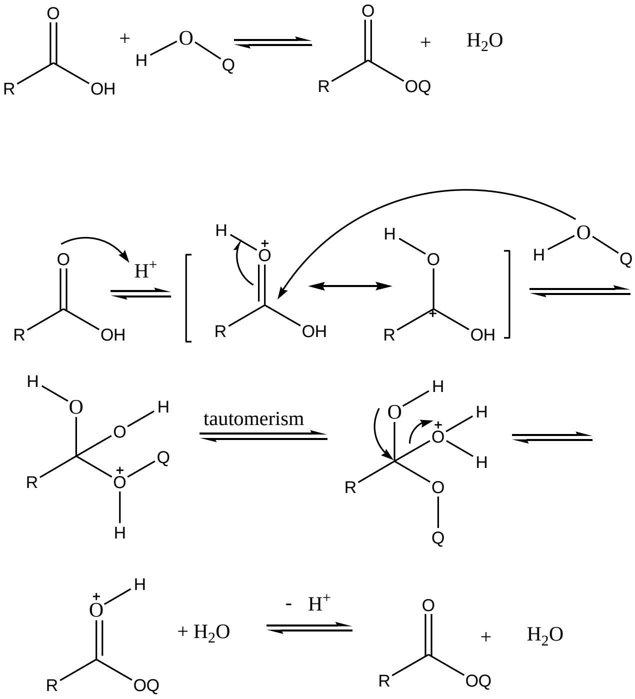

Figure 4-6: reaction scheme of Fischer's esterification

In the following paragraphs analysis calibration and analytical method validation is reported.

4.2.1 Analysis calibration using SUPELCOWAX 10 column

The analysis was calibrated using the dimethyl adipate (DMA) (Sigma Aldrich, >99.8%) and (3E)-hexenedioic dimethyl ester ((3E)HxDME) (Sigma Aldrich, 99%) were used as standard compound.
The instrument used for gas chromatographic analysis was "Master GC Fast Gas Chromatograph" (by Dani Instruments S.p.A) equipped with thermal conductivity detector (TCD). The sample (0.3 µL) was injected using a Hamilton syringe and subsequently vaporized at a temperature of 290 °C with a split ratio 1:3. Helium carrier flow was 15 mL/min. The chromatographic column used for the analysis was a SUPELCOWAX 10 (Sigma Aldrich) 60 meters long with a diameter of 0.53 mm and thickness of the inner coating film of 1 µm in PEG. The instrument operates in a temperature ramp starting from 60 °C. The temperature ramp was the following:
from 60 °C to 120 °C with a ramp of 18 °C/min;
from 120 °C to 160 °C with a ramp of 20 °C/min;
from 160 °C to 260 °C with a ramp of 15 °C/min;
isotherm at 260 °C for 1 minute.
Each analysis lasts 13 minutes.
The analysis was carried out using a TCD detector set at 240 °C.
A solution of butanol in methanol 0.035 (wt/wt) (Sigma Aldrich 99.9%) was used as internal standard.

4.2.1.1 Calibration of (3E)-hexenedioic dimethyl ester

0.259 g of (3E)-hexenedioic dimethyl ester ((3E)HxDME) were solubilized in 15.164 g of MeOH obtaining a solution with a weight ratio of 1.708E-02. The solution of the internal standard was prepared using 0.662 g of ButOH in 18.893 g of MeOH obtaining a solution with a weight ratio of 3.502E-02. Different solutions were then prepared for the calibration analyses using MeOH as solvent (Table 4-4). MeOH and ButOH density was considered 0.791 and 0.81 g/mL, respectively.

Table 4-4:calibration data of (3E)HxDME

# STD	$W_{sol.(3E)HxDME}$ (g)	$W_{sol.ButOH}$ (g)	W_{MeOH} (g)	$W_{totMeOH}$ (g)	$W_{(3E)HxDME}$ (g)	W_{ButOH} (g)
1	4.010	0.507	0.000	4.430	6.85E-02	1.77E-02
2	5.06E-01	1.007	6.022	7.490	8.64E-03	3.53E-02
3	1.531	0.508	2.005	4.000	2.61E-02	1.78E-02

The total amount of ButOH and (3E)HxDME was evaluated using the Eq.4-4

$$amount_i = W_{sol,i} \cdot weight\ ratio_i \qquad \text{(Eq.4-3)}$$

$$total\ amount\ of\ MeOH = W_{MeOH} + \sum W_{sol,i} - amount_i \qquad \text{(Eq.4-4)}$$

where:

amount$_i$ *(g)* = amount of (3E)HxDME or ButOH;

$W_{sol,i}$ (g)= amount of the mother solution used for the sample preparation;

Weight ratio$_i$ = 1.708E-02 and 3.502E-02 for (3E)HxDME and ButOH, respectively;

total amount of MeOH (g)= total weight of MeOH contained in the sample;

W_{MeOH} *(g)* = MeOH added for the sample preparation.

Table 4-5:chromatographic results for (3E)HxDME calibration

# STD	A_{ButoOH}	$A_{(3E)HxDME}$	$A_{(3E)HxDME}/A_{ButoOH}$
1	18.068	56.731	3.139
	20.666	67.518	3.267
	20.336	65.514	3.221
		average	3.203
2	23.718	4.731	0.199
	22.947	4.652	0.202
	23.699	4.834	0.204
		average	0.202
3	21.424	27.379	1.278
	22.16	26.334	1.188
	20.183	25.8	1.278
		average	1.248

Table 4-6: results for (3E)HxDME calibration

# STD	$A_{(3E)HxDME}/A_{ButoOH}$	$C_{(3E)HxDME}$ (mol/L)	C_{MeOH} (mol/L)	$C_{(3E)HxDME}/C_{ButoOH}$
1	3.203	7.07E-02	4.26E-02	1.66
2	0.202	5.27E-03	5.00E-02	1.05E-01
3	1.248	2.99E-02	4.73E-02	0.63

The concentration of (3E)HxDME was evaluated using the Eq.4-5

$$C_{(3E)HxDME} = \frac{\frac{W_{(3E)HxDME}}{MW_{HxDME}} \cdot 1000(\frac{mL}{L})}{\frac{W_{MeOH}}{\rho_{MeOH}} + \frac{W_{ButOH}}{\rho_{ButOH}}} \quad \text{(Eq.4-5)}$$

where:

$W_{(3E)HxDME}$ (g) = amount of (3E)HxDME calculated with Eq.3;

$MW_{(3E)HxDME}$ (g/mol) = 172.18;

W_{MeOH} (g) = amount of MeOH calculated with Eq.4;

MW_{ButOH} (g/mol) = 74.12;

ρ_{MeOH} (g/mL) = density of methanol;

ρ_{MeOH} (g/mL) = density of butanol;

A= chromatographic area.

An analogue equation was used to evaluate ButOH concentration.

The calibration curve obtained is reported in Figure 4-7.

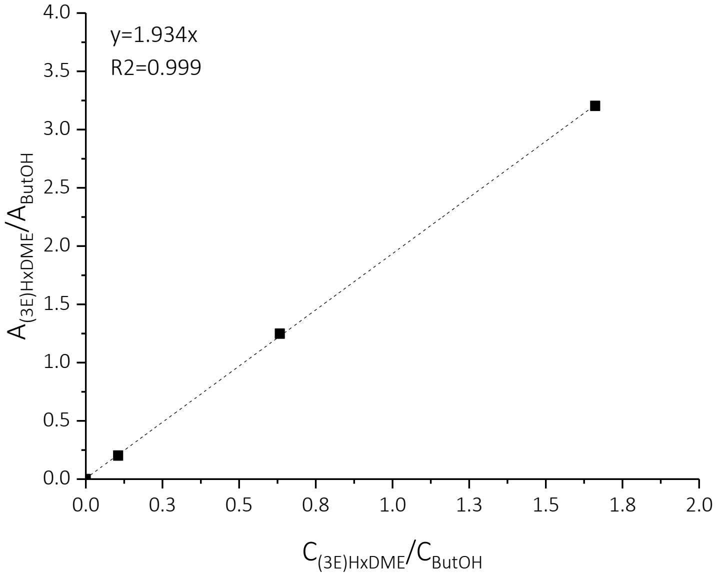

Figure 4-7: calibration of (3E)HxDME

A linear correlation was established. The calculated linear regression equation is $A_{(3E)HxDME} / A_{ButOH} = 1.934 \cdot C_{(3E)HxDME} / C_{ButOH}$ with R^2=0.999. During the period of research different analysis calibrations were performed obtaining different linear regressions equations.

4.2.1.2 Calibration of dimethyl adipate

0.363 g of dimethyl adipate (DMA) were solubilized in 20.295 g of MeOH obtaining a solution with a weight ratio of 1.787E-02. The solution of the internal standard was prepared using 0.662 g of ButOH in 18.893 g of MeOH obtaining a solution with a weight ratio of 3.502E-02. Different solutions were then prepared for the calibration analyses using MeOH as solvent (Table 4-7) MeOH and ButOH density was considered 0.791 and 0.81 g/mL, respectively.

The calibration obtained using the same equations reported in the previous paragraph is reported below.

Table 4-7: sample preparation for DMA calibration

# STD	$W_{sol.DMA}$ **(g)**	$W_{sol.ButOH}$ **(g)**	W_{MeOH} **(g)**	$W_{tot.MeOH}$ **(g)**	W_{DMA} **(g)**	W_{ButOH} **(g)**
1	4.006	0.507	0.000	4.422	7.159E-02	1.770E-02
2	0.501	1.001	6.002	7.459	8.941E-03	3.506E-02
3	1.506	0.505	2.012	3.978	2.691E-02	1.767E-02

Table 4-8: chromatographic results for DMA calibration

# STD	A_{ButoOH}	A_{DMA}	$A_{(DMA}$ /A_{ButoOH}
1	18.280	72.797	3.982
	19.787	76.112	3.847
	16.325	58.333	3.573
		average	3.801
2	23.105	5.725	0.247
	22.563	5.661	0.250
	20.572	5.08	0.246
		average	0.249
3	20.272	29.754	1.467
	17.731	26.818	1.512
	21.167	31.249	1.476
		average	1.485

Table 4-9: results for DMA calibration

A_{DMA}/A_{ButOH}	C_{DMA} (mol/L)	C_{ButOH} (mol/L)	C_{DMA}/C_{ButOH}
3.802	7.245E-02	4.211E-02	1.721
0.2481	5.412E-02	4.991E-02	0.108
1.495	3.042E-02	4.703E-02	0.648

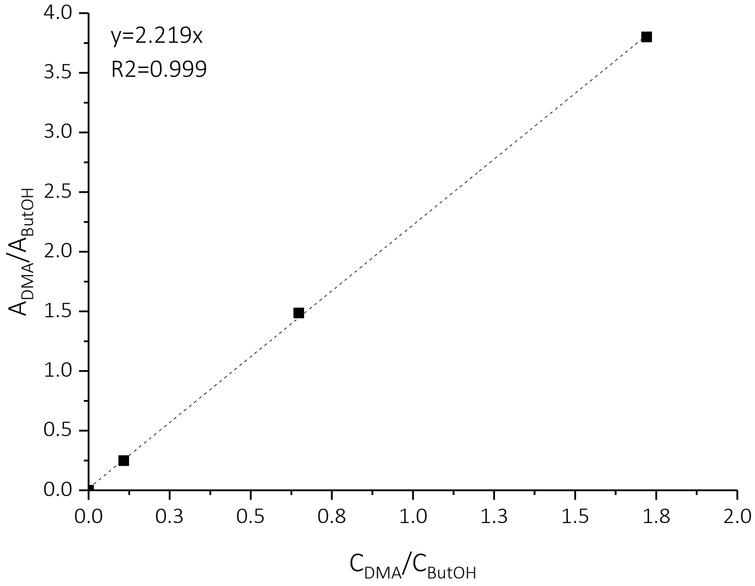

Figure 4-8: calibration of DMA

A linear correlation was established. The calculated linear regression equation is $A_{DMA}\ /A_{ButOH} = 2.219 \cdot C_{DMA}\ /C_{ButOH}$ with R^2= 0.999. During the period of research different analysis calibrations were performed obtaining different linear regressions equations.

4.2.2 Analysis calibration using SP-2380 column

SP-2380 (Sigma Aldrich) column is a highly polar cyan-siloxane column commonly used for separation of geometric (*cis/trans*) fatty acid methyl ester (FAME) isomers as a group. The stationary phase is stabilized with poly (90% biscyanopropyl/10% cyanopropyl-phenyl siloxane). The possibility to work in isotherm analysis to separate geometric isomers allowed performing several analyses in short period time. A SP®-2380 Capillary GC Column L × I.D. 60 m × 0.25 mm, film thickness 0.20 µm column was used during the last year of the research work.

We decided to use FID detector due to its higher sensibility compared with the TCD one.

Dimethyl glutarate (>99%, Fluka) was used as internal standard allowing the quantification of the different products.

The analysis was performed setting the following parameters:

- Oven temperature: 180 °C (isothermal condition);
- Injector temperature= 220 °C;
- Injector He gas flow= 1.8 mL/min;
- Split= 90;
- Detector temperature: 220 °C;

- Detector He flow= 43 mL/min;
- Detector air flow= 310 mL/min;
- Detector H_2 flow= 38 mL/min;
- Injection volume= 1.5 µL;
- Time of analysis= 8 min.

4.2.2.1 Calibration of (2E)hexenedioic dimethyl ester

The calibration of (2E)hexenedioic acid ((2E)HxDME) was performed using a standard purchase from Sigma Aldrich (purity >99.9%).

0.0329 g of (2E)hexenedioic acid ((2E)HxDME) were solubilized in 11.256 g (14.23 mL) of MeOH. (2E)HxDME concentration is equal to 1.34E-05 M. It is useless to prepare concentrated solution because the amount of the compound in the reaction mixture is very low. DMG and (2E)HxDME molecular weight is equal to 160.17 g/mol and 172.18 g/mol, respectively, while MeOH density was considered equal to 0.791 g/mL. The density of the mother solution was considered equal to the density of MeOH.

Different standard solutions were prepared starting from the mother solution and then analyzed by GC-FID analysis. The results are reported in the following tables.

Table 4-10: sample preparation for (2E)HxDME calibration (SP-2380 column)

#STD	DMG (g)	(2E)HxDME $_{mother\_solution}$ (g)	(2E)HxDME $_{mother\_solution}$ (mL)	DMG (mol)	(2E)HxDME (mol)	A_{DMG}	$A_{(2E)HxDME}$
1	3.80E-02	9.85E-01	1.245	2.37E-04	1.67E-05	798.18	129.149
						1270.60	205.151
						1135.6	187.523
2	4.04E-02	1.63E+00	2.055	2.52E-04	2.76E-05	445.906	107.291
						437.661	110.002
						602.327	149.909
3	4.02E-02	2.32E+00	2.934	2.51E-04	3.94E-05	376.665	134.445
						252.659	82.565
						494.279	179.431

Table 4-11:chromatographic results for (2E)HxDME calibration (SP-2380 column)

A_{DMG}	$A_{(2E)HxDME}$	$A_{(2E)HxDME}$ /A_{ButOH}	mol$_{(2E)HxDME}$/molDMG
798.18	129.149	0.162	0.0705
1270.60	205.151	0.161	
1135.6	187.523	0.165	
	average	0.162	
445.906	107.291	0.241	0.109
437.661	110.002	0.251	
602.327	149.909	0.249	
	average	0.246	
376.665	134.445	0.357	0.157
252.659	82.565	0.327	
494.279	179.431	0.363	
	average	0.348	

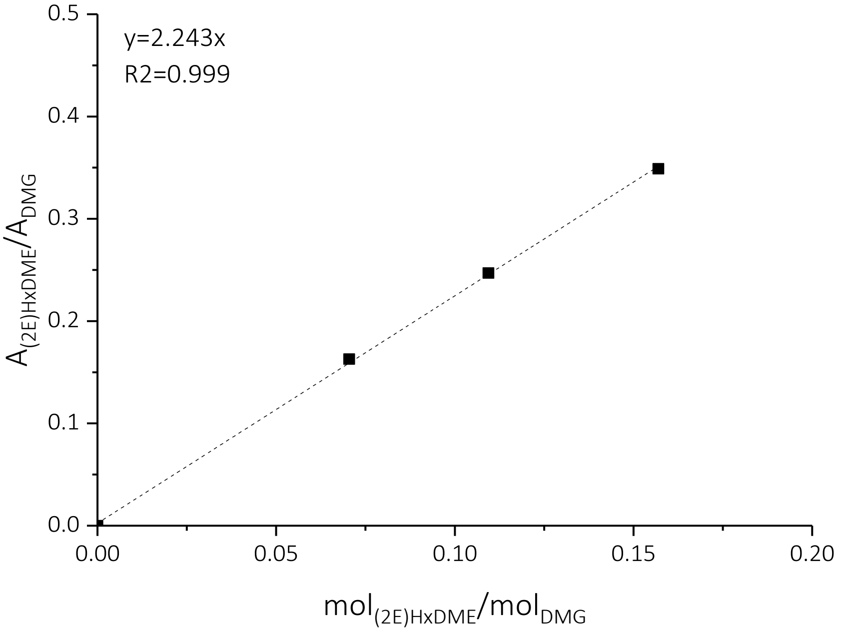

Figure 4-9: calibration of (2E)HxDME (SP-2380 column)

A linear correlation was established. The calculated linear regression equation is $A_{(2E)HxDME}$ / $A_{DMG} = 2.243 \cdot mol_{(2E)HxDME}\ /mol_{DMG}$ with R^2= 0.999. During the period of research different analysis calibrations were performed obtaining different linear regressions equations.

4.2.2.2 Calibration of (3E)hexenedioic dimethyl ester

The calibration of (3E)hexenedioic acid ((3E)HxDME) was performed using a standard purchase from Sigma Aldrich (purity >99.9%).

0.223 g of (3E)hexenedioic acid ((3E)HxDME) were solubilized in 5.00 mL of MeOH. (3E)HxDME concentration is equal to 0.258 M. DMG and (3E)HxDME molecular weight is equal to 160.17 g/mol and 172.18 g/mol, respectively, while MeOH density was considered equal to 0.791 g/mL. The density of the mother solution was considered equal to the density of MeOH.

Different standard solutions were prepared starting from the mother solution and then analyzed by GC-FID analysis. The results are reported in the following tables.

Table 4-12: sample preparation and chromatographic results for (3E)HxDME calibration (SP-2380 column)

#STD	DMG (g)	(3E)HxDME $_{mother\_solution}$ (μL)	MeOH (μL)	DMG (mol)	(3E)HxDME (mol)	A_{DMG}	$A_{(3E)HxDME}$
1	2.08E-02	170	430	1.29E-04	4.39-05	1627.342	492.988
						1197.833	361.656
						807.015	223.315
2	1.51E-02	200	400	9.42E-05	5.16E-05	886.641	420.343
						1118.37	561.842
						14871.53	7324.091
3	1.03E-02	140	460	6.43E-05	3.61E-05	4852.977	2449.083
						3055.243	1567.744
						3262.192	1723.621
4	1.19E-02	302	200	7.43E-05	9.83E-06	390.345	46.765
						277.731	33.461
						101.714	11.342
5	1.39E-02	570	350	8.67E-05	1.86E-05	59.764	8.707
						54.983	9.815
						62.057	12.227

Table 4-13: results for (3E)HxDME calibration (SP-2380 column)

$A_{(3E)HxDME}/A_{ButOH}$		$mol_{(3E)HxDME}/molDMG$
	0.303	0.338
	0.302	
	0.278	
average	0.294	
	0.474	0.547
	0.502	
	0.492	
average	0.489	
	0.505	0.562
	0.513	
	0.528	
average	0.515	
	0.119	0.132
	0.120	
	0.111	
average	0.117	
	0.146	0.214
	0.178	
	0.197	
average	0.173	

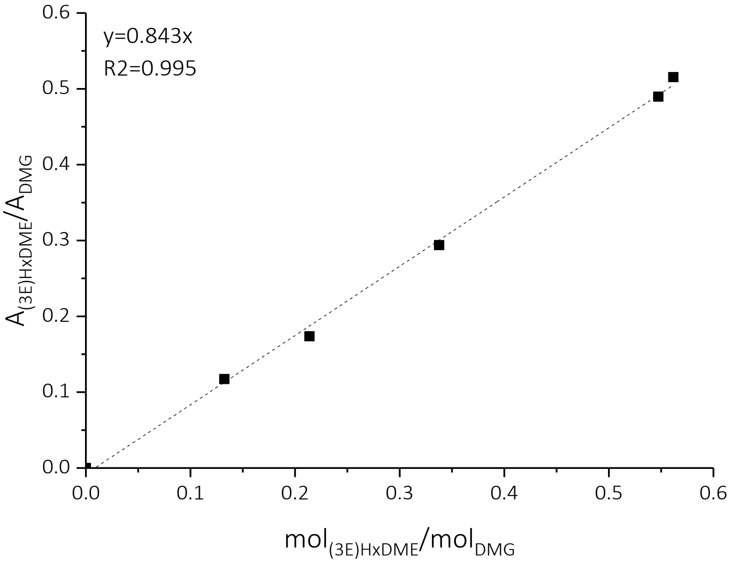

Figure 4-10: calibration of (3E)HxDME (SP-2380 column)

A linear correlation was established. The calculated linear regression equation is $A_{(3E)HxDME} / A_{DMG} = 0.843 \cdot mol_{(3E)HxDME} / mol_{DMG}$ with R^2= 0.995. During the period of research different analysis calibrations were performed obtaining different linear regressions equations.

4.2.2.3 Calibration of dimethyl adipate

The calibration of dimethyl adipate (DMA) was performed using a standard purchase from Sigma Aldrich (purity >99.9%) dissolved in MeOH

DMG and DMA molecular weight is equal to 160.17 g/mol and 174.19 g/mol, respectively. Different standard solutions were prepared and then analyzed by GC-FID analysis. The results are reported in the following tables.

Table 4-14: samples preparation and chromatographic results for DMA calibration (SP-2380 column)

#STD	DMG (g)	DMA (g)	MeOH (g)	DMG (mol)	DMA (mol)	A_{DMG}	A_{DMA}
1	0.079	0.147	0.698	4.98E-04	8.45E-04	137.75	292.84
						321.73	687.05
						136.24	293.71
2	0.045	0.100	0.644	2.82E-04	5.76E-04	231.48	562.57
						481.87	1179.65
						1026.43	2533.73
3	0.074	0.098	1.00	4.60E-04	5.65E-04	637.55	956.20
						611.02	915.68
						493.70	725.97
4	0.093	0.082	1.31	5.83E-04	4.71E-04	1411.03	1409.62
						542.82	535.89
						630.66	613.88
5	0.075	0.045	0.879	4.71E-04	2.64E-04	715.04	484.34
						1354.94	941.849
						1758.70	1219.6

Table 4-15: results for DMA calibration (SP-2380 column)

mol_{DMA}/mol_{DMG}		A_{DMA}/A_{DMG}
1.698		2.126
		2.136
		2.156
	average	2.139
2.0449		2.430
		2.448
		2.468
	average	2.449
1.229		1.500
		1.499
		1.470
	average	1.490
0.8072		0.999
		0.987
		0.973
	average	0.986
0.5597		0.677
		0.695
		0.693
	average	0.689

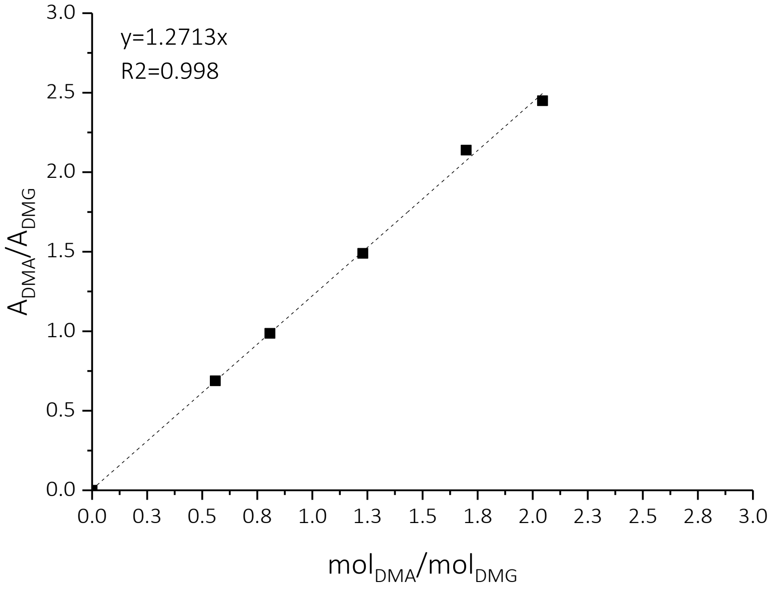

Figure 4-11: calibration of DMA (SP-2380 column)

A linear correlation was established. The calculated linear regression equation is $A_{DMA}\ /A_{DMG} = 1.2713 \cdot mol_{DMA}\ /mol_{DMG}$ with R^2=0.998. During the period of research different analysis calibrations were performed obtaining different linear regressions equations.

4.3 Application of the developed analytical method

The application of this analytical method involves many different passages and the possibility to loss material during the steps is tangible. For this reason, the material balance evaluation is mandatory to verify the concrete possibility to use this analytical method. Due to the equilibrium reaction of Fischer's reaction, an optimization of the esterification was required to correctly evaluate the selectivity. In the next paragraphs the application of the developed analytical method, its optimization and material balance calculation are described.

4.3.1 Data elaboration

4.3.1.1 Evaluation of the conversion through UV-Vis analysis

After the end of the reaction 1 g of the reacted mixture is used for the UV analysis sample preparation. Two or three dilutions are necessary to read an absorbance below 1. The samples are prepared weighting the reacted mixture and water (or ethanol).

1 g of sample collected from the reaction is diluted in 3 g of water (1st dilution). Then from this sample 1 g is withdrawn and added to 24 g of water (2nd dilution). Finally, from the 2nd dilution 1 g is withdrawn and added to 24 g of water (3rd dilution). The third sample is then analyzed using UV-Vis instrument performing the analysis from 500 to 190 nm. Distilled water (or ethanol) was used as blank. The value of absorbance is kept at 264 nm (maximum of the absorbance).

An example of UV-Vis analysis is reported below.

- 1st dilution: 1.022 g of reacted mixture in 3.231 g of distilled water;
- 2nd dilution: 1.039 g of 1st dilution sample in 25.092 g of distilled water;
- 3rd dilution: 1.070 g of 2nd dilution sample in 25.071 g of distilled water.

3 ml of the 3rd dilution sample was introduced in a quartz cuvette and the absorbance was recorded. Sample density was considered equal to 1 g/ml.

Table 4-16:diluition table for UV-Vis sample preparation

1st dilution (sample 0)		2nd dilution (sample 1)		3rd dilution (sample2)			
Reacted mixture (g)	Water$_1$ (g)	1stdil. sample (g)	Water$_2$ (g)	2nddil. sample (g)	Water$_3$ (g)	[sample2] (M)	Abs. 264nm
1.022	3.231	1.039	25.092	1.070	25.071	3.763E-06	0.116
w$_{1tot\ (g)}$=	4.253	w$_{2tot}$=	26.131	w$_{3tot}$=	26.141		

$$[sample0] = [sample2] \cdot \frac{w_{tot3}}{2^{nd} dil. sample} \cdot \frac{w_{tot2}}{1^{st} dil. sample} \cdot \frac{w_{tot1}}{reacted\ mixture} \cdot \qquad \text{(Eq.4-6)}$$

$$[sample2] = \frac{Abs.}{angular\ coeff. calibration} \qquad \text{(Eq.4-7)}$$

$$MA\ Conversion\ _i(\%) = \frac{C_i^{in} - [sample0]}{C_i^{in}} \cdot 100 \qquad \text{(Eq.4-8)}$$

where:

Abs.= the absorbance of the sample2 at 642nm;

C_i^{in} (mol/L)= MA starting concentration of the solution used for the reaction;

[sample0] (mol/L)= MA concentration of the reacted solution.

4.3.1.2 Sample preparation for Fischer's esterification

After the hydrogenation reaction (see next chapter) the reacted solution is filtered to eliminate the catalyst. The solution is filtered within a test tube. The solution is then dried in oven at 70 °C for 2 days and then Fischer's esterification is directly performed within the tube. Knowing the amount of the dried sample, H_2SO_4 98% (catalytic amount_30 µL + amount to acidified sodium muconate) and MeOH (in large excess) was added in the tube. Fischer's esterification was performed in the oven at 70 °C for 48 h. Finally, the sample is cooled and, after the addition of the internal standard, is analyzed by GC method.

An example of the evaluation of the amount of H_2SO_4 and MeOH to use during the esterification reaction is reported below.

Dried powder recovered= 0.086 g

$$H_2SO_{4\,neutr.} = \frac{dried\ powder\ (g) * MW_{H_2SO_4} \cdot 0.98}{MW_{Na-muc} \cdot \rho_{H_2SO_4}} = 2.39 \cdot 10^{-2} \qquad \text{(Eq.4-9)}$$

where:

$H_2SO_{4\,neutrl}$ (mL) = is the amount of sulphuric acid required to acidify sodium muconate;

MW_{H2SO4} (g/mol)= 98.08;

$MW_{Na\text{-}muc}$ (g/mol)= 188.1;

ρ_{H2SO4} (g/mL)= 1.84.

Therefore, the total amount of H_2SO_4 is equal to the sum of the acid necessary to neutralize sodium muconate and the catalytic amount required for the reaction. In this case the total amount is equal to 53.9 µL.

Methanol amount is instead evaluated as reported below.

Considering methanol/muconic acid ratio (mL/g) equal to 73, the amount of MeOH required for the esterification reaction is

$$MeOH = \frac{dried\ powder \cdot MW_{MA} \cdot MeOH/MA\ ratio}{MW_{Na-muc}} = 5.8 \qquad \text{(Eq.4-10)}$$

where:

MW_{MA} (g/mol)= 142.1;

MeOH/MA ratio= 73 (mL_{MeOH}/g_{MA}).

4.3.1.3 Gas chromatographic analysis with SUPELCOWAX-10 column

After esterification reaction the sample is ready for gas chromatographic analysis. In the case of SUPELCOWAX-10 column a solution of butanol (ButOH) (Sigma Aldrich, analytical grade) in methanol was used as internal standard. Sample preparation and data elaboration are reported below.

Internal standard solution (STD) was prepared weighting 0.713 g of ButOH and 18.019 g of MeOH. The weight ratio ButOH/MeOH is equal to 3.955E-02.

Therefore, 1.026 g of standard solution were added to the cool esterified sample.

STD (g)	**ButOH (g)**	**ButOH (mol)**
1.026	4.056E-02	5.472E-04

ButOH (g) was calculated knowing the ButOH/MeOH ratio:

$$ButOH(g) = STD\ (g) \cdot \left(\frac{ButOH}{MeOH}\right)_{ratio} \tag{Eq.4-11}$$

while ButOH (mol) was simply derived dividing ButOH (g) for the molecular weight of ButOH (74.12 g/mol)

GC analysis was performed injecting the sample three times to control data reproducibility and minimize analysis error. A are the chromatographic areas.

Table 4-17: results of GC analysis

	Rt= 3.5 min	Rt= 8.5 min	
#	A_{ButOH}	A_{DMA}	A_{DMA}/A_{ButOH}
1	173.259	24.254	0.140
2	180.560	25.610	0.141
3	178.908	24.987	0.139
		average	0.140

	Rt= 3.5 min	Rt= 9.1 min	
#	A_{ButOH}	$A_{(2Z)HxDME}$	$A_{(2Z)HxDME}/A_{ButOH}$
1	173.259	0.000	0.000
2	180.560	0 .000	0.000
3	178.908	0.000	0.000
		average	0.000

	Rt= 3.5 min	Rt= 9.3 min	
#	A_{ButOH}	$A_{(2E)HxDME}$	$A_{(2E)HxDME}/A_{ButOH}$
1	173.259	3.242	0.019
2	180.560	4.031	0.022
3	178.908	3.656	0.020
		average	0.020

	Rt= 3.5 min	Rt= 9.7 min	
#	A_{ButOH}	A_{DMM}	A_{DMM}/A_{ButOH}
1	173.259	9.210	0.053
2	180.560	10.021	0.055
3	178.908	9.765	0.054
		average	0.054

GC analysis is able to separate DMM, but this compound is not completely soluble in methanol at room temperature. During the cooling down process DMM precipitated is clearly visible on the bottom of the tube. For this reason, a good quantification is only possible using UV-Vis analysis.

After the collection of the chromatographic areas is possible to evaluate the selectivity of the reaction. Due to the lack of (2Z)HxDME standard, the evaluation of the selectivity toward this compound was performed using the same response factor of the (2Z)HxDME compound.

Using the calibration, it was possible to calculate the molar ratio between the compound and the internal standard.

In general, the molar ratio is evaluated with the following equation

$$mol_i\ /mol_{ButOH} = \frac{A\ /A_{ButOH}}{response\ factor} \qquad \text{(Eq.4-12)}$$

where the response factor is the angular coefficient of the calibrations.

mol_{DMA}/mol_{ButOH}	$mol_{(2Z)HxDME}\ /mol_{ButOH}$	$mol_{(2E)HxDME}\ /mol_{ButOH}$
6.307E-02	0.000	9.675E-03

The evaluation of the mole for each compound was performed using the following equation:

$$mol_i = mol_i\ /mol_{ButOH}\ \cdot\ mol_{ButOH} \qquad \text{(Eq.4-13)}$$

DMA (mol)	(2Z)HxDME (mol)	(2E)HxDME (mol)
3.451E-05	0.000	5.295E-06

Finally, the selectivity of each compound was evaluated using Eq.14

$$Selectivity_n\ (\%) = \frac{mol_n}{\sum mol_i + mol_n} \cdot 100 \qquad \text{(Eq.4-14)}$$

where:

$Selectivity_n$ =is the selectivity of the n compound;

mol_n= is the number of moles of the considered reaction product;

$\sum mol_i$=is the sum of the moles of all the other reaction products.

Sel_{DMA} (%)	$Sel_{(2Z)HxDME}$ (%)	$Sel_{(2E)HxDME}$ (%)
86.70	0.00	13.30

4.3.1.4 Gas chromatographic analysis with SP-2380 column

In the case of SP-2380 column pure dimethylglutarate (DMG) (Sigma Aldrich, analytical grade) was used as internal standard. 0.031 g of DMG were weighted in the cool sample and then the sample was analyzed.

In this case the DMG moles were directly evaluated using the amount of DMG weighted and dividing it for its molecular weight (160.17 g/mol).

The elaboration of the obtained data is described in the previous section.

4.3.2 Optimization of the Fischer's esterification reaction

To verify the complete reaction of the acids into the correspondent dimethyl ester, (3E)-hexenedioic acid (Sigma Aldrich 98%) and AdA (Sigma Aldrich 99.8%) were esterified and the state of conversion was compared using a simple GC calibration performed on dimethyl (3E)-3-hexenedioate and AdA.

0.012 g of (3E)-hexenedioic acid and AdA were esterified in two different 2 necks bottom flasks using 15 ml of pure methanol (Sigma Aldrich, anhydrous 99.8%). A catalytic amount of H_2SO_4 (30 µL) (Sigma Aldrich, 98%) was then added and the reaction was heated in an oil bath at 70 °C. Different samples were collected at different reaction times to verify the conversion.

The conversion was evaluated using the following equation:

$$Conversion\ _i(\%) = \frac{mol_i^{in} - mol_i^{end}}{mol_i^{in}} \cdot 100 \qquad \text{(Eq.4-15)}$$

where:

mol_i^{in}= starting moles of the specie *i*;

mol_i^{end}= number of moles of the specie *i*.

GC sample was prepared as described in section 4.3.1.2.

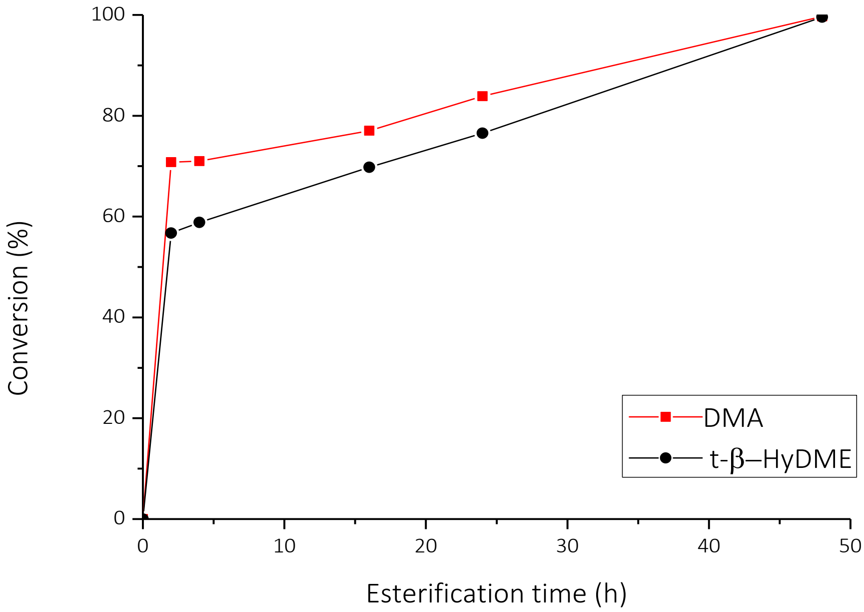

Figure 4-12:evaluation of the DMA and (3E)HxDME formation during esterification reaction

As reported in Figure 4-12. a full conversion of acids into their respective esters is achieved after 48 h of reaction. Therefore 2 days of reaction are mandatory to have an accurate selectivity evaluation.

4.3.3 Influence of Fischer esterification on stereoisomers

Before proceeding to develop the suitable GC analytical method the study of the influence of Fischer's reaction on the stereoisomers is mandatory. In fact, if the esterification causes any transformation of the stereocenter, the reaction products, quantification and the study of the reaction pathway could be invalidated. Different esterification reactions have been performed and analyzed using GC-TCD technique and SUPELCOWAX column. As reported in Figure 4-13 the esterification reaction does not convert any stereoisomer, therefore the analytical method developed is releasable.

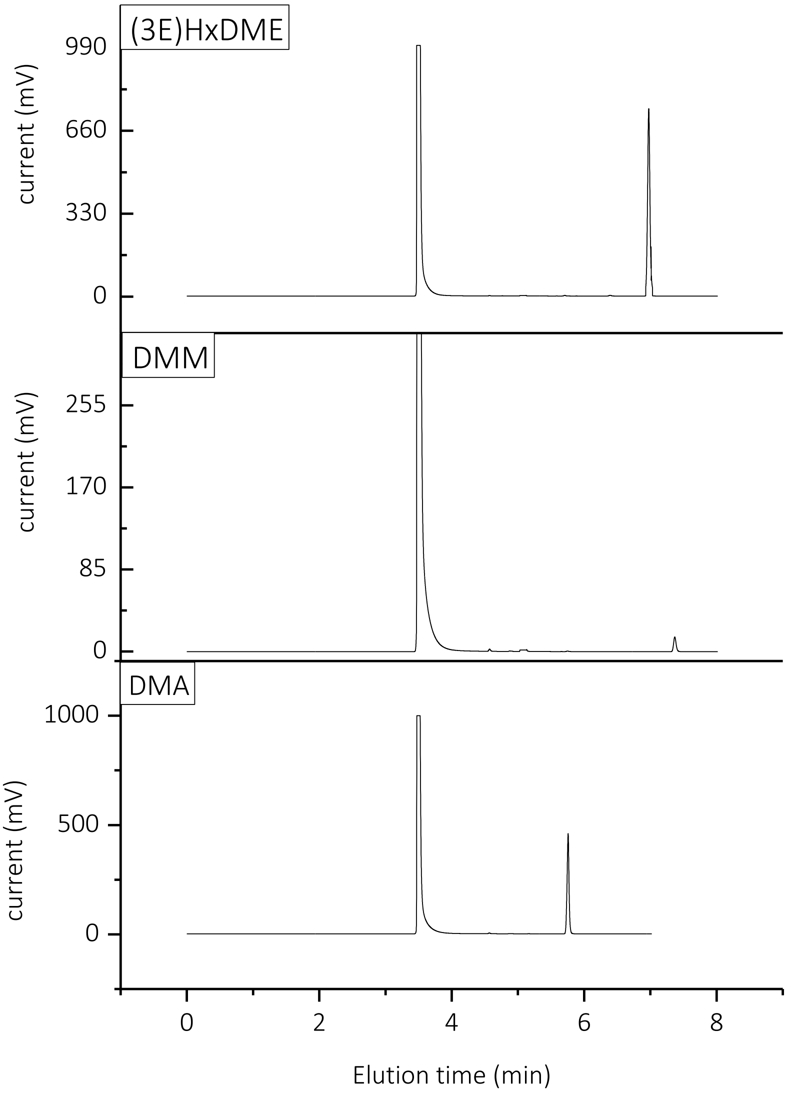

Figure 4-13: chromatogram of esterified t,t-MA, AdA and (3E)-hexenedioic acid for isomerization evaluation

4.3.4 Stereoisomer separation: set up of the chromatographic parameter for SUPELCOWAX column

The separation of stereoisomers is the real bottleneck of this analytical method. Setting a correct gas flow and using proper temperature ramps it is possible to separate compound that are very similar. An appropriate temperature ramp was set (Figure 4-14) and in this way the analysis is able to correctly separate the monounsaturated compound (in Z and E configuration) from AdA and MA.

The analysis is performed using the following parameters:

- Injector temperature: 290 °C;
- Split mode= 1:3;
- Gas carrier: Helium 15 mL/min;
- Column: SUPELCOWAX 10 (Length 60m; diameter 0.53mm; film thickness 1 µm);
- Temperature ramp (starting temperature= 60 °C):
    - from 60 °C to 120 °C with a ramp of 18 °C/min;
    - from 120 °C to 160 °C with a ramp of 20 °C/min;
    - from 160 °C to 260 °C with a ramp of 15 °C/min;
    - isotherm at 260 °C for 1 minute;
- TCD temperature: 240 °C.

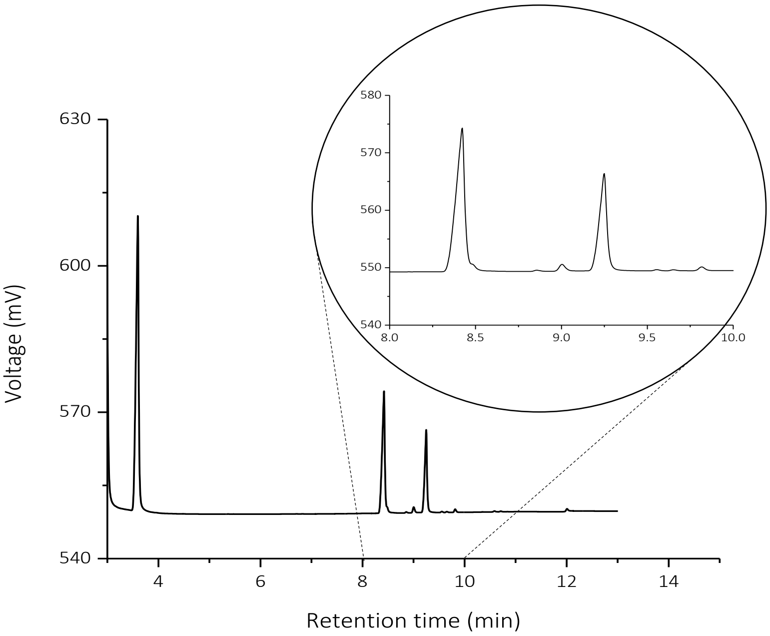

Figure 4-14: chromatographic separation of DMA, DMM and (3E)HxDME

A solution of butanol in methanol was used as internal standard (the detailed description is reported in section 4.4.1.3). In Figure 4-14 the separation of DMA, DMM, and (3E)HxDME compounds is reported

In Table 4-18 the retention times for each compound are reported.

Table 4-18: retention times for SUPELCOWAX 10 column

Compound	Retention time (min)
Butanol	3.86
DMA	8.46
DMHy	8.95
DMHy cis	9.09
DMHy trans	9.32
DMM	9.80

4.3.5 Stereoisomer separation: set up of the chromatographic parameter for SP-2380 column

SP-2380 column is strictly designed for the separation of methyl esters and the respective isomers. Due to this particular feature an isothermal analysis is sufficient to well separate the compounds, allowing to minimize analysis time.

The analysis was performed setting the following parameters:

- Oven temperature: 180 °C (isothermal condition);
- Injector temperature= 220 °C;
- Injector He gas flow= 1.8 mL/min;
- Split= 90;
- Detector temperature: 220 °C;
- Detector He flow= 43 mL/min;
- Detector air flow= 310 ml/min;
- Detector H_2 flow= 38 mL/min;
- Injection volume= 1.5 µL;
- Time of analysis= 8 min.

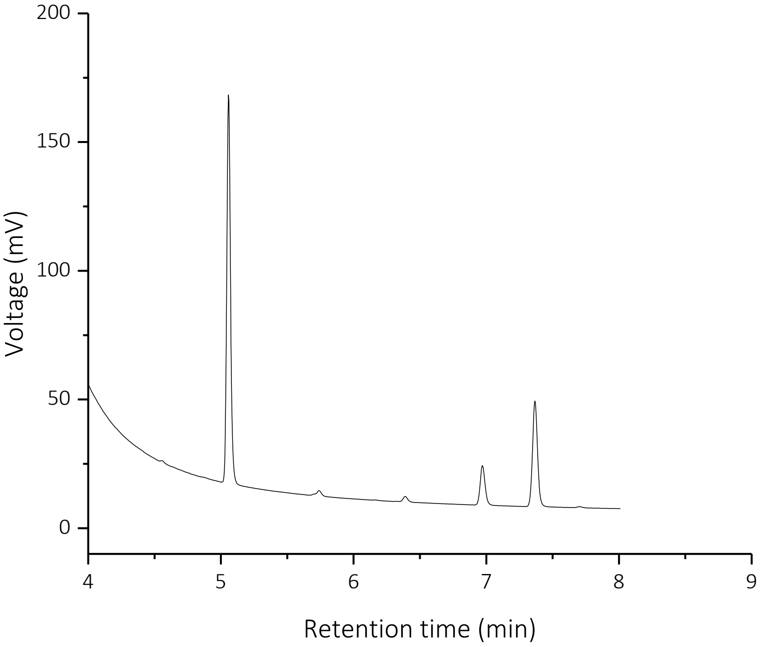

Figure 4-15: chromatogram from SP 2380 column

Table 4-19: retention time using SP 2380 column

Compound	Retention time (min)
DMG	5.06
DMA	5.74
(3E)HxDME	6.40
(2E)HxDME	6.97
ttDMM	7.36
ccDMM	7.70

4.3.6 Material balance

An analytical method can be considered robust and valid if all the operative steps and the analyses are sufficiently accurate, and if it remains unaffected by small, but deliberate variations in method parameters. In this sense the material balance can help to establish if all the steps performed before analyzing the sample, and the results of the analyses are adequately precise for this kind of evaluation. In the following table an example of material balance is reported. The material balance was performed on two different reactions and at different reaction time.

Table 4-20: mass balance evaluation

V (mL)	MA_{in} (mol)	$V_{UV\text{-}Vis}$ (g)	Conv (%)	MA_{cuv} (mol)	Residue (g)	MA_{res} (g)	S_{int} (%)	S_{AdA} (%)	int+AdA (g)	Int (g)	AdA (g)	Out (mol)	Mass balance (%)
10.78	7.51E-04	1.12E+00	30.50	7.77E-05	9.34E-02	6.49E-02	50.04	49.96	2.85E-02	1.43E-02	1.42E-02	7.31E-04	97.35
10.64	7.40E-04	9.80E-01	87.90	6.82E-05	9.32E-02	1.13E-02	8.64	91.36	8.19E-02	7.08E-03	7.48E-02	7.09E-04	95.74
10.60	7.38E-04	1.46E+00	89.50	1.02E-04	9.35E-02	9.82E-03	23.37	76.63	8.37E-02	1.96E-02	6.41E-02	7.45E-04	101.01
10.32	7.18E-04	1.21E+00	49.90	8.41E-05	9.12E-02	4.57E-02	41.02	58.98	4.55E-02	1.87E-02	2.68E-02	7.19E-04	100.06
10.69	8.40E-04	1.36E+00	18.90	1.07E-04	9.98E-02	8.09E-02	73.45	26.55	1.89E-02	1.39E-02	5.01E-03	8.06E-04	95.97
10.08	7.92E-04	9.36E-01	38.90	7.36E-05	9.82E-02	6.00E-02	70.84	29.16	3.82E-02	2.71E-02	1.11E-02	7.60E-04	95.93
13.46	1.06E-03	1.04E+00	14.9	8.14E-05	1.37E-01	1.16E-01	66.81	33.19	2.04E-02	1.36E-02	6.76E-03	1.04E-03	98.28
10.42	8.19E-04	9.29E-01	79.10	7.30E-05	1.05E-01	2.19E-02	49.42	50.58	8.31E-02	4.10E-02	4.20E-02	8.00E-04	97.60
9.90	7.78E-04	1.08E+00	98.30	8.49E-05	9.93E-02	1.69E-03	21.11	78.89	9.76E-02	2.06E-02	7.70E-02	7.67E-04	98.52
10.86	8.54E-04	9.53E-01	97.50	7.49E-05	1.09E-01	2.74E-03	10.63	89.37	1.07E-01	1.13E-02	9.53E-02	8.25E-04	96.63
10.49	8.25E-04	1.19E+00	100.00	9.34E-05	1.04E-01	0.00E+00	0.00	100	1.04E-01	0.00E+00	1.04E-01	8.07E-04	97.85

where:

V *(mL)*= volume used during the reaction;

MA_{in} *(mol)*= starting amount of muconic acid (or sodium muconate) used for the reaction;

$V_{UV\text{-}Vis}$ *(mL)*= volume of the reacted mixture used for the UV-Vis analysis;

Conv *(%)*= MA or (Na-Muc) conversion evaluated through UV-Vis analysis (using Eq.4-8);

MA_{cuv} *(mol)*= amount of muconic acid within the $V_{UV\text{-}Vis}$;

Residue *(g)*= amount of dried reacted mixture;

MA_{res} *(g)*= amount of MA (or sodium muconate) in the residue;

S_{int} *(%)*= selectivity towards the intermediates evaluated through GC analysis;

S_{AdA} *(%)*= selectivity towards AdA evaluated through GC analysis;

Int+AdA *(g)*= sum of the amount of intermediates and AdA;

Int *(g)*= amount of intermediates in the reaction products;

AdA *(g)*= amount of intermediates in the reaction products;

Out *(g)*= is the sum of the total number of moles in the products;

Balance *(%)*= mass balance.

The equations used to calculate the mass balance (%) are reported below.

$$MA_{in}(mol) = \frac{V\ (mL)}{1000\ (\frac{ml}{L})} \cdot C_{MA}(\frac{mol}{L}) \tag{Eq.4-16}$$

$$MA_{cuv}\ (mol) = \frac{V_{UV-Vis} \cdot MA_{in}}{V_{tot}} \tag{Eq.4-17}$$

$$MA_{res}(g) = residue\ \cdot (1 - \frac{Conv\ (\%)}{100}) \tag{Eq.4-18}$$

$$int + AdA\ (g) = residue -\ MA_{res} \tag{Eq.4-19}$$

$$Int\ (g) = (int + AdA) \cdot \frac{S_{int}}{100} \tag{Eq.4-20}$$

$$AdA\ (g) = (int + AdA) \cdot \frac{S_{AdA}}{100} \tag{Eq.4-21}$$

$$Out\ (mol) = \frac{MA_{res}}{MW_{MA}} + \frac{Int}{MW_{int}} + \frac{AdA}{MW_{AdA}} + MA_{cuv} \tag{Eq.4-22}$$

$$Balance\ (\%) = \frac{out}{MA_{in}} \cdot 100 \tag{Eq.4-23}$$

As reported in Table 4-20 the Mass balance is always between 96 and 101%, therefore, the developed method can be considered valid and robust.

Conclusion

A robust analytical method was developed to evaluate the conversion of MA and the selectivity towards the different reaction intermediates.

In particular, MA (or sodium muconate) conversion was evaluated using UV-Vis analysis due to the low solubility of dimethyl muconate in MeOH at room temperature. Different calibrations curves were performed changing solvent and substrate.

The selectivity was evaluated by GC analysis after a derivatization of reaction products. In fact, even if carboxylic acid can be separated and revealed during gas chromatographic analyses, the response of the instrument toward these compounds is not linear and reproducible. A Fischer's esterification reaction was then performed and optimized allowing a good selectivity evaluation. Different calibrations were performed, and two different gas chromatographic columns were used during the period of the project. The developed gas chromatographic method is able to separate AdA from monounsaturated intermediates and MA, and it is also able to separate the different stereo isomers. This allows to achieve a detailed study on the reaction pathway and the development of a regression model.

Using SUPELCOWAX 10 column a temperature ramp and TCD detector are mandatory to reach suitable results. Instead, using SP-2380 column an isothermal analysis and FID detector are sufficient to separate all the reaction products and reveal them. Finally, the mass balance range between 96 and 101% suggest that the developed analytical method is sufficiently robust.

Bibliography

1. Vardon, D. R. *et al.* Adipic acid production from lignin. *Energy Environ. Sci.* **8,** 617–628 (2015).
2. She, X., Brown, H. M., Zhang, X., Ahring, B. K. & Wang, Y. Selective hydrogenation of trans,trans-muconic acid to adipic acid over a titania-supported rhenium catalyst. *ChemSusChem* **4,** 1071–1073 (2011).
3. Skoog, D. A., Holler, F. J. & Crouch, S. R. *Principles of Instrumental Analysis*. (Thomson Brooks/Cole, 2007).
4. Buijs, K. & Maurice, M. J. Some considerations on apparent deviations from lambert-beer's law. *Anal. Chim. Acta* **47,** 469–474 (1969).

Chapter 5

Muconic acid hydrogenation using commercial Pt and Pd catalysts

This chapter describes the results obtained using commercial Pt and Pd catalyst supported on activated carbon. Initially, two different reactors were designed allowing to explore different range of hydrogen pressure. We decided to use a stainless-steel autoclave (with a working volume of 10 mL) for high pressurized reactions while a glass reactor (with a working volume of 100 mL) was used for atmospheric hydrogenation at low temperature (allowing to increase the volume of the solution used during the reaction).

Moreover, an optimization of initial operating parameters was performed as well as the check of the kinetic and diffusional regime.

Finally, recycling tests and catalyst characterization pre and post used was performed to understand the reaction mechanism and how the catalyst works during the reaction. A part of the chapter was published on Applied Catalysis B Journal (DOI: 10.1016/j.apcatb.2017.06.060).

5.1 Overview on heterogeneous catalyzed hydrogenation reaction

Heterogeneous catalysts are preferable to homogenous counterparts for industrial application due to the facility of the recovering from the reaction mixture.[1] In fact, in these types of reactions the catalyst and the reagents exist in two different phases, so a simple filtration can be often performed to separate liquid products from the catalyst.[2]

The properties required for an industrial heterogeneous catalyst are:

- high activity and selectivity: they depend on the choice of the metal and the support, the amount of the metal anchored on the support;
- fast filtration rate;
- recycle capability;
- high stability.

Activity and selectivity are greatly dependent on the choice of metal. This influences the strength of adsorption of reactants, the rate of desorption of reaction products and the rate of chemical reactions. The most frequently used metals for heterogeneous catalytic hydrogenation are palladium, platinum, rhodium, nickel, cobalt and ruthenium.[3] Heterogeneous catalyst may be supported or unsupported, the former directly uses the active phase in the reaction media, while in the latter the metallic active phase is anchored to a support (i.e. carbon, metal oxides…). Examples of unsupported catalysts include cobalt and Raney nickel. These are made by chemically dissolving the aluminum out of nickel-aluminum or cobalt-aluminum alloys and they are used for the reduction of nitriles, oximes and carbonyl functions. On the contrary in the supported catalysts, the metal is deposited on an inert (or not) material such as carbon, graphite, alumina or inorganic salts. For example, supported Pd catalysts are used for the reduction of carbon-carbon multiple bonds, multiple bond isomerization and hydrogenolysis while supported Pt is used for carbon-carbon and carbon-heteroatom double bonds.[4] Supported catalysts present advantages such as easy separation from the reaction medium and more effective use of the metal surface, as the metal is generally deposited as nanoparticles (between 1 to 10 nm in diameter). Its interaction with the support can also influence the properties of the catalyst, as well as providing stabilization against particle conglomeration/sintering.[5] The metal may be present in oxidic or reduced form, depending on the method of catalyst preparation. Oxidic type catalysts are reduced in situ to reach the metal 0 oxidation state and therefore frequently show an induction period.[6]

A peculiar feature of Pt and Pd is that they are active under very mild pressure and temperature conditions.[7] Therefore, they are often used in the liquid-phase hydrogenation reaction at room temperature and atmospheric, or only slightly, pressure of hydrogen.[8]

The use of high reaction temperatures and pressure is generally favorable for increasing the reaction rate, but in case of reaction that involves different phases (such as a gas and a liquid) elevated temperatures mean lower gas solubility (Henry’s law). Therefore, in the case of hydrogenation reaction, a compromise between pressure and temperature must be considered. The amounts of catalyst to be used may also be reduced under these conditions, unless the catalyst is deactivated, as is often the case with unsupported platinum metals.

Hydrogenation reactions under mild conditions are advantageous to study the conversion and thus achieve selective hydrogenation. For fast hydrogenations, care must be taken to guarantee that the reaction does not occur too violently, particularly in a large-scale hydrogenation. Therefore, an accurate study about the optimization of the amount of catalyst, the hydrogen pressure and the reaction temperature must be performed.

Heterogeneous catalytic hydrogenations reactions can be divided in three main groups depending on the hydrogen source.[9]

- *Ex-situ hydrogen sources*

In these kind of reactions, the hydrogen is supplied from an external source (such as a cylinder) or is produced within the plant and then fed using proper gas lines.

- *Hydrogen transfer reaction*

Hydrogen can be extracted ("transferred") from "hydrogen-donors" instead of H_2 gas. Hydrogen donors, which often serve as solvents include hydrazine, dihydronaphthalene, dihydroanthracene, isopropanol, and formic acid.[10]

Transfer hydrogenation is useful for the asymmetric reduction of ketones, aldehydes, and imines. Non-noble metal catalyst can be used in this reaction such as molybdenum oxide, super acid catalyst, zeolites, acid resins…

- *Electrochemical reaction*

Electrochemical hydrogenation and hydrogenolysis (ECH) does not require external hydrogen source and offers a sustainable way to produce chemicals at room temperature and pressure when matching with renewable electricity sources. Bio-based chemicals can be produced in isolated locations where hydrogen is not readily available. Another advantage of electrochemical reactions is that the reaction on the electrocatalyst can be controlled by current or potential changes.[11]

5.1.1 Hydrogenation equipment

Nowadays bench chemist has three main different choices of hydrogenation equipment:

- *Batch reactor under atmospheric conditions*

Batch reactor under atmospheric condition is the simplest and common configuration used in teaching laboratories. This process is commonly performed by adding solid catalyst to a round bottom flask (or a jacket glass reactor) of dissolved reactant. The hydrogen gas is then supplied from a H_2 cylinder after an evacuation using helium. The resulting three phases mixture is stirred to promote mixing.

- *Batch reactor at high temperature and/or pressure*

Pressurized system is widely used in hydrogenation of aromatic system or hydrogenolysis reactions. In these cases, catalyst is added to a solution of reactant under an inert atmosphere in an autoclave. Hydrogen is added directly from a cylinder. Heat may also be used, as the pressure compensates for the associated reduction in gas solubility.

- *Flow reactor*

Flow hydrogenation is used to increase the process scale. This technique involves a continuous flowing of dissolved reactant over a fixed bed catalyst in the presence of hydrogen. This technique allows to reach high pressure (100 bar) and temperature.

- *Industrial reactor*

Catalytic hydrogenation is performed in tubular plug-flow reactor (PFR) packed with a supported catalyst. Temperature and pressure can be high, although this depends on the catalyst. Catalyst loading is typically much lower than in laboratory batch hydrogenation. Usually various promoters are added to the metal to improve activity, selectivity and stability.

5.2 Set up of the hydrogenation reactor

Two different hydrogenation reactors were used depending on the operating conditions of the reaction. A stainless-steel autoclave was used to perform hydrogenation reaction at mild pressure, while a glass reactor was used for hydrogenation reaction performed at atmospheric pressure and low temperature.

5.2.1 Stainless-steel autoclave for high pressure reactions

The laboratory scale autoclave and a schematic picture of the system are reported in Figure 5-1. The cylindrical reactor (1) is placed inside a heating jacket (2) placed above a hot plate (3) with a display for setting the temperature and the stirring.

The maximum temperature reachable is 400 °C, while the maximum stirring is 1000 rpm.

The temperature is monitored by means of a thermocouple (4) connected to the hot plate, which is inserted inside the holes on the outer casing, thus directly measuring the temperature of the reactor placed inside it.

The stainless-steel reactor catalyzes hydrogenation reactions due to the presence of different active metal within the steel. For this is the reason the hydrogenation reaction was performed into a cylindrical glass insert.

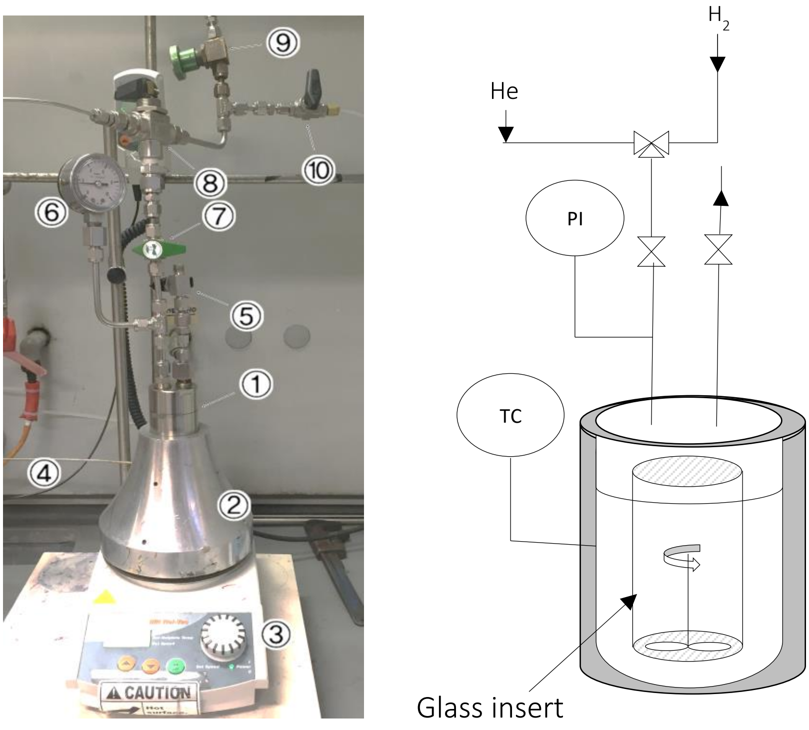

Figure 5-1: picture and schematic representation of autoclave reactor

On the head of the reactor there are two conduits, both of which have a Teflon ring at the base.

The right-hand duct has an "open and close" valve (5) through which the reagent mixture is injected using a syringe. The left duct has a pressure gauge (6) for measuring the pressure; this instrument has a sensitivity of 0.4 bar and a maximum measurement fixed at 10 bar.

Another "open and close" valve (7) is positioned for the gas intake into the reactor. A three-way valve (8) above the previous one has the function of switching the helium and hydrogen flow inside the reactor. Helium is used both for inerting and quenching the reaction. In the picture two other valves are reported: one with a pin (9) and the other "open and close" (10); they are safety valves which can be respectively used to introduce and remove hydrogen.

The plant can not work in continuous for practical reasons, so each point of the kinetics is obtained by performing a new test in the same operating conditions by varying only the reaction time.

5.2.1.1 Pre-treatment of the catalyst

The hydrogenation reaction requires a well-activated catalyst, so the noble metal that catalyzes the reaction must not be in oxidized form and therefore a pretreatment reduction is mandatory.

An amount of known catalyst of about 100 mg was charged inside the glass insert, equipped with a magnetic stirrer, which was placed inside the reactor.

Once the reactor was closed, a switch on in the reaction environment is started: 4/5 cycles of loading and removal of hydrogen were then performed to ensure complete reducing environment. Once completed, the activation step was performed: hydrogen fully charges the reactor at the desired pressure (6 bar) and at the reduction temperature of 200 °C (obtained from TPR analyses described in the following paragraph) for 3 hours.

In any case, the catalyst is placed on the bottom of the reactor, therefore it reaches the set temperature. Once the catalyst activation phase was completed, the reactor was cooled to room temperature.

5.2.1.2 Temperature programmed reduction (TPR)

TPD/R/O 1100 ThermoQuest Instruments was used for TPR study. An amount 40 mg of catalyst was dried in oven and then analyzed. The sample was pre-treated with argon flow from room temperature to 200 °C with a temperature ramp of 30 $°C \cdot min^{-1}$ and maintained at this temperature for 60 min. The analysis was then conducted from 50 °C to 900 °C at 8 $°C \cdot min^{-1}$ at 1 bar. The gaseous mixture was 5.04% of hydrogen in argon and it was fluxed within the instrument at 14 $mL \cdot min^{-1}$.

The peaks in Figure 5-2 correspond to the material's reduction temperatures.

The peak at 200-210 °C can be correlated to the platinum reduction temperature, so it was used in the pre-treatment step to make it active in the reduction of muconic acid to AdA. The second peak is due to the reduction-degradation of carbon; in fact, it is almost superimposable to the peak of pure carbon (red line). The shift is probably caused by platinum interactions. The TPR profile shows that the catalyst needs an activation at 200 °C. The chosen pressure (6 bar) is higher than that used during TPR analysis in order to guarantee a complete activation.

Three hours are a reasonable time to be sure to have a total activation of the catalyst.

A well activated catalyst is a positive starting point to obtain good results.

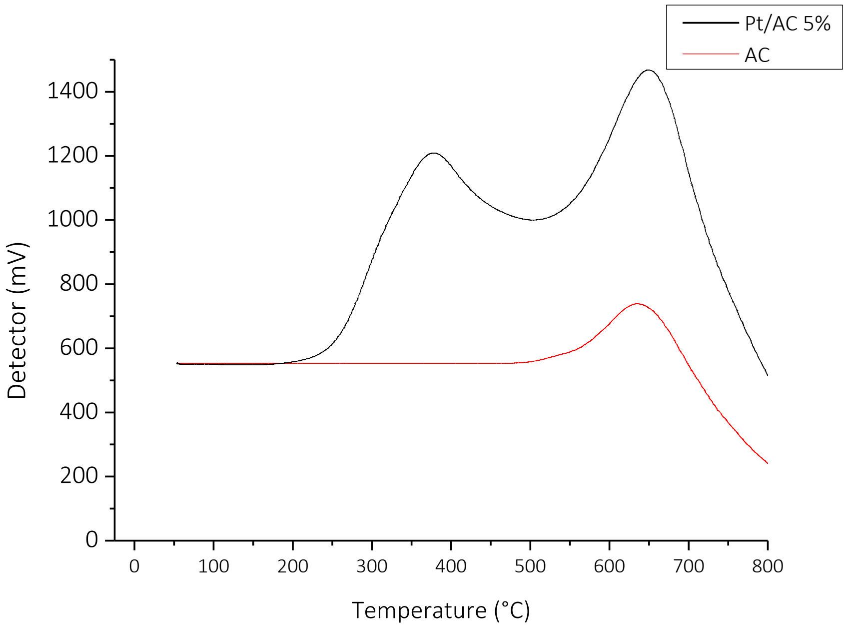

Figure 5-2: TPR analysis of the commercial Pt/C 5% (black line) and carbon support (red line)

5.2.1.3 Hydrogenation reaction of muconic acid

A known amount of about 10 g of reagent solution was weighed and loaded with a syringe by opening the valve 5 and inserting the needle inside the right duct. This operation was mandatory for different reasons: to prevent the spreading of the solution, to avoid catalyst re-oxidation and to prevent catalyst burning due to the presence of carbon support that is extremely pyrophoric. Once the solution has been charged inside the reactor, hydrogen cycles were carried out to eliminate each other gasses in the reaction environment. Then hydrogen is charged to the desired pressure (1-4 bar), and the stirring rate (700-1200 rpm) and temperature (40-70 °C) were set. Once the kinetic test was complete, the heating was switched off and the hydrogen was discharged by opening the valve 10 and venting the hydrogen outside. To be sure of having removed the hydrogen, quenching was carried out with helium. The quenching was conducted opening the three-way valve (Figure 5-1 (8)) toward the helium line that was flushed inside the reactor for a few seconds.

At the beginning, fresh catalyst was used for each kinetic point. When the reaction ends, the reacted mixture was filtered to separate the liquid solution from the heterogeneous catalyst. The conversion was evaluated using UV-Vis analysis as described in Chapter 4. During the recyclability tests of the reactor was cooled at room temperature and extracted from the stainless-steel autoclave. Then the catalyst is left to decant at the bottom of the glass insert. At this point the solution was recovered with a Pasteur pipette and re-used for a new kinetic point.

5.2.1.4 Work up of the reaction: conversion and selectivity evaluation

After the end of the reaction 1 g of the reacted mixture is used for the UV analysis sample preparation. Two or three dilutions were necessary to read an absorbance below 1. The samples are prepared weighting the reacted mixture and water. 1 g of sample collected from the reaction is diluted in 3 g of water (1st dilution). Then from this sample 1 g is withdrawn and added to 24 g of water (2nd dilution). Finally, from the 2nd dilution 1 g is withdrawn and added to 24 g of water (3rd dilution). The third sample is then analyzed using UV-Vis instrument performing the analysis from 500 to 190 nm. Distilled water was used as blank. The value of absorbance was kept at 264 nm (maximum of the absorbance). The concentration of the sample was evaluated using the Lambert-Beer's law, while the conversion was calculated using the Eq. 5-1

$$Conversion\ _i(\%) = \frac{mol_i^{in} - mol_i^{end}}{mol_i^{in}} \cdot 100 \qquad \text{(Eq. 5-1))}$$

where:

mol_i^{in}= starting moles of the specie *i (t,t*-MA or Na-Muc*)*;

mol_i^{end}= number of moles of the specie *i* at the desired reaction time.

Subsequently, the remaining filtered sample was dried at rotavapor or placed in an oven at 70 °C to remove water or the reaction solvent; in this way a white/yellow solid product was obtained. This is possible because the volatility difference between the solvent and the reaction product is high, in fact the boiling temperature of the product and the solvent are 300 °C and 80-100 °C, respectively. During this operation, the mixture was not subjected to strong boiling to prevent the product from being drawn by the developed vapors. The solid white product is then subjected to an esterification reaction. The esterified samples were analyzed by gas chromatographic analysis to evaluate the selectivity (Eq.5-2)

$$Selectivity_n\ (\%) = \frac{mol_n}{\sum mol_i + mol_n} \cdot 100 \qquad \text{(Eq.5-2)}$$

where:

$\mathrm{Selectivity_n}$ =is the selectivity of the n compound;

$\mathrm{mol_n}$= is the number of moles of the considered reaction product;

$\sum \mathrm{mol_i}$=is the sum of the moles of all the other reaction products.

Finally, products yield was calculated multiplying the selectivity with the respective conversion.

$$Yield_n\ (\%) =\cdot \frac{Selectivity_n\ (\%)}{100} \cdot Conversion\ (\%) \qquad \text{(Eq.5-3)}$$

where:

$Yield_n$(Y)= yield of the n compound.

5.2.2 Low pressure reactor

Glass low pressure reactor (Figure 5-3)was designed to perform hydrogenation reaction up to 3 bar and low temperatures. This reactor allows also to use a high amount of reagent solution increasing the amount of catalyst needed for the characterization.

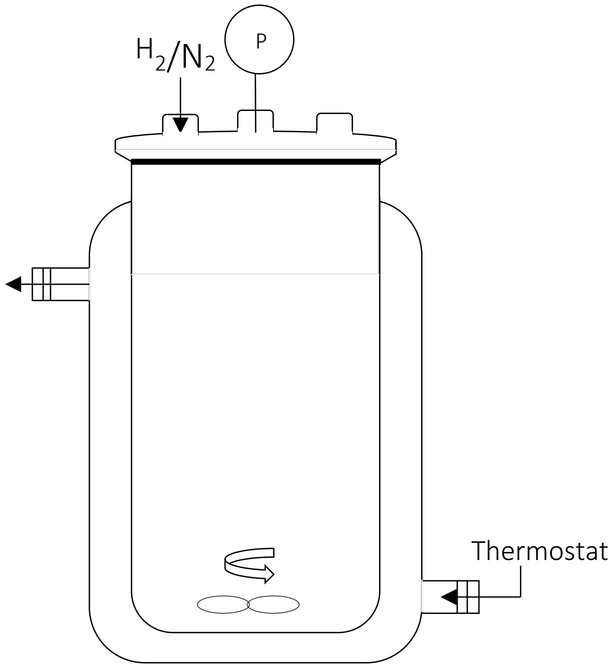

Figure 5-3: glass reactor configuration

The glass reactor was equipped with a pressure controller and an external jacket linked to a thermostatic water bath. The low-pressure hydrogen was added using a proper line. The third neck of the glass cap was equipped with a silicon septum that allows to make a withdrawal at different reaction times without stopping the reaction or losing pressure. The glass reactor was placed on a hot plate for the magnetic stirring.

A known amount of reagent solution was placed in the reactor and it was thermostated at the desired temperature under magnetic stirring. Then the catalyst was added, and the hydrogen was inserted at the desired pressure after the removal of the air. The air was removed adding hydrogen three times and degassing the reactor.

The zero time of the reaction was taken after the addition of the hydrogen at the desired temperature. The sample was collected using a syringe equipped with a needle of the proper length. The sample was filtered using a paper filter to remove the solid catalyst.

Then the conversion and selectivity were evaluated as described in section 5.2.1.4.

5.3 Evaluation of the starting operating parameters

Whenever a new reactor is designed, and a new reaction is performed, it is more advisable to select suitable starting operating parameter to avoid mass transfer limitation or to use high pressure (that is not suitable when pure hydrogen is used).

5.3.1 Hydrogen solubility in water in function of pressure and temperature

One of the most important parameter involved in hydrogenation reaction is hydrogen pressure. The solubility of hydrogen in water strictly depends on pressure and temperature. Starting from a study of Sander[12] hydrogen concentration in water was evaluated at mild pressure and temperature. The results of the study are reported in Table 5-1 and Figure 5-4.

Henry's constant in function of temperature (T (K)) was calculated using Eq.5-4 in accordance with Sander's work.

$$H(T) = H_{ref} \cdot e^{\left[\frac{dH}{d(\frac{1}{T})} \cdot \left(\frac{1}{T} - \frac{1}{T_{ref}}\right)\right]} \qquad \text{(Eq.5-4)}$$

$$C_{H_2}\left(\frac{mol}{L}\right) = H(T) \cdot P(bar) \qquad \text{(Eq.5-5)}$$

where:

$H(T)$ = Henry's constant at temperature T (expressed in Kelvin);

H_{ref}= Henry's constant at 298.15 K;

$dH/(d(1/T))$ = 530;[12]

T_{ref}= 298.15 K;

$P(bar)$ = considered pressure;

C_{H2} (mol/L) = hydrogen molar concentration in water.

Table 5-1: hydrogen concentration in function of temperature and pressure evaluated with Henry's Law

T [K]	298.15	303.15	308.15	313.15	318.15	323.15	328.15	333.15	338.15	343.15	348.15
H(T)	7.80E-04	7.57E-04	7.36E-04	7.16E-04	6.98E-04	6.80E-04	6.63E-04	6.47E-04	6.32E-04	6.18E-04	6.04E-04
P (bar)	**Hydrogen concentration in water (mol/L)**										
1	7.80E-04	7.57E-04	7.36E-04	7.16E-04	6.98E-04	6.80E-04	6.63E-04	6.47E-04	6.32E-04	6.18E-04	6.04E-04
1.2	9.36E-04	9.09E-04	8.84E-04	8.60E-04	8.37E-04	8.16E-04	7.96E-04	7.77E-04	7.58E-04	7.41E-04	7.25E-04
1.4	1.09E-03	1.06E-03	1.03E-03	1.00E-03	9.77E-04	9.52E-04	9.28E-04	9.06E-04	8.85E-04	8.65E-04	8.46E-04
1.6	1.25E-03	1.21E-03	1.18E-03	1.15E-03	1.12E-03	1.09E-03	1.06E-03	1.04E-03	1.01E-03	9.88E-04	9.67E-04
1.8	1.40E-03	1.36E-03	1.33E-03	1.29E-03	1.26E-03	1.22E-03	1.19E-03	1.16E-03	1.14E-03	1.11E-03	1.09E-03
2	1.56E-03	1.51E-03	1.47E-03	1.43E-03	1.40E-03	1.36E-03	1.33E-03	1.29E-03	1.26E-03	1.24E-03	1.21E-03
2.2	1.72E-03	1.67E-03	1.62E-03	1.58E-03	1.53E-03	1.50E-03	1.46E-03	1.42E-03	1.39E-03	1.36E-03	1.33E-03
2.4	1.87E-03	1.82E-03	1.77E-03	1.72E-03	1.67E-03	1.63E-03	1.59E-03	1.55E-03	1.52E-03	1.48E-03	1.45E-03
2.6	2.03E-03	1.97E-03	1.91E-03	1.86E-03	1.81E-03	1.77E-03	1.72E-03	1.68E-03	1.64E-03	1.61E-03	1.57E-03
2.8	2.18E-03	2.12E-03	2.06E-03	2.01E-03	1.95E-03	1.90E-03	1.86E-03	1.81E-03	1.77E-03	1.73E-03	1.69E-03
3	2.34E-03	2.27E-03	2.21E-03	2.15E-03	2.09E-03	2.04E-03	1.99E-03	1.94E-03	1.90E-03	1.85E-03	1.81E-03
3.2	2.50E-03	2.42E-03	2.36E-03	2.29E-03	2.23E-03	2.18E-03	2.12E-03	2.07E-03	2.02E-03	1.98E-03	1.93E-03
3.4	2.65E-03	2.58E-03	2.50E-03	2.44E-03	2.37E-03	2.31E-03	2.25E-03	2.20E-03	2.15E-03	2.10E-03	2.05E-03
3.6	2.81E-03	2.73E-03	2.65E-03	2.58E-03	2.51E-03	2.45E-03	2.39E-03	2.33E-03	2.28E-03	2.22E-03	2.18E-03
3.8	2.96E-03	2.88E-03	2.80E-03	2.72E-03	2.65E-03	2.58E-03	2.52E-03	2.46E-03	2.40E-03	2.35E-03	2.30E-03
4	3.12E-03	3.03E-03	2.95E-03	2.87E-03	2.79E-03	2.72E-03	2.65E-03	2.59E-03	2.53E-03	2.47E-03	2.42E-03
4.2	3.28E-03	3.18E-03	3.09E-03	3.01E-03	2.93E-03	2.86E-03	2.78E-03	2.72E-03	2.65E-03	2.59E-03	2.54E-03
4.4	3.43E-03	3.33E-03	3.24E-03	3.15E-03	3.07E-03	2.99E-03	2.92E-03	2.85E-03	2.78E-03	2.72E-03	2.66E-03
4.6	3.59E-03	3.48E-03	3.39E-03	3.30E-03	3.21E-03	3.13E-03	3.05E-03	2.98E-03	2.91E-03	2.84E-03	2.78E-03
4.8	3.74E-03	3.64E-03	3.53E-03	3.44E-03	3.35E-03	3.26E-03	3.18E-03	3.11E-03	3.03E-03	2.97E-03	2.90E-03
5	3.90E-03	3.79E-03	3.68E-03	3.58E-03	3.49E-03	3.40E-03	3.32E-03	3.24E-03	3.16E-03	3.09E-03	3.02E-03

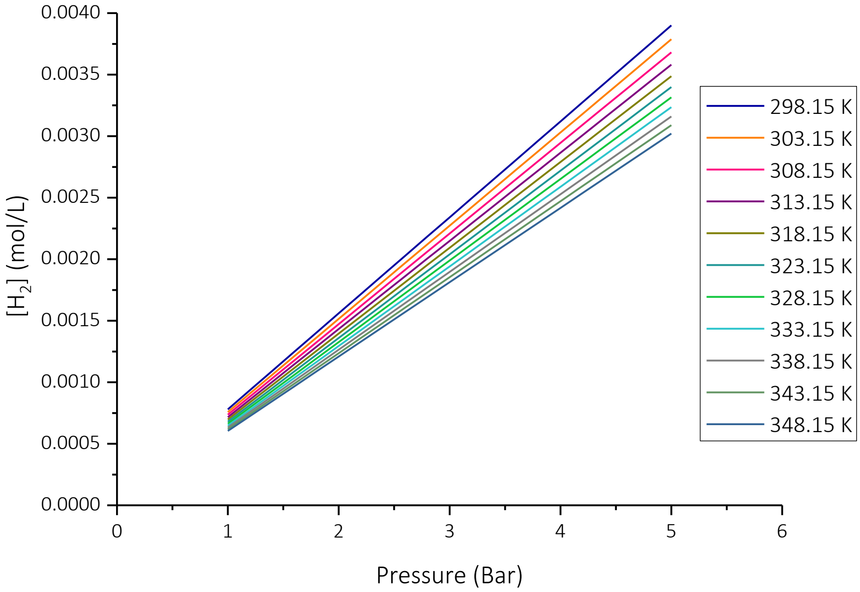

Figure 5-4: hydrogen concentration in water at different temperatures and pressures

As reported in Figure 5-4 for low pressure the hydrogen concentration in water does not strictly depend on temperature, while increasing the pressure, hydrogen solubility is higher for low temperature. For this reason, we decide to start the hydrogenation reaction using **4 bar of hydrogen** and temperature between **50 and 70 °C**.

5.3.2 Control of kinetic regime

An aspect that could significantly affect the performance of a slurry reactor is the insurgence of mass-transfer resistances between the gas (hydrogen), the liquid (solvent and reactants dissolved) and the solid (catalyst particles) phase. Although slurry reactors usually minimize transport phenomena issues, the confirmation of a pure kinetic regime is necessary if the reactor layout and the results are meant for further mechanism studies. Some practical criteria to exclude mass transfer resistances were by Chaudari and Rajashekharam.[13,14] They proposed qualitative indexes to evaluate whether any external or intraparticle mass transfer phenomena are the rate determining step, rather than the reaction itself. The value of the parameters cited below are reported in Table 5-2.

The calculation is based on the definition of initial rate, defined as:

$$R_A = \lim_{t \to 0} \frac{1}{\nu_i} \frac{dC_i}{dt} \qquad \text{(Eq.5-6)}$$

where C_i is the concentration of a reference specie, in this case MA.

The calculated value is of the order of 1.26 kmol·m^{-3}·s^{-1}.

The contribution of gas-liquid mass transfer is evaluated by the index defined in Eq.5-7, which should be lower than 0.1 to exclude its contribution to the overall kinetics.

$$\alpha_1 = \frac{R_A}{k_l a_B C^*_{H_2}} < 0.1 \qquad \text{(Eq.5-7)}$$

where:

$k_l a_B$ (s^{-1})= the overall mass transfer coefficient (gas side-film theory) for stirred reactors,

C^*_{H2} ($kmol \cdot m^{-3}$) = the equilibrium concentration of hydrogen. Machado[15,16] addressed the problem of estimating the gas-liquid mass transfer coefficient for bench-scale stirred reactors.

The range of 0.05-0.5 s^{-1} was considered representative for the smaller hydrogenation reactors. Even with the more conservative values, the system under study resulted in α1 values lower than 0.05. The calculated value is 0.03 that is safely under the threshold to exclude gas-liquid resistance.

Liquid-liquid mass transfer limitation was excluded performing a series of hydrogenations under the same conditions but varying the stirring speed from 250 to 700 rpm. The essays revealed that for higher speed than 500 rpm the system is no more sensitive to stirring rate, hence no more liquid-liquid transport is relevant on the overall kinetics Figure 5-5 the reactor can be considered a CSTR, therefore the hydrogen concentration in liquid bulk is assumed constant.[17]

Liquid-solid mass transfer can be assessed by the index in equation 5-8.

$$\alpha_2 = \frac{R_A}{k_s a_p C^*_{H_2}} < 0.1 \qquad \text{(Eq.5-8)}$$

where:

k_S (s^{-1}) = the liquid-solid mass transfer coefficient;

a_p ($m^2 \cdot m^{-3}$) = the interface area of liquid-solid boundary (external surface area of the catalyst per unit volume.

The latter is defined by equation 5-9:

$$a_p = \frac{6w}{\rho_p d_p} \qquad \text{(Eq.5-9)}$$

Where:

w ($kg \cdot m^{-3}$) = the catalyst load;

ρ_P and d_P(m)= particle density and diameter respectively.

Particles diameter was set using sieves and it was at about 40 µm (325 and 400 mesh –TYLER series)

The parameter k_S is obtained using a literature correlation:[18]

$$\frac{k_s d_p}{D_{H_2} F_c} = 2 + 0.4\left(\frac{d_p^4 \rho_l^3 e}{\mu_l^3}\right)^{0.25}\left(\frac{\mu_l}{\rho_l D_{H_2}}\right)^{0.33} \qquad \text{(Eq.5-10)}$$

where:

D_{H_2} ($m^2 \cdot s^{-1}$) = the molecular diffusion of hydrogen in water;

F_c is a shape factor assumed to be 1 for spherical particles;

μ_l (P) and ρ_l ($kg \cdot m^{-3}$) = liquid viscosity and density respectively;

e = energy supplied to the liquid by the stirrer, given in equation 5-11

$$e = \frac{N_p n^5 l^5}{V} \qquad \text{(Eq.5-11)}$$

where:

N_p = impeller power number;

l (m)= impeller diameter;

n (rps)= rotation speed.

The calculated value for α_2 is 0.019, which allows excluding liquid-solid mass transfer limitations.

Finally, pore diffusion can be considered negligible if the parameter Φ_{exp} is lower than 0.2:

$$\Phi_{exp} = d_p \left(\frac{\rho_P R_A}{w D_e c^*_{H_2}} \right)^{0.5} < 0.2 \qquad \text{(Eq.5-12)}$$

where:

d_p (m)= particle diameter;

w ($kg \cdot m^{-3}$) = catalyst load;

D_e =effective diffusivity calculated as

$$D_e = \frac{D_\varepsilon}{\tau} \qquad \text{(Eq.5-13)}$$

where:

ε = catalyst porosity;

τ= tortuosity factor.

The latter parameter is usually little characterized: it is a complex function of the type of charcoal, of the adsorbed substrate, and the reaction medium, often regressed from indirect diffusion measurements.[19] Nonetheless, in carbon-supported platinum hydrogenation catalysts, the parameter was estimated in the range between 3 and 7.[20]

The calculated ϕ_{exp} was lower than 0.04 even for the most conservative values of tortuosity in the conditions of this study, allowing the exclusion of pore diffusion mass transfer.

In the case of Pt/AC 5% (Sigma Aldrich) the check on the mass transfer limitation was performed applying the parameters reported in Table 5-2.

Table 5-2: parameters used for mass transfer evaluation

Reaction conditions	
Hydrogen pressure	4 bar
Hydrogen gas-liq. transf. rate ($k_l a_B$)	0.1 s^{-1}
Liquid density	1000 $kg \cdot m^{-3}$
Liquid viscosity	6.5 x 10^{-4} Pa s
Reactor properties	
Volume	0.025 L
Reactor materials	glass
Impeller power number	5
Diameter of the impeller	2.5 mm
Rotation speed	8.33 rps
Catalyst properties	
Support	Activated charcoal
Pt content	5% wt/wt
Catalyst loading	10 $g_{cat} \cdot (L_{AM\ solution})^{-1}$
Catalyst porosity	0.95
Particle diameter	40 x10^{-6} m
Particle skeletal density	2 x 10^3 $kg \cdot m^{-3}$

In our reaction conditions the system was not affected to any mass transfer limitation, so the reaction occurred only in kinetic regime.

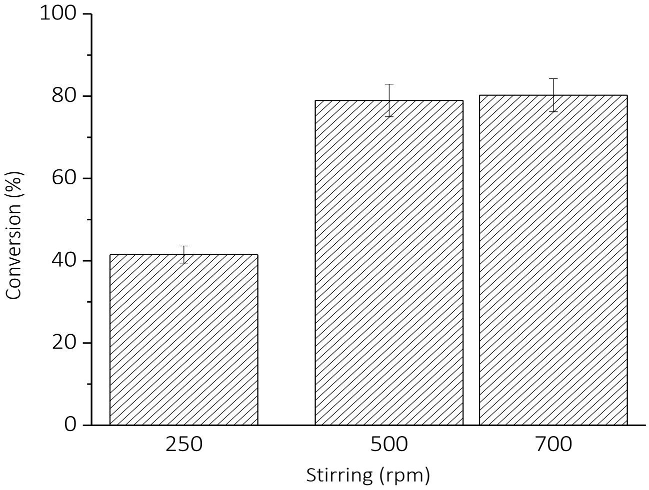

Figure 5-5: Sodium muconate conversion evaluation at 250, 500 and 700 rpm T=60 °C, $P(H_2)$= 4 bar, reaction time= 60 min, sub/cat= 10 (wt/wt) and [MA]= $7 \cdot 10^{-2}$M

5.4 Pt/AC 5% commercial catalyst

5.4.1 *t,t*-MA hydrogenation in water

The first set of hydrogenation reaction was performed using Pt/AC 5% (Sigma Aldrich) on sodium muconate solution. The catalyst was pre-treated at 200 °C for 3 h under 6 bar of static hydrogen. After cooling, 10 mL of degassed muconate solution (0.07 M) were added to the reactor. The batch hydrogenations were conducted at 50 °C, 60 °C and 70 °C at 2-4 bar of static hydrogen with a magnetic stirring of 500 rpm up to 4 h.

Finally, experiments were performed at 70 °C, 4 bar of hydrogen and 500 rpm on *cis,cis*-muconic acid using a synthetic salt solution which reproduces a clarified fermentation broth as the one of Niu et.al.[21] This test considers the possibility to avoid a MA crystallization step before hydrogenation reaction, preventing the solution acidification and the risk of MA isomerization. The synthetic fermentation broth contained *cis,cis*-muconic acid (Sigma Aldrich) (28 g/L), Na_2HPO_4 (50 g/L), KH_2PO_4 (15 g/L), NaCl (2.5 g/L) and NaOH (40 g/L).

After every reaction, the catalyst was removed by filtration and the solution analyzed as described in paragraph 4.3.1. The filtrate was analyzed by ICP-OES to check a possible metal leaching.

5.4.2 Influence of pressure

Due to the influence of pressure on the hydrogen solubility in water, the impact of static hydrogen pressure was studied to evaluate how conversion and yield are affected by it.

As reported in Figure 5-6 the conversion is slightly affected by the pressure, while the yield toward adipic acid (YAdA) strongly depends on hydrogen pressure.

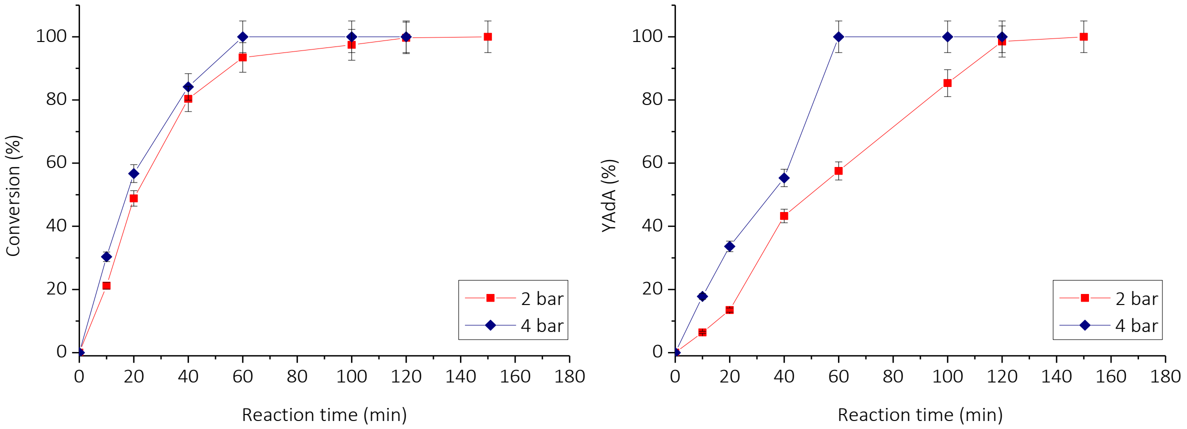

Figure 5-6: dependence of conversion and AdA yield on the hydrogen pressure at 70°C, cat/sub=200 (wt/wt), [Na-Muc]=7.56E-02 M

For this reason, 4 bar of hydrogen pressure was selected to perform the successive kinetic studies.

5.4.2.1 Catalyst-substrate ratio optimization

Firstly, the catalyst/substrate ratio was studied to optimize the amount of catalyst to use during the reaction. Different tests were performed varying the amount of catalyst and Na-Muc concentration used to perform the reaction. The operating conditions were 60 °C of temperature, 4 bar of static hydrogen and 500 rpm of stirring. The reaction occurred in a stainless-steel autoclave for 60 min. The results are reported in Table 5-3.

Table 5-3: results of the catalyst/substrate ratio optimization

Pd/AC 5% (g)	Pd (g)	Pd (mol)	Na-Muc (mol/L)	Volume (mL)	Na-Muc (mol)	Na-Muc/Pd (mol/mol)	Conv (%)	S_{AdA} (%)
0.0943	4.96E-03	2.54E-05	0.0700	9.59	6.71E-04	26.37	56.9	55.5
0.023	1.21E-03	6.21E-06	0.0749	10.38	7.77E-04	125.21	30.1	62.6
0.0428	2.25E-03	1.15E-05	0.0749	10.00	7.49E-04	64.86	49.3	57.9
0.1542	8.12E-03	4.16E-05	0.0749	10.22	7.66E-04	18.40	47.7	32.5
0.0715	3.76E-03	1.93E-05	0.0773	10.29	7.96E-04	41.24	47.9	44.1
0.0406	2.14E-03	1.10E-05	0.0773	10.49	8.11E-04	74.01	37.3	48.9
0.1086	5.72E-03	2.93E-05	0.0700	10.11	7.08E-04	24.15	58.1	41.3

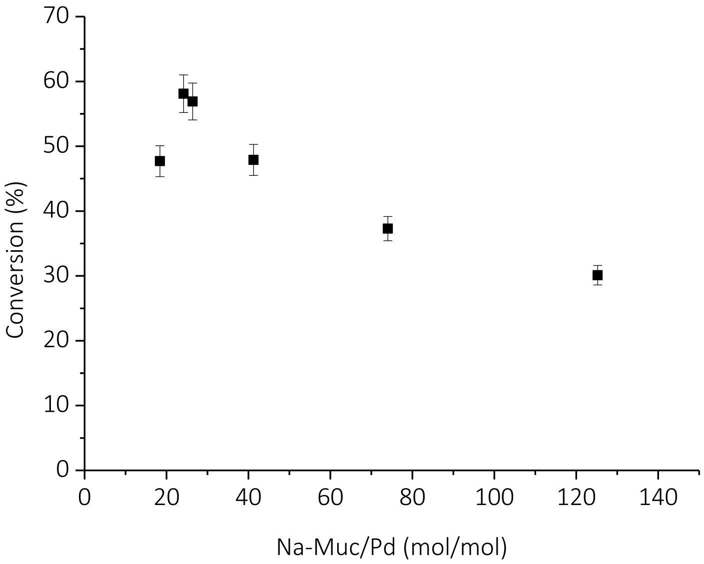

Figure 5-7: substrate/catalyst ratio optimization performed at T=60 °C, stirring rate =500 rpm, P(H_2)=4 bar

5.4.2.2 Influence of temperature

Once the pressure and catalyst/substrate ratio were selected, different reactions were performed varying the temperature. This parameter could affect the adsorption and desorption rate of the species on the catalyst surface as well as the overall reaction rate. The results are reported in Figure 5-8. Na-Muc conversion is higher increasing the temperature. This behavior is common, a raise in the temperature facilitates the reaction rate and the desorption and adsorption steps. Figure 5-9 shows the yield and therefore the selectivity toward the monounsaturated compounds and AdA. For low reaction time (2Z)HxAc is the predominant intermediates, while for long reaction time the two

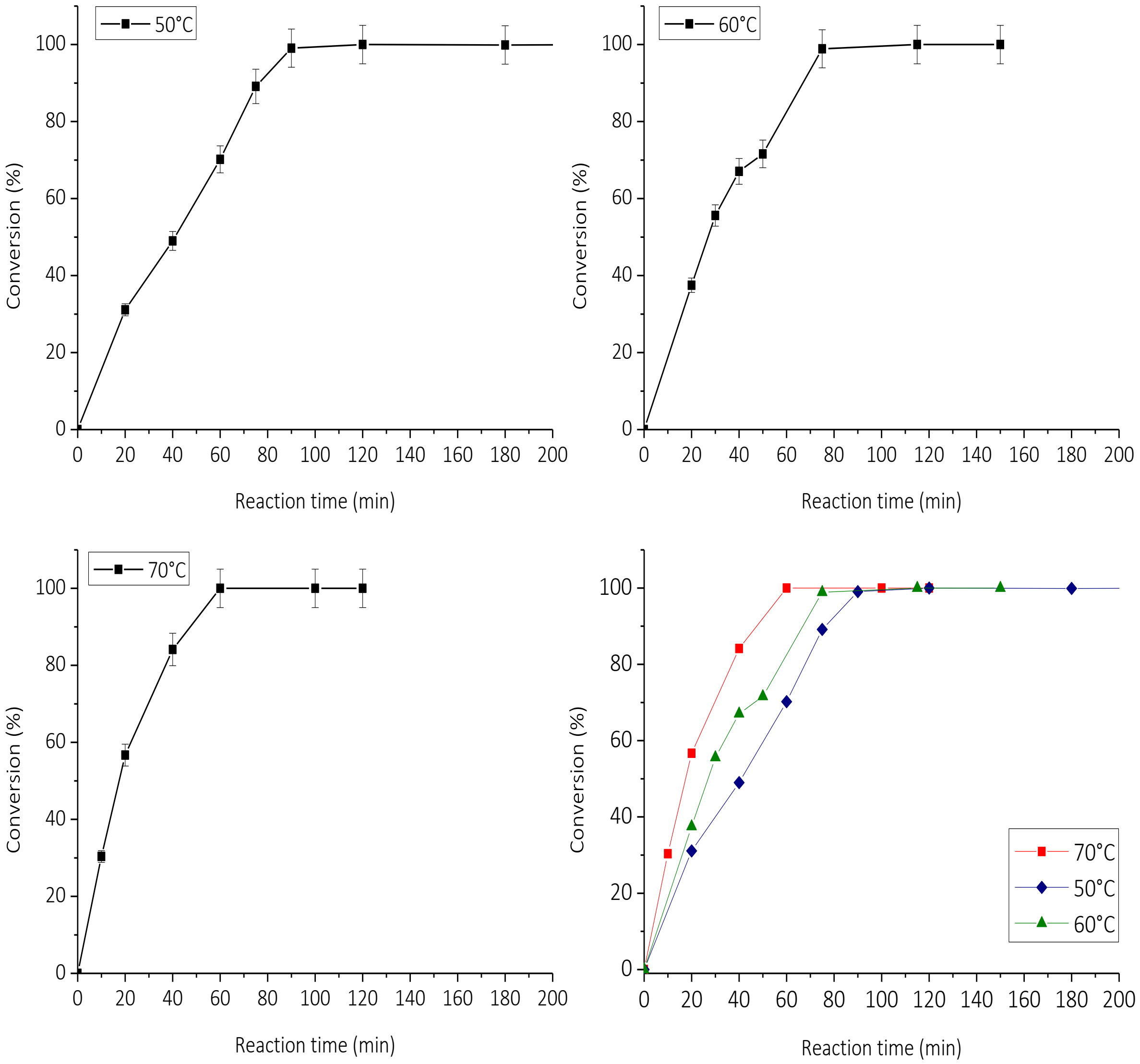

Figure 5-8: conversion of Na-Muc at different temperatures. Stirring=500 rpm, $P(H_2)$=4 bar, sub/cat=24 (mol_{sub}/mol_{Pd}), [Na-Muc]=$7\cdot10^{-2}$M

intermediates were fully converted into AdA. At high temperature the yield toward AdA increases; in particular at 70 °C after 60 min, Na-Muc is fully converted to AdA (Figure 5-9 D).

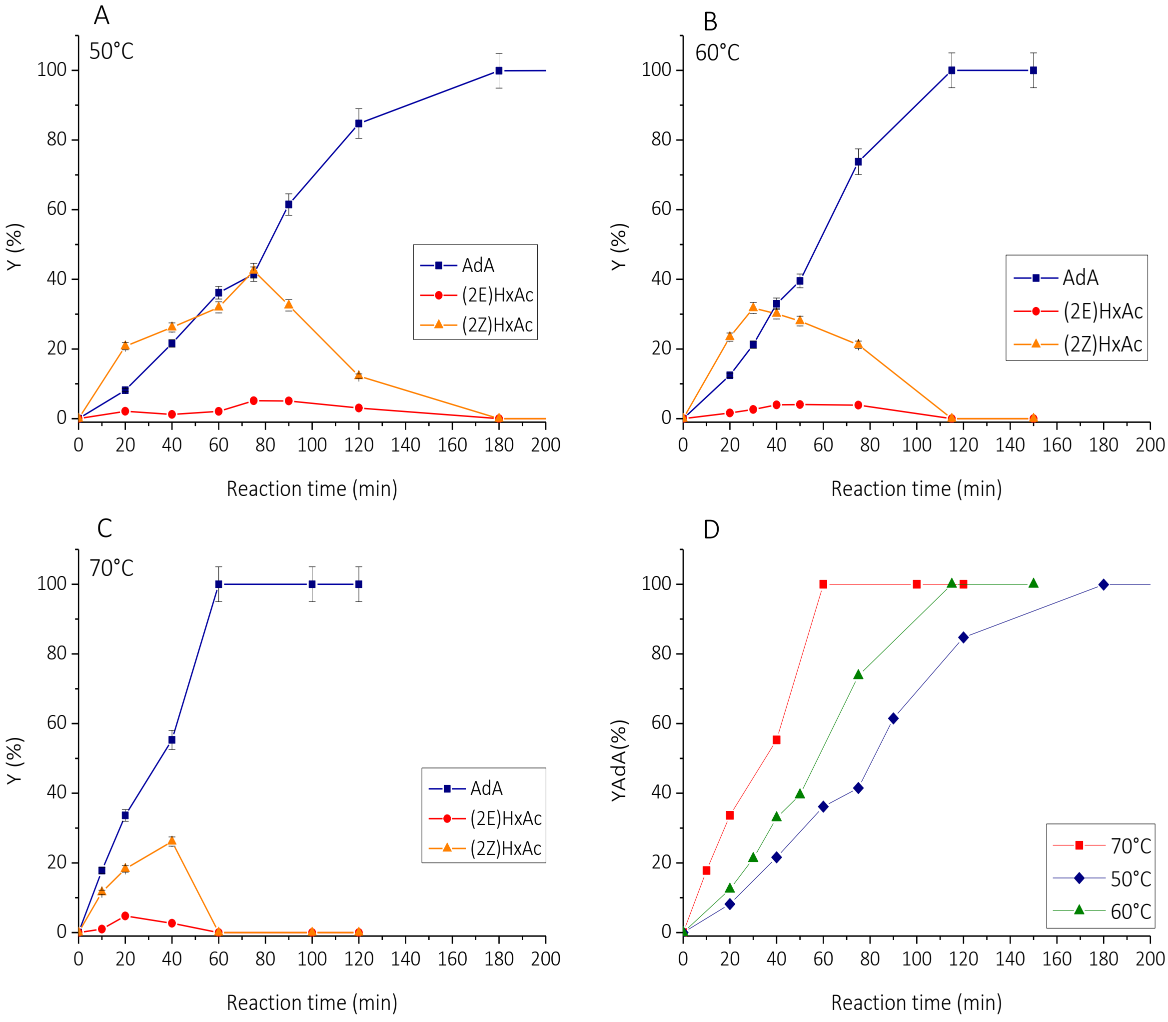

Figure 5-9: yields of the different compounds at different temperatures and AdA yield

5.4.2.3 Recycling test

The possibility to reuse the catalyst many times before its completely deactivation is one of the most important features for the choice of potential industrial catalyst. During the recycles test the catalyst was separated from the reacted mixture by centrifugation and reused for the next reaction. Therefore, the same sample of catalyst was reused for 10 consecutive kinetic tests keeping all the operating parameter constant (T=70 °C, P(H_2)= 4 bar, stirring= 500 rpm, reaction time= 180 min, [Na-Muc]=$7.00 \cdot 10^{-2}$ M, V=10 mL). After each test, conversion and selectivity were evaluated.

After 10 reactions the conversion and the yield for AdA were 100% (Figure 5-10). Therefore, the catalyst can be used many times before its completely deactivation.

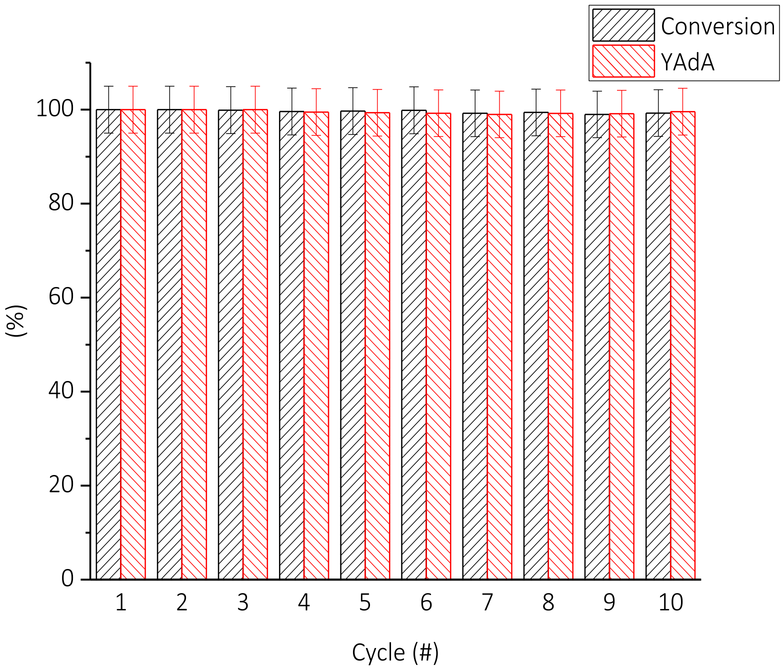

Figure 5-10: results of the recycling test

5.4.3 Fresh and used catalyst characterization

5.4.3.1 Transmission electron microscopy coupled with Energy Dispersive X-ray spectroscopy (TEM-EDX)

TEM images were obtained using Philips 208 Transmission Electron Microscope.

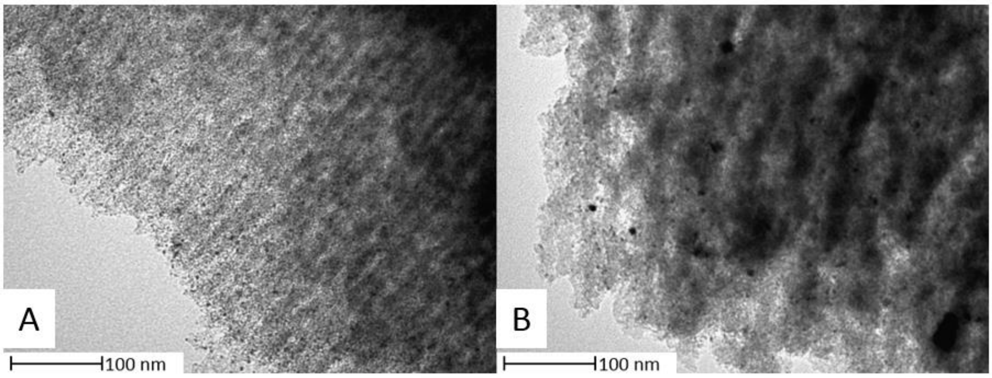

Figure 5-11: Characterization by TEM of A) fresh and B) used catalyst

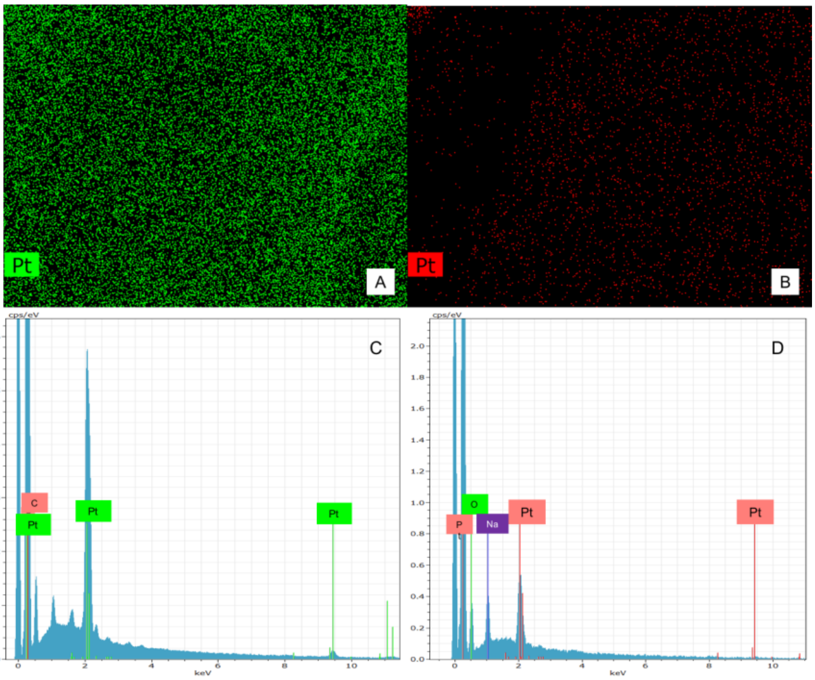

Figure 5-12: EDX mapping analysis of the (A-C) fresh Pt/C 5% catalyst and (B-D) the pre-treated ones

TEM analysis of the fresh and used catalysts are reported in Figure 5-11 (A,B), respectively. The fresh catalyst is characterized by a homogeneous distribution of Pt aggregates (black color) on the carbon surface (grey color). The size of these Pt aggregates can be estimated of about 4 nanometers. In the sample after the pre-activation procedure and the reaction (Figure 5-11 B) it is possible to observe three times greater Pt particles than the corresponding ones present in the fresh sample. This result can be explained considering a sintering of Pt particle during the pre-treatment step. EDX analysis reported in Figure 5-12 shows for fresh catalyst (Figure 5-12 A) a good dispersion of Pt on the surface of carbon support, while after reaction (Figure 5-12 B) Pt particle was less dispersed. In Figure 5-12 C and D the catalyst composition in fresh and used catalyst is reported. While in the fresh sample it is possible to confirm the theoretical catalyst composition, in the used sample sodium element was detected (Figure 5-12 D), due to the adsorption of sodium hydroxide used for muconic acid salification.

5.4.3.2 Scanning electron microscopy (SEM)

SEM images were obtained using a Field Emission Gu Electron Scanning Microscopy LEO 1525 (Zeiss). The samples were investigated by Inlens detector for secondary electrons, AsB detector for backscattered electrons and elemental composition was determined using Bruker Quantax EDX.

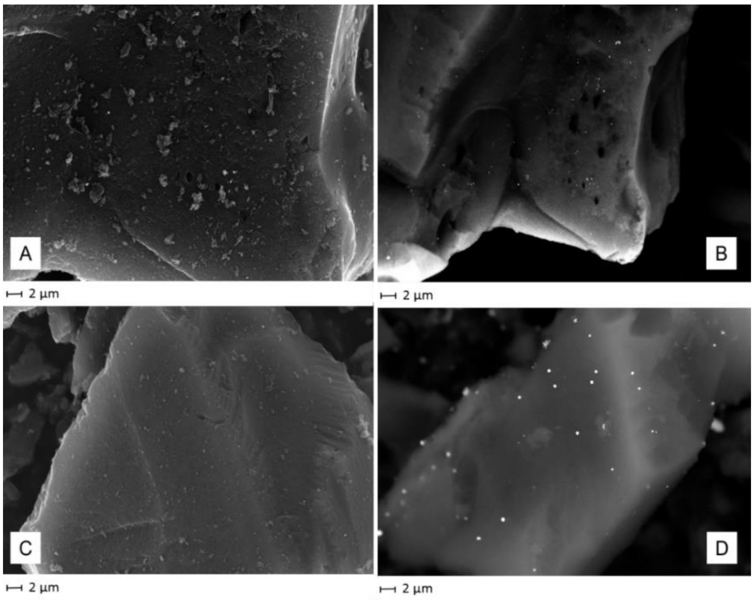

Figure 5-13: *Characterization by SEM of fresh (A, B) and used catalyst (C, D) in different zones*

SEM analysis on fresh and used catalyst are reported in Figure 5-13, where two different particles of the same sample were analyzed, i.e. A) and B) for fresh catalyst and C) and D) for the used one. Images A) and C) were collected using secondary electron detectors, while B) and D) using backscattered electrons detector. By making a comparison between the different zones it is possible conclude that the catalyst is homogeneous for what concerns both its morphology and Pt distribution. Moreover, the same observation previously discussed on the basis of TEM analysis is confirmed also by SEM.

5.4.3.3 X-ray powder diffraction (XRPD)

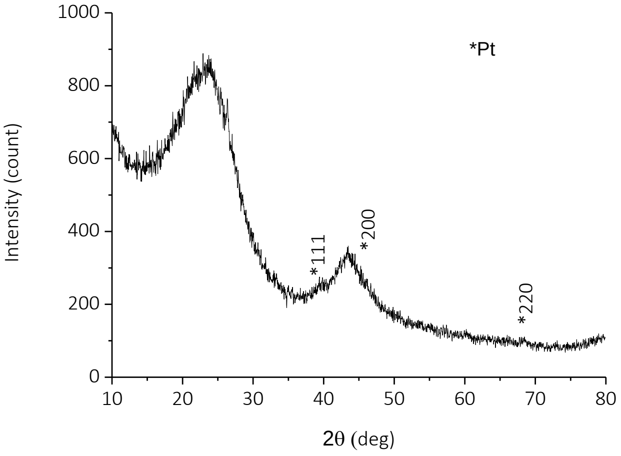

Figure 5-14: XRPD of Pt/AC 5%

The XRPD analysis

Figure 5-14 shows the presence of very small crystal domains (< 10 nm) of Pt (Sherrer's equation). The peak at 25° can be attributed to the graphite crystal domains present in the carbon support. The peak at 38° is ascribable to Pt (111), while the peaks at 44° and 77° are Pt (200) and Pt (220), respectively.

5.4.4 *t,t*-MA hydrogenation in synthetic fermentation broth

Once proven the good performances of the catalyst on MA, the same hydrogenation conditions were repeated on the *cis,cis*-MA, with the same good results. However, thinking to the industrial process, a solution with the sole *cis,cis* isomer is unlikely to be found, given the spontaneous rearrangement to the *cis,trans* form in acidic environment. Still, the *cis,cis* form could be preserved, as long as any crystallization step on the fermentation broth is excluded. Consequently, we tried to hydrogenate a synthetic solution, which could mimic the salt buffer of the fermentation, assuming that the broth was previously clarified from the microorganisms and treated by means of ultrafiltration and activated carbon to remove all the biological matter. The synthetic fermentation broth contained *cis,cis*-muconic acid (Sigma Aldrich) (28 g/L), Na_2HPO_4 (50 g/L), KH_2PO_4 (15 g/L), NaCl (2.5 g/L) and NaOH (40 g/L).

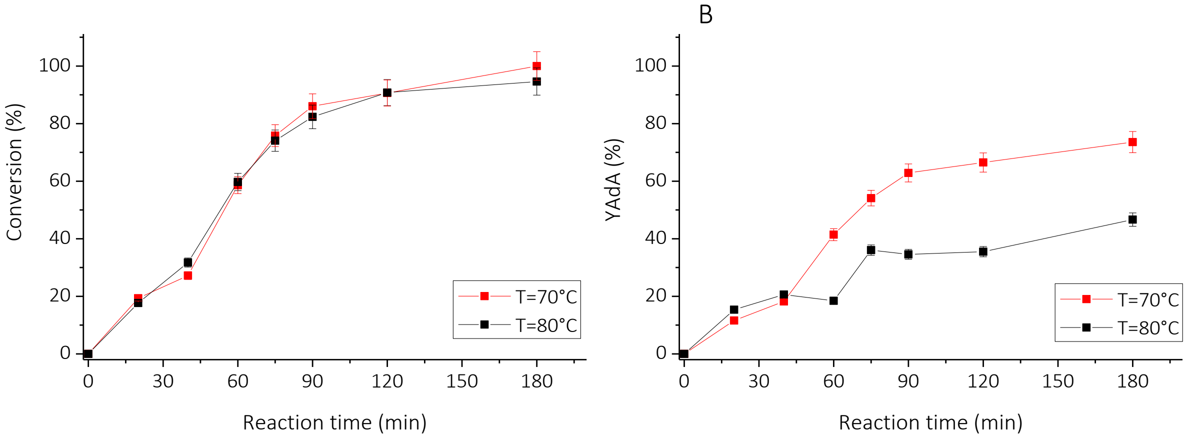

Figure 5-15: conversion of sodium muconate (A) and AdA yield (B) in M9 fermentation broth

In presence of salt, the reaction is sensibly slower (Figure 5-15): AdA yield after 180 min is only 73% despite the conversion reaches value of 100%. This result can be explained considering the salts concurrent adsorption on the catalyst surface and confirms the need to perform the hydrogenation on a substrate with the highest reachable purity. This would be beneficial also on the duration of the catalyst, as in absence of the growth support salts the noble metal poisoning would be prevented. To verify the adsorption of salty species on the surface of the catalyst or within its pores, a conductivity analysis was performed on M9 broth without and with catalyst and without/with muconic acid.

Conductivity analyses performed on M9 fermentation broth and the reacted solution revealed that the addition of MA to M9 broth increased the conductivity from 55.2 mS from 77.4 mS. This could be explained due to the dissociation of MA into muconate ions. The catalyst recovered from the reacted solution was washing with 10 ml of hot distilled water at 70 °C for 10 minutes under magnetic stirring. The results are reported in Table 5-4.

After 8 washes the water used during the washing has the same conductivity of distilled water (Figure 5-16). The washings help to clean the catalyst that might be adsorbed different salty species, blocking the pores. The conductivity study was also performed on M9 broth in presence of Pt/AC catalyst without the addition of MA. M9 growth support has a conductivity of 81.31 mS at 80 °C. After the addition of Pt/AC 5% the conductivity decreases of about 30% after 30 min, this means that the catalyst adsorbs the different salts. When MA was added higher values of conductivity were measure respect to Pt+M9 sample. Therefore, MA must compete with all the other species to reach and to be adsorbed on the catalyst surface, that implies low reaction rate and low conversion respect to the reaction performed in distilled water.

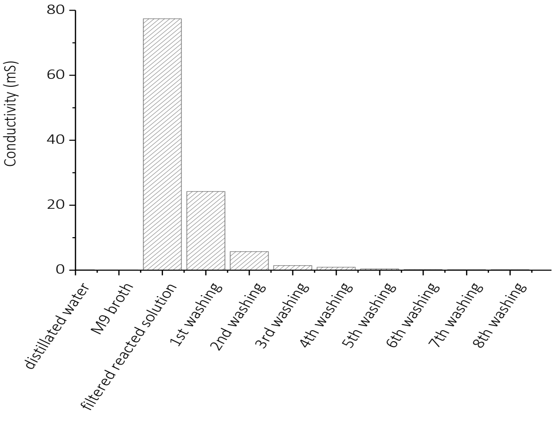

Figure 5-16: conductivity measurement on Pt/AC 5% in M9 broth with t,t-MA during the catalyst washing test

Table 5-4: conductivity tests on M9 broth and catalyst washing

	Conductivity (mS)
Distilled water (70 °C)	0.106
M9 broth (70 °C)	55.2
Filtered reacted solution (70 °C)	77.4
Washing with water (70 °C)	
1st washing	24.2
2nd washing	5.7
3rd washing	1.4
4th washing	0.880
5th washing	0.366
6th washing	0.180
7th washing	0.152
8th washing	0.141
Pt in M9 no MA (80 °C)	
M9 (80 °C)	82.31
Pt+M9 (30 min)	58.62
Pt+M9 (70 min)	61.21
Pt+M9 (110 min)	61.02
Pt+M9 (180 min)	60.83
Pt in M9 with MA (80 °C)	
Pt+M9+MA (30 min)	86.6
Pt+M9+MA (60 min)	86.7
Pt+M9+MA (120 min)	91.3
Pt+M9+MA (180 min)	89.4

5.4.5 *t,t*-MA hydrogenation in light alcoholic solvent

Hydrogenation of *t,t*-MA was tested using ethanol and methanol. In this case, due to the higher solubility of muconic acid in organic solvent, no salification was performed. The reactions occurred in the stainless-steel autoclave at different temperature keeping constant all the other operating parameters.

- H_2 pressure= 4 bar;
- Temperature= 50-90 °C;
- Stirring= 500 rpm;
- Catalyst: commercial Pt/AC 5% (0.1 g) pretreated at 200 °C for 3h at 6 bar of hydrogen;
- [*t,t*-MA]= 0.054 M (10 mL).

5.4.5.1 Ethanol

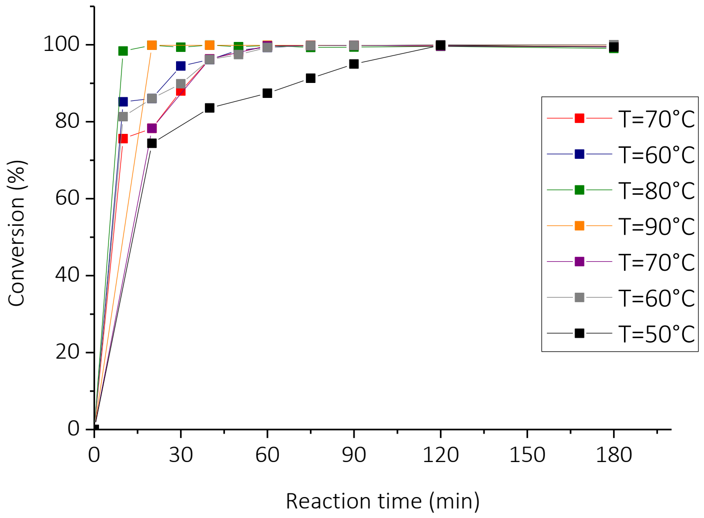

Figure 5-17: t,t-MA conversion in EtOH at different temperatures

As reported in Figure 5-17 the conversion rate is low at 50 °C, while for 60 and 70 °C the conversion is more or less equal. Increasing the temperature, the conversion increases and after 15 min full conversion of MA was reached.

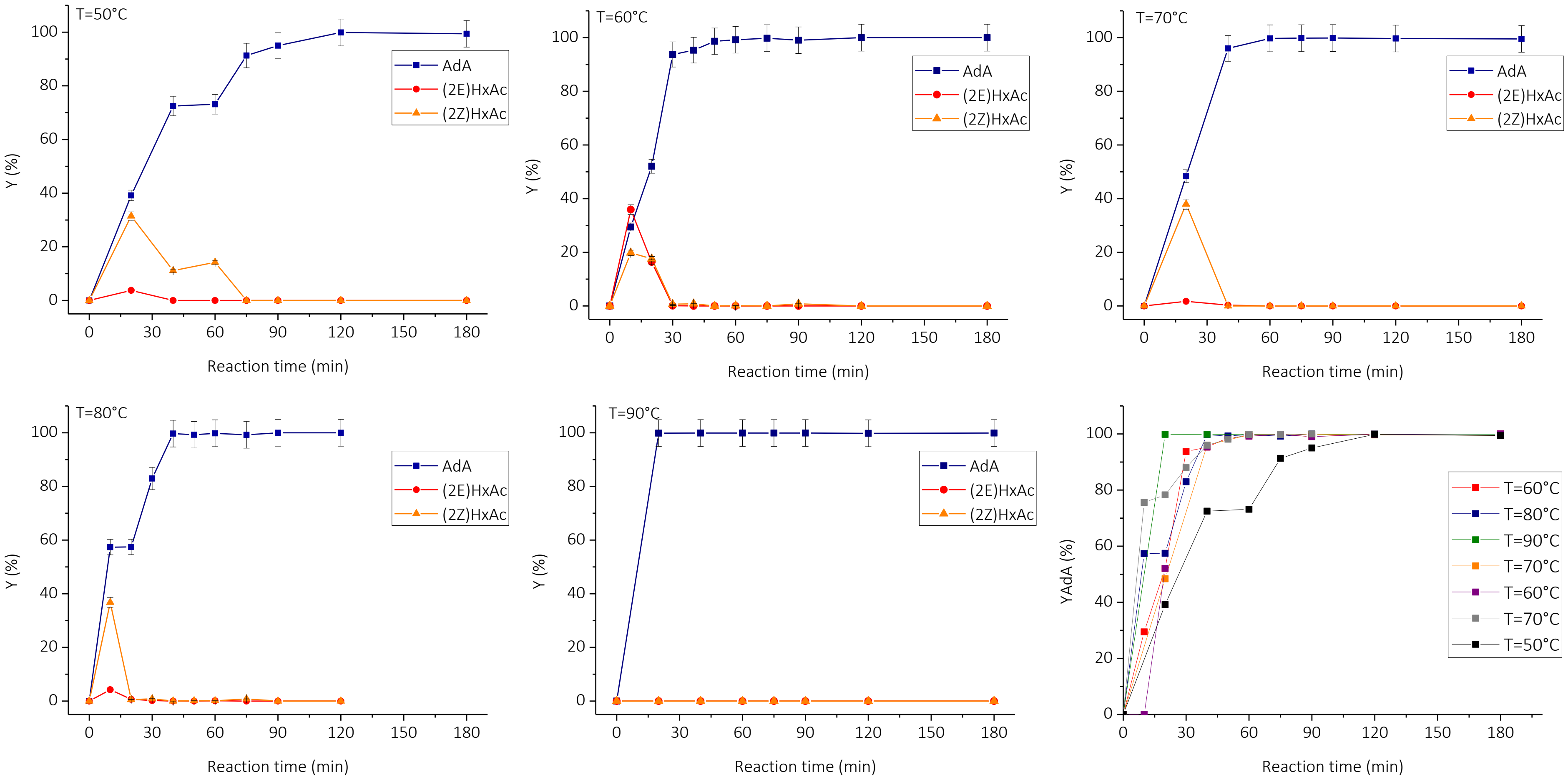

Figure 5-18: yield of the reaction products (A,B,C,D,E) and AdA at different temperatures in EtOH at P(H_2)=4 bar, [t,t-MA]=0.054 M (10 mL)

The yield of all the compounds and the yield to AdA at different temperature are reported in Figure 5-18. For temperature between 50 and 80 °C (2Z)HxAc was observed as main reaction intermediate, while at 90 °C no intermediates formation were observed. Therefore, the reaction tends to directly produce AdA. AdA yield follows the temperature raise, but the differences are more evident for 50 and 90 °C. At 50 °C full yield to AdA was reached only after 120 min of reaction, while for temperature equal to 90 °C a full yield to AdA was obtained after 15 minutes.

Comparing the results with the ones obtained using Na-Muc in water, it is possible to asses that in EtOH the reaction proceeded faster and also AdA yield achieved greater values in lower reaction time. This behavior could be explain hypothesizing a parallel mechanism of reaction that is able to produce hydrogen useful for the reaction: the hydrogen transfer catalysis.

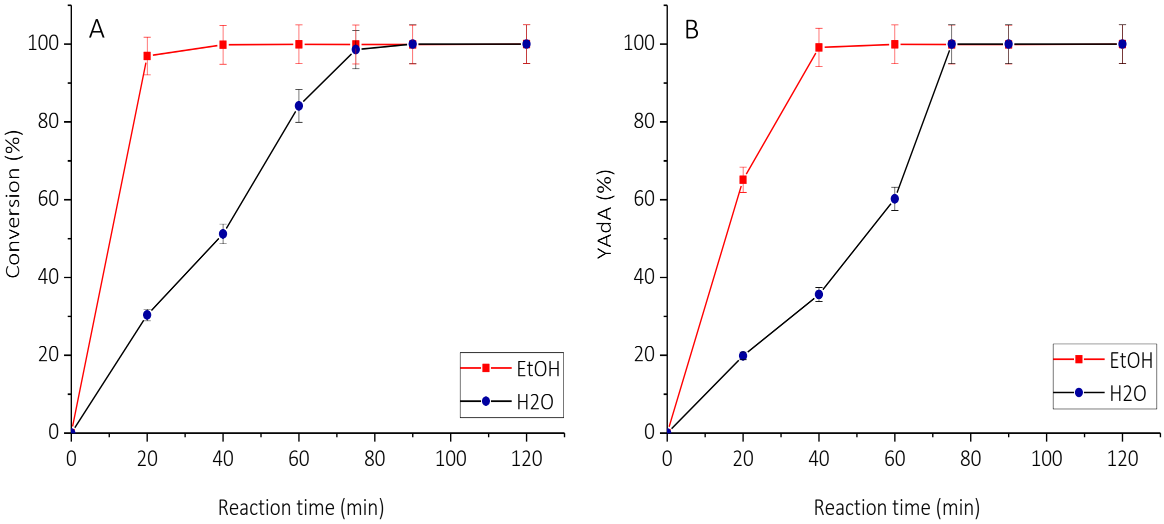

Figure 5-19: comparison of the conversion (A) and AdA yield (B) in water and EtOH at T=70 °C P(H_2)= 4 bar, stirring= 500 rpm

5.4.5.2 Methanol

The same reaction was also performed in Methanol (MeOH) to explore the behavior of the reaction. Full conversion and selectivity toward AdA were achieved in 90 minutes, while for EtOH the same results were obtained in 60 min (Figure 5-20).

In Figure 5-21 a comparison between the results obtained using EtOH and MeOH as solvent are shown. *t,t*-MA conversion and AdA yield are comparable although in AdA yield seems that EtOH is able to faster convert MA into AdA than MeOH. Due to the higher toxicity of MeOH, the choice between these two alcoholic solvents falls back (without doubt) on ethanol, which is also used into MA crystallization and purification steps (see Chapter 8).

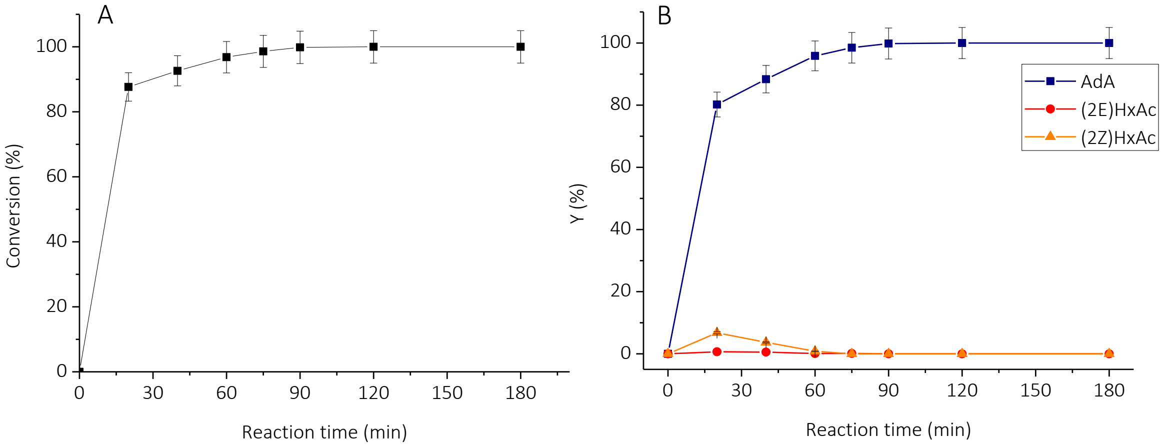

Figure 5-20: conversion (A) and AdA yield (B) in MeOH at T=70 °C and P(H_2) = 4 bar

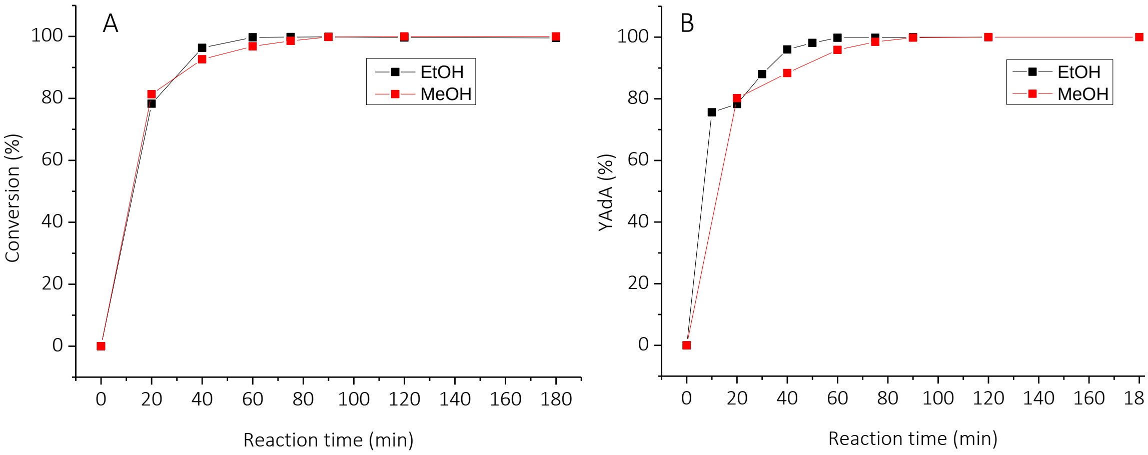

Figure 5-21:comparison of the results in term of t,t-MA conversion (A) and AdA yield (B) in alcoholic solvent at 70 °C and P(H_2) = 3 bar

5.5 Pd/AC 5% commercial catalyst

Palladium based catalysts are known as good catalyst for hydrogenation reactions.
The possibility to directly use the catalyst without pre-treatment,[22,23] the high activity of the catalyst at low temperature and atmospheric pressure[24] and the lower price respect to the Pt based catalyst make this material a good substitute of the expensive Pt/AC.[25] A systematic study varying the operating conditions was performed, trying to decrease the amount of catalyst as much as possible, and working at low temperature (50-70 °C) and atmospheric pressure (1-3 bar). Moreover, a double comparison between sodium muconate and *t,t*-MA hydrogenation was also performed to study the different activity of the catalyst toward these compounds. MA production, recovery, and purification processes affect the final chemical configuration of MA. MA is produced through bacterial fermentation as *cis,cis*-sodium muconate but after its separation from the bacterial cells (for example using acidic environment) it is converted to *cis,cis* and *cis,trans*-MA.[26] Further purification step that occurs in ethanol and hydrochloridric acid isomerizes almost completely the *cis-cis* form into *trans-trans* configuration. Therefore, we decided to use sodium muconate and *t,t*-MA as substrate to study and find the best choice regarding the starting substrate.

5.6 Fresh catalyst characterization

5.6.1.1 BET

Bet surface area of the fresh Pd/AC 5% commercial catalyst is 812.3 m^2/g. The desorption pore diameter was evaluated using BJH method[27] and the result is 3.79 nm. The total pore volume for pores with diameter less than 147.03 nm (at $P/P_0=0.9868$) is 0.732 cc/g, while using the DR method[28] the cumulative desorption pore volume is 0.363 cc/g.

5.6.1.2 XRD

XRD pattern was collected using Bruker D8XR instrument. Figure 5-22 shows the results of the analysis for the fresh catalyst. The broad peaks at 25° and 45 ° corresponds to the (002) and (101) planes of low-graphitized carbonaceous structure, this indicates that the porous carbon material is disordered or amorphous.[29,30] Other peaks were also observed at 2θ= 40°, 46° and 68 °, attributed to the (111), (200) and (220) planes of the face-centred cubic (fcc) crystal structure of palladium oxide.[31]

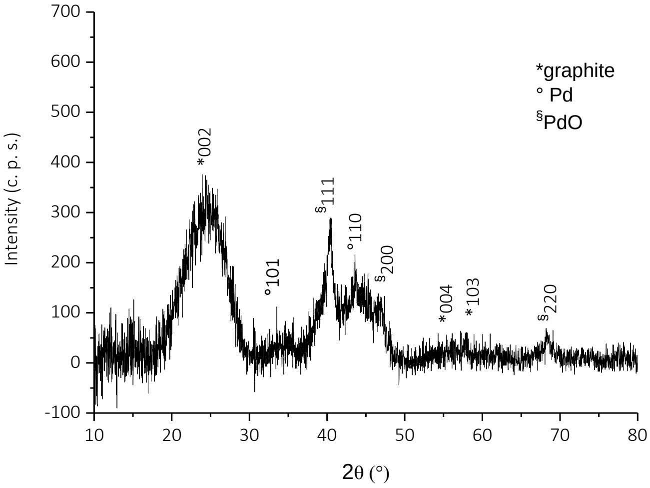

Figure 5-22: XRD pattern of commercial fresh Pd/AC 5%

5.6.1.3 SEM/EDX

SEM/EDX analysis was performed using a HITACHI analytical TableTop Microscope / Benchtop SEM TM3030.

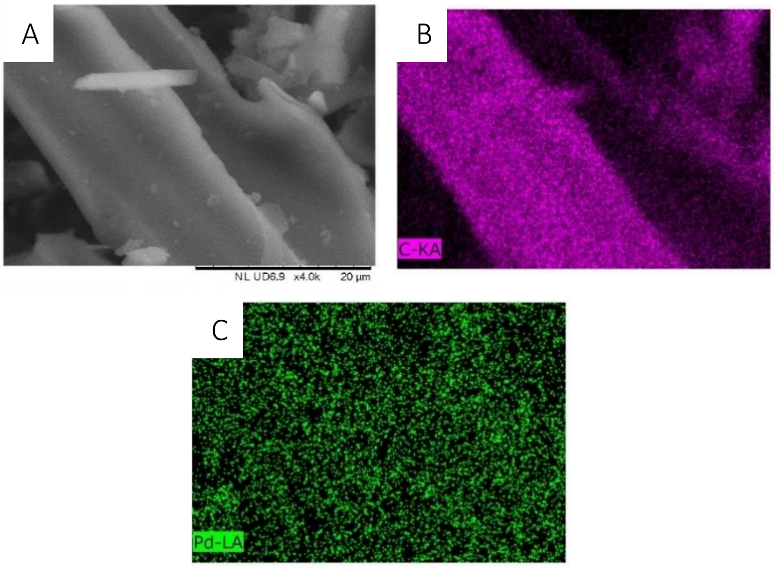

Figure 5-23: TEM of fresh Pd/AC 5% catalyst (A) and EDX maps of the image (B, C)

Pd NPs were well dispersed on the surface of the carbon support (Figure 5-23). This allows to perform different reactions with different batch of catalyst without affecting reproducibility. Fresh catalyst is composed by coal grains that have very different size (5-100 µm) (Figure 5-24).

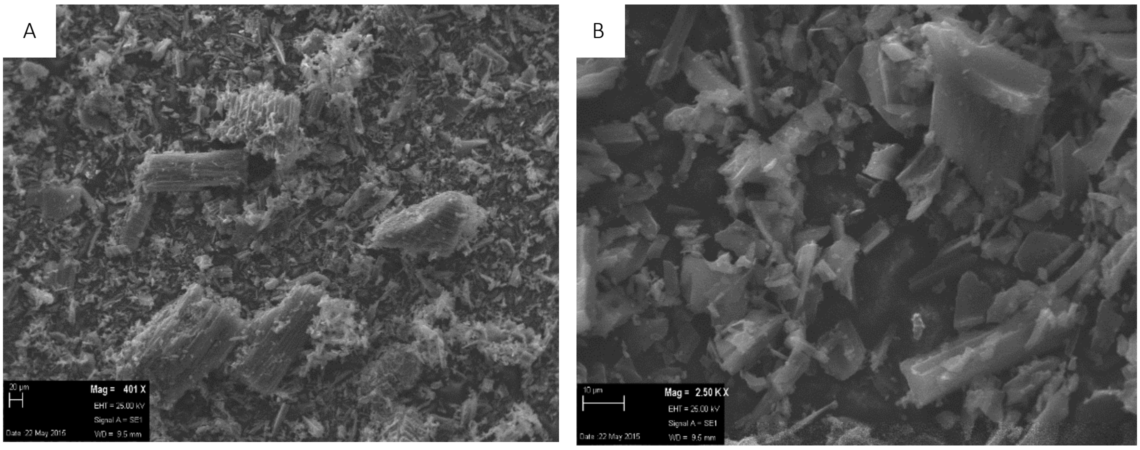

Figure 5-24: SEM images of fresh Pd/AC 5% at 40 KX (A) and 250 KX (B)

An elemental analysis was also performed to evaluate the amount of different chemical element present in the catalyst. A huge portion of particle was chosen allowing a good composition evaluation. The results are reported in Table 5-5.

Table 5-5: elemental analysis on fresh Pd/AC 5%

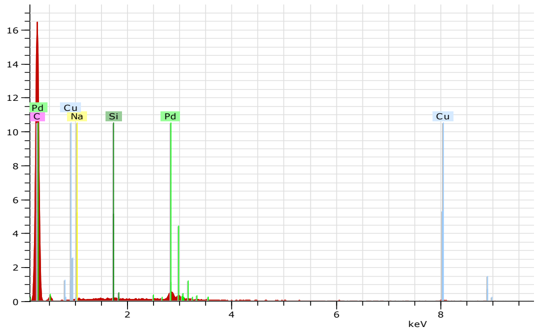

Element	AN series	Norm (wt%)	C atom (at%)	Error
Carbon	6 K	89.78	98.06	6.1
Palladium	46 L	5.12	0.63	0.1
Copper	29 K	4.27	0.88	0.1
Sodium	11 K	0.44	0.25	0.0
Silicon	14 K	0.38	0.18	0.0

The activated carbon is not only composed by carbon and oxygen, but there is the presence of copper, sodium and silicon in traces. The palladium amount is 5.12 % (error 0.1) that exactly corresponds to the specification sheet of the home maker.

5.6.1.4 TEM

Transmission electron microscopy (TEM) and scanning transmission electron microscopy (STEM) were performed on a JEOL JEM-2100 operating at 200 kV. Energy dispersive X-ray analysis (EDX) was done using an Oxford Instruments X-Max^N 80 detector and the data analysed using the Aztec software. Samples were prepared by dispersion in ethanol by sonication and deposited on 300 mesh copper grids coated with holey carbon film.

At about 200 NPs were considered to evaluate the particle size distribution (PSD). The study was performed using ImageJ program. The PSD was calculated using the Lognormal distribution.

Metal Pd particles are well dispersed on the carbon support Figure 5-25 (A and B) and their average size is 3.3±0.3 nm (Figure 5-25 C) . Moreover, Figure 5-25 (B) revealed 0.225 nm spacing of the lattice fringes which is consistent with the Pd(111) lattice plane.[32]

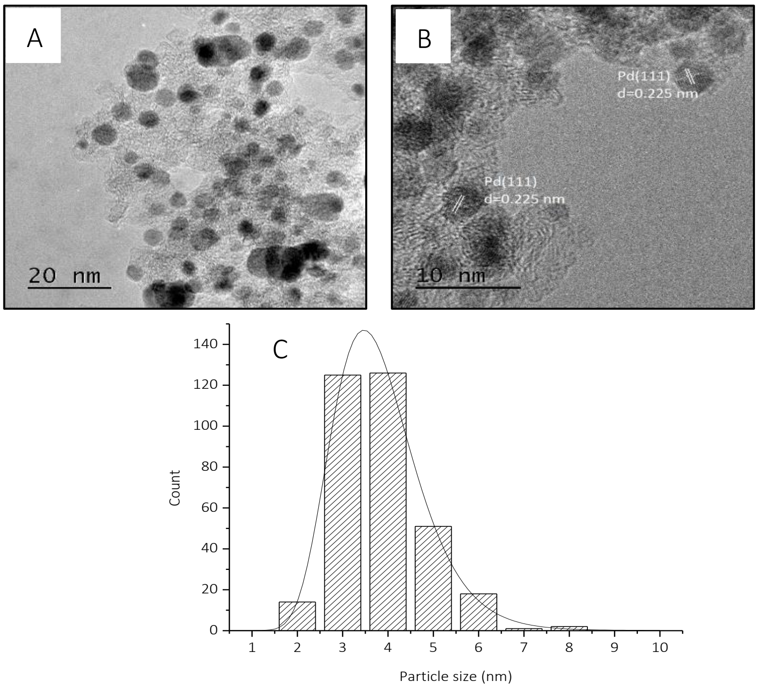

Figure 5-25: TEM images(A), evaluation of the lattice fringe of Pd(111) specie (B) and particle size distribution (C) for fresh commercial Pd/AC 5% catalyst

5.6.1.5 X-ray photoelectron spectroscopy (XPS)

X-ray photoelectron spectroscopy (XPS) was performed on a Thermo Scientific K-alpha$^+$ spectrometer. Samples were analyzed using a monochromatic Al x-ray source operating at 72 W (6 mA x 12 kV), with the signal averaged over an oval-shaped area of approximately 600 x 400 microns. Data was recorded at pass energies of 150 eV for survey scans and 40 eV for high resolution scan with a 1eV and 0.1 eV step size respectively.

Charge neutralization of the sample was achieved using a combination of both low energy electrons and argon ions (less than 1 eV) which gave a C(1s) binding energy of 284.8 eV.

All data were analyzed using CASAXPS (v2.3.17 PR1.1) using Scofield sensitivity factors and an energy exponent of -0.6.

Figure 5-26 shows the fitted Pd 3d core-level XPS spectra of the fresh commercial Pd/AC 5%.

Each Pd species displayed two peaks due to the Pd $3d_{3/2}$ and Pd $3d_{5/2}$ transition. Pd(0) $3d_{5/2}$ core electron binding energy is at 335.6 eV, while the Pd(0) $3d_{3/2}$ is at 340.54 eV. The Pd(II) peaks are at

343.46 and 338.18 eV, and they are identified as $3d_{3/2}$ and $3d_{5/2}$ transition, respectively. These binding energy values are in good agreement with that data reported in Chen et al. and Sanchez et al.[32,33]
As reported in Table 5-6, fresh Pd/AC catalyst is equally composed by Pd oxide and Pd metal. Despite the active phase for hydrogenation reactions is the bare metal, it is possible to directly use the catalyst avoiding the pre-treatment. In fact, in reducing conditions the metal oxide can be easily transform to the active metal 0 state.

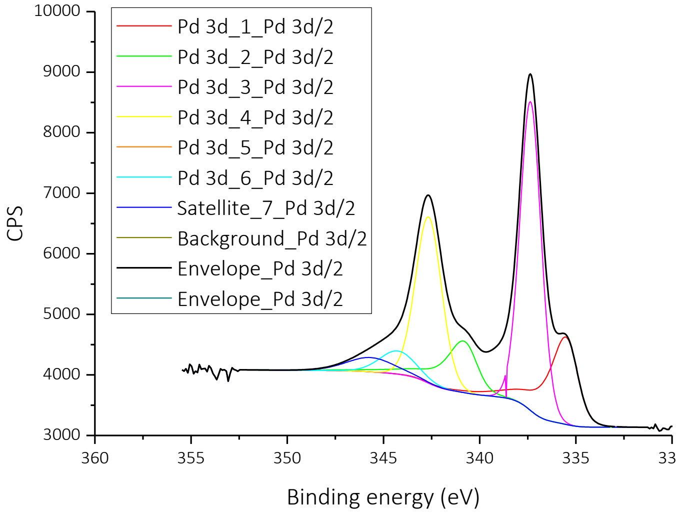

Figure 5-26: XPS analysis on fresh commercial Pd/AC 5% catalyst

Table 5-6: evaluation of the percentage of Pd(0) and Pd(II) in the fresh catalyst

	$Area_{Pd(0)}$	$Area_{Pd(II)}$	Sum	$Area_{Pd(0)}$ (%)	$Area_{Pd(II)}$ (%)
$Pd3d_{5/2}$	3672	3222	6894	53.3	46.7
$Pd3d_{3/2}$	3220	3098	6318	50.9	49.1

The ratio between Pd and PdO for the $3d_{5/2}$ and $3d_{3/2}$ configurations are 1.14 and 0.52, respectively.

5.6.1 Hydrogenation reaction in stainless steel autoclave

Hydrogenation reactions were performed both in autoclave and in glass reactor. Substrate/catalyst ratio, temperature, stirring, substrate concentration and pressure were varied using *t,t*-MA an Na-Muc as substrate and distilled water as solvent The tests at 2 and 3 bar of hydrogen were performed in the autoclave. Tests at 1 bar were also performed in the glass reactor, allowing to use a large amount of substrate and to collect a proper amount of post reaction catalyst to use for the characterization.

5.6.1.1 Catalyst to substrate ratio optimization

The catalyst/substrate ratio is one of the most important parameters because it affects the mass transport and diffusion phenomena, and in industry, it might influence the cost of the process (in particular if noble metals are involved in the reaction).

Different hydrogenation reactions were performed varying the amount of catalyst and keeping constant all the other operating parameter. The reactions were performed using the following operating parameter:

- temperature=70 °C;
- static pressure of hydrogen= 3 bar;
- concentration of *t,t*-MA and Na-Muc= 1.43E-02 M;
- magnetic stirring= 500 rpm;
- solvent= distilled water;
- catalyst= Pd/AC 5% (Sigma Aldrich);
- reaction time= 60 min;
- reactor= stainless steel reactor.

The catalyst/substrate ratio is expressed as mol of metal divided by the mol of substrate used for the reaction. The results are reported in Table 5-7 and Figure 5-27.

Table 5-7: Results for catalyst/substrate ratio optimization

Cat/substrate (mol_{Pd}/mol_{sub})	*t,t*-MA		Na-Muc	
	Conversion (%)	YAdA (%)	Conversion (%)	YAdA (%)
1/10	99.42	99.09	98.87	98.69
1/100	99.13	99.13	92.82	69.79
1/200	99.62	99.49	97.68	41.89
1/500	98.65	98.23	90.12	37.26

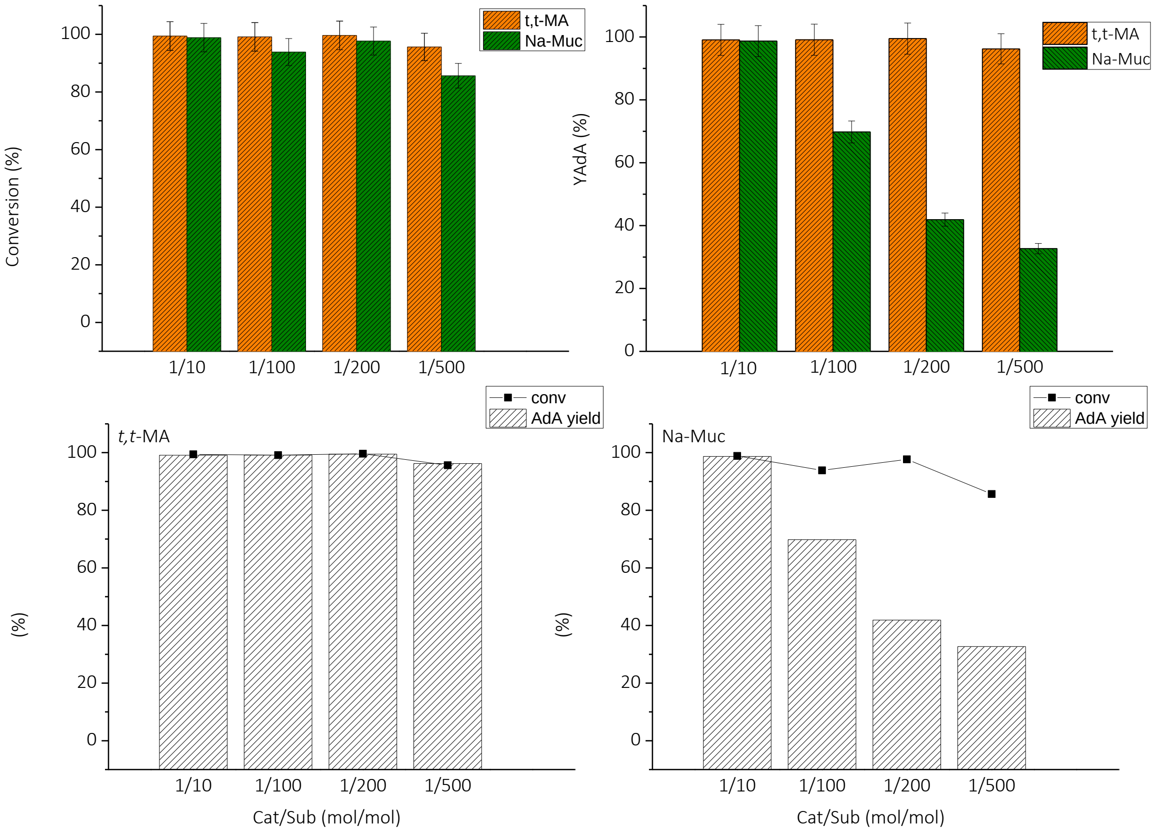

Figure 5-27: conversion and YAdA evaluation at different cat/sub (mol$_{Pd}$/mol$_{sub}$) ratio for t,t-MA and Na-Muc

As reported in Figure 5-27 the fast hydrogenation of *t,t*-MA did not allow to study the dependence of the conversion from the catalyst/substrate ratio: the conversion is high for all the tests. Different results were obtained using Na-Muc, the conversion decreases reducing the amount of catalyst.

For high amount of catalyst, the conversion and the selectivity are higher than the results obtained using lower amount of catalyst. With a cat/sub ratio equal to 1/200 the yield to AdA produced from Na-Muc hydrogenation is the half respect to the one obtained using *t,t*-MA. The behaviour might be explained considering the different pH of the substrate solution: *t,t*-MA has a pH equal 3.66 while Na-Muc solution is a pH equal to 11.45. In fact, pH has a wide influence on the ionic state of MA. At low pH AdA is completely undissociated while at high pH it is completely dissociated; this behaviour might deeply affect the adsorption/desorption process the reactivity and therefore the reaction rate.[34]

We decided to perform the further hydrogenation reaction using the catalyst to substrate ratio equal to 1/200 to allow a good and precise weight of the catalyst.

5.6.1.2 Pressure effect

The hydrogen pressure plays a key role in hydrogenation reactions because it has to be enough to completely saturate the double bonds, but it might be not in too large excess to avoid the whole coverage of the catalyst surface. Moreover, the solubility and the amount of hydrogen in the reaction medium are strictly connected to the pressure. For this reason, different reactions were performed varying the pressure from 1 to 3 bar. The reactions were performed using the following operating parameters:

- temperature=70 °C;
- static pressure of hydrogen= 1-2-3 bar;
- concentration of *t,t*-MA and Na-Muc= 1.43E-02 M;
- magnetic stirring= 500 rpm;
- solvent= distilled water;
- catalyst/substrate (mol_{Pd}/mol_{sub}) =1/200;
- reaction time= 10 min;
- catalyst: commercial Pd/AC 5%;
- reactor= stainless-steel autoclave.

The results are expressed in term of initial activity (Eq.5-14) that was evaluated considering the amount of catalyst used for each test, the conversion and the time of the reaction.

$$Initial\ activity\ (s^{-1}) = \frac{Conversion\ (\%) \cdot C_s^0 \cdot V}{n_{Pd} \cdot reaction\ time \cdot 60\frac{s}{min}} \qquad \text{(Eq. 5-14)}$$

where:

C^0_s (M)= initial concentration of the substrate;

V (L)= liquid volume of the solution;

n_{Pd} (mol)= moles of Pd introduced in the reactor;

reaction time (min)= considered reaction time.

Table 5-8: value of the initial activity at different hydrogen pressures

Pressure (bar)	*t,t*-MA Initial activity (s^{-1})	Na-Muc Initial activity (s^{-1})
1	0.6034	0.2645
2	0.5532	0.2766
3	0.6034	0.3045

As shown in Figure 5-28 and in Table 5-8 the initial activity does not strictly depends on the pressure used to conduct the reaction both on *t,t*-MA or Na-Muc. However, a little difference is shown considering the initial activity at 1 and 3 bar for Na-Muc hydrogenation. Despite the initial activity (calculated starting from the conversion) is equal at the considering pressures, it is reasonable to suppose that the pressure may influence AdA yield. Therefore, to better understand the effect of hydrogen pressure on the reaction, kinetics studies were performed evaluating the conversion and the yield toward the intermediates and AdA. The results are reported in Figure 5-29 and Figure 5-30. Two different hydrogenation reactions were performed at 3 and 1 bar, respectively using Na-Muc as substrate. The pressure seems not to have a huge effect on the conversion (E) but AdA selectivity is widely affected by the pressure. At 1 bar of pressure and after 2 hours of reaction AdA yield is about 60%, while at 3 bar AdA yield is 100% after 2 hours.

Regarding the hydrogenation of *t,t*-MA the pressure does not affect the conversion, while it has a little influence on the yield of AdA. This behavior might be explained considering that the solubility of hydrogen is higher for electrolyte solution than in pure water containing organic acid.

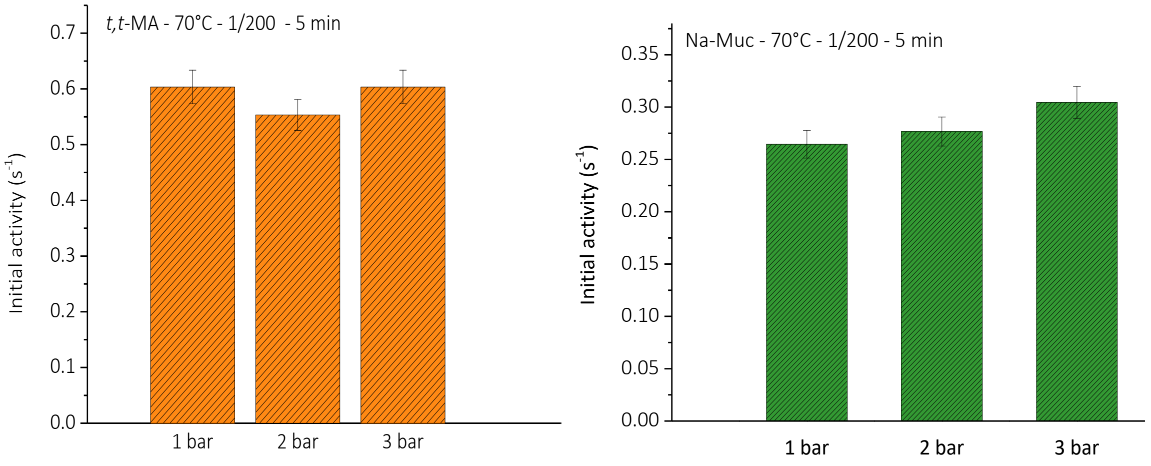

Figure 5-28: Initial activity at different pressure for t,t-MA (orange) and Na-Muc (green) hydrogenation

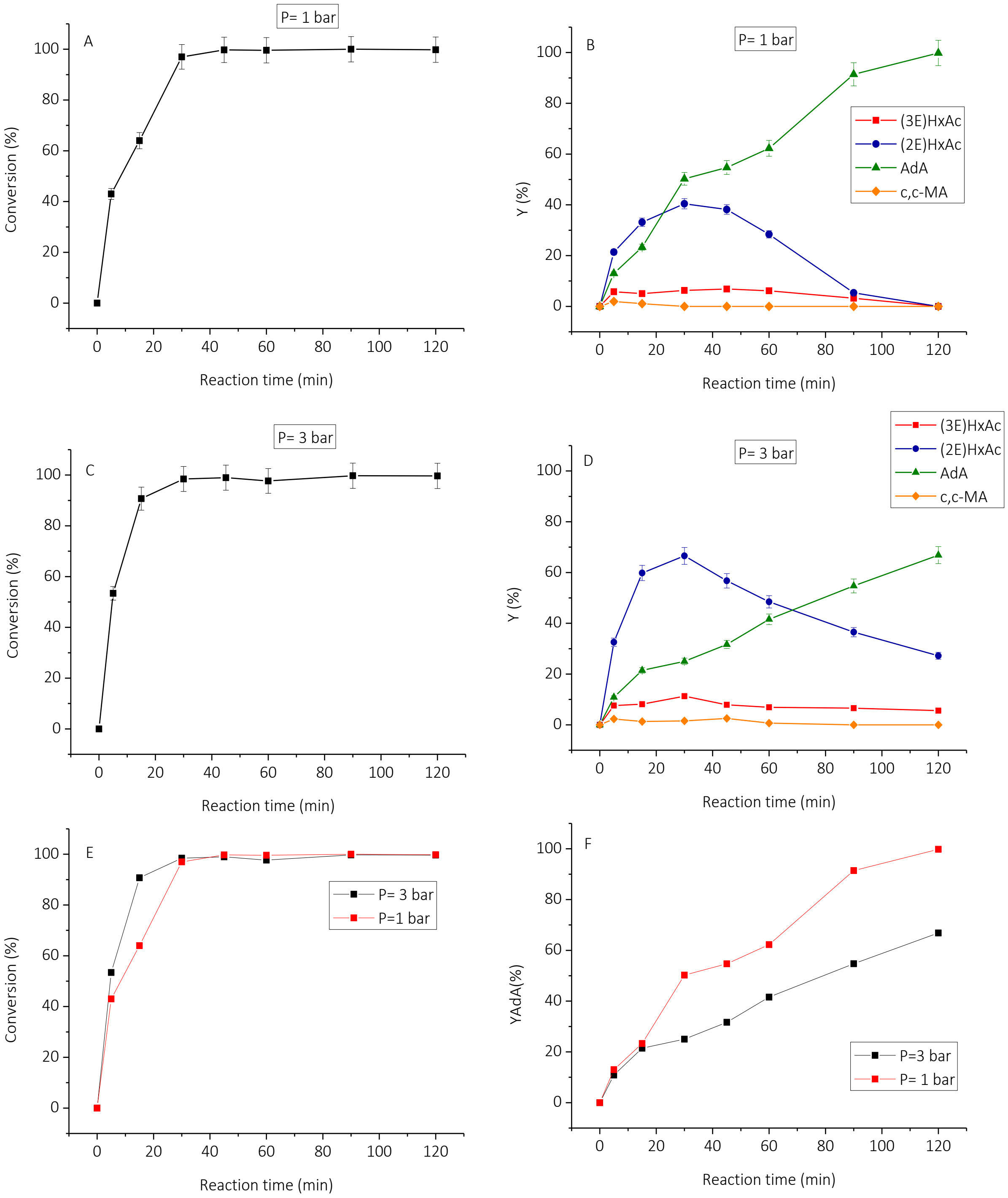

Figure 5-29: Pressure effects on conversion and yield using Na-Muc as substrate

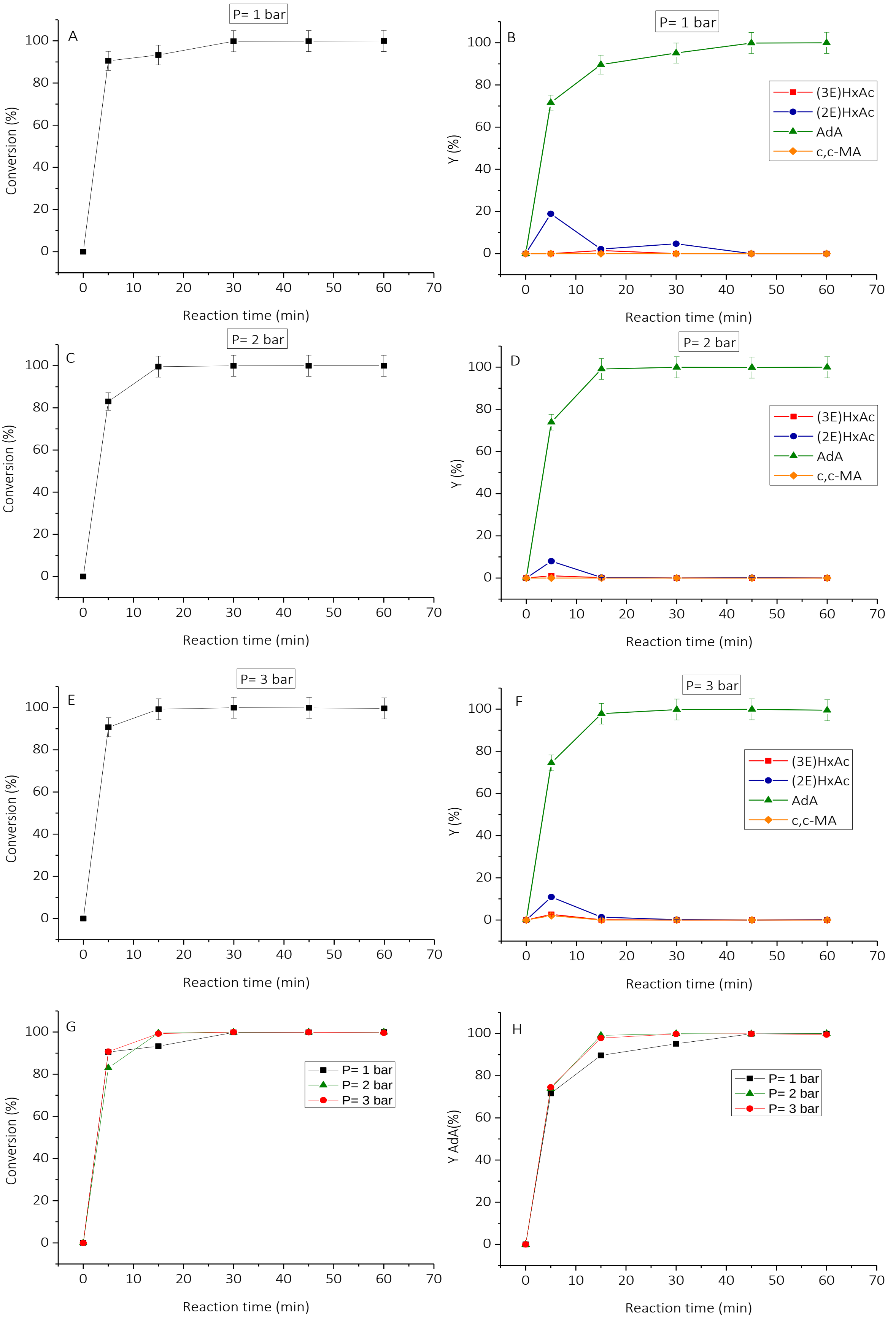

Figure 5-30: Pressure effects on conversion and yield using t,t-MA as substrate

5.6.1.3 Effect of sodium muconate concentration

The reaction was performed at:

- temperature=70 °C;
- static pressure of hydrogen= 1-3 bar,
- concentration of Na-Muc= 0.0101 M, 0.0143 M and 0.0184 M;
- magnetic stirring= 500 rpm;
- solvent= distilled water;
- catalyst/substrate (mol_{Pd}/mol_{sub}) =1/200;
- reaction time= 60 min;
- reactor= stainless-steel autoclave.

The effect of sodium muconate concentration was performed keeping constant the catalyst/substrate ratio and varying the starting concentration of Na-Muc solution. At the lowest concentration the conversion is 74.45% and 64.99% at 1 bar and 3 bar, respectively, while at higher concentration the conversion is constant. The yield of AdA changes varying the concentration and pressures. In fact, for high pressure AdA yield is greater than the one obtained at 1 bar of hydrogen. This behavior is also explained considering the results obtained in the previous paragraph.

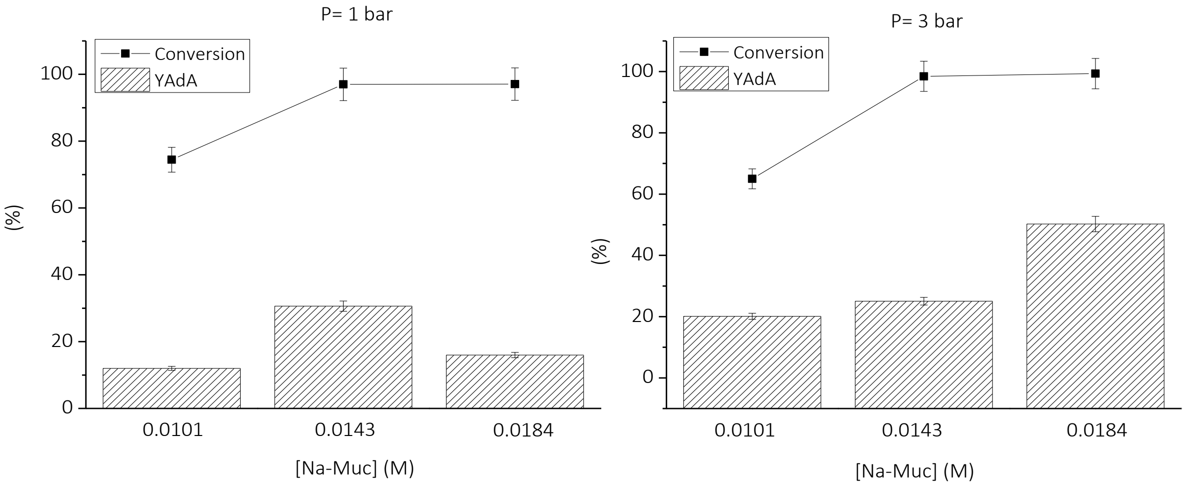

Figure 5-31: effect of Na-Muc concentration at different pressure

Table 5-9: results of the different concentration and pressure on Na-Muc conversion and YAdA

[Na-Muc] (M)	P=1 bar		P= 3 bar	
	Conversion (%)	YAdA (%)	Conversion (%)	YAdA (%)
0.0101	74.45	12.00	64.99	20.12
0.0143	97.00	30.63	98.45	25.06
0.0184	97.07	15.98	99.34	50.23

5.6.1.4 Temperature effect

Temperature effect was studied to evaluate the activation energy of the reaction and to verify the possibility to decrease the reaction temperature from 30 °C to 70 °C. In fact, thinking in industrial terms, can perform a reaction at 20 °C implies significant energy savings and therefore a lower cost of production. Hydrogenation reactions were performed at 30, 50, and 70 °C evaluating the conversion and the yield of AdA.

The operating parameters were:

- temperature=30-50-70 °C;
- static pressure of hydrogen= 1 bar,
- concentration of Na-Muc= 0.0143 M;
- magnetic stirring= 1200 rpm;
- solvent= distilled water;
- catalyst/substrate (mol_{Pd}/mol_{sub}) =1/200;
- catalyst: commercial Pd/AC 5%
- reaction time= 0-120 min;
- reactor= glass reactor.

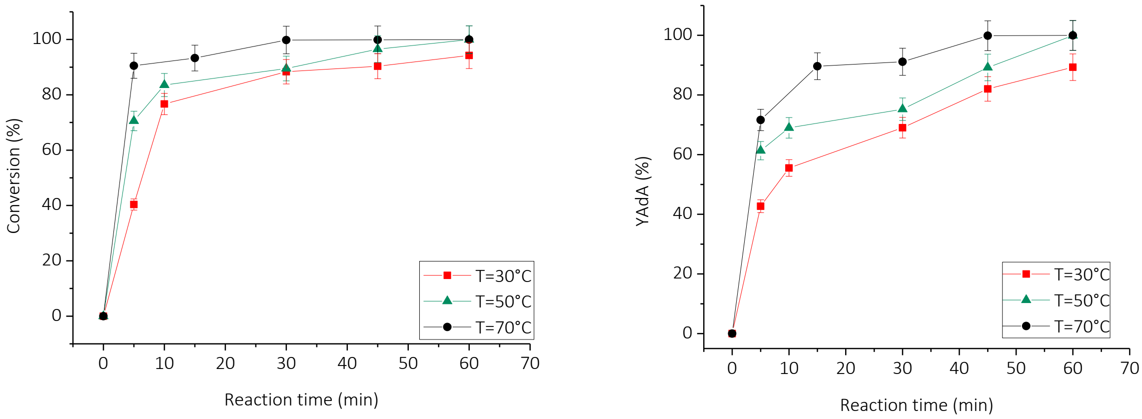

Figure 5-32: effect of temperature during t,t-MA hydrogenation

Higher the temperature higher is the conversion and in particular AdA yield (Figure 5-32). The temperature seems to have a positive effect on AdA yield even after 60 min 100% of AdA was reached at 50 °C and 70 °C. At 30 °C no full conversion and AdA yield were obtained after 1 hour of reaction. Figure 5-33 shows the production of the different reaction intermediates: (2E)HxAc is the main intermediate that is further hydrogenated to AdA, while the isomerization of *t,t*-MA to *c,c*-MA is negligible

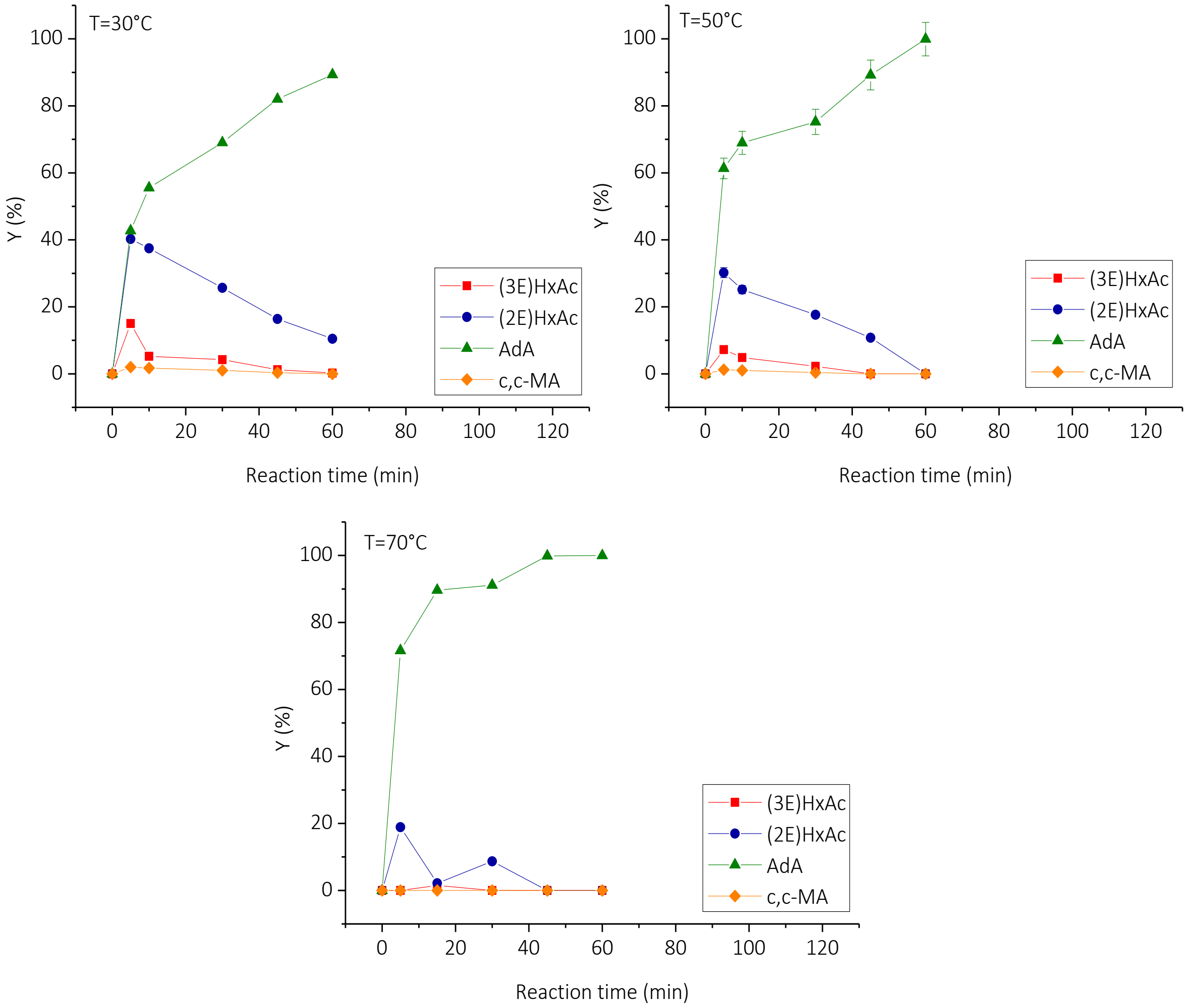

Figure 5-33: yield of the intermediates and AdA during t,t-MA hydrogenation reaction at different temperatures

Differently than shown during *t,t*-MA hydrogenation, the temperature is a discriminant operating parameter during Na-Muc hydrogenation. Conversion and AdA yield are rather affected from the temperature (Figure 5-34). At 30 °C after 90 min Na-Muc is completely converted to AdA but with a conversion of 67.55%. On the other hand, AdA yield strongly depends from the reaction temperature. Greater the temperature, higher the AdA yield. This behavior might be explained considering that the reaction rate depends on the temperature as well as the adsorption and desorption processes. Therefore, an increment in the temperature helps the adsorption/desorption process increasing the rate of the reaction and allowing to have more free active sites during the reaction. Interesting are the yield of the intermediates. At 50 °C (2E)HxAc is the main intermediates that is converted to AdA after 30 minutes of reaction (Figure 5-35).

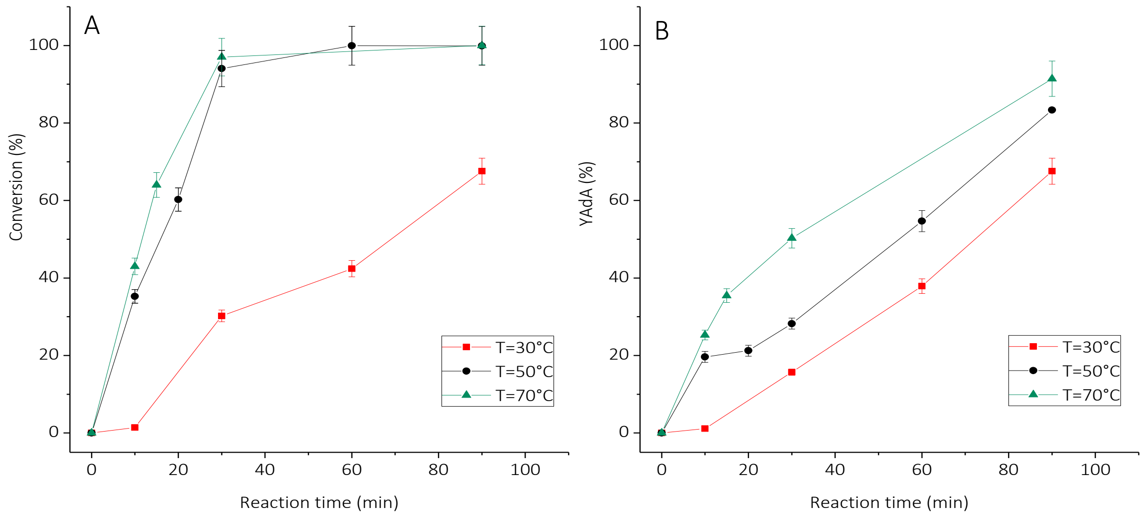

Figure 5-34: effect of temperature on conversion (A) and YAdA (B) during Na-Muc hydrogenation

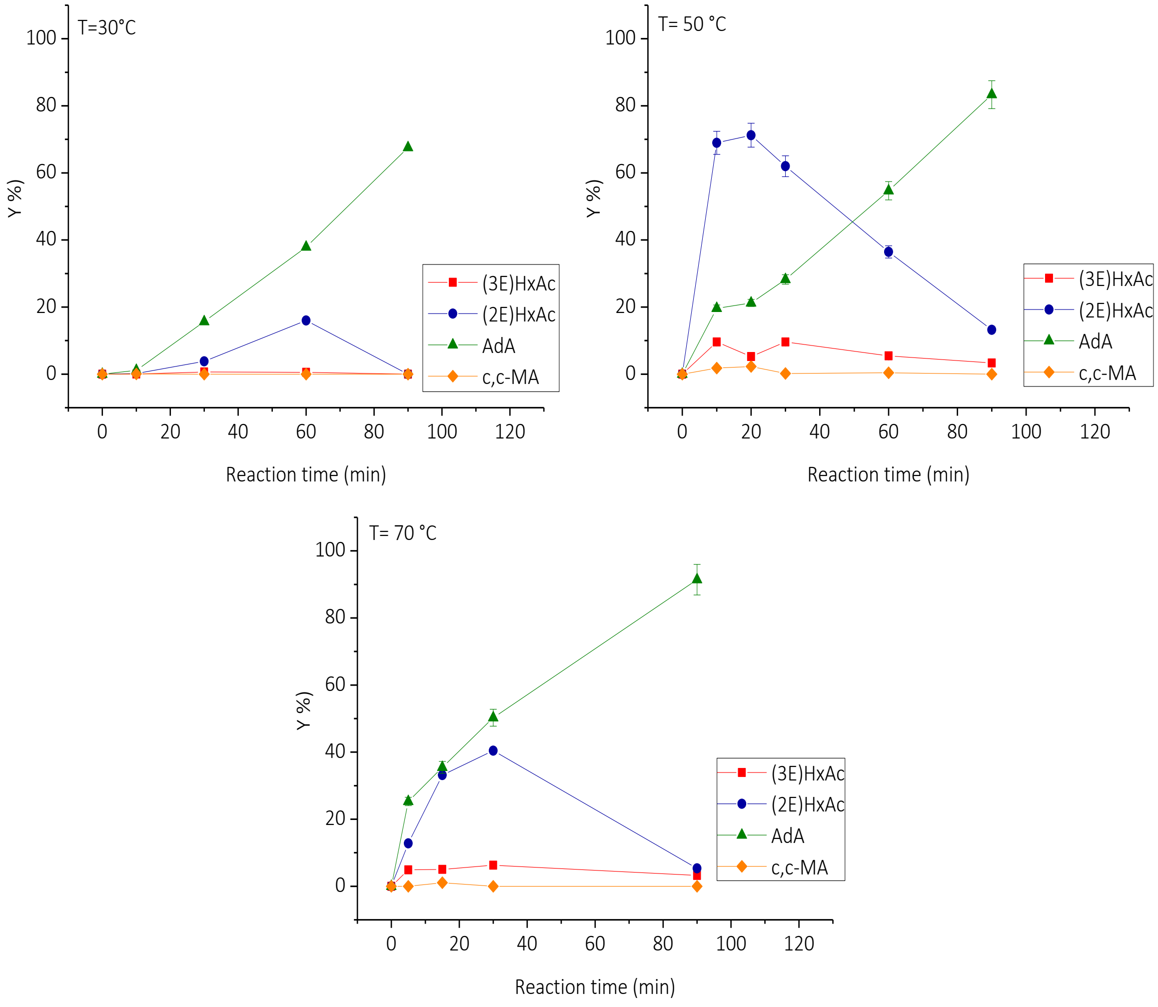

Figure 5-35: yield of the intermediates and AdA during Na-Muc hydrogenation reaction at different temperatures

5.6.1.5 Evaluation of the apparent activation energy

The study of the effect of temperatures allowed to evaluate the apparent activation energy of the two reactions. The activation energy was evaluated considering the Arrenhius' equation. Arrhenius' equation describes the effect of a change of temperature on the rate coefficient and therefore on the rate of the reaction:

$$k = A \cdot e^{\frac{-E_a}{RT}} \qquad \text{(Eq.5-15)}$$

where:

A= pre-exponential factor or the steric factor, which includes factors like the frequency of collisions and their orientation. It varies slightly with temperature, although not much. It is often taken as constant across small temperature ranges;

E_a= activation energy;

R= universal gas constant;

T(K)= the thermodynamic temperature;

k= kinetic constant.

The Eq.5-15 can be written equivalently as:

$$\ln k = lnA - \frac{E_a}{RT} \qquad \text{(Eq.5-16)}$$

Eq.5-16 has the same form of as an equation for a straight line y=mx + q, where x is the reciprocal of T. So, when a reaction has a rate constant that obeys Arrhenius' equation, a plot of ln(k) versus T^{-1} gives a straight line, whose gradient and intercept can be used to determine E_a and A. This procedure has become so common in experimental chemical kinetics that practitioners have taken to using it to define the activation energy for a reaction. That is the activation energy is defined to be (−R) times the slope of a plot of ln(k) vs. (1/T). This method can be applied considering a pseudo first order for the firsts minutes of reaction.

The data of the study are reported in Table 5-10 while the results are reported in Figure 5-36.

Table 5-10: data for the construction of the Arrhenius' plot

			ln(initial activity)	
Temperature (°C)	**Temperature (K)**	**Temperature (K^{-1})**	***t,t*-MA**	**Na-Muc**
30	303	0.00331	-1.87	-3.38
50	323	0.00310	-1.78	-2.42
70	343	0.00292	-1.69	-1.66

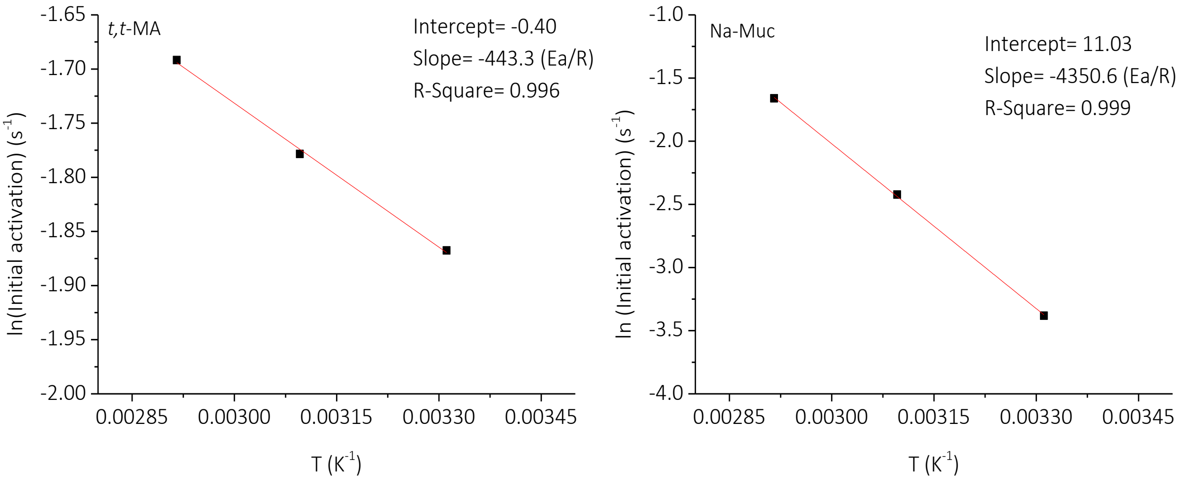

Figure 5-36: Arrhenius' plot for the apparent activation energy evaluation

The apparent activation energy was evaluated multiplying the slope by the universal gas constant R (8.314 J K^{-1} mol^{-1}). Therefore the calculated activation energy is: 3685 KJ/mol for the reduction of *t,t*-MA and 36170 KJ/mol for the hydrogenation of Na-Muc. Apparent activation energy for Na-Muc is one order of magnitude greater than the one related to the hydrogenation of *t,t*-MA. This confirm the behaviour previously found where Na-Muc reduction is slower than *t,t*-MA one. Moreover, at high temperature (so at low 1/T), the ln(initial activity) for the two reactions is similar, while for lower temperature we can verify the different conducts. As shown in Figure 5-37 increasing the temperature the gap between Na-Muc (dash line) and *t,t*-MA (solid line) raises.

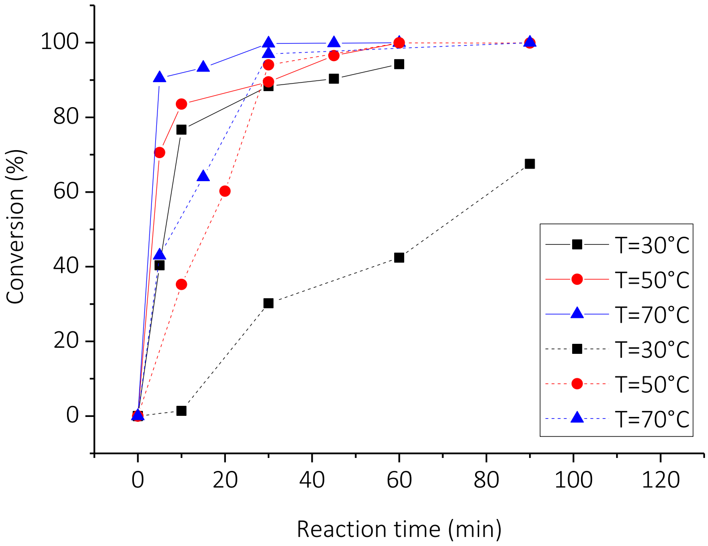

Figure 5-37: conversion of t,t-MA (solid line) and Na-Muc (dash line) at different temperatures

5.6.2 Hydrogenation reaction in glass reactor

Hydrogenation reactions at different catalyst/substrate ratio were performed using the glass reactor. This allowed better verifying the kinetic regime due to higher amount of substrate solution that it is possible to introduce in the reactor, and therefore a larger amount of catalyst, decreasing the weight error. The reactions were performed both on *t,t*-MA and Na-Muc solutions keeping constant all the operating parameters except the amount of catalyst.

The operating parameters were:

- temperature=70 °C;
- static pressure of hydrogen= 1 bar,
- concentration of Na-Muc and *t,t*-MA= 0.0143 M;
- magnetic stirring= 1200 rpm;
- solvent= distilled water;
- catalyst/substrate (mol_{Pd}/mol_{sub}) =1/10-1/700;
- reaction time= 10 min.

The results are reported in Table 5-11-12 and Figure 5-38.

Table 5-11: check of kinetic regime for t,t-MA hydrogenation

Cat/Sub (mol_{Pd}/mol_{sub})	t,t-MA initial activity (s^{-1})
1/10	0.02762
1/100	0.27536
1/200	0.5363
1/500	0.5563

Table 5-12: check of kinetic regime for Na-Muc hydrogenation

Cat/Sub (mol_{Pd}/mol_{sub})	Na-Muc initial activity (s^{-1})
1/200	0.2914
1/500	0.3274
1/700	0.3143

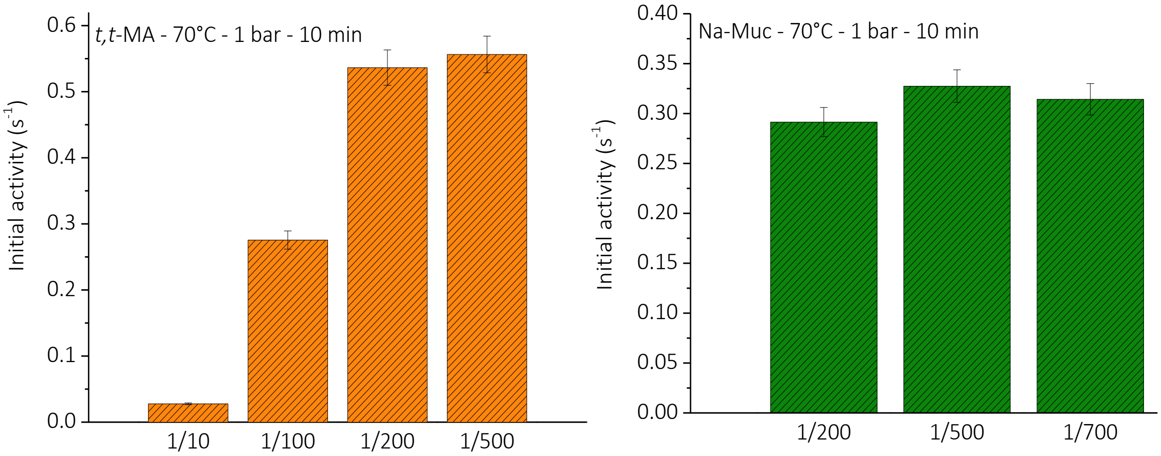

Figure 5-38: control of the kinetic regime during t,t-MA (orange) and Na-Muc (green)

From cat/sub ratio greater than 200 the initial activity is constant (Figure 5-38). Therefore, the reaction is occurring in kinetic regime avoiding the interference of mass transfer limitation. It is possible to reduce the amount of catalyst, but this implies a lower conversion. (Figure 5-39). Industrially speaking, the choice of the amount of catalyst is a compromise between the production and selectivity.

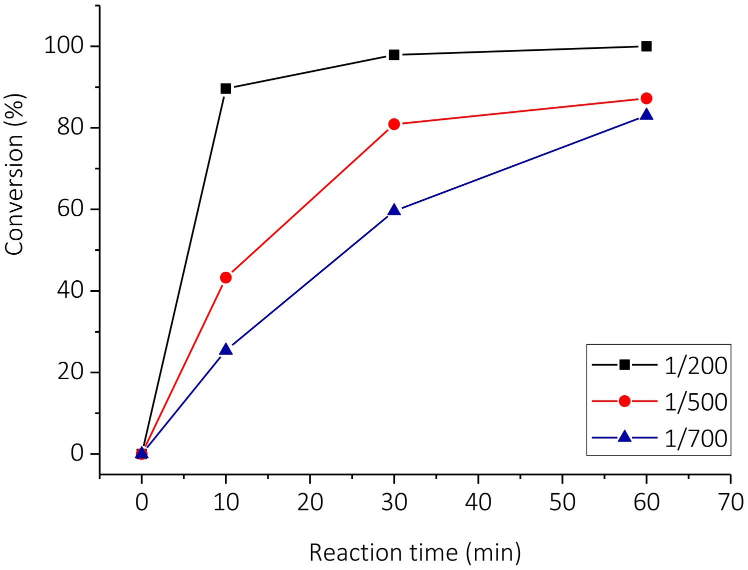

Figure 5-39: Na-Muc conversion at different cat/sub ratios

5.6.3 Used catalyst characterization

5.6.3.1 XPS (*t,t*-MA hydrogenation reaction)

Used catalyst recovered after the filtration was analyzed by XPS to understand the change in oxidations state of Pd during the reaction. Fresh catalyst and 3 samples of used catalyst at 15, 30 and 60 min have been characterized. Both Pd and C element were analyzed (Figure 5-40 and Figure 5-43, respectively).

Figure 5-41 shows the fitted Pd 3d core-level XPS spectra of the used commercial Pd/AC 5%.

Each Pd species displayed two peaks due to the Pd $3d_{3/2}$ and Pd $3d_{5/2}$ transition. Pd(0) $3d_{5/2}$ core electron binding energy is at 335.6 eV, while the Pd(0) $3d_{3/2}$ is at 340.54 eV. The Pd(II) peaks are at 343.46 and 338.18 eV, and they are identified as $3d_{3/2}$ and $3d_{5/2}$ transition, respectively. These binding energy values are in good agreement with that data reported in Chen et al. and Sanchez et al.[32,33]

Analysing the area of the deconvolution peaks the evaluation of the percentage of the two species was calculated as reported in Table 5-14. The oxidation state of the Pd varied during the reaction (Figure 5-41). In particular the two initial peaks of fresh catalyst were split in two. The yellow and red peak appear during the reaction while the blue and green ones disappear. Observing the deconvolution it is possible to notice that the red and yellow peaks belong to the Pd(0) state while the blue and green one at Pd(II) oxidation state. This means that during the reaction and in reducing environment the Pd(II) presents on the surface of the catalyst is reduced to metallic Pd.

Plotted the reaction time versus the Pd(0)% it is possible to see how the metal Pd amount increases during the reaction reaching a value of 95% (Figure 5-42).

Table 5-13: percentage of Pd(II) and Pd(0) at different reaction time

Sample	Pd 3d (II) (%)	Pd 3d (0) (%)
0 min	49.90	50.10
15 min	31.26	68.74
30 min	24.97	75.03
60 min	5.03	94.67

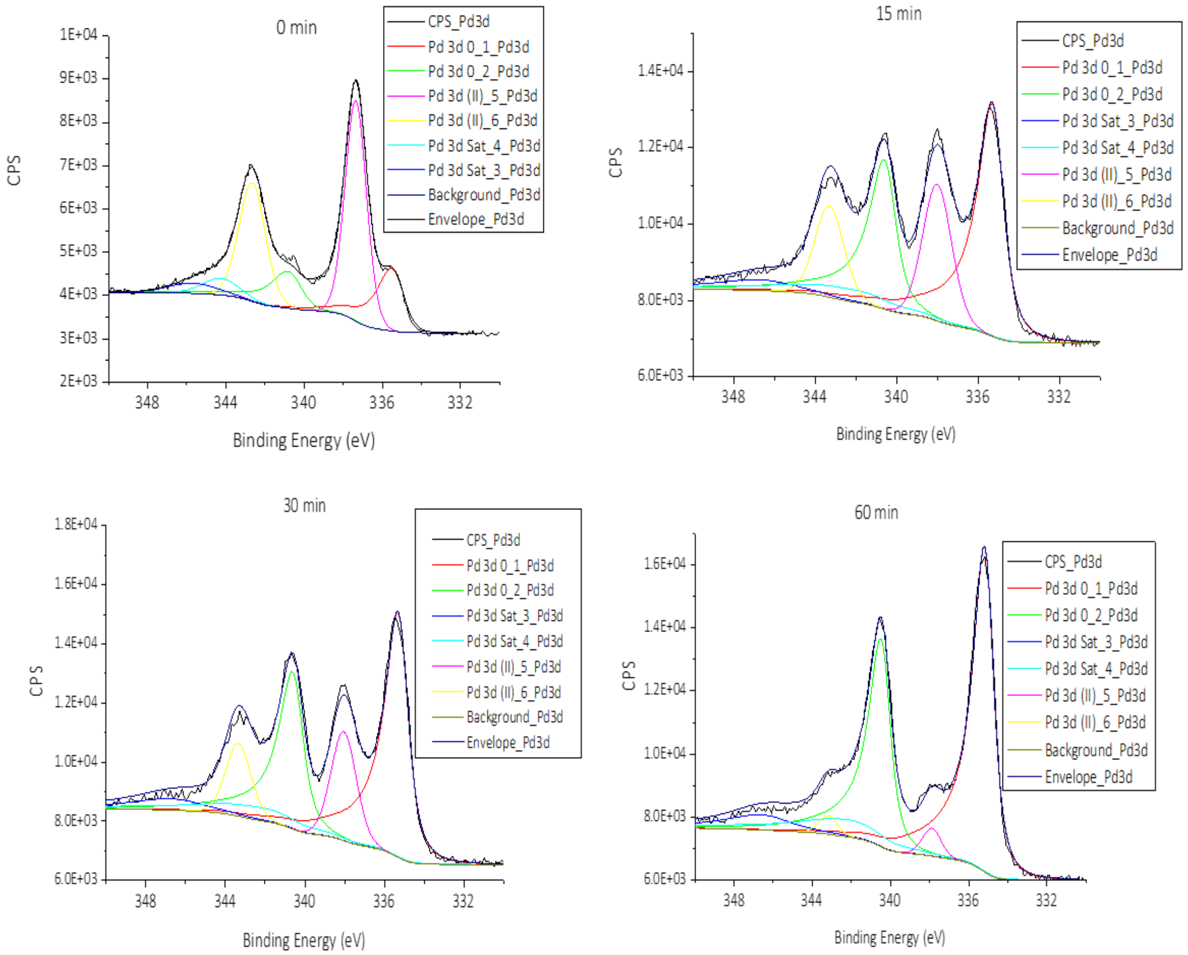

Figure 5-40: XPS and deconvolution of Pd species at different reaction times

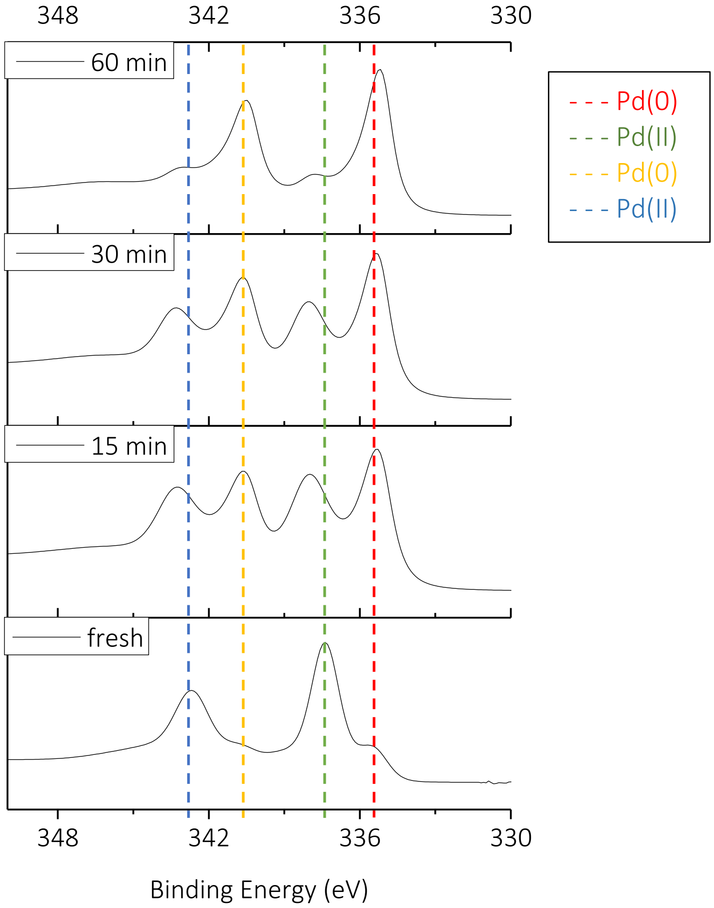

Figure 5-41: comparison of XPS results for Pd element during t,t-MA hydrogenation

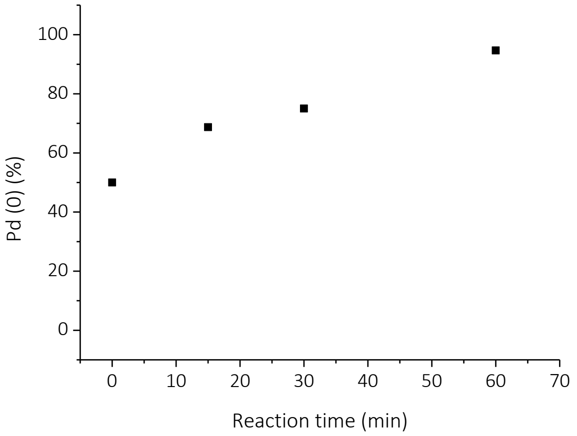

Figure 5-42: Pd(0) percentage during the hydrogenation reaction

The C groups were also analyzed and deconvoluted as reported (Figure 5-43). The binding energy of the different C groups are reported in Table 5-14.

Table 5-14: Binding energy for the different C groups

Group	Binding Energy (eV)
C sp2	284.29
C-O	286.77
C=O	288.73
C sp3	284.80

Table 5-15 shows the percentage of the different C groups in the catalyst, while Figure 5-44 represents the comparison among the C groups at different reaction times.

Table 5-15: percentage of different C species in the catalyst used for t,t-MA hydrogenation

Sample	C 1s (%)	C pi b (%)	C pi s (%)	C sp2 (%)	C sp3 (%)	C-O (%)	C=O (%)
15 min	49.05	0.15	2.10	23.65	16.40	2.48	6.16
30 min	48.82	0.19	2.57	28.94	13.32	3.02	3.12
60 min	48.67	0.18	2.45	27.61	14.31	3.79	3.00

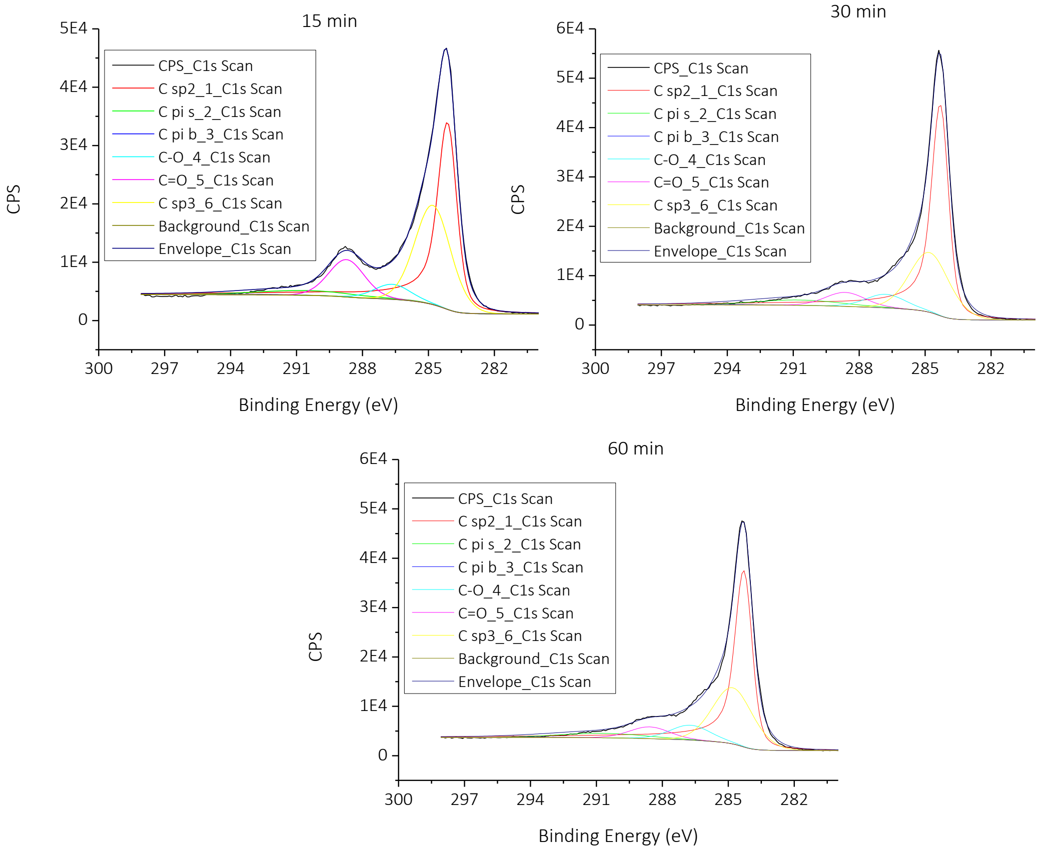

Figure 5-43: C deconvolution of catalyst samples recovered during t,t-MA hydrogenation

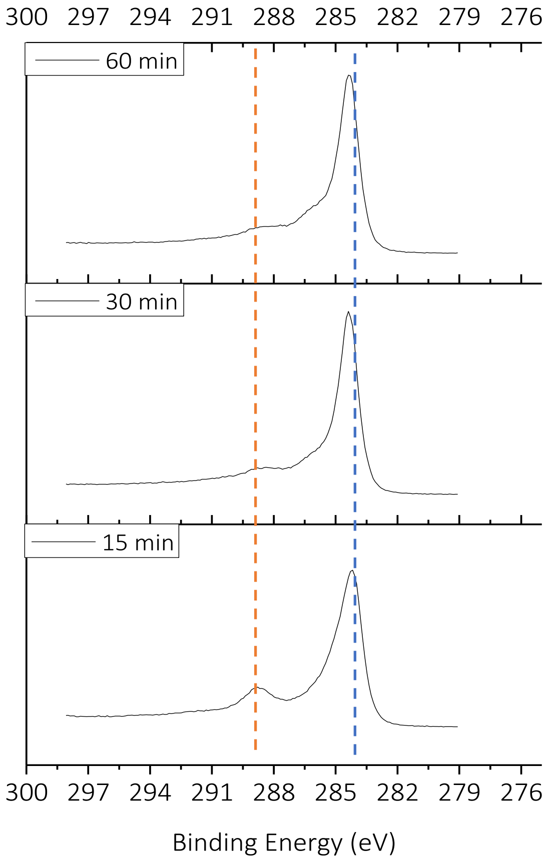

Figure 5-44: comparison of C species in the catalyst used for t,t-MA hydrogenation

During the reaction C sp3 and C=O percentages decreases, while Csp2 and C-O amount increases (Figure 5-45). Therefore, the reducing environment not only affects the oxidation state of Pd, but also reduces the carboxylic groups and Csp3 species to C-O and Csp2, respectively.

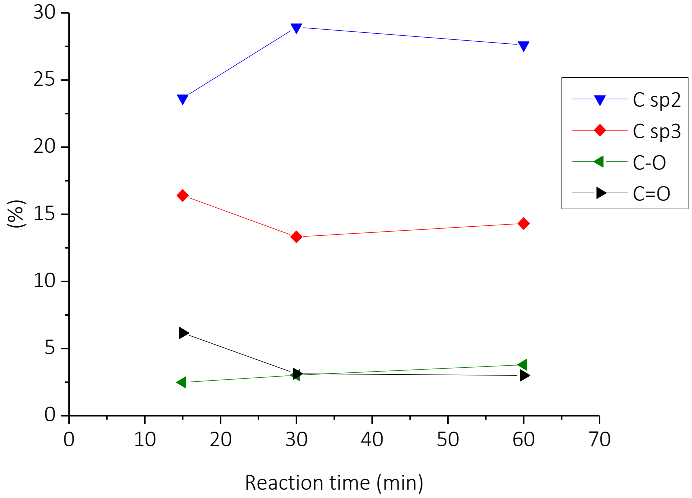

Figure 5-45: reduction of C=O and Csp3 specie during the hydrogenation reaction of t,t-MA

5.6.3.2 XPS (Na-Muc hydrogenation reaction)

XPS analysis was also performed on used catalyst recovered from Na-Muc reduction. Both Pd and C element were analyzed (Figure 5-46 and Figure 5-49, respectively). Figure 5-46 shows the fitted Pd 3d core-level XPS spectra of the used commercial Pd/AC 5%. Each Pd species displayed two peaks due to the Pd $3d_{3/2}$ and Pd $3d_{5/2}$ transition. Pd(0) $3d_{5/2}$ core electron binding energy is at 335.6 eV, while the Pd(0) $3d_{3/2}$ is at 340.54 eV. The Pd(II) peaks are at 343.46 and 338.18 eV, and they are identified as $3d_{3/2}$ and $3d_{5/2}$ transition, respectively. These binding energy values are in good agreement with that data reported in Chen et al. and Sanchez et al.[32,33] Analysing the area of the deconvolution peaks the evaluation of the percentage of the two species was calculated as reported in Table 5-16.

Table 5-16: percentage of Pd(II) and Pd(0) at different reaction time

Sample	Pd 3d (II) (%)	Pd 3d (0) (%)
0 min	49.90	50.10
30 min	14.00	86.00
120 min	8.87	91.13

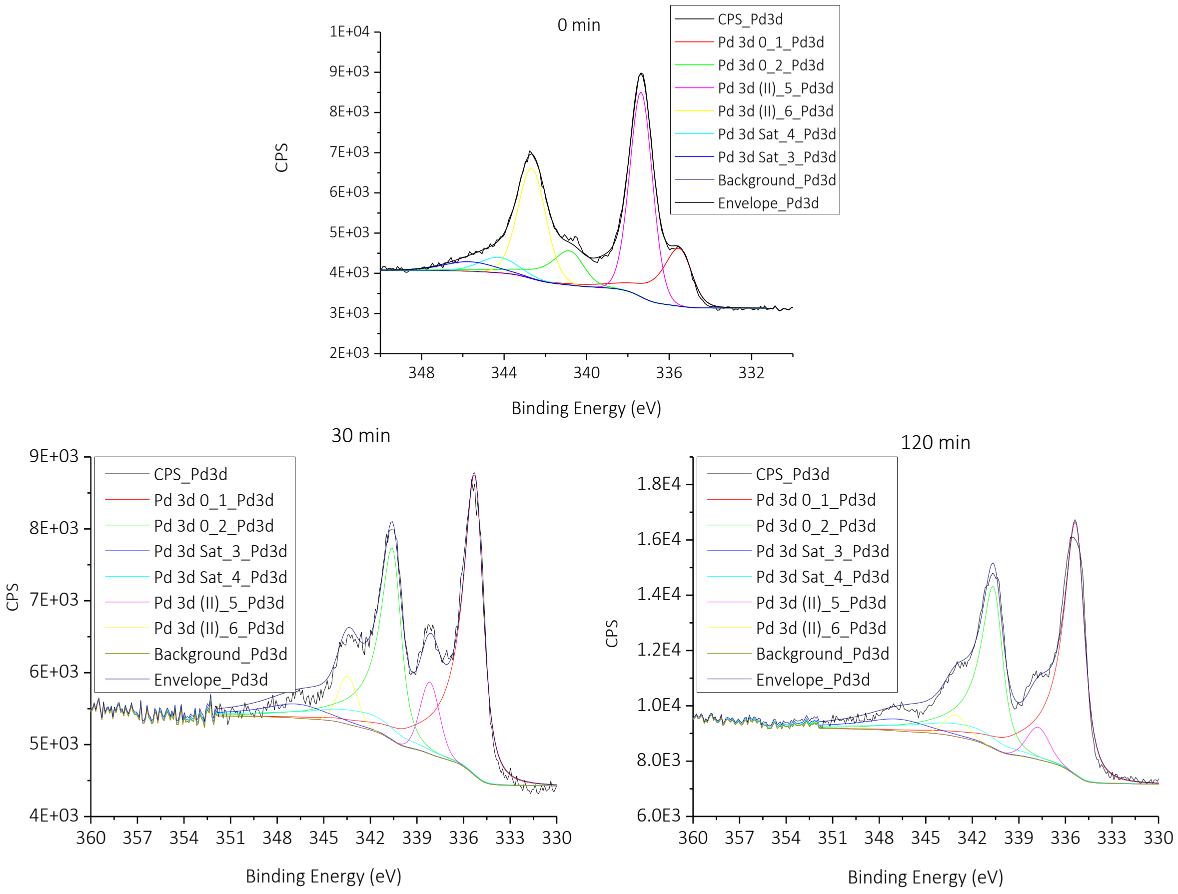

Figure 5-46: XPS and deconvolution of Pd species during Na-Muc hydrogenation reaction

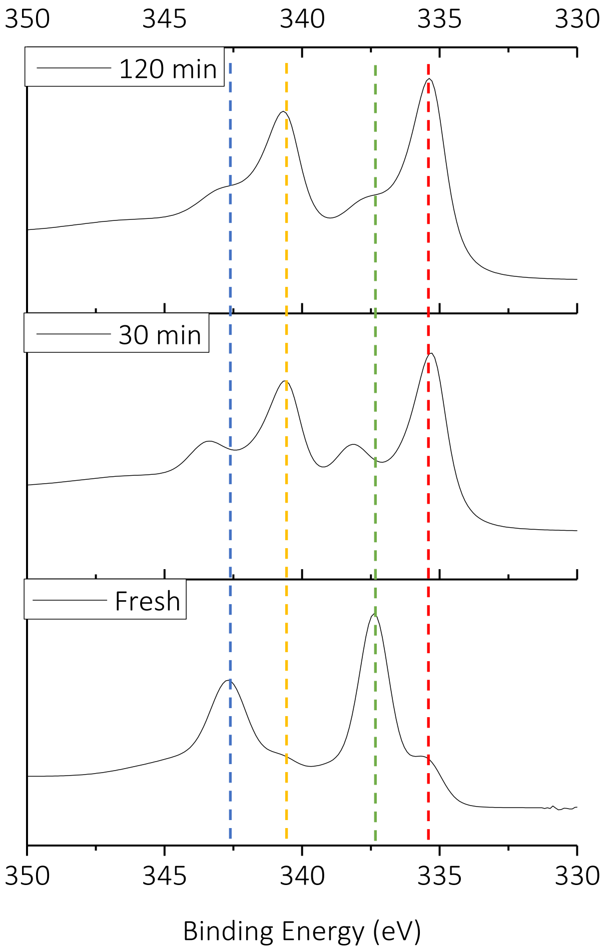

Figure 5-47: comparison of XPS results for Pd element during Na-Muc hydrogenation

The oxidation state of the Pd varied during the reaction (Figure 5-47). In particular the two initial peaks of fresh catalyst were split in two. The yellow and red peak appeared during the reaction while the blue and green one disappeared. Observing the deconvolution it is possible to notice that the red and yellow peaks belong to the Pd(0) state while the blue and green one at Pd(II) oxidation state. This means that during the reaction and in reducing environment the Pd(II) presents on the surface of the catalyst is reduced to metallic Pd. Plotted the reaction time versus the Pd(0)% it is possible to see how the metal Pd amount increases during the reaction reaching a value of 91% (Figure 5-48:).

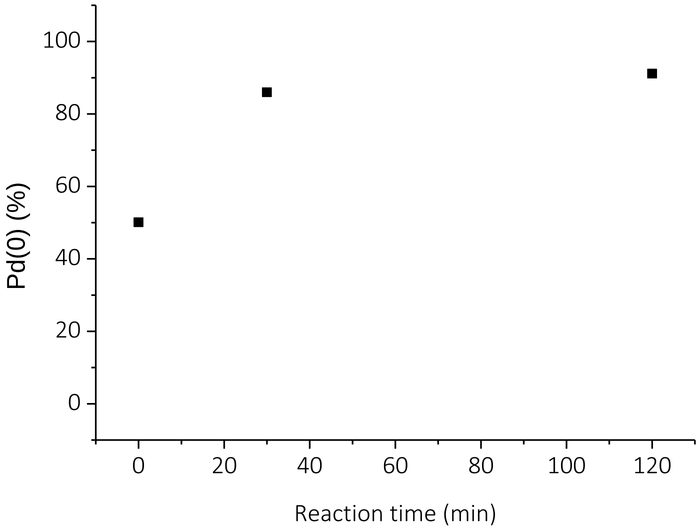

Figure 5-48: Pd(0) percentage during the hydrogenation reaction

The C groups were also analyzed and deconvoluted as reported in Figure 5-49:.

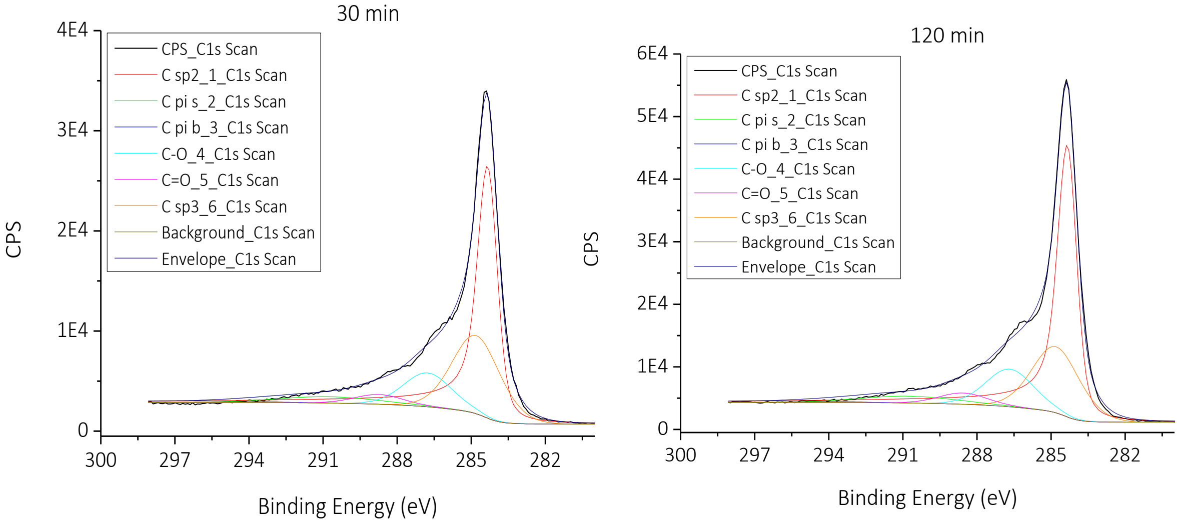

Figure 5-49: C deconvolution of catalyst's sample recovered during Na-Muc hydrogenation

The binding energy of the different C groups are reported in Table 5-17.

Table 5-17: Binding energy for the different C groups

Group	Binding Energy (eV)
C sp2	284.29
C-O	286.77
C=O	288.73
C sp3	284.80

Table 5-18 shows the percentage of the different C groups in the catalyst while Figure 5-50 represents the comparison among the C groups at different reaction times. No significative differences were found between the catalyst recovered at 30 and 120 minutes of reaction. The catalyst is mainly composed by C 1s specie while C=O is about 2%.

Table 5-18: percentage of different C species in the catalyst used for Na-Muc hydrogenation

Sample	C 1s (%)	C pi b (%)	C pi s (%)	C sp2 (%)	C sp3 (%)	C-O (%)	C=O (%)
30 min	48.88	0.17	26.87	26.87	13.91	6.03	1.73
120 min	49.01	0.18	28.00	28.00	11.68	6.66	1.99

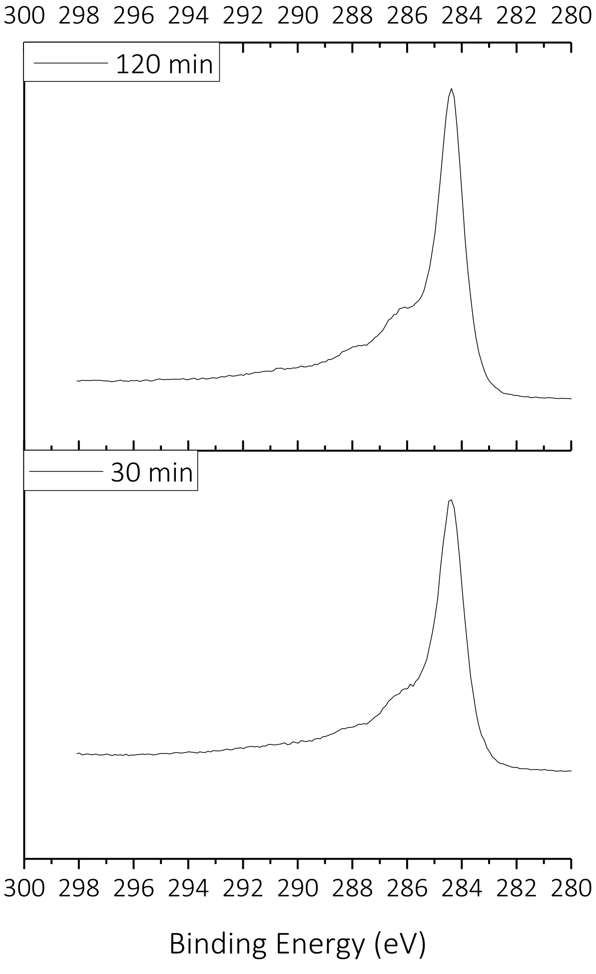

Figure 5-50: comparison of C species in the catalyst used for Na-Muc hydrogenation

Conclusion

This work addressed the production of adipic acid from renewable, focusing on the hydrogenation of muconic acid, an intermediate achieved by fermentation of lignocellulosic biomass

The experiments were performed in a batch slurry reactor in kinetic regime using water as a reaction medium. The reaction achieved a complete conversion and total yield to AdA at the low hydrogen pressure of 4 bar and mild temperature, paving the way to the scalability of the technology. Tests on the catalyst recyclability showed the possibility to reuse up to 10 times without loss in activity and selectivity. The pre-treatment of the catalyst causes the sintering of Pt particles and moreover the carbon support during the reaction of sodium muconate adsorbs Na.

The same reaction and operating conditions were applied to the fermentation broth containing the MA. The reaction occurs slow and no complete AdA yield was observed. Conductibility tests showed that several washings are mandatory to restore the starting surface condition of the catalyst, therefore the large amount of salts in the fermentation broth is responsible of its poor activity.

After that the solvent was changed opting for alcoholic solvents like methanol and ethanol. Alcoholic solvents can solubilize a greater amount of MA than water, allowing to work with higher concentration of MA. Using Pt/AC 5% as catalyst the results for the two alcoholic solvents are similar but considering the dangerousness of the methanol the choice of ethanol is without any doubt the best option.

Then commercial Pd/AC 5% was tested due to its lower commercial price and the possibility to directly use it without any pre-treatment. Na-Muc and *t,t*-MA were used as substrate. Firstly, the optimization of the main reaction operating parameters was performed allowing to find the best catalyst to substrate ratio (1/200 mol_{Pd}/mol_{sub}) and working pressure (1 bar). Therefore, the effect of substrate concentration and temperatures was study. Decreasing the temperature, the conversion decreases for both the systems. Using *t,t*-MA as substrate the reaction is fast and after 60 minutes full conversion to AdA was established (except for T= 30 °C). On the contrary Na-Muc hydrogenation is slow and only at T= 70 °C and after 90 minutes of reaction complete conversion was reached.

The characterization of the used catalyst shows that during the reaction Pd(II) is reduced to Pd(0) and a small shift in the signal was observed probably due to the change of the carbon support.

Bibliography

1. de Vries, J. G. & Jackson, S. D. Homogeneous and heterogeneous catalysis in industry. *Catal. Sci. Technol.* **2,** 2009 (2012).
2. Beeck, O. Hydrogenation catalysts. *Discuss. Faraday Soc.* **8,** 118–128 (1950).
3. Rylander, P. N. *Catalytic Hydrogenation in Organic Synthesis*. (Academic Press Limited, 1979).
4. Polkovnikov, B. D., Nefedov, O. M., Mikos, É. P. & Novitskaya, N. N. Sequence of hydrogenation of the double bonds of cycloheptatriene over palladium, platinum, and rhodium catalysts. *Bull. Acad. Sci. USSR, Div. Chem. Sci.* **17,** 1175–1178 (1968).
5. Rodríguez-reinoso, F. The role of carbon materials in heterogeneous catalysis. *Carbon N. Y.* **36,** 159–175 (1998).
6. Nerozzi, F. Heterogeneous Catalytic Hydrogenation. *Platin. Met. Rev.* **56,** 236–241 (2012).
7. Upare, P. P. *et al.* Selective hydrogenation of levulinic acid to γ-valerolactone over carbon-supported noble metal catalysts. *J. Ind. Eng. Chem.* **17,** 287–292 (2011).
8. Capelli, S. *et al.* Bio-adipic acid production by catalysed hydrogenation of muconic acid in mild operating conditions. *Appl. Catal. B Environ.* **218,** 220–229 (2017).
9. Singh, U. K. & Vannice, M. A. Kinetics of liquid-phase hydrogenation reactions over supported metal catalysts — a review. *Appl. Catal. A Gen.* **213,** 1–24 (2001).
10. van Es, T. & Staskun, B. Aldehydes from Aromatic Niriles: 4-Formylbenzenesulfonamide. in *Organic synthesis database online* (John Wiley and Sons, Inc., 2003). doi:https://doi.org/10.1002/0471264180.os051.06
11. Bard, A. J. & Faulkner, L. R. *Electrochemical methods (Fundamentals and applications)*. (John Wiley and Sons, Inc., 2001).
12. Sander, R. Compilation of Henry's law constant (version 4.0) for water as solvent. *Atmos. Chem. Phys.* **15,** 4399–4981 (2015).
13. Chaudhari, R. V. *et al.* Kinetics of hydrogenation of maleic acid in a batch slurry reactor using a bimetallic Ru-Re/C catalyst. *Chem. Eng. Sci.* **58,** 627–632 (2003).
14. Rajashekharam, M. V, Nikalje, D. D., Jaganathan, R. & Chaudhari, R. V. Hydrogenation of 2,4-Dinitrotoluene Using a Pd/Al2O3 Catalyst in a Slurry Reactor: A Molecular Level Approach to Kinetic Modeling and Nonisothermal Effects. *Ind. Eng. Chem. Res.* **36,** 592–604 (1997).
15. Machado, R. M. Foundamentals of mass transfer and kinetics for the hydrogenation of nitrobenzene to aniline. *ALR Appl. note* **1,** 1–14 (2007).
16. Fillion, B., Morsi, B. I., Heier, K. R. & Machado, R. M. Kinetics, Gas−Liquid Mass Transfer, and Modeling of the Soybean Oil Hydrogenation Process. *Ind. Eng. Chem. Res.* **41,** 3052 (2002).
17. Hájek, J. & Murzin, D. Y. Liquid-Phase Hydrogenation of Cinnamaldehyde over a Ru−Sn Sol−Gel Catalyst. 1. Evaluation of Mass Transfer via a Combined Experimental/Theoretical Approach. *Ind. Eng. Chem. Res.* **43,** 2030–2038 (2004).
18. Sano, Y., Yamaguchi, N. & Adachi, T. Mass transfer coefficients for suspended particles in agitated vessels and bubble columns. *J. Chem. Eng. Japan* **7,** 255–261 (1974).
19. McKetta Jr., J. J. *Encylopedia of Chemicals Processing and design: Volume 46-Pumps: Bypass to Reboilers*. (Taylor & Francis, 1993).
20. Acres, G. J. K. & Cooper, B. J. Carbon-supported platinum metal catalysts for hydrogenation reactions. Mass transport effects in liquid phase hydrogenation over Pd/C. *J. Appl. Chem. Biotechnol.* **22,** 769–785 (2018).
21. Niu, W., Draths, K. M. & Frost, J. W. Benzene-free synthesis of adipic acid. *Biotechnol. Prog.* **18,** 201–211 (2002).

22. Bard, A. J. & Faulkner, L. R. *Electrochemical Methods: Fundamentals and Applications*. (Jhon Wiley & Sons, 2000).
23. Ĉerveny, L. Palladium Catalysts In Hydrogenation Reactions. *Chem. Eng. Commun.* **83,** 31–63 (1989).
24. Belskaya, O. B. *et al.* A Study of Pd/C Catalysts in the Liquid-phase Hydrogenation of 1,3,5-Trinitrobenzene and 2,4,6-Trinitrobenzoic Acid. Selection of Hydrogenation Conditions for Selective Production of 1,3,5-Triaminobenzene. *Procedia Eng.* **152,** 110–115 (2016).
25. Cooper, J. & Beecham, J. A Study of Platinum Group Metals in Three-Way Autocatalysts. *Platin. Met. Rev.* **57,** 281–288 (2013).
26. Carraher, J. M., Pfennig, T., Rao, R. G., Shanks, B. H. & Tessonnier, J.-P. cis,cis-Muconic acid isomerization and catalytic conversion to biobased cyclic-C $_6$ -1,4-diacid monomers. *Green Chem.* 21–25 (2017). doi:10.1039/C7GC00658F
27. Kumar, A. & Jena, H. M. Preparation and characterization of high surface area activated carbon from Fox nut (Euryale ferox) shell by chemical activation with H3PO4. *Results Phys.* **6,** 651–658 (2016).
28. Jagiello, J. & Thommes, M. Comparison of DFT characterization methods based on N2, Ar, CO2, and H2 adsorption applied to carbons with various pore size distributions. *Carbon N. Y.* **42,** 1227–1232 (2004).
29. Yang, G., Han, H., Li, T. & Du, C. Synthesis of nitrogen-doped porous graphitic carbons using nano-CaCO3as template, graphitization catalyst, and activating agent. *Carbon N. Y.* **50,** 3755–3765 (2012).
30. Yu, W. *et al. Nanosizing Pd on 3D porous carbon frameworks as effective catalysts for selective phenylacetylene hydrogenation*. *RSC Adv.* **7,** (2017).
31. Shang, S., Yang, X. & Tao, X. ming. Easy synthesis of carbon nanotubes with polypyrrole nanotubes as the carbon precursor. *Polymer (Guildf).* **50,** 2815–2818 (2009).
32. Chen, X. *et al. Non-covalently modified graphene supported ultrafine nanoparticles of palladium for hydrogen gas sensing*. *RSC ADVANCES* **3,** (2013).
33. Sanchez, F. *et al.* Hydrogen Generation from Additive-Free Formic Acid Decomposition Under Mild Conditions by Pd/C: Experimental and DFT Studies. *Top. Catal.* **61,** 254–266 (2018).
34. Ebbesen, S. D., Mojet, B. L. & Lefferts, L. Effect of pH on the Nitrite Hydrogenation Mechanism over Pd/Al2O3 and Pt/Al2O3: Details Obtained with ATR-IR Spectroscopy. *J. Phys. Chem. C* **115,** 1186–1194 (2011).

Chapter 6

Mechanism identification and regression of kinetic parameters

In this chapter, the mechanism identification and kinetic model definition are described. The study was developed using the results obtained from the hydrogenation reaction of sodium muconate in water at different temperatures using Pt/AC 5% commercial catalyst.

The empirical study allowed identifying a catalyst with optimal performances in very mild conditions, providing the data for the first kinetic study on the mechanism of muconic acid hydrogenation. At the beginning of the study, the reaction was modelled using LHHW mechanism and kinetic parameters at constant temperature were regressed. This reaction model showed an overestimation of the reactant and the intermediate concentrations due to the group of the different intermediates. Divided the intermediates and introducing the different reaction temperatures the model is able to predict the concentration of the different species during the reaction. The results of this study are published in Chemical Engineering Transaction Journal 57, 931-936 (2017).

6.1 State of art

Previous studies on muconic acid hydrogenation addressed only *cis,cis*-muconic acid (ccMA), without considering that the *cis,cis* isomer is the most unstable of the three possible forms and spontaneously evolves into the configurational isomer *cis,trans* (ctMA) in acidic environment at temperatures above 30 °C.[1] Also, it has been extensively proven that both ccMA and ctMA tend to isomerize to *trans,trans*-muconic acid (ttMA) in presence of metals that strongly bind hydrogen molecules.[2,3] The choice of ccMA for previous kinetic studies was motivated by the fact that the *cis,cis* isomer is the one produced by the microorganism: this assumption still is not entirely acceptable from a full-process perspective. Considering in fact the most plausible downstream operations for the ccMA rich fermentation broth, the *cis,cis* form is unlikely to be preserved. Indeed, the filtered broth undergoes to a crystallization step achieved by pH shift, and, due to the thermal deactivation of the bacteria and the evaporation steps, an increase of temperature above 80 °C is required. The coupled conditions of acidic environment and higher temperatures are therefore a realistic scenario, and the hydrogenation will be possibly performed on a mixture of the three isomers. The presence of muconic lactones, which actually can be formed in these conditions (and can reduce the hydrogenation selectivity), can be avoided by shorter treatments.[4]

Therefore, *trans,trans*-muconic acid (ttMA) was selected as the model chemical for this hydrogenation study. Even though a real application would probably deal with mixtures of MA isomers from the purified broth (as assumed during the development of the superstructure in Chapter 3), the analysis on the sole ttMA has several advantages. First, due to the lower solubility and higher heat of formation, ttMA is the most recalcitrant isomer to react.[5] Therefore, the reaction conditions valid for ttMA apply also for the other isomers, leaving space for further optimizations. Second, the analytics are simplified and accelerated, removing some of the other possible intermediates: 3-hexanedioic acid, for example, is detected when hydrogenating ccMA,[6] but it is not formed in measurable amounts with ttMA.[7] Finally, for the sake of the mechanism modelling, ttMA allows excluding the isomerization equilibria of the reactant between *cis,cis*, *cis,trans* and *trans,trans* forms, reducing the number of equations and parameters to regress. In this way, a deeper understanding of the reaction mechanism is possible, removing parallel or concurrent pathways. All the analyses in water were performed on sodium muconate salts, as ttMA is very insoluble in water in its acid form.

6.2 Materials and Methods

6.2.1 Experimental

The substrates were *trans,trans*-muconic acid (Sigma Aldrich, purity 98 %), Pt/C 5% (Taminco), butanol (Sigma Aldrich, purity >99 %), sulfuric acid 98 % (Sigma Aldrich), sodium hydroxide (Sigma Aldrich, purity >99 %), adipic acid (AA) (Sigma Aldrich), (2E)-2-hexenedioic acid (Sigma Aldrich, purity 98 %), dimethyl adipate (Sigma Aldrich, purity ≥99 %). Reagents and solvent were used without further purification.

The hydrogenation of MA was performed on the sodium muconate salt that was obtained adding to the aqueous solution a stoichiometric amount of solid sodium hydroxide. The reaction was carried out in a cylindrical batch autoclave equipped with two different gas lines. Helium was used to clean the reactor and to quench the reaction, while hydrogen was used for catalyst pre-treatment and as reagent for the hydrogenation reaction. The reaction took place in a cylindrical glass tube to avoid that the Nickel contents in the steel could interfere. All the system was heated through an external metal jacket and the temperature monitored with a thermocouple. The reaction mixture was stirred with a magnetic stirrer at a stirring rate of 500 rpm. The catalyst (0.1 g) pre-treatment occurred in situ at 6 bar of static hydrogen for 3 hours at 200 °C. The hydrogenation reaction was achieved in the aqueous solution (10 mL, 0.7x10-2 M). The hydrogenation tests were performed varying temperature (40-70 °C) and keeping constant the hydrogen pressure, the amount of catalyst, the agitation speed and reactor configuration. The reaction tests were performed in batch condition using a fresh catalyst at the beginning of all the tests.

Sodium muconate conversion was evaluated by UV-Vis analysis. A reaction mixture sample collected after the catalyst filtration was analysed in a spectrophotometer T60 UV-Visible Spectrophotometer PRIXMA from 400 to 190 nm. The maximum absorption was at 264 nm. The calibration of the analysis was performed with sodium muconate prepared from *trans,trans*-muconic acid. The selectivity toward AA and monounsatured compounds was estimated by GC analyses on derivative methyl esters (Master GC Fast Gas Cromatograph Dani Instrument equipped with an Aldrich Supelcowax 10: 60 m x 0.53 mm, film thickness 1 μm) with TCD detector operating in splitless mode. Butanol was used as internal standard.

The recognition of the reaction intermediates was carried out with GC coupled with mass detector on derivatized esterified products.

6.2.2 Kinetic modelling

The studied Pt/C 5 % catalyst outperformed all the others previously tested in terms of conversion and selectivity (>99 %), even at milder pressure (4 bar). Therefore, the reaction was investigated to characterize the kinetic parameters, which represent the basis for the scale up of laboratory data to industry. Since *trans,trans*-muconic acid is a double unsaturated compound, it is reasonable to assume a multi-step reaction, in which mono-unsaturated hexenedioic acid is formed as an intermediate product and then is hydrogenated to AA. The presence of a solid catalyst in a slurry reactor involves adsorption-desorption equilibria of the reacting species, thus Langmuir-Hinshelwood-Hougen-Watson (LHHW) expressions were used to model the reaction rates.[8,9] These models, originally developed for gas phase reaction, proved to be effective also for liquid reactions, in which competitive adsorption of hydrogen and organic molecules occurs.[10,11]

The macroscopic performance of a slurry reactor can be affected by the insurgence of mass-transfer resistances among the gas (hydrogen), the liquid (water and reactants dissolved) and the solid (catalyst particles) phases. Even though slurry reactors and the use of a catalyst in fine powder (40 µm) usually minimize transport phenomena issues, the validation of a pure kinetic regime was necessary. Chaudari et al developed some qualitative indexes to assess whether any external or intraparticle mass transfer phenomena are the rate determining step, taking care of the initial reaction rate, of the stirring speed, and of the catalyst properties.[10,12,13] The hydrogen concentration was assumed to be constant throughout the reaction, given the fixed pressure and the exclusion of gas-liquid mass transfer limitation. The nonlinear regression of model parameters, coupled with the solution of the differential equations for the material balances in the reactor, were performed in C++ language applying Bzz-Math libraries.[14] The library covers many fields of numerical analysis for Windows and Linux users, includes parallel computations automatically enabled when possible, and self-selects the best algorithms during computations. It is used in all continents and is the kernel of many industrial solutions for process modeling, simulation, control, and optimization. In the simplified mechanism, all the intermediates were considered as a single pseudo-component “IN”.

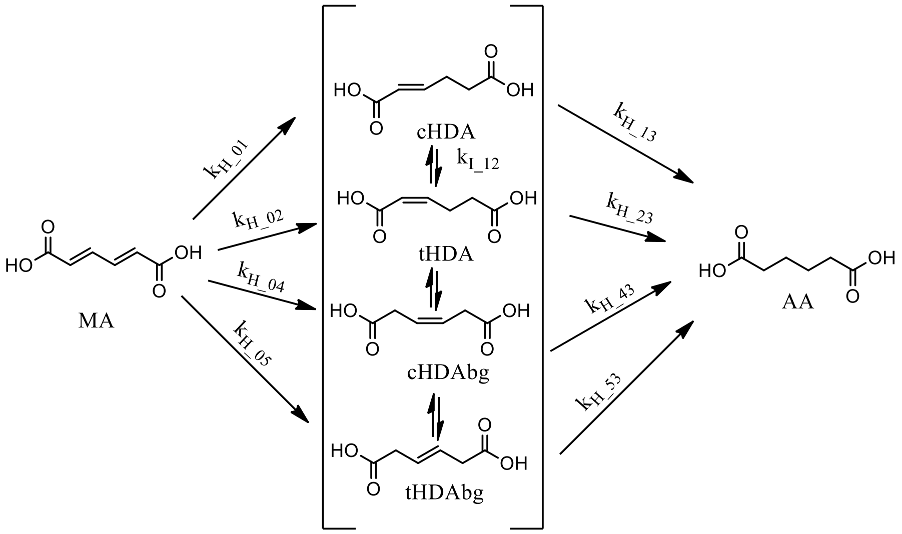

Figure 6-1: reaction scheme with all possible monounsaturated intermediate isomers. The species reported are trans,trans-muconic acid (MA), α,β cis-hexenedioc acid (cHDA), α,β trans-hexenedioic acid (tHDA), β,γ cis-hexenedioic acid (cHDAbg), β,γ trans-hexenedioic acid (tHDAbg) and adipic acid (AA)

6.2.3 LHHW models and nonlinear regression

The Langmuir-Hinshelwood-Hougen-Watson (LHHW) model was used to express the reaction rate equations, assuming as the rate-determining step the reaction on the surface.[15] This formulation, which decomposes the mechanism of adsorption-reaction-desorption occurring on the catalyst into elementary steps, allows considering the competitive adsorption equilibria of the species, and the hypotheses of molecular or dissociated hydrogen reaction. A preliminary study at fixed temperature, identified a LHHW competitive adsorption with hydrogen dissociation mechanism. The generic reaction rate equation is:[15]

$$R_j = \frac{k_j C_t K_{H_2} C_{H_2} K_i C_i}{(1 + \sum_k K_k C_k)^n} \qquad \text{(Eq.6-1)}$$

where

K_i = the adsorption constants for the specie i;

k_j = the kinetic constant of reaction j;

C_i (mol/L)= the concentration of the specie i;

C_t (mol/L)= the active sites concentration.

The denominator exponent expresses the hydrogen dissociation, according to the Yang and Hougen tables.[8]

The kinetic constant temperature dependence can be expressed by the Arrhenius equation:

$$k_j = A_j \cdot exp\left(-\frac{E_{att,j}}{RT}\right) \tag{Eq.6-2}$$

Also k_j can be expressed in function of temperature using the Van't Hoff formulation, but for liquid phase hydrogenations the temperature dependence of adsorption can be neglected in the hypothesis of high surface coverage:[16] The number of parameters was therefore reduced. However, even though LHHW is among the most popular models in reaction engineering, its mathematical structure is little suitable for nonlinear regression applications, as the parameters are strongly collinear and can lead to ill-conditioning problems.[17] This means that while performing the parameters regression, the error minimization becomes difficult even for robust solvers, and the results can be strongly affected by any small perturbation of the input data due to unavoidable experimental error. These shortcomings are particularly relevant for models with many reaction steps and adaptive parameters, which require the solution of large size nonlinear regression problems, coupled with the dynamic solution of the stiff ODEs system derived from the chemical species material balances. To reduce the computational effort, a common approach is the re-parametrization of the model, and, if possible, the removal of the less significant parameters. Eq. 6-1 was therefore re-parametrized as:

$$R_j = \frac{\widetilde{k_j} C_i C_{H_2}}{(1 + \sum_k K_k C_k)^3} \tag{Eq.6-3}$$

where the kinetic constant of the numerator was expressed as a modified Arrhenius' equation as reported in Eq.6-2:

$$k_j = exp\left(\widetilde{A_j} - \frac{E_{att,ij}}{R}\left(\frac{1}{T} - \frac{1}{\bar{T}}\right)\right) \tag{Eq.6-4}$$

where $\bar{T}$ is an average temperature of the ones explored (333K). The constant contribution at the numerator of Eq.6-1 (i.e. K_{H2} , K_{ttMA}, C_t) were all lumped in the factor $\widetilde{A_j}$, which was calculated as one of the arguments of the exponential function. The Eq.6-4 is fully equivalent to Eq.6-2, but, from a mathematical perspective, helps in reducing the condition number and therefore simplifies the optimization problem.[17] The equations could be possibly further re-parametrized, but this would result in non-physically interpretable parameters, which does not allow the definition of physical constraints to the kinetic constants to reduce the search space. The advantage of this formulation is in fact that the activation energies of the Arrhenius' equations or the adsorption constants of LHHW model can be bounded in the well-known ranges available in literature. In particular, the apparent activation energy for double bond hydrogenations on noble metal catalysts can be bounded in a range between 10 and 120 kJ mol-1. [12,18–21] As for the adsorption constants, values taken from similar systems modelled with LHHW span between 10^{-1} and 10^{4} L·mol^{-1}:[19,22,23] This wide range was enough to reduce sensibly the convergence time. The objective function to be minimized for the parameters calculation was the sum of squared errors (SSE):

$$SSE = \sum_i \left(C_{i,exp} - C_{i,calc}\right)^2 \qquad \text{(Eq.6-5)}$$

where:

$C_{i,exp}$ (mol/L)= experimental concentration of specie i;

$C_{i,calc}$ (mol/L)= calculated concentration of specie i.

The model fitting quality was assessed comparing the final value of the SSE and the coefficient of determination, defined as:

$$R^2\% = 1 - \frac{SSE}{\sum_i \left(C_{i,exp} - \widetilde{C_{\iota,exp}}\right)^2} \qquad \text{(Eq.6-6)}$$

where:

$\widetilde{C_{\iota,exp}}$= average experimental value.

The optimization method adopted to achieve the best parameters was based on the class of robust minimization of BzzMath library in C++ language.[17] The 95% confidence interval on the regressed parameters were calculated using least square method analysis tools both in Matlab environment (lsqnonlin function) and C++ (BzzMath nonLinReg), to confirm the results applying different solvers.

6.3 Results and discussion

6.3.1 Preliminary study at constant temperature

Since the main purpose of the study was to demonstrate the feasibility of MA hydrogenation in mild conditions, lower pressures and lower temperatures were studied preferably. The reaction at 40 °C (Figure 6-2) showed an induction period and did not achieve full conversion after 4 hours: this denotes too slow kinetics for any practical application. A lag time is often detected in heterogeneous catalytic systems at low temperatures, and it is due to the strong absorption of the organic species on the active sites of the catalyst that gradually are deactivated. Low temperatures have not been sufficient to sustain the desorption step, and full conversion cannot be achieved. Vardon et al.[6] suggested a similar explanation. An increase of temperature to 60 °C eliminated the lag time and allowed complete conversion in only 1.5 hours. The kinetic study was then performed on the data at 60 °C, in line with the suggestions of Scelfo et al.[24] Many batches were necessary to provide a sufficient amount of experimental data at different times. Also, the complex and time-demanding workout to characterize the samples limited the number of the available points. To accelerate the data collection, the intermediates were considered initially as a single pseudo-component, referred as "IN" in Table 6-1. Two models based on LHHW adsorption mechanism were evaluated. Model A, considered the dissociation of molecular hydrogen when it is adsorbed on the catalyst, while model B, assumed no dissociation. The reaction rate equations are summarized in Table 6-1. Each hydrogenation step was considered irreversible and rate-determining, if compared to the kinetics of adsorption and desorption of all the species.

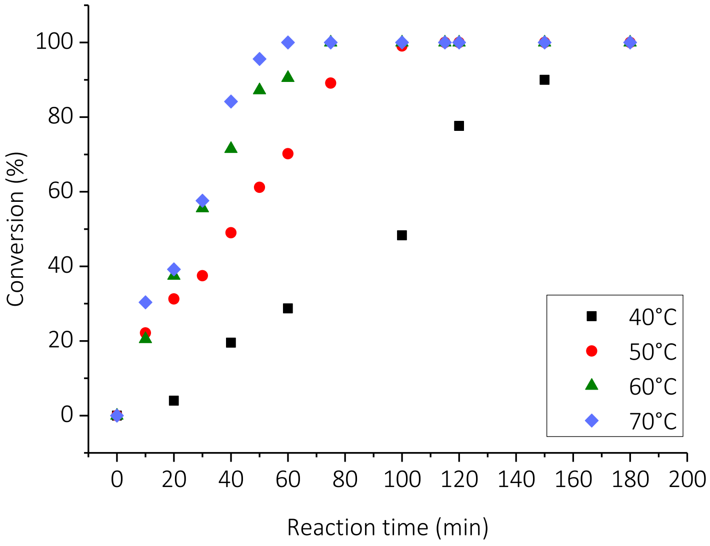

Figure 6-2: hydrogenation at different temperatures

Table 6-1: generic equations for the simplified mechanism with intermediate pseudo component. Dual site L-H model according to Yang and Hougen tables, n=2 without H2 dissociation, n=3 with dissociation

Kinetic equation	Reaction step	
$R_1 = \dfrac{k_1 C_{MA} C_{H_2}}{(1 + K_{MA}C_{MA} + K_{H_2}C_{H_2} + K_{IN}C_{IN+}K_{AA}C_{AA})^n}$	MA hydrogenation to IN	Eq.6-7
$R_2 = \dfrac{k_2 C_{IN} C_{H_2}}{(1 + K_{MA}C_{MA} + K_{H_2}C_{H_2} + K_{IN}C_{IN+}K_{AA}C_{AA})^n}$	IN hydrogenation to AA	Eq.6-8

where:

k_1= kinetic constant of MA hydrogenation to IN;

C_{MA} (mol/L) = concentration of MA;

C_{H2} (mol/L) = concentration of H_2;

K_{MA} (m^3/kmol) = adsorption constant of MA;

K_{H2} (m^3/kmol) = adsorption constant of AA;

C_{IN} (mol/L) = concentration of the intermediates;

K_{IN} (m^3/kmol) = adsorption constant of MA;

K_{AA} (m^3/kmol) = adsorption constant of AA;

C_{AA} (mol/L) = concentration of AA;

k_2 = kinetic constant for the hydrogenation of INT to AA.

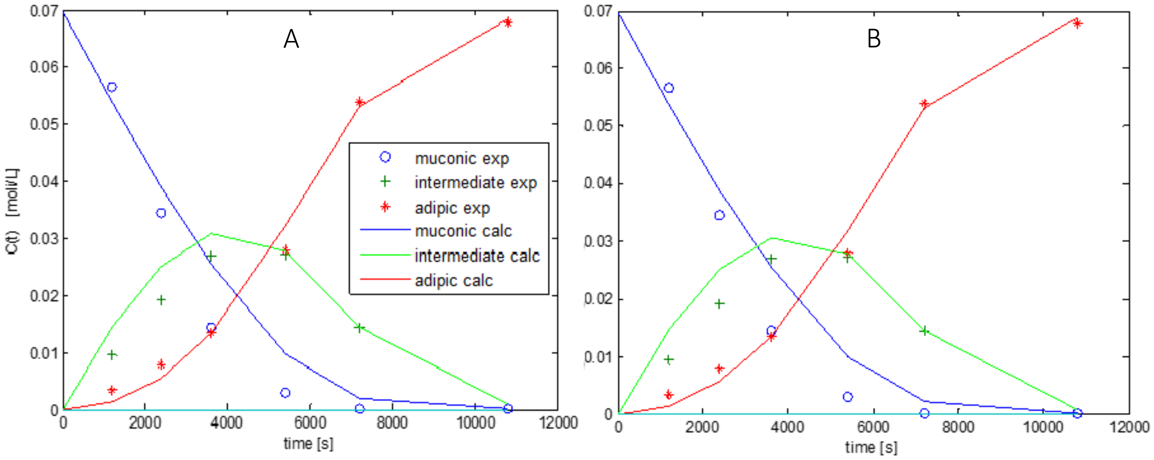

Figure 6-3: comparison between experimental and calculated values from model A (left) and B (right)

In both the cases, the calculations failed to represent properly the experimental data. In particular, the model showed an overestimation of the reactant and the intermediate concentrations. This trend, common in both the models, introduced a doubt on the reliability of the experimental measures, later confirmed by the material balances. A lack of molar quantities up to -20 % was observed during the reaction, which reduced to 0 as long as the reactants were consumed. This peculiar trend could only be explained by some errors in the quantification of the intermediate. After repeating the experiments and increasing the resolution of the gas chromatograph, it was possible to identify two distinct intermediates with different retention times. The analytical technique was then improved, so that all the possible intermediates were considered (Table 6-2) in the following modelling.

Table 6-2: concentration of the different compound at T= 60 °C

Reaction time (min)	C_{MA} (mol/L)	C_{cHDA} (mol/L)	C_{tHDA} (mol/L)	C_{AA} (mol/L)
0	7.00E-02	0.00E+00	0.00E+00	0.00E+00
20	5.69E-02	1.36E-03	8.25E-03	3.48E-03
40	4.28E-02	9.79E-03	9.50E-03	7.94E-03
60	2.93E-02	2.85E-03	1.53E-02	2.26E-02
90	1.46E-02	4.69E-03	2.00E-02	3.28E-02
120	1.19E-03	3.52E-03	1.10E-02	5.43E-02
180	1.75E-03	0.00E+00	0.00E+00	6.10E-02
240	1.00E-09	1.00E-09	1.00E-09	7.00E-02

6.3.2 Refined mechanism and model

Since the hydrogenation catalyst promotes double bond rotation,[3] all the four isomers are possible. However, the β,γ unsaturated intermediates were not detected in significant amounts, therefore the reaction scheme was simplified.

Three pathways were taken into consideration:

- Model C: LHHW mechanism without hydrogen dissociation (n=2) with irreversible isomerization of cHDA to tHDA;
- Model D: LHHW mechanism with hydrogen dissociation (n=3) with irreversible isomerization of cHDA to tHDA;
- Model E: LHHW mechanism with hydrogen dissociation (n=3) with isomerization equilibrium between cHDA and tHDA.

The equations used for modelling the reaction rates are reported in Table 6-3. Given the higher number of species and reactions with respect to the first modelling attempt, the number of kinetic parameters increases, resulting in different models which all performed a fairly good fitting (R^2 higher than 95% in all the cases). The residues were 0.0327, 0.0249 and 0.0226 for model C, D, and E, respectively. The comparison of the residues of model C and D, equivalent in the number of parameters, showed that hydrogen dissociates on the catalyst surface. Model E therefore assumes the hydrogen dissociation and includes the isomerization reaction. Another tested model, analogous to Model E but without dissociation, gave a poorer fit, confirming once again the dissociation of hydrogen.

Table 6-3: generic *equations for the refined mechanism with intermediates: dual site L-H model according to Yang and Hougen tables, n=2 without H2 dissociation, n=3 with dissociation*

Kinetic equation	Reaction step	
$R_{H\_01} = \frac{k^*_{\_h01} C_1 C_{H_2}}{(1+\sum K_i C_i)^n}$	MA hydrogenation to cHDA	(Eq.6-9)
$R_{H\_02} = \frac{k^*_{\_h02} C_1 C_{H_2}}{(1+\sum K_i C_i)^n}$	MA hydrogenation to tHDA	(Eq.6-10)
$R_{H\_13} = \frac{k^*_{\_h13} C_1 C_{H_2}}{(1+\sum K_i C_i)^n}$	cHDA hydrogenation to AdA	(Eq.6-11)
$R_{H\_23} = \frac{k^*_{\_h23} C_2 C_{H_2}}{(1+\sum K_i C_i)^n}$	tHDA hydrogenation to AdA	(Eq.6-12)
$R_{I\_21} = \frac{k^*_{\_i21} C_2}{(1+\sum K_i C_i)^n}$ and $R_{I\_12} = \frac{k^*_{\_i12} C_1}{(1+\sum K_i C_i)^n}$	Isomerization cHDA <-> tHDA	(Eq.6-13)

Table 6-4: calculated parameters for the three models, adsorption constants Ki are in L/mol

	K_{MA}	K_{cHDA}	K_{tHDA}	K_{AdA}	K_{H2}	$k_{\_h01}$	$k_{\_h02}$	$k_{\_h13}$	$k_{\_h23}$	$k_{\_i12(i21)}$
C	67.36	77.17	2.14E-3	2.83	1.75E-1	6.61E-1	5.96E-1	4.60	5.09E-1	1.01E-3
D	15.90	2.60E-1	1.87E-2	3.25	2.33E-2	1.86E-1	1.70E-1	1.28	1.51E-1	1.00E-1
E	12.46	14.91	1.00E-5	2.92E-2	1.08E-2	1.13E-1	9.93E-2	9.52E-1	1.00E-5	2.27E-4 (5.14E-4)

Observing the parameter values of Table 6-4, however, it was clear that the model had to be further refined. In fact, the *trans* configuration of the intermediate should be theoretically favored due to its lower steric hindrance, however, comparing the two kinetic constants reported, the reaction seems to move backward.

These results therefore served as an indication, before more experimental data became available. In addition, the kinetic constants showed an undue variability from model to model, especially for model D. However, it was impossible to compare the values to other published literature, since no data for muconic acid and derivatives are available for benchmarking. Nonetheless, some confirmation on the relative values of the adsorption constants can be found in Chaudhari et al.,[22] who studied the kinetics of hydrogenation of maleic acid to succinic acid in a slurry reactor, a similar system to MA. They observed that the unsaturated acid adsorbs preferably, confirming the relative magnitude of the calculated constants, even though their investigated temperatures were far higher than 230 °C.

6.3.2.1 Model regression with temperature dependence

The reaction mechanism identified in the preliminary tests is presented in Figure 6-4. The first step of hydrogenation on ttMA yields two isomers, namely (2Z)-2-hexenedioic acid (tHDA) and (2E)-2-hexenedioic acid (cHDA), in a single irreversible step. The concentration of the intermediates is regulated by an equilibrium isomerization reaction. The second step of hydrogenation yields adipic acid (AA) from both the intermediates.

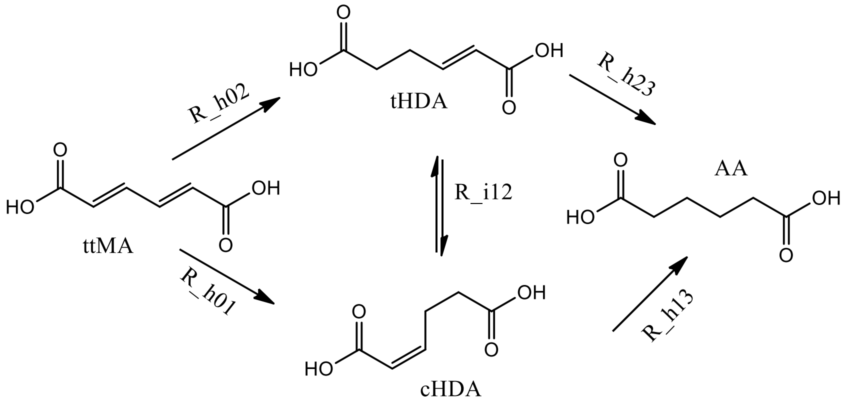

Figure 6-4: hypothesized reaction scheme of model LHHW_17P

The experimental data used for the regression are reported in Table 6-5.

Table 6-5: experimental data used for the regression of parameter

Time (s)	Temperature (K)	ttMA (mol/L)	cHDA (mol/L)	tHDA (mol/L)	AA (mol/L)	H_2 (mol/L)
0	323	6.96E-02	0.00E+00	0.00E+00	0.00E+00	2.73E-03
1200		4.80E-02	1.47E-03	1.45E-02	5.69E-03	2.73E-03
2400		3.55E-02	8.39E-04	1.82E-02	1.50E-02	2.73E-03
3600		2.07E-02	1.46E-03	2.22E-02	2.52E-02	2.73E-03
4500		7.56E-03	3.59E-03	2.96E-02	2.89E-02	2.73E-03
5400		6.47E-04	3.53E-03	2.26E-02	4.28E-02	2.73E-03
7200		0.00E+00	2.12E-03	8.51E-03	5.90E-02	2.73E-03
10800		6.96E-05	0.00E+00	0.00E+00	6.95E-02	2.73E-03
14400		0.00E+00	0.00E+00	0.00E+00	6.96E-02	2.73E-03
0	333	6.96E-02	0.00E+00	0.00E+00	0.00E+00	2.59E-03
1200		4.35E-02	1.13E-03	1.63E-02	8.67E-03	2.59E-03
1800		3.09E-02	1.83E-03	2.21E-02	1.48E-02	2.59E-03
2400		2.29E-02	2.76E-03	2.10E-02	2.29E-02	2.59E-03
3000		1.98E-02	2.82E-03	1.95E-02	2.75E-02	2.59E-03
4500		7.66E-04	2.72E-03	1.48E-02	5.13E-02	2.59E-03
6900		1.33E-03	0.00E+00	0.00E+00	7.00E-02	2.59E-03
9000		0.00E+00	0.00E+00	0.00E+00	7.00E-02	2.59E-03
0	343	6.96E-02	0.00E+00	0.00E+00	0.00E+00	2.47E-03
600		4.85E-02	6.87E-04	8.05E-03	1.24E-02	2.47E-03
1200		3.01E-02	3.32E-03	1.27E-02	2.34E-02	2.47E-03
2400		1.10E-02	1.86E-03	1.82E-02	3.85E-02	2.47E-03
3600		0.00E+00	0.00E+00	0.00E+00	6.96E-02	2.47E-03
6000		0.00E+00	0.00E+00	0.00E+00	6.96E-02	2.47E-03
7200		0.00E+00	0.00E+00	0.00E+00	6.96E-02	2.47E-03

The set of ordinary differential equations reported in Eq. 5.14-18 describes the mechanism (identified from now on as LHHW_17P) and presents 17 adaptive parameters. The results of the regression, listed in Table 6-6, seem particularly encouraging: the regression shows a R^2 close to 99%. The good fitting can be appreciated also in the concentration time profiles and in the dispersion diagram reported in Figure 6-5.

$$\frac{dC_{ttMA}}{dt} = -R_{h01} - R_{h02} = -\frac{k^*_{\text{h01}} \cdot C_{ttMA} \cdot C_{H_2}}{(1+\sum K_i C_i)^3} - \frac{k^*_{\text{h02}} \cdot C_{ttMA} \cdot C_{H_2}}{(1+\sum K_i C_i)^3} \qquad \text{(Eq.6-14)}$$

$$\begin{aligned}\frac{dC_{cHDA}}{dt} &= +R_{h01} - R_{h13} - \ R_{i12} \\ &= -\frac{k^*_{\text{h01}} \cdot C_{ttMA} \cdot C_{H_2}}{(1+\sum K_i C_i)^3} - \frac{k^*_{\text{h13}} \cdot C_{cHDA} \cdot C_{H_2}}{(1+\sum K_i C_i)^3} - \frac{k^*_{\text{i12}} \cdot \ C_{cHDA} - k^*_{\text{i12}} \cdot \ C_{tHDA}}{(1+\sum K_i C_i)^3}\end{aligned} \qquad \text{(Eq.6-15)}$$

$$\begin{aligned}\frac{dC_{tHDA}}{dt} &= +R_{h01} - R_{h23} + \ R_{i12} \\ &= -\frac{k^*_{\text{h02}} \cdot C_{ttMA} \cdot C_{H_2}}{(1+\sum K_i C_i)^3} - \frac{k^*_{\text{h23}} \cdot C_{tHDA} \cdot C_{H_2}}{(1+\sum K_i C_i)^3} - \frac{k^*_{\text{i12}} \cdot \ C_{cHDA} - k^*_{\text{i12}} \cdot \ C_{tHDA}}{(1+\sum K_i C_i)^3}\end{aligned} \qquad \text{(Eq.6-16)}$$

$$\frac{dC_{AA}}{dt} = R_{h13} + R_{h23} = -\frac{k^*_{\text{h13}} \cdot C_{cHDA} \cdot C_{H_2}}{(1+\sum K_i C_i)^3} - \frac{k^*_{\text{h23}} \cdot C_{tHDA} \cdot C_{H_2}}{(1+\sum K_i C_i)^3} \qquad \text{(Eq.6-17)}$$

$$\frac{dC_{H2}}{dt} = 0 \qquad \text{(Eq.6-18)}$$

Still, the statistical analysis of results showed little consistency on the regressed parameters with a wide confidence interval for all the parameters. This highlights that 17 adaptive parameters lead to a very flexible model which is not able to discriminate the outliers experimental points because it is able to follow the concentration profile in virtue of the many adaptive parameters. Another critical aspect of LHHW_17P model is the value of the activation energy for the first hydrogenation, which is close to the boundary limit. This model was therefore discarded, pursuing a simpler formulation. A 15 parameters model was hence obtained, excluding from the mechanism the reaction step R_h01. In effect this step assumes a combined isomerization and hydrogenation of ttMA: even possible, the isomerization reaction is unlikely in a strong reducing environment. In spite of the lower number of parameters, model LHHW_15P decreases its coefficient of determination of only 0.6%, while sensibly reducing the uncertainty of many of the parameters. Also, the values of the apparent activation energy assumed a value more in line with the previously estimated 70 kJ mol^{-1} for Pt/C in ethanol.[25]
However, the results were still unsatisfactory.

Table 6-6: Calculated values of the model parameters with 95% confidence interval and regression metrics

Parameter		LHHW_17P		LHHW_15P		LHHW_13P		LHHW_11P	
K_{ttMA}	$[L \cdot mol^{-1}]$	1.49E+01	±190%	6.97E+01	±35%	7.85E+02	±13%	8.10E+02	±7%
K_{cHDA}	$[L \cdot mol^{-1}]$	4.86E+03	±81%	9.16E+02	±56%	9.03E+03	±50%	9.85E+03	±45%
K_{tHDA}	$[L \cdot mol^{-1}]$	5.81E+00	±500%	1.00E+00	±43%	2.15E+02	±126%	2.19E+02	±102%
K_{aa}	$[L \cdot mol^{-1}]$	6.53E+01	±133%	3.57E+01	±35%	4.72E+01	±184%		
K_{H2}	$[L \cdot mol^{-1}]$	4.20E+02	±400%	1.02E+00	±96%	1.00E+00	±186%		
A_{h02}	$[s^{-1}]$	4.72E+00	±93%	3.86E+00	±27%	1.01E+01	±5%	1.02E+01	±2%
Ea_{h02}	$[kJ \cdot mol^{-1}]$	1.20E+05	±146%	7.41E+04	±34%	6.30E+04	±24%	6.20E+04	±13%
A_{h23}	$[s^{-1}]$	4.35E+00	±43%	2.31E+00	±46%	1.03E+01	±5%	1.04E+01	±2%
Ea_{h23}	$[kJ \cdot mol^{-1}]$	2.96E+04	±264%	1.23E+04	±140%	1.03E+05	±16%	1.02E+05	±16%
A_{i12}	$[s^{-1}]$	2.98E+00	±63%	5.51E+00	±42%	4.62E+00	±13%	4.59E+00	±10%
A_{i21}	$[s^{-1}]$	5.43E-01	±306%	3.61E+00	±65%	2.98E+00	±24%	2.98E+00	±19%
Ea_{i12}	$[kJ \cdot mol^{-1}]$	4.03E+04	±116%	1.63E+05	±119%	1.40E+05	±27%	1.37E+05	±20%
Ea_{i21}	$[kJ \cdot mol^{-1}]$	1.17E+05	±43%	2.24E+05	±83%	1.60E+05	±24	1.53E+05	±18%
A_{h13}	$[s^{-1}]$	8.63E+00	±19%	5.74E+00	±18%				
Ea_{h13}	$[kJ \cdot mol^{-1}]$	8.59E+04	±33%	8.37E+04	±27%				
A_{h01}	$[s^{-1}]$	6.45E+00	±25%						
Ea_{h01}	$[kJ \cdot mol^{-1}]$	7.77E+04	±60%						
SSE		2.51E-04		5.38E-04		5.58E-04		5.57E-04	
RR		99.49%		98.90%		98.86%		98.86%	

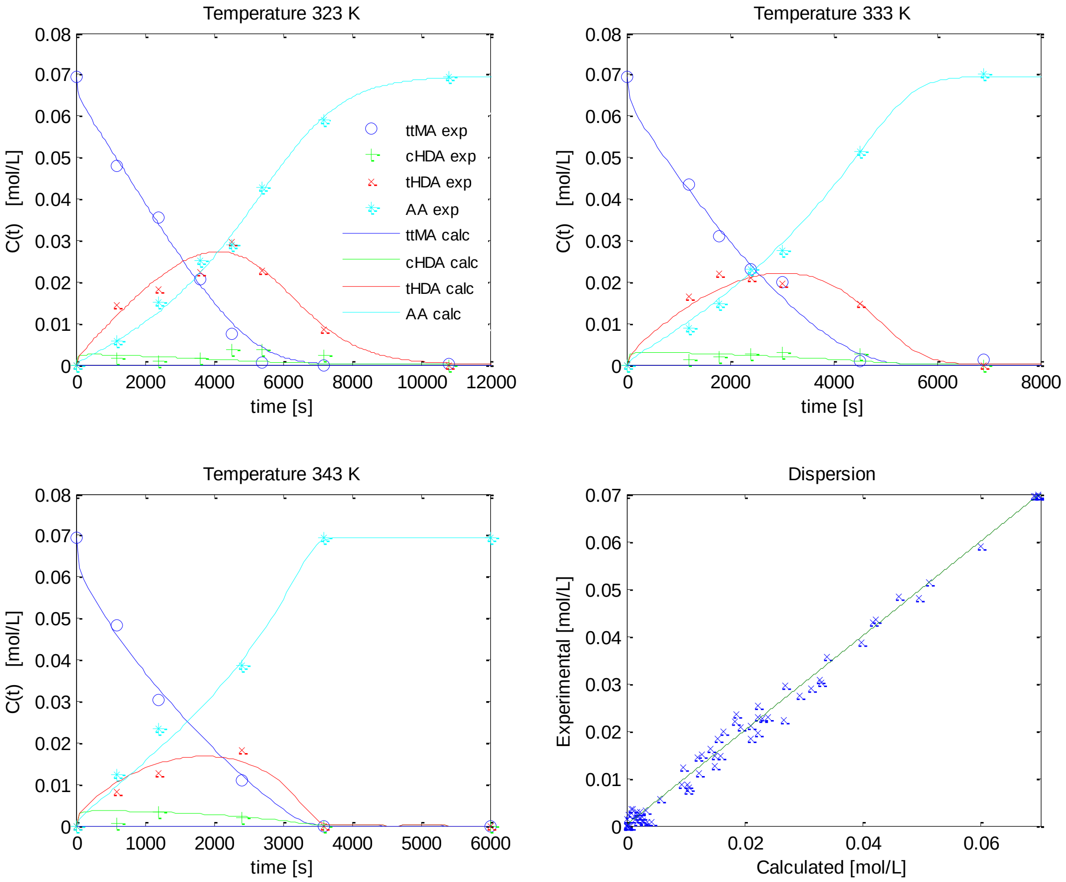

Figure 6-5: concentration profiles for the hydrogenation of ttMA on Pt/C 5% catalyst at 4 bar of hydrogen. Results of the regression with model LHHW_17P

It is clear that the equilibrium is strongly shifted towards tHDA, therefore, the hydrogenation of the cHDA intermediate is expected to have little effect on the overall mechanism. The reaction R_h13 was therefore neglected, obtaining a more simplified model with 13 parameters, referred as LHHW_13P with comparable residuals. Interestingly, the Arrhenius reaction rates parameters converged to acceptable values with a reduction of the confidence interval, but the adsorption constants saw a broadened confidence. Focusing on the adsorption constants of the dual site Langmuir Hinshelwood model, it should be noted that the values are still comparable with the estimates for 2,4-dinitrotoluene hydrogenation on carbon dispersed catalysts at similar temperatures.[17]

The large confidence interval for the adsorption constants depends on the fact that the denominator parameters are the most correlated, as shown by a least square analysis performed with BzzMath library tools. The t-test and p-test pointed K_{tHDA}, K_{AA} and K_{H2} as “redundant parameters”. This model was further analyzed performing a sensitivity analysis on the parameters, whose results are shown in Figure 6-6.

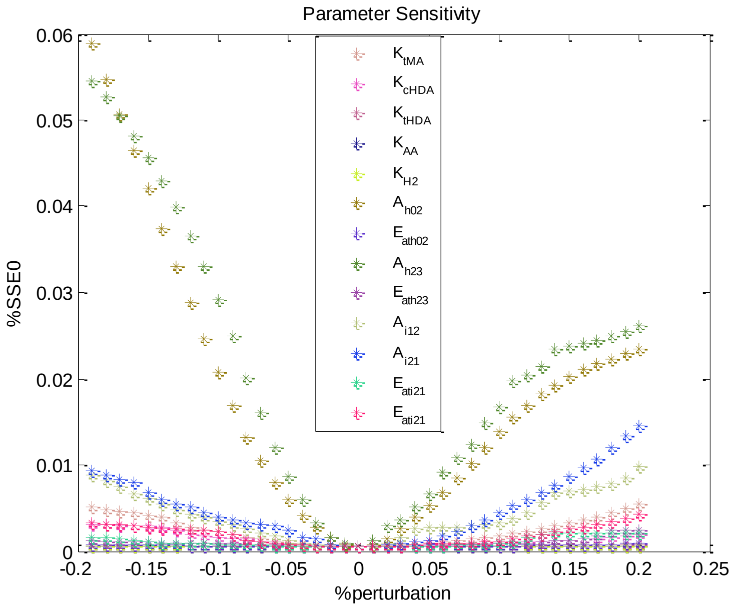

Figure 6-6: sensitivity analysis on the parameters of model LHHW_13P

The parameters that minimally affect the regression results were, in order from the less relevant, K_{H2}, K_{AA} and K_{tHDA}. Provided the constant concentration of H_2 and the lower value of the adsorption constant (close to the lower limit) the contribution of the group $K_{H2}C_{H2}$ could be neglected (<<1). Also, the group $K_{AA}C_{AA}$ was neglected, as the adsorption constants of saturated compounds was far lower than saturated ones. The obtained model had therefore 11 parameters (identified as LHHW_11P), resulting in a minimal reduction of the coefficient of determination. The statistical analysis showed that K_{tDA} was still affected by collinearity, but all the other values presented acceptable confidence intervals as shown in Table 6-6. The concentration time profiles and in the dispersion diagram for LHHW_11P are presented in Figure 6-7. In conclusion, the LHHW_11P model is to be preferred as simple but sound in representing some of the experimental data.

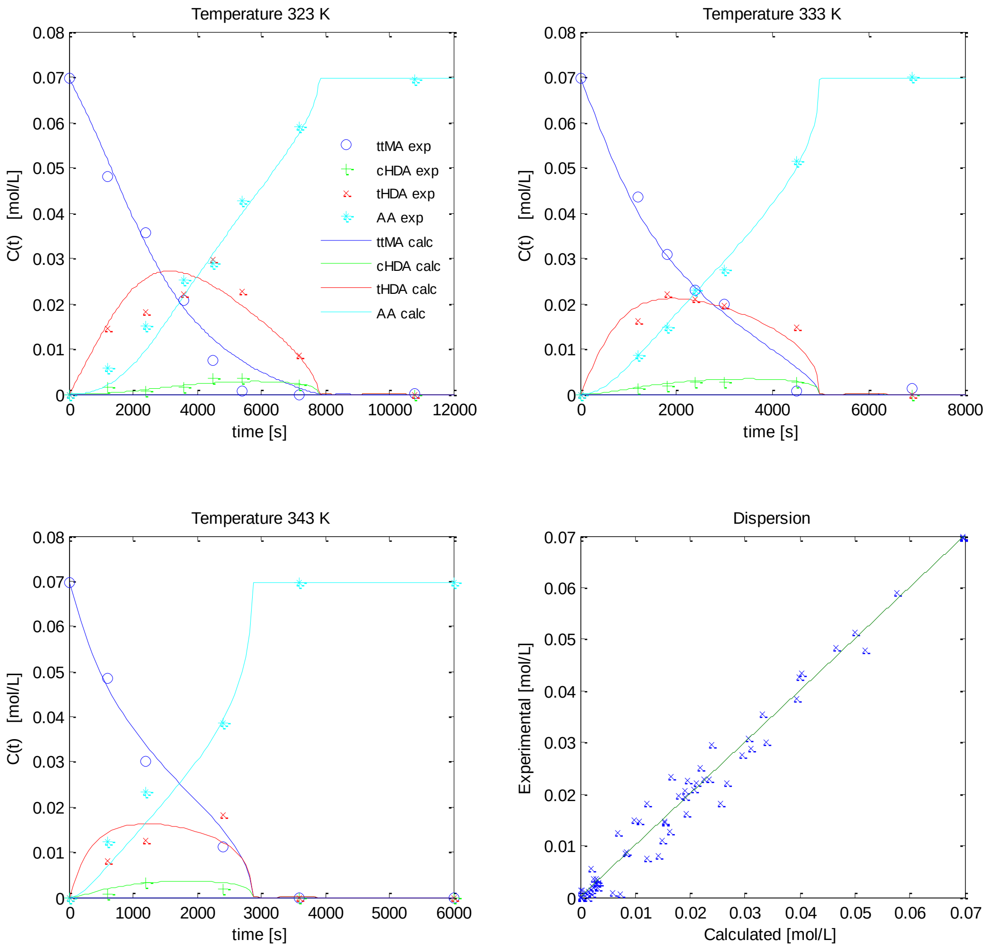

Figure 6-7: concentration profiles for the hydrogenation of ttMA on Pt/C 5% catalyst at 4 bar of hydrogen. Results of the regression with model LHHW_11P

6.3.2.2 Abbreviations Table

ttMA	trans,trans-muconic acid/ muconate salts
tHDA	(2E)-2-hexenedioic acid
cHDA	(2Z)-2-hexenedioic acid
AA	Adipic acid
LHHW	Langmuir-Hinshelwood-Hougen-Watson model
SSE	Sum of squared errors
R2	Coefficient of determination

Conclusion

Several models were used to interpret the experimental values, developed according to the LHHW theory, which considers the species adsorption-desorption equilibria of the involved species. A dual-step hydrogenation mechanism was demonstrated, characterized by hydrogen dissociation on the metal. The mechanism is the following: ttMA is hydrogenated first to tHDA, that undergoes an isomerization reaction to cHDA, promoted by the catalyst activation of the double bond. The intermediates are further hydrogenated to AA. This led to the formulation of a first model with 17 adaptive parameters, able to fit the data but strongly affected by multicollinearity. The parameters number was therefore reduced to 11, to achieve a final model with a good fit of the experimental data and characterized by kinetic constants in line with previous literature estimates of similar systems.

This very first detailed study of the hydrogenation of muconic acid provided an insight of the kinetic parameters, which currently are the sole reference values for this system. Even though the model was able to fit satisfactorily the experimental data, some topics deserve further investigation.

- An aspect that has a key role in the hydrogenation dynamics is the adsorption/desorption of the species on the catalyst. Even though LHHW model takes into account these phenomena, the model has been questioned, as performs many simplifications. For this reason, a specific study on the adsorption equilibria of muconates on the catalyst support needs to be performed. The aim is including in the kinetic equations an explicit and detailed temperature-dependent adsorption model. This will eventually reduce also the computational efforts for the kinetic regression.
- The present model can be further refined exploring and modelling the effects of a wider range of reaction conditions, collecting data on the effects of the catalyst amount, the initial species concentration, a wider span of temperatures, and possibly different reactor configurations. In this way the model could be better employed for simulating scaled-up applications, to estimate the performance and the costs of an industrial hydrogenation process of muconic acid.

In general, the hydrogenation model development and the optimization of the reaction conditions gave very encouraging results, but the work is still at its beginning.

Regression model and code

Code for the regression of the kinetic parameters of a LHHW model in C++ language. The results are then compared with the least squares analysis on Matlab and plotted

1. Leastsquares17PModel4 (C++)
2. LHHW_17P_confidence_diss.m (MATLAB)
3. LHHW_17P_print_diss.m (MATLAB)

Function 1: Leastsquares17PModel4 (C++)
Scope: Performs the SSE minimization to provide the kinetic parameters of a LHHW model of the hydrogenation of muconic acid to adipic acid.

```
#define BZZ_COMPILER 3
#include "BzzMath.hpp"
#define SSE_STD

/////////////////////////////////////////////////////////////////////////////////////////
/////////////////////////////////////////////////////////////////////
// GLOBAL VARIABLES

double ResMin(BzzVector &b); // Residues ycalc- yexp ->to be minimized
BzzMatrix ModelOdeMB(BzzVector &b, int &flag);                                         //
Function for calculating the y calc to regress b parameters [n°models, n°pt exp,
parameters, time, exp points]
void MatBalModel4(BzzVector&y, double t, BzzVector &f);    // mat bal function

BzzVector bOdeMB;                   // adaptive parameters
BzzVector tOdeMB;            // t integration time points
int numModels = 1;                  // Number of models
int numX;                                  // Nr columns input matrix
int numY;                                  // Nr input variables
int numExperiments;                        // Nr experimental points
double T;                                  // Temperature
int NumPar = 17;       // Number of adaptive parameters in the model

double R = 8.3144;                  // Universal gas constant J/mol/K
BzzVector bGL(NumPar);       // adaptive param of LHHV model, updated by function
ModelOdeMB
BzzMatrix X;                        // Input matrix acquired by file  X.dat
BzzMatrix Y;                        // Input matrix acquired by file  Y.dat
BzzMatrix Ycalc;                    // Calculated matrix by ModelOdeMB
BzzVector yexp;
FILE *risultati;                    // output file pointer
double RR;                          // RR relative residual, or normalized SSE
double SSE;                         // SSE sum of squared error
/////////////////////////////////////////////////////////////////////////////////////////
/////////////////////////////////////////////////////////////////////

void main(void)
{
        bzzOpenMP = 0;              // parallel computation deactivation
        bzzWarningWindow = 0;       // warning deactivation
        int maxIter = 10000;               // max iterations robust
        BzzVector pOpt;
```

```
        // print results
        risultati = fopen("myresults.txt", "w");
        fprintf(risultati, " %s\n ", "CALCOLO PARAMETRI CINETICI IDROGENAZIONE ACIDO
MUCONICO IN ACQUA");
        fprintf(risultati, " %s\n ", "Modello a 17 parametri (serie 4HYDnodiss)  vin
SMART, 2 run davero");

        printf(" %s\n ", "CALCOLO PARAMETRI CINETICI IDROGENAZIONE ACIDO MUCONICO IN
ACQUA");
        printf(" %s\n ", "Modello a 17 parametri (serie 4HYDnodiss)   vin SMART, 2 run
davero");

        //data acquisition
        BzzMatrix inputX;
        Load(&inputX, "Xinput.dat");
        BzzMatrix inputY;

        Load(&inputY, "Yinput.dat");
        numExperiments = inputX.Rows();    // nr lines= nr experimental points
        fprintf(risultati, "%s\t %i\n", "numero pti sperimentali", numExperiments);
        printf("%s\t\t %i\n\n\n", "numero pti sperimentali", numExperiments);
        numY = inputY.Columns();
// Measured variables (they are 5: MucA, Hdioc cis, Hdioc trans, AdiA, Hydr)
        numX = inputX.Columns();

// Measured variables in X (they are 7: Temperature, measured time, e y0)
        BzzMatrix Xload(numExperiments, numX, 1, 1, inputX);
        X = Xload;

        BzzMatrix Yload(numExperiments, numY, 1, 1, inputY);
// Exp points matrix. numExp lines, numY columns, taken from position 1,1, of input
matrix inputY
        Y = Yload;                                        Y.UseMatrixAsVector(&yexp);
        //vector experimental points
        ChangeDimensions(numExperiments, &tOdeMB); //vector tOdeMB is resized so that
measure times correspond to the calculated times

for (int i; i <= numExperiments; i = i + 1)
        {
                tOdeMB[i] = X[i][2];                                                   }

        BzzMinimizationRobust mr;          // Class minimization robust


        //  17 PARAMTETERS ++ CONSTRAINTS
        BzzVector  bL(NumPar, 0., 0., 0., 0., 0., 0., 2.5e4, 0., 2.5e4, 0., 0., 0., 0.,
0., 2.5e4, 0., 2.5e4);
        BzzVector  bU(NumPar, 1.e6, 1.e6, 1.e6, 1.e6, 1.e6, 1.e6, 6.e4, 1.e6, 6.e4, 1.e6,
1.e6, 1.e6, 1.e6, 1.e6, 6.e4, 1.e6, 6.e4);
        BzzVector b0(NumPar, 49.439346,     0.434629,      109.909861,   0.000154,
533.932809,    0.259200,     25446.403051, 1.786284,      25069.625964, 13.748135,
11.788726,     94.644664,    55778.595363, 2.729225,      59999.836649, 1.730708,
25000.005689);


        //NO CONSTRAINTS
        //BzzVector  bL(NumPar), bU(NumPar);              // Search limits
        //BzzVector b0(NumPar);
        //b0 = 1.;
        //bU = 1.e6;
        ////////////////////////////////////////////////////////////////////
        // CALCULATION
```

```
//1 step
        printf("\n\n%-s\n", "PrimoStep...");
        mr(b0, ResMin, bL, bU); // initialize object mr [1attempt, fun, min and max]
        mr(maxIter);
// Call
        mr.BzzPrint("Results 1");
        mr.GetSolution(&pOpt);

        // 2 Step
        printf("\n\n%-s\n", "SecondoStep...");
        mr(pOpt, ResMin, bL, bU);
        mr(maxIter);
        mr.BzzPrint("Results 2");
        mr.GetSolution(&pOpt);

        // 3 Step
        printf("\n\n%-s\n", "TerzoStep...");
        mr(pOpt, ResMin, bL, bU);
        mr(maxIter);
        mr.BzzPrint("Results 3");
        mr.GetSolution(&pOpt);

        //4 Step
        printf("\n\n%-s\n", "QuartoStep...");
        mr(pOpt, ResMin, bL, bU);
        mr(maxIter);
        mr.BzzPrint("Results 4");
        mr.GetSolution(&pOpt);


        //Plot screen
        pOpt.BzzPrint("\n\n\n\n%-s\n", "Parametri final:");
        printf("%s\t %f\n", "SSE", SSE);
                                                    // resudues and par
        printf("%s\t %f\n", "RR%", RR*100.);
        //plot to file myresults
        fprintf(risultati, "%s\t %f\n", "SSE", SSE);
        fprintf(risultati, "%s\t %f\n", "RR%", RR*100.);
        BzzMatrix rosematrice;
        rosematrice = Ycalc;
        int roserighe = rosematrice.Rows();
        int rosecolonne = rosematrice.Columns();
        int  rosenmat, rosemmat;
        fprintf(risultati, "\n\n %s\t\n %i\t %i\n   ", "matrice Ycalc ", roserighe,
rosecolonne);
        for (int rosenmat = 1; rosenmat <= roserighe; rosenmat++)
        {
                for (int rosemmat = 1; rosemmat <= rosecolonne; rosemmat++)
                {
                        fprintf(risultati, "%f\t", rosematrice[rosenmat][rosemmat]);
                }
                fprintf(risultati, "\n\n");
        }


} //END MAIN

/////////////////////////////////////////////////////////////////////////////////////////
///////////////////////////////////////////////////////////////////////////% Residues function
(Objective fun to be minimized)

double ResMin(BzzVector &b)
                                                    {
        int flag;
```

```
        Ycalc = ModelOdeMB(b, flag);       // calculated points


        //Convergence check

        if (flag == 1)
        {
                bzzUnfeasible = 1;
                //printf("\n%-s\n","cambiamo il giro...");

                return 0.;

        }
        #ifdef SSE_STD
        BzzVector ycalc, diff, prod, prodnorm;
        Ycalc.UseMatrixAsVector(&ycalc);    // big result matrix into vector
        diff = yexp - ycalc;                // SSE difference
        ElementByElementProduct(diff, diff, &prod);// squared difference

        SSE = prod.GetSumElements(); // Sum of squared difference
        #endif

        #ifdef SSE_NORM
        //printf("%s\t %f\n", "RR", RR);
        BzzVector ycalc, diff, prod, prodnorm;
        Ycalc.UseMatrixAsVector(&ycalc);
                                            /
        diff = yexp - ycalc;
        int sz = diff.Size();
        BzzVector diffnorm(sz);
        for (int i = 1; i <= sz; i = i + 1)
        {
                diffnorm[i] = fabs(diff[i] / (yexp[i] + 10.e-5));
        }
        //system("pause");
        //ElementByElementProduct(diffnorm, diffnorm, &prodnorm);
        double RR0;
        SSE = diffnorm.GetSumElements();
        double szf = sz*1.;
        RR = RR0 / szf;
        #endif

        return (SSE);

}

/////////////////////////////////////////////////////////////////////////////////////////
/////////////////////////////////////////////////////////////////////% Solution of the
material balances (ODE integration)

BzzMatrix ModelOdeMB(BzzVector &b, int &flag)
// generates the calculated Ycalc values
{
        flag = 0;
        bGL = b;                                                                      int
i = 1;
        BzzMatrix y0m(numExperiments, numY, 1, 3, X);      // initial conditions matrix
        BzzVector y0(numY);
                                                          // vector initial conditions,
correspond to the 3rd column of inpit matrix X
        BzzVector yMin(numY), yy(numY);                          // min y=0. Positive
value constraint
        BzzMatrix Ycalcload(numExperiments, numY);
        fprintf(risultati, "%s\n\n", "valori parziali parametri");
```

```
        //17 PARAM     fprintf(risultati, " %s\t %f\t %f\t %f\t %f\t %f\t %f\t %f\t %f\t
%f\t %f\t %f\t %f\t %f\t %f\t %f\t %f\t %f\n ", "parametri regrediti", bGL[1], bGL[2],
bGL[3], bGL[4], bGL[5], (bGL[6]), bGL[7], (bGL[8]), bGL[9], (bGL[10]), (bGL[11]),
bGL[12], bGL[13], bGL[14], bGL[15], bGL[16], bGL[17]);



        //  ODE SOLUTION
        BzzOdeStiff o;
        o.SetMinimumConstraints(&yMin); //  Constraint y>=0

        for (i = 1; i <= numExperiments; i = i + 1)
        {
                y0 = y0m.GetRow(i);
                o.SetInitialConditions(y0, 0., MatBalModel4HYD);
                T = X[i][1];   // Temperature considered, updated on the global
                yy = o(tOdeMB[i]);    // Integration: each step corresponds to the
experimental point. Integrates from 0 to tOdeMB[i]
                if (o.GetCalculationState() != 1 && o.GetCalculationState() != 2)
                {
                flag = 1;                            //If it does not converge
                }
                Ycalcload.SetRow(i, yy);

        }

        return (Ycalcload);
}
///////////////////////////////////////////////////////////////////////////////////////////
//////////////////////////////////////////////////////////////////////
// Regression models

void MatBalModel4(BzzVector&y, double t, BzzVector &f)     //LHHW with H2 dissociation ed
R_h13
{
        // Model: 17 parameters
        // Idrogenazione irreversibile muconico solo a intermedio trans, equilibrio
isomerizzazione trans cis, idrogenazione irreversibile del trans ad adipico
        // Le costanti sono LHHW CON  formulazione Arrhenius
        // Dissociazione idrogeno esplicito
        // Si idrogena anche int CIS

        bOdeMB = bGL;

        double k333_h02 = bOdeMB[6];
        double Ea333_h02 = bOdeMB[7];
        double k333_h23 = bOdeMB[8];
        double Ea333_h23 = bOdeMB[9];
        double k333_i12 = bOdeMB[10];
        double k333_i21 = bOdeMB[11];
        double Ea333_i12 = bOdeMB[12];
        double Ea333_i21 = bOdeMB[13];
        double k333_h13 = bOdeMB[14];
        double Ea333_h13 = bOdeMB[15];
        double k333_h01 = bOdeMB[16];
        double Ea333_h01 = bOdeMB[17];

        double n = 3.;
        double hydcon = bOdeMB[5] * y[5];
        double denexp1 = 1. + bOdeMB[1] * y[1] + bOdeMB[2] * y[2] + bOdeMB[3] * y[3] +
bOdeMB[4] * y[4] + pow(hydcon, 0.5);//Adsorptions (denominator)
```

```
       double R_h02 = exp(k333_h02 - Ea333_h02 / R*(1. / T - 1. / 333.)) * y[1] * y[5] /
pow(denexp1, n);
                                           // Hydrog ttMA to tHDA
       double R_h23 = exp(k333_h23 - Ea333_h23 / R*(1. / T - 1. / 333.)) * y[3] * y[5] /
pow(denexp1, n);                                  // Hydrog tHDA to AA
       double R_i12 = -exp(k333_i12 - Ea333_i12 / R*(1. / T - 1. / 333.)) * y[2] /
pow(denexp1, n) + exp(k333_i21 - Ea333_i21 / R*(1. / T - 1. / 333.)) * y[3] /
pow(denexp1, n);                    // Isomer cHDA->tHDA
       double R_h13 = exp(k333_h13 - Ea333_h13 / R*(1. / T - 1. / 333.)) * y[2] * y[5] /
pow(denexp1, n);                                  // Hydrog cHDA to AA
       double R_h01 = exp(k333_h01 - Ea333_h01 / R*(1. / T - 1. / 333.)) * y[1] * y[5] /
pow(denexp1, n);                                  // Hydrog ttMA to cHDA       f[1] = -
R_h02 - R_h01;        // tMA consumption
       f[2] = +R_i12 - R_h13 + R_h01;      // formation consumption cHDA
       f[3] = R_h02 - R_h23 - R_i12;       // formation consumption tHDA
       f[4] = R_h23 + R_h13;        // formation AA
       f[5] = 0.;                          //Hydrogen constant composition
}

/////////////////////////////////////////////////////////////////////////////////////////
//////////////////////// THE END ////////////////////////////////////
```

Input files: Xinput.dat

```
24 7

323.15 0      6.96E-02      0.00E+00      0.00E+00      0.00E+00      2.73E-03
323.15 1200   6.96E-02      0.00E+00      0.00E+00      0.00E+00      2.73E-03
323.15 2400   6.96E-02      0.00E+00      0.00E+00      0.00E+00      2.73E-03
323.15 3600   6.96E-02      0.00E+00      0.00E+00      0.00E+00      2.73E-03
323.15 4500   6.96E-02      0.00E+00      0.00E+00      0.00E+00      2.73E-03
323.15 5400   6.96E-02      0.00E+00      0.00E+00      0.00E+00      2.73E-03
323.15 7200   6.96E-02      0.00E+00      0.00E+00      0.00E+00      2.73E-03
323.15 10800  6.96E-02      0.00E+00      0.00E+00      0.00E+00      2.73E-03
323.15 14400  6.96E-02      0.00E+00      0.00E+00      0.00E+00      2.73E-03
333.15 0      6.96E-02      0.00E+00      0.00E+00      0.00E+00      2.59E-03
333.15 1200   6.96E-02      0.00E+00      0.00E+00      0.00E+00      2.59E-03
333.15 1800   6.96E-02      0.00E+00      0.00E+00      0.00E+00      2.59E-03
333.15 2400   6.96E-02      0.00E+00      0.00E+00      0.00E+00      2.59E-03
333.15 3000   6.96E-02      0.00E+00      0.00E+00      0.00E+00      2.59E-03
333.15 4500   6.96E-02      0.00E+00      0.00E+00      0.00E+00      2.59E-03
333.15 6900   6.96E-02      0.00E+00      0.00E+00      0.00E+00      2.59E-03
333.15 9000   6.96E-02      0.00E+00      0.00E+00      0.00E+00      2.59E-03
343.15 0      6.96E-02      0.00E+00      0.00E+00      0.00E+00      2.47E-03
343.15 600    6.96E-02      0.00E+00      0.00E+00      0.00E+00      2.47E-03
343.15 1200   6.96E-02      0.00E+00      0.00E+00      0.00E+00      2.47E-03
343.15 2400   6.96E-02      0.00E+00      0.00E+00      0.00E+00      2.47E-03
343.15 3600   6.96E-02      0.00E+00      0.00E+00      0.00E+00      2.47E-03
343.15 6000   6.96E-02      0.00E+00      0.00E+00      0.00E+00      2.47E-03
343.15 7200   6.96E-02      0.00E+00      0.00E+00      0.00E+00      2.47E-03
```

Input files: Yinput.dat

```
24 5

6.96E-02      0.00E+00      0.00E+00      0.00E+00      2.73E-03
4.80E-02      1.47E-03      1.45E-02      5.69E-03      2.73E-03
3.55E-02      8.39E-04      1.82E-02      1.50E-02      2.73E-03
2.07E-02      1.46E-03      2.22E-02      2.52E-02      2.73E-03
7.56E-03      3.59E-03      2.96E-02      2.89E-02      2.73E-03
6.47E-04      3.53E-03      2.26E-02      4.28E-02      2.73E-03
```

```
0.00E+00       2.12E-03       8.51E-03       5.90E-02       2.73E-03
6.96E-05       0.00E+00       0.00E+00       6.95E-02       2.73E-03
0.00E+00       0.00E+00       0.00E+00       6.96E-02       2.73E-03
6.96E-02       0.00E+00       0.00E+00       0.00E+00       2.59E-03
4.35E-02       1.13E-03       1.63E-02       8.67E-03       2.59E-03
3.09E-02       1.83E-03       2.21E-02       1.48E-02       2.59E-03
2.29E-02       2.76E-03       2.10E-02       2.29E-02       2.59E-03
1.98E-02       2.82E-03       1.95E-02       2.75E-02       2.59E-03
7.66E-04       2.72E-03       1.48E-02       5.13E-02       2.59E-03
1.33E-03       0.00E+00       0.00E+00       7.00E-02       2.59E-03
0.00E+00       0.00E+00       0.00E+00       7.00E-02       2.59E-03
6.96E-02       0.00E+00       0.00E+00       0.00E+00       2.47E-03
4.85E-02       6.87E-04       8.05E-03       1.24E-02       2.47E-03
3.01E-02       3.32E-03       1.27E-02       2.34E-02       2.47E-03
1.10E-02       1.86E-03       1.82E-02       3.85E-02       2.47E-03
0.00E+00       0.00E+00       0.00E+00       6.96E-02       2.47E-03
0.00E+00       0.00E+00       0.00E+00       6.96E-02       2.47E-03
0.00E+00       0.00E+00       0.00E+00       6.96E-02       2.47E-03
```

Function 2: LHHW_17P_confidence_diss.m (MATLAB)
Scope: Performs the SSE minimization to provide the kinetic parameters of a LHHW model of the hydrogenation of muconic acid to adipic acid.

```
%algorithm to calculate 95% confidence intervals for the parameters regressed with
lsqnonlin

function nonlinmatlab

global Xinput Yexp;
%Predictor variables:  time[s]; C_muc[mol/L]; C_cis[mol/L]; C_trans[mol/L];
C_adia[mol/L]; C_H2[mol/L];T[K];
Xinput=[0       6.96E-02    0.00E+00    0.00E+00    0.00E+00    2.73E-03    323.15
        1200    6.96E-02    0.00E+00    0.00E+00    0.00E+00    2.73E-03    323.15
        2400    6.96E-02    0.00E+00    0.00E+00    0.00E+00    2.73E-03    323.15
        3600    6.96E-02    0.00E+00    0.00E+00    0.00E+00    2.73E-03    323.15
        4500    6.96E-02    0.00E+00    0.00E+00    0.00E+00    2.73E-03    323.15
        5400    6.96E-02    0.00E+00    0.00E+00    0.00E+00    2.73E-03    323.15
        7200    6.96E-02    0.00E+00    0.00E+00    0.00E+00    2.73E-03    323.15
        10800   6.96E-02    0.00E+00    0.00E+00    0.00E+00    2.73E-03    323.15
        14400   6.96E-02    0.00E+00    0.00E+00    0.00E+00    2.73E-03    323.15
        0       6.96E-02    0.00E+00    0.00E+00    0.00E+00    2.59E-03    333.15
        1200    6.96E-02    0.00E+00    0.00E+00    0.00E+00    2.59E-03    333.15
        1800    6.96E-02    0.00E+00    0.00E+00    0.00E+00    2.59E-03    333.15
        2400    6.96E-02    0.00E+00    0.00E+00    0.00E+00    2.59E-03    333.15
        3000    6.96E-02    0.00E+00    0.00E+00    0.00E+00    2.59E-03    333.15
        4500    6.96E-02    0.00E+00    0.00E+00    0.00E+00    2.59E-03    333.15
        6900    6.96E-02    0.00E+00    0.00E+00    0.00E+00    2.59E-03    333.15
        9000    6.96E-02    0.00E+00    0.00E+00    0.00E+00    2.59E-03    333.15
        0       6.96E-02    0.00E+00    0.00E+00    0.00E+00    2.47E-03    343.15
        600     6.96E-02    0.00E+00    0.00E+00    0.00E+00    2.47E-03    343.15
        1200    6.96E-02    0.00E+00    0.00E+00    0.00E+00    2.47E-03    343.15
        2400    6.96E-02    0.00E+00    0.00E+00    0.00E+00    2.47E-03    343.15
        3600    6.96E-02    0.00E+00    0.00E+00    0.00E+00    2.47E-03    343.15
        6000    6.96E-02    0.00E+00    0.00E+00    0.00E+00    2.47E-03    343.15
        7200    6.96E-02    0.00E+00    0.00E+00    0.00E+00    2.47E-03
343.15];

%Response values experimental: C_muc[mol/L]; C_cis[mol/L]; C_trans[mol/L];
C_adia[mol/L]; C_H2[mol/L]
Yexp=[6.96E-02  0.00E+00    0.00E+00    0.00E+00    2.73E-03
      4.80E-02  1.47E-03    1.45E-02    5.69E-03    2.73E-03
      3.55E-02  8.39E-04    1.82E-02    1.50E-02    2.73E-03
      2.07E-02  1.46E-03    2.22E-02    2.52E-02    2.73E-03
      7.56E-03  3.59E-03    2.96E-02    2.89E-02    2.73E-03
      6.47E-04  3.53E-03    2.26E-02    4.28E-02    2.73E-03
      0.00E+00  2.12E-03    8.51E-03    5.90E-02    2.73E-03
      6.96E-05  0.00E+00    0.00E+00    6.95E-02    2.73E-03
      0.00E+00  0.00E+00    0.00E+00    6.96E-02    2.73E-03
      6.96E-02  0.00E+00    0.00E+00    0.00E+00    2.59E-03
      4.35E-02  1.13E-03    1.63E-02    8.67E-03    2.59E-03
      3.09E-02  1.83E-03    2.21E-02    1.48E-02    2.59E-03
      2.29E-02  2.76E-03    2.10E-02    2.29E-02    2.59E-03
      1.98E-02  2.82E-03    1.95E-02    2.75E-02    2.59E-03
      7.66E-04  2.72E-03    1.48E-02    5.13E-02    2.59E-03
      1.33E-03  0.00E+00    0.00E+00    7.00E-02    2.59E-03
      0.00E+00  0.00E+00    0.00E+00    7.00E-02    2.59E-03
      6.96E-02  0.00E+00    0.00E+00    0.00E+00    2.47E-03
      4.85E-02  6.87E-04    8.05E-03    1.24E-02    2.47E-03
      3.01E-02  3.32E-03    1.27E-02    2.34E-02    2.47E-03
      1.10E-02  1.86E-03    1.82E-02    3.85E-02    2.47E-03
      0.00E+00  0.00E+00    0.00E+00    6.96E-02    2.47E-03
      0.00E+00  0.00E+00    0.00E+00    6.96E-02    2.47E-03
      0.00E+00  0.00E+00    0.00E+00    6.96E-02    2.47E-03];
```

```
beta0=[ 14.945133    4859.685480     5.812822    65.303215   419.716329  4.722541
120000.000000   4.348464    29569.064584    2.979021    0.543381    40294.045485
116612.941311   8.631272    85886.851277    6.445348    77711.047153];
betaL=[ 1.,  1.,         1.,         1.,         1.,         1.e-8,      1.e4,
1.e-8,       1.e4,       1.e-8,      1.e-8,      1.e3,       1.e3,       1.e-8,
1.e4, 1.e-8,        1.e4];
betaU=[  1.e6, 1.e6, 1.e6, 1.e6, 1.e6, 1.e6, 1.2e5, 1.e6, 1.2e5, 1.e8, 1.e8, 1.e6,
1.e6, 1.e6, 1.2e5, 1.e6, 1.2e5];

options = optimoptions(@lsqnonlin,'TolX',1e-8);



[beta,resnorm,residual,exitflag,output,lambda,jacobian]=lsqnonlin(@fun, beta0,
betaL, betaU,options);
disp(beta);
ci = nlparci(beta,residual,'jacobian',jacobian)
beta=beta';
stdev=ci(:,2)-beta;

beta_out = sprintf('%0.6e\n',beta)
stdev_out=sprintf('%0.6e\n',stdev)
% Calculation least squares value
function yy=fun(beta)
global Xinput Yexp;


texp323=Xinput(1:9,1);
C0323=Xinput(1,2:6);

texp333=Xinput(10:17,1);
C0333=Xinput(10,2:6);

texp343=Xinput(18:24,1);
C0343=Xinput(18,2:6);

[tls323,Cls323] = ode23s(@BMDIFF323,texp323,C0323,[],beta);
[tls333,Cls333] = ode23s(@BMDIFF333,texp333,C0333,[],beta);
[tls343,Cls343] = ode23s(@BMDIFF343,texp343,C0343,[],beta);
Ycalc=[Cls323;Cls333;Cls343];
YVcalc=reshape(Ycalc, [],1);
YVexp=reshape(Yexp, [],1);
yy=YVcalc-YVexp;


%% ---------------- FUNCTION MATERIAL BAL  323K-------------------
function dy = BMDIFF323(t,C,par)
% C  Cexp(1) muconic Cexp; (2) intermediate cis;  Cexp(3)intermediate trans;
Cexp(4) adipic;  Cexp(5) hydrogen
T=323;
 R=8.314;
k333_h02 = par(6); % par from 1 to 5 are LHHW adsorption constants
Ea333_h02 = par(7);
k333_h23 = par(8);
Ea333_h23 = par(9);
k333_i12 = par(10);
k333_i21 = par(11);
Ea333_i12 = par(12);
Ea333_i21 = par(13);
k333_h13=par(14);
Ea333_h13 = par(15);
k333_h01 = par(16);
Ea333_h01 = par(17);
denexp=(1+par(1)*C(1)+par(2)*C(2)+par(3)*C(3)+par(4)*C(4)+(par(5)*C(5)))^3;

R_h02 = exp(k333_h02 - Ea333_h02/R*(1/T-1/333))*C(1)*C(5)/denexp;      %trans int
formation
```

```
R_h23 = exp(k333_h23 - Ea333_h23 / R*(1 / T - 1 / 333))*C(3)*C(5)/denexp;
%trans int hydrog to aa
R_i12= (-exp(k333_i12 - Ea333_i12 / R*(1 / T - 1 / 333))*C(2)+exp(k333_i21 -
Ea333_i21 / R*(1 / T - 1 / 333))*C(3))/denexp; %isomerization cis->trans (e
contrario)
R_h13=exp(k333_h13 - Ea333_h13 / R*(1 / T - 1 / 333))*C(2)*C(5)/denexp;      %cis
int hydrog to aa
R_h01= exp(k333_h01 - Ea333_h01/R*(1/T-1/333))*C(1)*C(5)/denexp;      %trans cis
formation

    dC(1) = -R_h02-R_h01;           %BM ttMA
    dC(2) = R_i12-R_h13+R_h01;      %BM cHDA
    dC(3) = R_h02-R_h23-R_i12;      %BM tHDA
    dC(4) = R_h23+R_h13;            %BM AA
    dC(5) = 0.;                     %BM Const H2
    dy=dC';

%% ---------------- FUNCTION MATERIAL BAL 333K-------------------
function dy = BMDIFF333(t,C,par)
% C  Cexp(1) muconic Cexp; (2) intermediate cis;  Cexp(3)intermediate trans;
Cexp(4) adipic;  Cexp(5) hydrogen
T=333;
R=8.314;
k333_h02 = par(6);
Ea333_h02 = par(7);
k333_h23 = par(8);
Ea333_h23 = par(9);
k333_i12 = par(10);
k333_i21 = par(11);
Ea333_i12 = par(12);
Ea333_i21 = par(13);
k333_h13=par(14);
Ea333_h13 = par(15);
k333_h01 = par(16);
Ea333_h01 = par(17);
denexp=(1+par(1)*C(1)+par(2)*C(2)+par(3)*C(3)+par(4)*C(4)+(par(5)*C(5)))^3;

R_h02 =exp(k333_h02 - Ea333_h02/R*(1/T-1/333))*C(1)*C(5)/denexp;      %trans int
formation
R_h23 =exp(k333_h23 - Ea333_h23 / R*(1 / T - 1 / 333))*C(3)*C(5)/denexp;
%trans int hydrog to aa
R_i12= (-exp(k333_i12 - Ea333_i12 / R*(1 / T - 1 / 333))*C(2)+exp(k333_i21 -
Ea333_i21 / R*(1 / T - 1 / 333))*C(3))/denexp; %isomerization cis->trans (e
contrario)
R_h13=exp(k333_h13 - Ea333_h13 / R*(1 / T - 1 / 333))*C(2)*C(5)/denexp;      %cis
int hydrog to aa
R_h01= exp(k333_h01 - Ea333_h01/R*(1/T-1/333))*C(1)*C(5)/denexp;      %trans cis
formation

    dC(1) = -R_h02-R_h01;           %BM ttMA
    dC(2) = R_i12-R_h13+R_h01;      %BM cHDA
    dC(3) = R_h02-R_h23-R_i12;      %BM tHDA
    dC(4) = R_h23+R_h13;            %BM AA
    dC(5) = 0.;                     %BM Const H2
    dy=dC';

%% ---------------- FUNCTION MATERIAL BAL  343K-------------------
    function dy = BMDIFF343(t,C,par)
T=343;
  R=8.314;
k333_h02 = par(6);                  % par da 1 a 5 sono le costanti di
adsorbimento secondo LHHW
Ea333_h02 = par(7);
k333_h23 = par(8);
Ea333_h23 = par(9);
k333_i12 = par(10);
k333_i21 = par(11);
```

```
Ea333_i12 = par(12);
Ea333_i21 = par(13);
k333_h13=par(14);
Ea333_h13 = par(15);
k333_h01 = par(16);
Ea333_h01 = par(17);
denexp=(1+par(1)*C(1)+par(2)*C(2)+par(3)*C(3)+par(4)*C(4)+(par(5)*C(5)))^3;

R_h02 =exp(k333_h02 - Ea333_h02/R*(1/T-1/333))*C(1)*C(5)/denexp;      %trans int
formation
R_h23 =exp(k333_h23 - Ea333_h23 / R*(1 / T - 1 / 333))*C(3)*C(5)/denexp;
%trans int hydrog to aa
R_i12= (-exp(k333_i12 - Ea333_i12 / R*(1 / T - 1 / 333))*C(2)+exp(k333_i21 -
Ea333_i21 / R*(1 / T - 1 / 333))*C(3))/denexp; %isomerization cis->trans (e
contrario)
R_h13=exp(k333_h13 - Ea333_h13 / R*(1 / T - 1 / 333))*C(2)*C(5)/denexp;      %cis
int hydrog to aa
R_h01= exp(k333_h01 - Ea333_h01/R*(1/T-1/333))*C(1)*C(5)/denexp;      %trans cis
formation

    dC(1) = -R_h02-R_h01;            %BM ttMA
    dC(2) = R_i12-R_h13+R_h01;       %BM cHDA
    dC(3) = R_h02-R_h23-R_i12;       %BM tHDA
    dC(4) = R_h23+R_h13;             %BM AA
    dC(5) = 0.;                      %BM Const H2
    dy=dC';
```

Function 3: LHHW_17P_print_diss.m (MATLAB)
Scope: Calculates the concentration profiles of the species and plots them against the experimental values, given the regressed model parameters.

```
%% PRINTING TOOL
%% REFERRED TO LHHW 17P

function fitDIFF

 close all           % per chiudere eventuali finestre di grafici
 clear all
 clc
 global npoint;

 %%%% Temperature 323
input='input_int';                     % opens input dfile
C0323=xlsread(input,3,'B2:F2');            % conc matrix col1 ttMA, col2 cHDA,
col3 tHDA, col4 AA, col 5 H2
npoint=xlsread(input,3,'A20');          % nr exp points
rM=xlsread(input,3,'A2:F10');           % matrice input (grezza)
Cexp323=rM(1:npoint,2:end);                % matrice concentrazione specie col1
muconico, col2 intermedio cis,  col3 intermedio trans, col4 adipico, col 5 hydr
texp323 =rM(1:npoint,1);                   % vettore dei tempi sperimentali
Cexp_muc323=[texp323, Cexp323(1:npoint,1)];
Cexp_cis323=[texp323, Cexp323(1:npoint,2)];
Cexp_trans323=[texp323, Cexp323(1:npoint,3)];
Cexp_aad323=[texp323, Cexp323(1:npoint,4)];

%%%% Temperature 333
C0333=xlsread(input,4,'B2:F2');            conc matrix col1 ttMA, col2 cHDA,  col3
tHDA, col4 AA, col 5 H2
npoint=xlsread(input,4,'A20');          % nr exp points
rM=xlsread(input,4,'A2:F9');           % matrice input (grezza)
Cexp333=rM(1:npoint,2:end);                % matrice concentrazione specie col1
muconico, col2 intermedio cis,  col3 intermedio trans, col4 adipico, col 5 hydr
texp333 =rM(1:npoint,1);                   % vettore dei tempi sperimentali
Cexp_muc333=[texp333, Cexp333(1:npoint,1)];
Cexp_cis333=[texp333, Cexp333(1:npoint,2)];
Cexp_trans333=[texp333, Cexp333(1:npoint,3)];
Cexp_aad333=[texp333, Cexp333(1:npoint,4)];

%%%% Temperature 343
C0343=xlsread(input,5,'B2:F2'); % initial conc ttMA, cHDA, tHDA, AA, H2
npoint=xlsread(input,5,'A20');          % nr exp points
rM=xlsread(input,5,'A2:F8');           % matrice input (grezza)
Cexp343=rM(1:npoint,2:end);           % conc matrix col1 ttMA, col2 cHDA,  col3
tHDA, col4 AA, col 5 H2
texp343 =rM(1:npoint,1);                   % exp times
Cexp_muc343=[texp343, Cexp343(1:npoint,1)];
Cexp_cis343=[texp343, Cexp343(1:npoint,2)];
Cexp_trans343=[texp343, Cexp343(1:npoint,3)];
Cexp_aad343=[texp343, Cexp343(1:npoint,4)];

% Insert final parameters
par=[14.945133   4859.685480     5.812822    65.303215   419.716329  4.722541
120000.000000   4.348464    29569.064584    2.979021    0.543381    40294.045485
116612.941311   8.631272    85886.851277    6.445348    77711.047153];

tsmooth323=[0:60:14400];
tsmooth333=[0:60:9000];
tsmooth343=[0:60:7200];
[tg323,Ctg323] = ode23s(@BMDIFF323,tsmooth323,C0323,[],par);
[tg333,Ctg333] = ode23s(@BMDIFF333,tsmooth333,C0333,[],par);
[tg343,Ctg343] = ode23s(@BMDIFF343,tsmooth343,C0343,[],par);
```

```
% LEAST SQUARE CALC
[tls323,Cls323] = ode23s(@BMDIFF323,texp323,C0323,[],par);
[tls333,Cls333] = ode23s(@BMDIFF333,texp333,C0333,[],par);
[tls343,Cls343] = ode23s(@BMDIFF343,texp343,C0343,[],par);

Clscalc=[reshape(Cls323(:,1:4), numel(Cls323(:,1:4)),1);reshape(Cls333(:,1:4),
numel(Cls333(:,1:4)),1);reshape(Cls343(:,1:4), numel(Cls343(:,1:4)),1)];
Clsexp=[Cexp_muc323(:,2);Cexp_cis323(:,2);Cexp_trans323(:,2);Cexp_aad323(:,2);Cexp
_muc333(:,2);Cexp_cis333(:,2);Cexp_trans333(:,2);Cexp_aad333(:,2);Cexp_muc343(:,2)
;Cexp_cis343(:,2);Cexp_trans343(:,2);Cexp_aad343(:,2); ];
SSE = sum((Clscalc-Clsexp).^2);
disp('SSE');
disp(SSE);
RR= (1-SSE/sum((Clsexp-mean(Clsexp)).^2))
disp ('RR');
disp(RR);



%PLOT
figure
plot (Clscalc, Clsexp, 'x', [0:0.000001:0.07],[0:0.000001:0.07], '-' )

 figure (1)

plot(Cexp_muc323(:,1),Cexp_muc323(:,2),'ob',
Cexp_cis323(:,1),Cexp_cis323(:,2),'+g',
Cexp_trans323(:,1),Cexp_trans323(:,2),'xr',
Cexp_aad323(:,1),Cexp_aad323(:,2),'*c', tg323,Ctg323(:,1),'b',
tg323,Ctg323(:,2),'g', tg323,Ctg323(:,3),'r', tg323,Ctg323(:,4),'c',
tg323,zeros(size(tg323)));
title('Temperature 323K')
 xlabel('time [s]'),ylabel('C(t)   [moli/L]');
 legend('muconic exp','intermediate cis exp', 'intermediate trans exp','adipic
exp','muconic calc','intermediate cis calc','intermediate trans calc', 'adipic
calc' );

 figure (2)
 plot(Cexp_muc333(:,1),Cexp_muc333(:,2),'ob',
Cexp_cis333(:,1),Cexp_cis333(:,2),'+g',
Cexp_trans333(:,1),Cexp_trans333(:,2),'xr',
Cexp_aad333(:,1),Cexp_aad333(:,2),'*c', tg333,Ctg333(:,1),'b',
tg333,Ctg333(:,2),'g', tg333,Ctg333(:,3),'r', tg333,Ctg333(:,4),'c',
tg333,zeros(size(tg333)));
title( 'Temperature 333K')
 xlabel('time [s]'),ylabel('C(t)   [moli/L]');
 legend('muconic exp','intermediate cis exp', 'intermediate trans exp','adipic
exp','muconic calc','intermediate cis calc','intermediate trans calc', 'adipic
calc' );


 figure (3)
plot(Cexp_muc343(:,1),Cexp_muc343(:,2),'ob',
Cexp_cis343(:,1),Cexp_cis343(:,2),'+g',
Cexp_trans343(:,1),Cexp_trans343(:,2),'xr',
Cexp_aad343(:,1),Cexp_aad343(:,2),'*c', tg343,Ctg343(:,1),'b',
tg343,Ctg343(:,2),'g', tg343,Ctg343(:,3),'r', tg343,Ctg343(:,4),'c',
tg343,zeros(size(tg343)));
 title('Temperature 343K')
 xlabel('time [s]'),ylabel('C(t)   [moli/L]');
 legend('muconic exp','intermediate cis exp', 'intermediate trans exp','adipic
exp','muconic calc','intermediate cis calc','intermediate trans calc', 'adipic
calc' );


 figure (4)
```

```
 subplot(2,2,1);
 plot(Cexp_muc323(:,1),Cexp_muc323(:,2),'ob',
Cexp_cis323(:,1),Cexp_cis323(:,2),'+g',
Cexp_trans323(:,1),Cexp_trans323(:,2),'xr',
Cexp_aad323(:,1),Cexp_aad323(:,2),'*c', tg323,Ctg323(:,1),'b',
tg323,Ctg323(:,2),'g', tg323,Ctg323(:,3),'r', tg323,Ctg323(:,4),'c',
tg323,zeros(size(tg323)));
axis([0 12000 0 0.08 ])
 title('Temperature 323 K')
 xlabel('time [s]'),ylabel('C(t)   [mol/L]');

  subplot(2,2,2);
 plot(Cexp_muc333(:,1),Cexp_muc333(:,2),'ob',
Cexp_cis333(:,1),Cexp_cis333(:,2),'+g',
Cexp_trans333(:,1),Cexp_trans333(:,2),'xr',
Cexp_aad333(:,1),Cexp_aad333(:,2),'*c', tg333,Ctg333(:,1),'b',
tg333,Ctg333(:,2),'g', tg333,Ctg333(:,3),'r', tg333,Ctg333(:,4),'c',
tg333,zeros(size(tg333)));
axis([ 0 8000 0 0.08])
 title( 'Temperature 333 K')
 xlabel('time [s]'),ylabel('C(t)   [mol/L]');

 subplot(2,2,3);
 plot(Cexp_muc343(:,1),Cexp_muc343(:,2),'ob',
Cexp_cis343(:,1),Cexp_cis343(:,2),'+g',
Cexp_trans343(:,1),Cexp_trans343(:,2),'xr',
Cexp_aad343(:,1),Cexp_aad343(:,2),'*c', tg343,Ctg343(:,1),'b',
tg343,Ctg343(:,2),'g', tg343,Ctg343(:,3),'r', tg343,Ctg343(:,4),'c',
tg343,zeros(size(tg343)));
 axis([ 0 6000 0 0.08])
 title('Temperature 343 K')
 xlabel('time [s]'),ylabel('C(t)   [mol/L]');
legend('ttMA exp','cHDA exp', 'tHDA exp','AA exp','ttMA calc','cHDA calc','tHDA
calc', 'AA calc' );

subplot(2,2,4);
 plot (Clscalc, Clsexp, 'x', [0:0.000001:0.07],[0:0.000001:0.07], '-' )
 axis([0 0.07 0 0.07])
 title('Dispersion')
 xlabel('Calculated [mol/L]'),ylabel('Experimental [mol/L]');



 figure (5)
plot (Clscalc, Clsexp, 'x', [0:0.000001:0.07],[0:0.000001:0.07], '-' )
```

Bibliography

1. Carraher, J. M., Matthiesen, J. E. & Tessonnier, J.-P. Comments on "Thermodynamics of cis,cis-muconic acid solubility in various polar solvents at low temperature range". *J. Mol. Liq.* **224,** 420–422 (2016).
2. Li, X. *et al.* Highly efficient chemical process to convert mucic acid into adipic acid and DFT studies of the mechanism of the rhenium-catalyzed deoxydehydration. *Angew. Chemie - Int. Ed.* **53,** 4200–4204 (2014).
3. Frost, J. W., Miermont, A., Schweitzer, D. & Bui, V. Preparation of trans, trans muconic acid and trans, trans muconates. (2013).
4. Carraher, J. M., Pfennig, T., Rao, R. G., Shanks, B. H. & Tessonnier, J.-P. cis,cis-Muconic acid isomerization and catalytic conversion to biobased cyclic-C $_6$ -1,4-diacid monomers. *Green Chem.* 21–25 (2017). doi:10.1039/C7GC00658F
5. Matthiesen, J. E. *et al.* Electrochemical Conversion of Biologically Produced Muconic Acid: Key Considerations for Scale-Up and Corresponding Technoeconomic Analysis. *ACS Sustain. Chem. Eng.* **4,** 7098–7109 (2016).
6. Vardon, D. R. *et al.* cis,cis-Muconic acid: separation and catalysis to bio-adipic acid for nylon-6,6 polymerization. *Green Chem.* **18,** 3397–3413 (2016).
7. She, X., Brown, H. M., Zhang, X., Ahring, B. K. & Wang, Y. Selective hydrogenation of trans,trans-muconic acid to adipic acid over a titania-supported rhenium catalyst. *ChemSusChem* **4,** 1071–1073 (2011).
8. Yang, K. H. & Hougen, O. A. Determination of mechanism of catalyzed gaseous reactions. *Chem. Eng. Prog.* **46,** 146–157 (1950).
9. Rostrup-Nielsen, J. Chapter 5 Reaction kinetics/reactor design. *Catal. Today* **22,** 295–311 (1994).
10. Chaudhari, R. V & Ramachandran, P. A. Three phase slurry reactors. *AIChE J.* **26,** 177–201 (1980).
11. Piskun, A. S., van de Bovenkamp, H. H., Rasrendra, C. B., Winkelman, J. G. M. & Heeres, H. J. Kinetic modeling of levulinic acid hydrogenation to γ-valerolactone in water using a carbon supported Ru catalyst. *Appl. Catal. A Gen.* **525,** 158–167 (2016).
12. Rajashekharam, M. V, Nikalje, D. D., Jaganathan, R. & Chaudhari, R. V. Hydrogenation of 2,4-Dinitrotoluene Using a Pd/Al2O3 Catalyst in a Slurry Reactor: A Molecular Level Approach to Kinetic Modeling and Nonisothermal Effects. *Ind. Eng. Chem. Res.* **36,** 592–604 (1997).
13. Chaudhari, R. V *et al.* Kinetics of hydrogenation of maleic acid in a batch slurry reactor using a bimetallic Ru–Re/C catalyst. *Chem. Eng. Sci.* **58,** 627–632 (2003).
14. Buzzi-Ferraris, G. & Manenti, F. *Interpolation and Regression Models for chemical engineer: Solving Numerical Problems*. (Jhon Wiley & Sons, 2010).
15. Froment, G. F., Bischoff, K. B. & De Wilde, J. *Chemical reactor analysis and design*. (Wiley New York, 2011).
16. Lylykangas, M. S., Rautanen, P. A. & Krause, A. O. I. Hydrogenation and Deactivation Kinetics in the Liquid-Phase Hydrogenation of Isooctenes on Pt/Al2O3. *Ind. Eng. Chem. Res.* **43,** 1641–1648 (2004).
17. Buzzi-Ferraris, G. & Manenti, F. *Interpolation and Regression Models for the Chemical Engineer: Solving Numerical Problems*. (John Wiley & Sons, 2010).
18. Vardon, D. R. *et al.* Adipic acid production from lignin. *Energy Environ. Sci.* **8,** 617–628 (2015).
19. Neri, G., Musolino, M. G., Milone, C. & Galvagno, S. Kinetic Modeling of 2,4-Dinitrotoluene Hydrogenation over Pd/C. *Ind. Eng. Chem. Res.* **34,** 2226–2231 (1995).
20. Veldsink, J. W., Bouma, M. J., Schöön, N. H. & Beenackers, A. A. C. M. Heterogeneous Hydrogenation of Vegetable Oils: A Literature Review. *Catal. Rev.* **39,** 253–318 (1997).
21. Jones, W. H. *Catalysis in Organic Syntheses*. (Elsevier Science, 2013).
22. Chaudhari, R. V. *et al.* Kinetics of hydrogenation of maleic acid in a batch slurry reactor using a bimetallic Ru-Re/C catalyst. *Chem. Eng. Sci.* **58,** 627–632 (2003).
23. Zhang, Z., Jackson, J. E. & Miller, D. J. Kinetics of Aqueous-Phase Hydrogenation of Lactic Acid to

Propylene Glycol. *Ind. Eng. Chem. Res.* **41,** 691–696 (2002).

24. Scelfo, S., Pirone, R. & Russo, N. Highly efficient catalysts for the synthesis of adipic acid from cis,cis-muconic acid. *Catal. Commun.* **84,** 98–102 (2016).
25. Vardon, D. R. *et al.* Adipic acid production from lignin. *Energy Environ. Sci.* **8,** 617–628 (2015).

Chapter 7

t,t-MA and Na-Muc hydrogenation using Pd/AC home-made catalyst

This chapter describes the results for *t,t*-MA hydrogenation reaction performed using Pd/AC 1% home-made-catalyst. The catalysts were prepared using the colloidal-immobilization technique which allow synthesizing noble metal nanoparticles that can be immobilized to a solid powder support. Different carbon supports were used to prepare the catalyst and a reaction screening allowed to choose the best catalyst to use for a deeper analysis. The home-made catalysts were characterize using the most common techniques and a comparison between the best home-made catalyst and the commercial Pd/AC 5% was finally performed.

7.1 Overview about the synthesis of colloidal metal nanoparticles

Colloids are a class of material in which different materials co-exist with at least one dimension not greater than micrometre or two or more phases of same or different material co-exist. Colloids may be particles, plates or fibres (Figure 7-1). Nanomaterials are a sub-class of colloids, in which one of the dimensions of colloids is about 1 to 100 nm range.

Organic and inorganic materials can be dispersed into each other to form colloids.

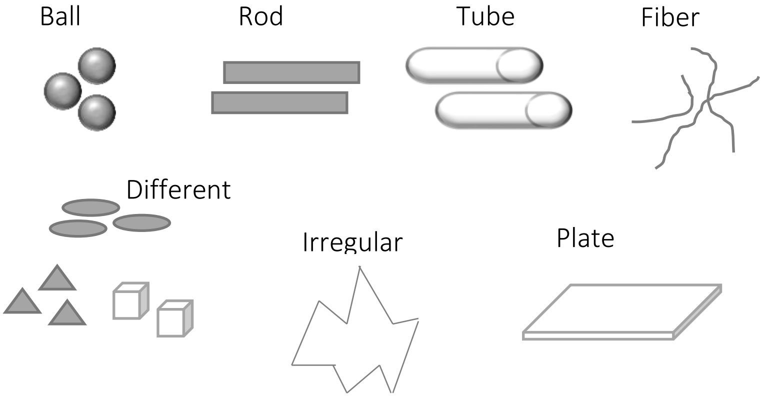

Figure 7-1: different types of colloids

Although chemical synthesis of nanoparticles (NPs) may appear as a complex process, by understanding how nucleation and growth of particles takes place, it is possible to control the various steps and try to achieve mono-dispersed (i.e. particles of nearly same size) nanoparticles. This can be done with the help of LaMer diagram shown in Figure 7-2. As we keep on increasing the concentration of the reactants in the solution. at certain concentration called C_0, the formation of nuclei begins.

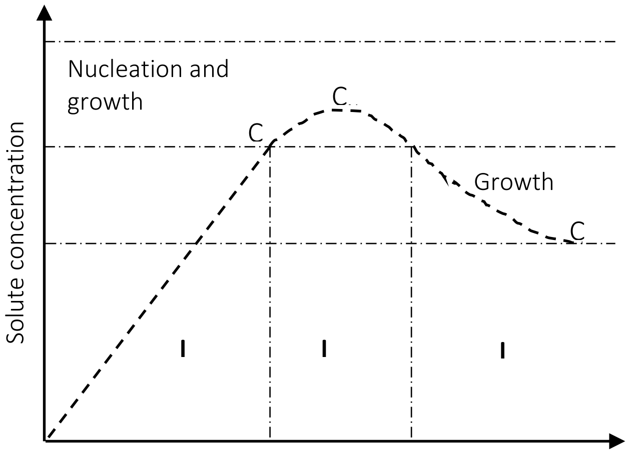

Figure 7-2: Lamer's diagram

There is no precipitate at this concentration. Further increase in concentration increases nuclei formation up to a concentration $C_{n,}$ above which there is a “super saturation” between C_n and C_s. Concentration C_n denotes the maximum rate of nuclei formation. When nuclei formation reduces, again C_0 the minimum concentration for nucleation is reached. No new nuclei can be formed, and crystal growth reduces the concentration. At this concentration C_s equilibrium is obtained. If new nuclei are formed during the growth of particles, particles with large size distribution are obtained. Therefore, it is very important to adjust the concentration of the solute and its diffusion to obtain more stable NPs and a constant rate grow of littler particles. Growth mode recognized as Ostwald ripening. Experimentally it was found that there is sometimes aggregation of particles. Aggregation also reduces the energy of the system. Thus Ostwald ripening and aggregation are competing processes and either of them is responsible to reduce the surface free energy.[1]

Colloidal metal nanoparticles (NPs) can be prepared by two different approaches: the “top-down method” which utilizes physical methods to subdivide the bulk meals and the “bottom-up method” in which the solution-phase colloidal chemistry is employed. Colloidal chemical synthetic method cab be used to synthesize uniform NPs with controlled particle size and shape in solution.[2] In general there are three main approaches to chemically produced metal NPs: chemical reduction of metal salt precursors, controlled decomposition of organometallic compounds and metal-surfactant complexes, and electrochemical synthesis. In all the above methods, a large variety of stabilizer (donor ligands, polymers and surfactants) are used to control the growth of the initially forms nanocluster and to prevent NPs agglomeration.

Colloidal methods are well established and simple wet chemistry precipitation processes where the solutions of the different metal precursors, stabilizer and reducing agents are mixed under controlled temperature. The schematic approach for producing NPs is reported below:

$$xM^{n+} + nxe^{-} + \text{stabilizer} \rightarrow M^{0}n \text{ (cluster)}$$ [3]

After the NPs colloidal formation and stabilization, the support is added under vigorous stirring and only after the solution is colourless the catalyst is filtered and dried in oven.

7.2 Pd/AC 1% catalyst: activated carbon effect

7.2.1 Catalyst synthesis

The home-made catalysts were prepared using colloidal-immobilization synthesis. 400 mL of HPLC grade water (Fischer Scientific) were added in a 600 ml flask. The water was stirred at 800 rpm using a magnetic stirring. Then 2 mL of K_2PdCl_4 (5 mg_{Pd}/mL) (Fisher Scientific) water solution and 0.65 mL of a solution of polyvinyl alcohol 87-90% hydrolyzed (PVA) in water (1% wt) were added to water under magnetic stirring using a PVA/met ratio= 0.65 (wt/wt). Therefore, 0.2 M solution of $NaBH_4$ was prepared weighting 0.0756 g of $NaBH_4$ in 10 mL of distillated water. Then 4.698 mL of the $NaBH_4$ solution were added to the aqueous metal precursor solution ($NaBH_4$/met= 10). Then the colloidal solution was maintained under stirring for 30 min to stabilize the NPs formed during the reduction process. Activated carbon (AC) support (0.99 g) was the added and two drops of sulfuric acid (98 %, Sigma Aldrich) were dropped into the colloidal solution. At low pH (acid environment) the surface of the carbon support is charged with a negative value, while the Pd-PVA complex remains negative. Therefore, there is an electrostatic attraction between the carbon and the metal NPs which helps the anchoring of the NPs on the support. The mixture was maintained under magnetic stirring for 1 h. Finally, the prepared catalyst was separated from the aqueous solution by vacuum filtration. During the filtration the catalyst was washed with 1 L of distillated water. Then the filtered black powder was dried in oven at 100 °C for 16 hours (Figure 7-3). The water recovered from the filtration step was analyzed by ICP analysis and negligible amount (<2 %) was lost during the whole catalysts synthesis. Three different activated carbon supports were used: activated carbon Darco KB 100 mesh, Norit ® and Darco G60 100 mesh activated charcoal provided by Sigma Aldrich. The list of the synthesized catalyst is reported in Table 7-1.

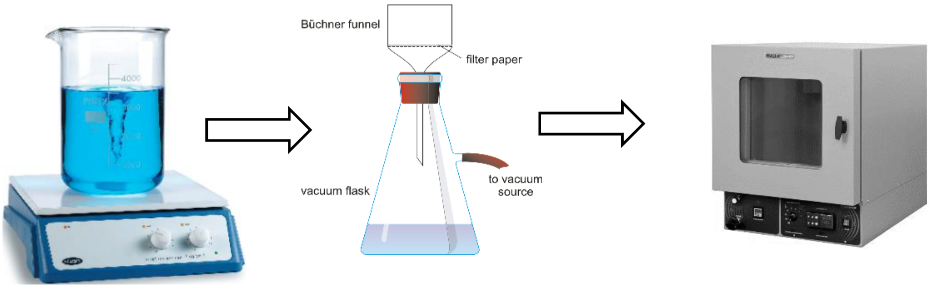

Figure 7-3: 3 steps fro the synthesis of the home-made catalysts

Table 7-1: list of prepared catalysts

Sample	Label	PVA 1% (wt) ml	Support
Pd/Darco G60 1%	Pd/G60	0.65	Activated carbon Darco G0 100 mesh
Pd/Darco KB 1%	Pd/KB	0.65	Activated carbon Darco KB 100 mesh
Pd/Norit 1%	Pd/Norit	0.65	Activated charcoal Norit

7.2.2 Catalyst characterization

The activated carbon supports were analysed by BET method to evaluate the surface area, pore size distribution, total pore volume… Figure 7-4 shows the isotherms of the different carbon supports.
The adsorption isotherm of the three commercial activated carbons belong to type IV isotherm. According to IUPAC classification, the type IV isotherm indicates mixture of microporous and mesoporous material. The adsorption on mesoporous solids proceeds via multilayer adsorption followed by capillary condensation taking place in mesopores. The characteristic features of the type IV isotherm are its hysteresis loop and the limiting uptake over a range of high p/p^0. The adsorption isotherm clearly shows the mesoporous nature of activated carbon (Figure 7-2). The structural heterogeneity of porous material is generally characterized in terms of the pore size distribution.[4] This pore size distribution is closely associated to both equilibrium and kinetic properties of porous material, and maybe it is the most important feature for characterizing the structural heterogeneity of porous materials used in industrial application. The pore size distribution of activated carbon is reported in Figure 7-5. These figures show that the commercial activated carbons contain micro (>2 nm) and mesoporous (2-50 nm) structure. In particular G60 sample shows a greater amount of mesoporous then KB one. The surface area, micropore volume, total pore volume, micropore area and average pore radius (Table 7-2). KB activated carbon support has the highest surface area (1604 m^2/g) and micropore volume (0.523 cm^3/g), and the lowest average pore radius (2.0 nm). G60 activated carbon support has the lowest surface area (802 m^2/g) and the highest average pore radius (18.7 nm). Norit activated carbon has the lowest micropore volume (0.191 cm^3/g) and the lowest micropore area (440 m^2/g).

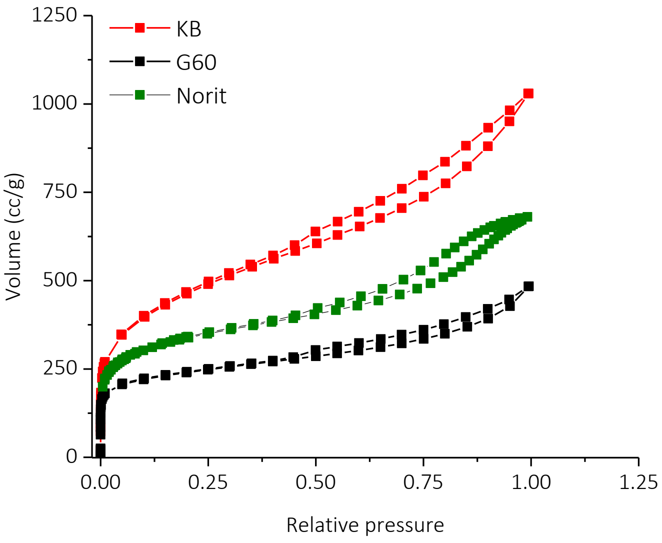

Figure 7-4: N_2 adsorption isotherm for the differen carbon support

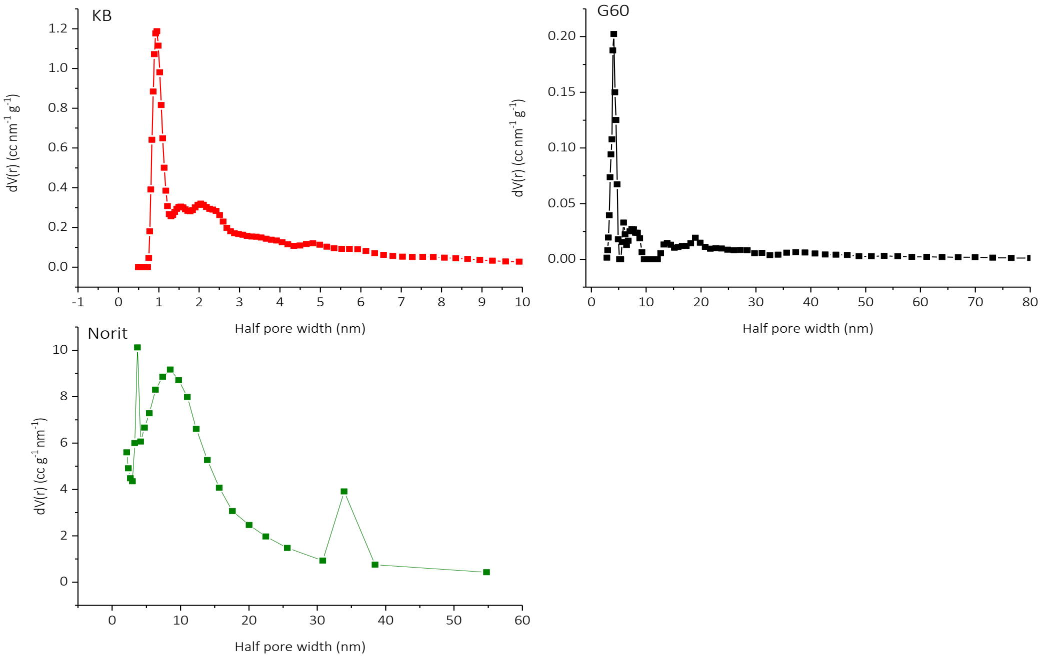

Figure 7-5: pore size distribution of the activated carbon support

Table 7-2: results of BET analysis on activated carbon supports

Sample	BET (m^2/g)	Micropore volume (cm^3/g)	Total pore volume (cm^3/g)	Micropore area (m^2/g)	Average pore radius (nm)
KB	1604	0.523	1.59	999	2.0
G60	802	0.227	0.75	555	18.7
Norit	1195	0.191	0.80	440	5.5

7.2.2.1 TEM

TEM of fresh catalyst reveals that Pd/KB 1% and Pd/Norit 1% are composed by Pd NPs that have an average diameter of about 2.6 nm (Figure 7-6 and 7-7). On the contrary, the Pd/G60 1% sample shows an average Pd NPs diameter of 3.5 nm (Figure 7-8). Therefore, starting from the same colloidal NPs solution, the support can influence the final size of the metal NPs. Norit and KB support showing a surface area higher than 1000 m^2/g are able to stabilize small Pd NPs during the immobilization.

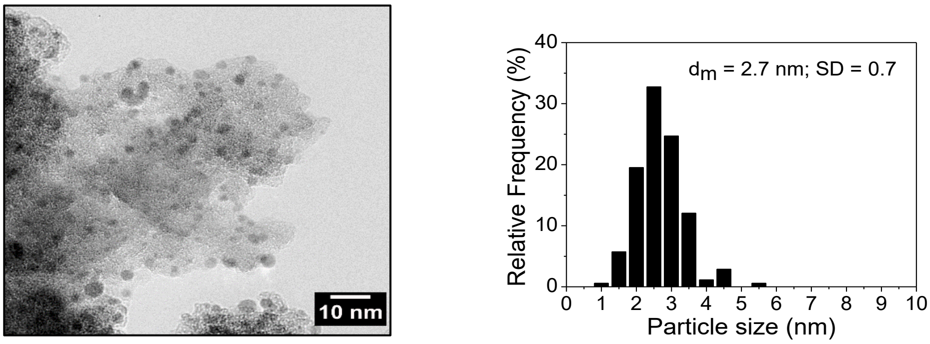

Figure 7-6: TEM of Pd/KB 1%

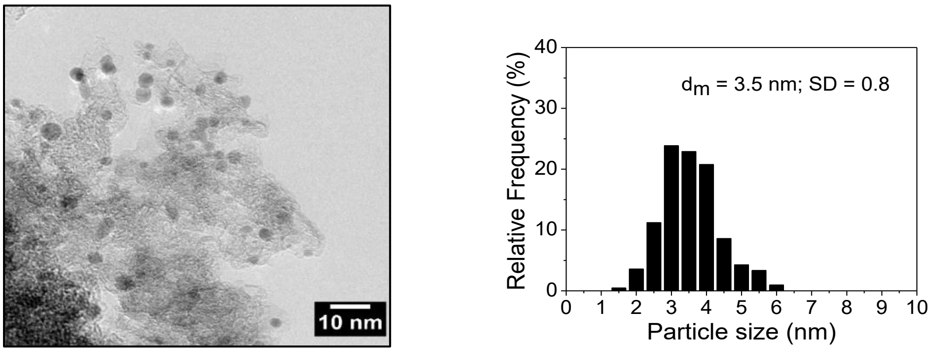

Figure 7-7: TEM of Pd/G60 1%

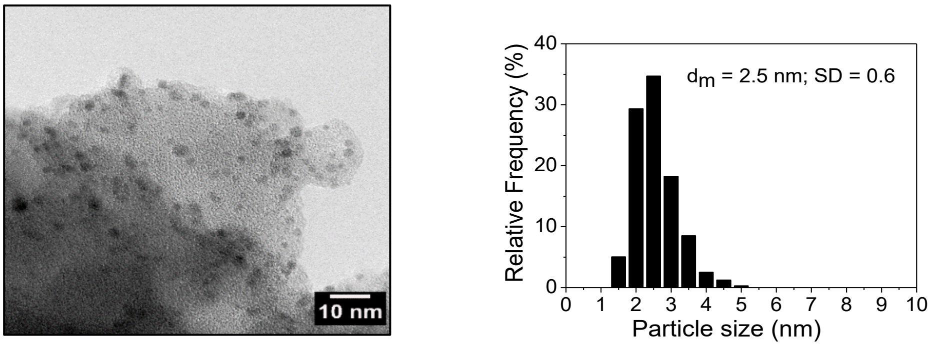

Figure 7-8: TEM of Pd/Norit 1%

7.2.3 Hydrogenation reaction in glass reactor

Hydrogenation reactions were performed in the glass reactor using the following operating conditions:

- temperature: 50 °C;
- stirring: 1200 rpm;
- substrate (*t,t*-MA and Na-muc): 1.42E-02 M;
- volume: 100 mL;
- H_2 pressure: 1.2 bar;
- Pd/substrate= 1/200 (mol_{Pd}/mol_{sub});
- reaction time: 0-90 min.

Substrate conversion and intermediates and products selectivity were evaluated by UV-Vis and GC analysis, respectively as reported in Chapter 3. The hydrogenation reactions were performed using Na-Muc and *t,t*-MA (using the procedure described in Chapter 5) to study the effect of the substrate on the catalytic activity. The results of the study are reported in the following paragraphs.

7.2.3.1 Hydrogenation reaction on *t,t*-MA

Figure 7-6 shows the results of the hydrogenation reactions performed using the catalyst prepared with the standard PVA/met weight ratio of 0.65. In terms of conversion the catalysts showed a similar behaviour, while AdA yield was influenced by the type of carbon support. The Pd/KB catalyst reached the best results in term of AdA yield, after 90 min of reaction a 100% of *t,t*-MA is converted to AdA. For Pd/G60 and Pd/Norit the maximum AdA yield after 90 min of reaction was 65% and 48%, respectively (Figure 7-9). In all the cases the production of AdA is similar to (2E)HxAc for low reaction time, while after 60 min the (2E)HxAc intermediate is hydrogenated to AdA (Figure 7-10).

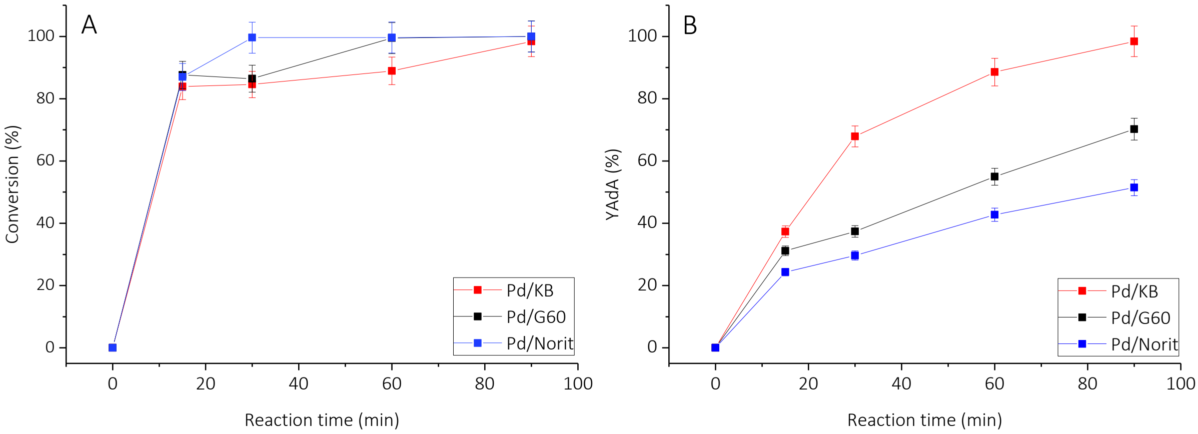

Figure 7-9: t,t-MA conversion (A) and YAdA (B)

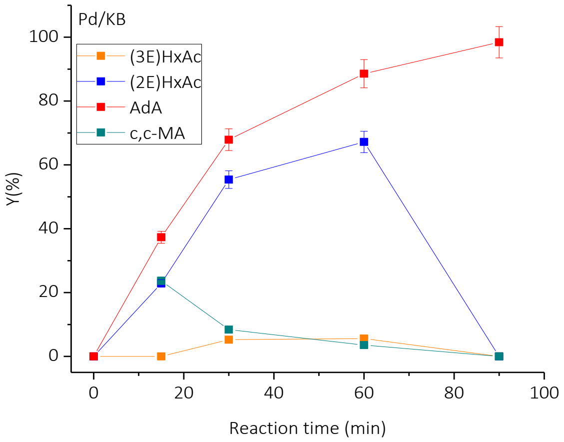

Figure 7-10: yield of reaction intermediates and AdA during t,t-MA hydrogenation

7.2.3.2 Hydrogenation on Na-Muc

Figure 7-8 shows the results of the hydrogenation reactions performed using the catalyst prepared with the standard PVA/met ratio of 0.65. The conversion of Na-Muc seems not to be affected by the activated carbon, but AdA yield largely depends on the support. As already observed for *t,t*-MA hydrogenation, the best result was obtained using KB activated carbon as support: after 90 minutes of reaction 50% of yield of AdA was achieved. For Pd/G60 and Pd/Norit the maximum AdA yield reached after 90 min was 20% and 18%, respectively (Figure 7-11). In all the cases the main intermediate is the (2E)HxAc that is further hydrogenated to AdA. In particular a large amount of (2E)HxAC is produced for low reaction time and it is gradually reduced to AdA during the reaction (Figure 7-11)

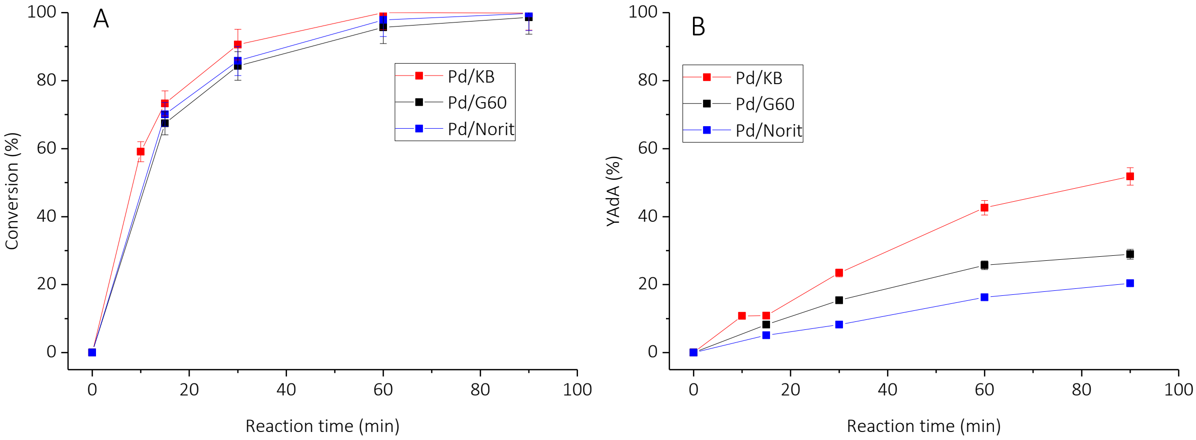

Figure 7-11: Na-Muc conversion (A) and YAdA (B)

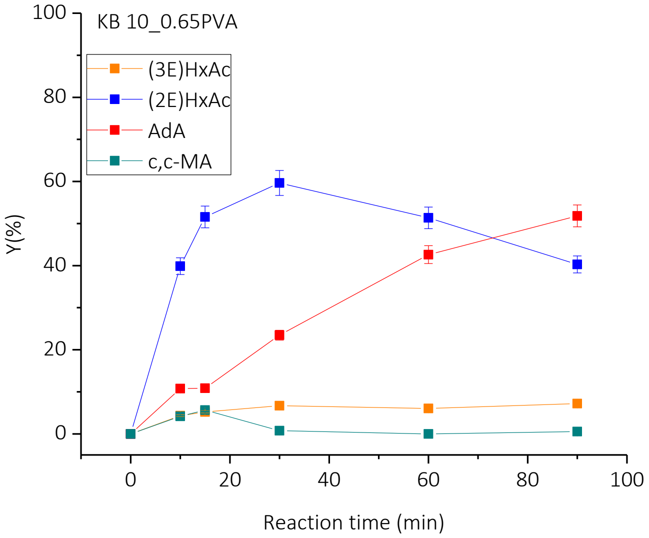

Figure 7-12: yield of reaction intermediates and AdA during Na-Muc hydrogenation

In both cases KB showed the best performance in term of AdA yield. This behaviour could be explained considering the highest surface area and the lowest Pd NPs size. A high surface area helps the adsorption of the reagents while small Pd NPs are more active than the bigger one.

Due to the good results obtaining by using Darco KB 100 mesh as activated carbon support, we decided to prepare a series of catalyst varying the PVA/met ratio from 0.0 to 1.2. The results are reported in the following paragraphs.

7.3 Pd/AC 1% catalyst: effect of the amount of stabilizer

7.3.1 Catalyst synthesis

The home-made catalysts were prepared using colloidal-immobilization synthesis varying the amount of the stabilizing agent from 0.0 to 1.2 (wt/wt) (Table 7-3). 400 mL of HPLC grade water (Fischer Scientific) were added in a 600 ml flask. The water was stirred at 800 rpm using a magnetic stirring. Then 2 mL of K_2PdCl_4 (5 mg_{Pd}/mL) (Fisher Scientific) water solution and 0-1.2 mL of a solution of polyvinyl alcohol 87-90% hydrolyzed (PVA) in water (1% wt) were added to water under magnetic stirring using a PVA/met ratio from 0.0 to 1.2 (wt/wt). Therefore, 0.2 M solution of $NaBH_4$ was prepared weighting 0.0756 g of $NaBH_4$ in 10 mL of water. Then 4.698 mL of the $NaBH_4$ solution were added to the aqueous metal precursor solution ($NaBH_4$/met= 10). It is important to use fresh solution of $NaBH_4$ to exploit the maximum hydrogen production useful for the reduction of the metal precursor. Then the colloidal solution was maintained under stirring for 30 min to stabilize the NPs formed during the reduction process. KB Darco 100 mesh Activated carbon (AC) support (0.99g) was then added and to facilitate the immobilization of the NPs 2 drops of sulfuric acid (98 %, Sigma Aldrich) were dropped into the colloidal solution. The mixture was maintained under magnetic stirring for 1 h. Finally, the prepared catalyst was separated from the aqueous solution by vacuum filtration. During the filtration the catalyst was washed with 1 L of distillated water. Then the filtered black powder was dried in oven at 100 °C for 16 hours. The water recovered from the filtration step was analyzed by ICP analysis and < 2% of the total Pd was detected in all the samples. The list of the synthesized catalyst is reported in Table 7-3.

Table 7-3: list of KB series samples prepared with different amount of PVA

Sample	**Label**	**PVA 1% wt** (mL)	**Support**
Pd/AC 1%	10_0.0PVA	0.00	Activated carbon Darco KB 100 mesh
	10_0.1PVA	0.10	
	10_0.3PVA	0.30	
	10_0.65PVA	0.65	
	10_1.2PVA	1.20	

7.3.2 Fresh catalyst characterization

7.3.2.1 BET of fresh KB series

The catalysts prepared varying the amount of PVA has the same surface area (≈1500 m^2/g) but higher average pore radius than the bare support. In fact, the bare support had an average pore radius equal to 2.0 nm while the bare catalyst at about 4.6 nm (Figure 7-13). The same observations are also worth for micropore volume, which decreased from 0.523 to 0.10 cm^3/g, and micropore area that was reduced from 999 m^2/g to ≈250 m^2/g. The sample KB_0.1PVA shows the presence of some pores that have a diameter between 40 and 50 nm (Table 7-4).

Table 7-4: BET results of KB series catalyst

Sample	BET (m^2/g)	Micropore volume (cm^3/g)	Micropore area (m^2/g)	Average pore radius (nm)
10_0.1PVA	1570	0.10	242	4.7
10_0.3PVA	1550	0.10	245	4.6
10_0.65PVA	1530	0.11	268	4.6
10_1.2PVA	1490	0.11	258	4.6

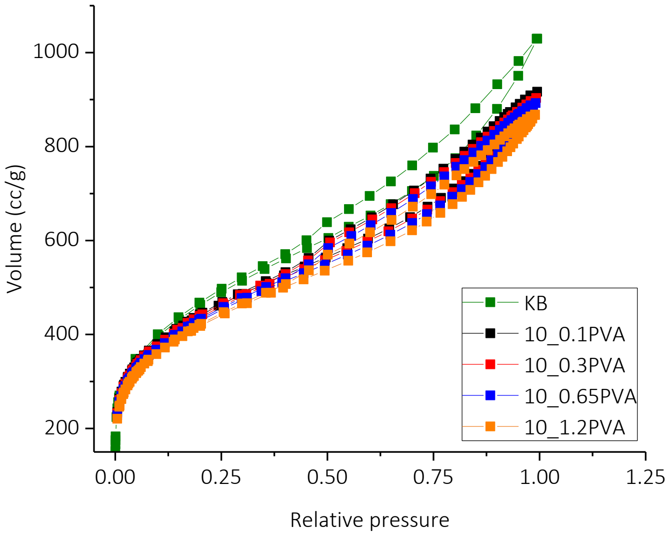

Figure 7-13: N_2 adsorptioin isotherm of KB series

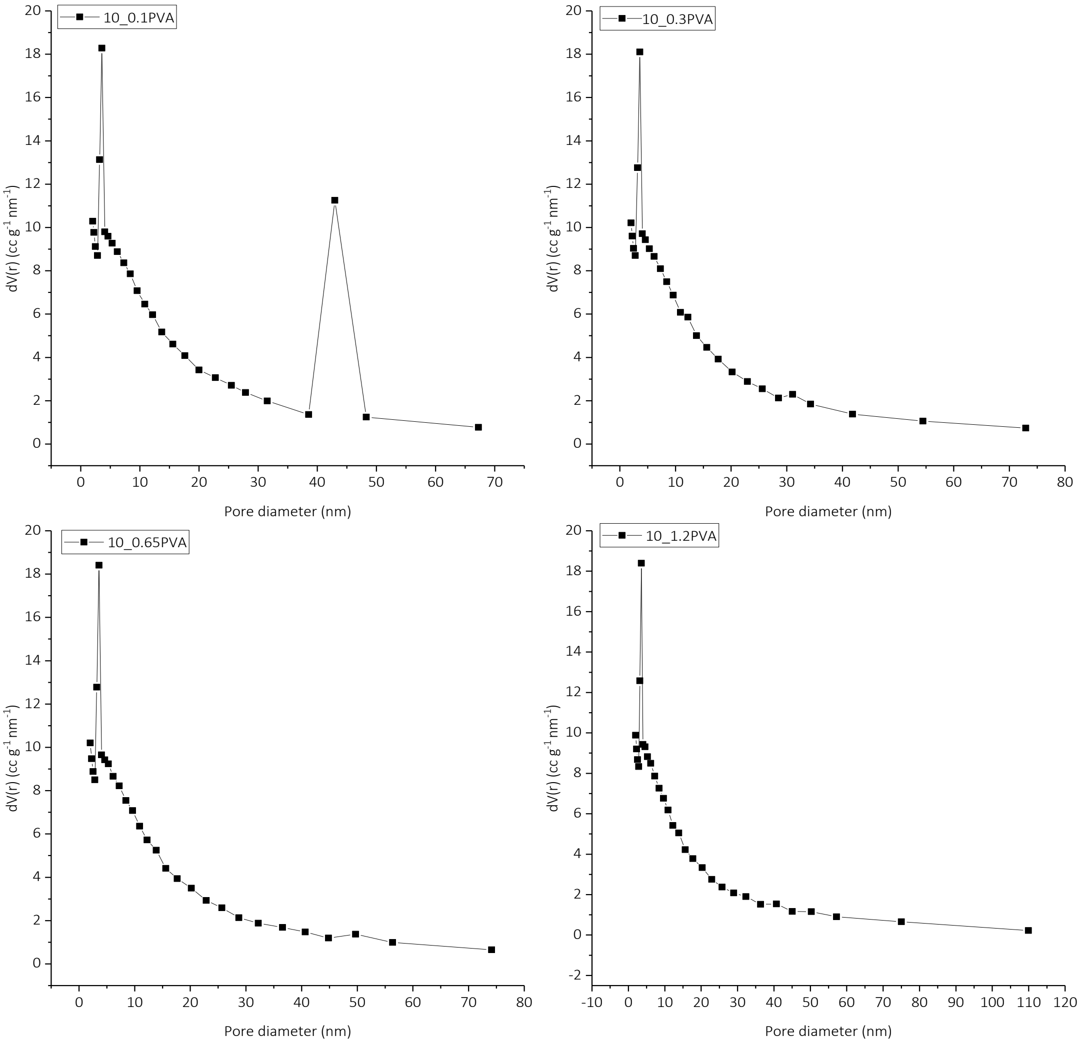

Figure 7-14: pore size distribution of KB series

7.3.2.2 TEM

TEM images of KB series catalyst shows the presence of well dispersed Pd NPs on their surfaces. Particles size is not the same for all the samples; in particular 10_0.3PVA and 10_1.2PVA have a similar average particle diameter of 3.6 nm and 3.7 nm, respectively (Figure 7-15 and 7-17). The sample 10_0.65PVA shows a lower average particle size of 2.7 nm (Figure 7-16). Therefore, the PVA amount influences the particle size: a low amount of PVA is not sufficiently able to stabilize, for example in 10_0.0PVA (Figure 7-18) wide NPs aggregates are immobilized on KB activated carbon surface.

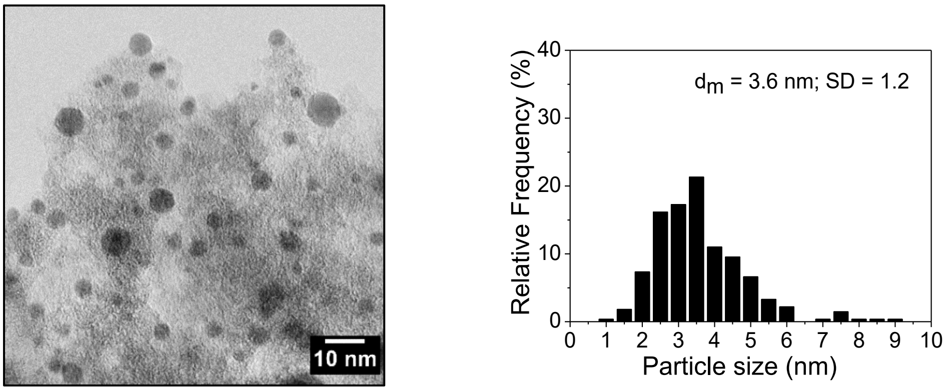

Figure 7-16: TEM of 10_0.3PVA

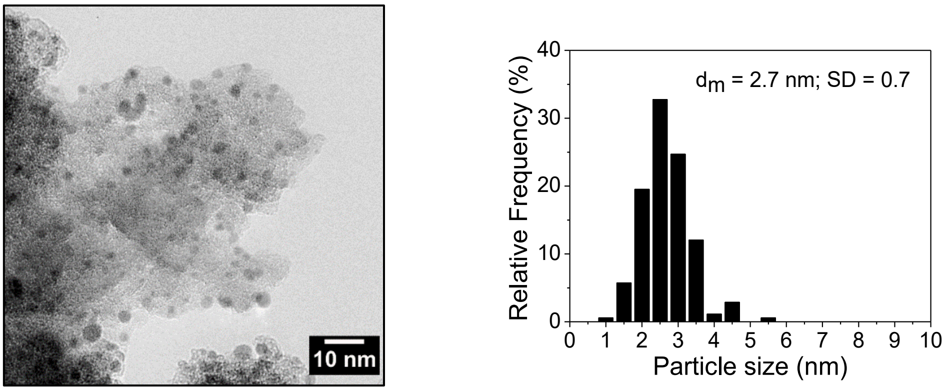

Figure 7-15:TEM of 10_0.65PVA

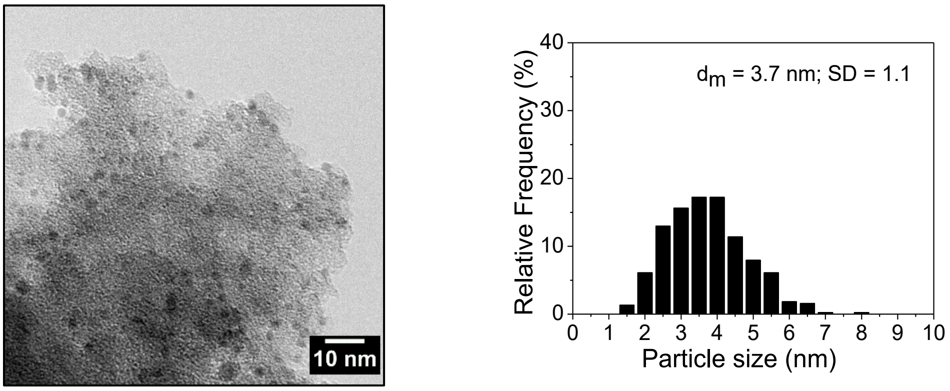

Figure 7-17: TEM of 10_1.2PVA

On the contrary a large excess of PVA slows down the immobilization process facilitating the aggregation of the NPs that are in solution. Finally, the addition of sulfuric acid decreases the pH of the solution decreasing the NPs stability. Therefore, lower is the immobilization rate, higher is the possibility to form large aggregates.

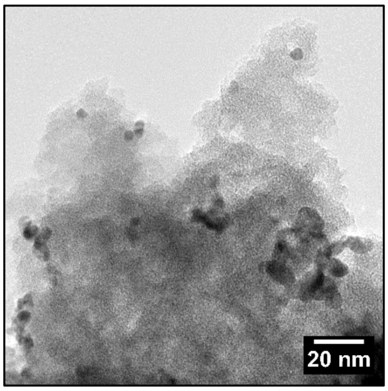

Figure 7-18: TEM of 10_0.0PVA

7.3.2.3 XPS of fresh KB series

XPS analyses of the fresh KB series were performed and Pd and C spectra were elaborated.

The survey spectra were elaborated with CasaXPS software, and the atomic percentage for each element was calculated. Due to the increment of PVA and the constant amount of Pd, the ratio between Pd and C should decrease. Therefore, the Pd surface exposition decreases increasing the amount of PVA; this behaviour might be explained considering that the higher is the amount of PVA the greater is the presence of the stabilizer that is covering the catalyst surface. The results are reported in Table 7-5 and Figure 7-19. The catalyst that has the highest Pd surface exposition is the 10_0.1PVA that has a Pd/C ratio equal to 0.039, while the 10_0.0PVA has the lowest value (0.012). This difference might be explained considering the non-homogeneity of the catalyst and thus the analysed sample could be no completely significative.

Table 7-5: atomic percentage of C, O and Pd in the KB sample

Sample	C (%)	O_2 (%)	Pd (%)	Pd/C
10_0.0PVA	87.8	11.1	1.2	0.012
10_0.1PVA	82.9	13.8	3.2	0.039
10_0.3PVA	81.9	15.3	2.7	0.033
10_0.65PVA	82.8	14.8	2.4	0.029
10_1.2PVA	80.9	16.8	2.4	0.029

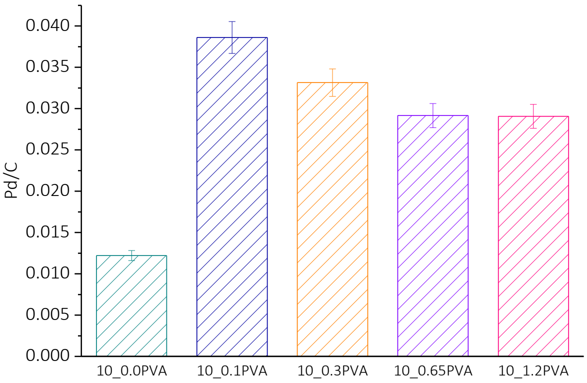

Figure 7-19: Pd/C ratio evaluated from the Survay spectra

From the deconvolution of C specie 4 different groups were detected: C sp2, C sp3, C=O and C-O at 284.09 eV, 284.80 eV, 287.66 eV and 287.71 eV, respectively (Table 7-6).

The percentage of the different C species evaluated from the C spectra were estimated and the results are reported in Table 7-7. The last column shows the ratio between the sum of the percentage of the Csp3 and C-O species, and the Csp2 that is ≈0.38. Csp2 was chosen as the reference species because it is present only in the carbon support, therefore the C sp2 % is constant (33.7-37.4 %) while the C sp3 and C-O should increase due to the presence of a larger amount of PVA. The only sample that shows different results is the catalyst prepared without the PVA as reported in Figure 7-20.

Table 7-6: Binding energy for the C species

Specie	Binding Energy (eV)
C sp2	284.09
C sp3	284.80
C=O	287.66
C-O	287.71

Table 7-7: percentage of the different C species of KB series catalysts

Sample	C 1s (%)	C sp2 (%)	C sp3 (%)	C-O (%)	C=O (%)	Csp3+C-O (%)	Csp3+C-O/C sp2 ratio
10_0.0PVA	50.5	37.4	9.9	1.2	0.9	11.2	0.30
10_0.1PVA	50.4	33.8	11.9	2.6	1.2	14.6	0.43
10_0.3PVA	50.2	33.7	12.2	1.3	2.6	13.5	0.40
10_0.65PVA	50.5	34.9	11.7	0.6	2.2	12.3	0.35
10_1.2PVA	50.8	34.9	10.2	2.6	1.6	12.7	0.37

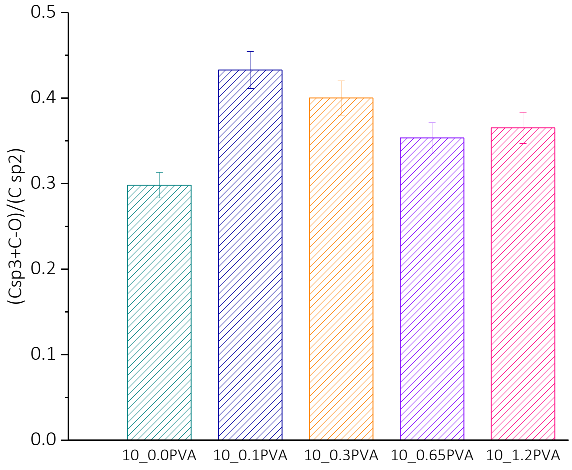

Figure 7-20: (Csp3+C-O)/Csp2 ratio of KB series catalysts

Regarding the deconvolution of Pd species, this metal displayed two different peaks (Figure 7-22 A) ascribable to the Pd $3d_{3/2}$ and Pd $3d_{5/2}$ transition. Pd(0) $3d_{5/2}$ core electron binding energy is at 335.60 eV, while the Pd(0) $3d_{3/2}$ is at 340.54 eV. The Pd(II) peaks are at 338.15 eV and 343.47 eV, and they are identified as $3d_{3/2}$ and $3d_{5/2}$ transition, respectively (Table 7-8). These binding energy values are in good agreement with that data reported in Chen et al. and Sanchez et al.[5,6]

Table 7-8: BE of the detected Pd species

Specie	Binding Energy (eV)
Pd 3d $_{5/2}$(0)	335.60
Pd $3d_{5/2}$ (II)	338.15
Pd $3d_{3/2}$ (0)	340.54
Pd $3d_{3/2}$ (II)	343.47

Moreover, the percentage of the different Pd species evaluated from the Pd spectra were estimated and the results are reported Table 7-9. The 10_1.2PVA catalyst has the higher amount of Pd(II) (32.2%), while the 10_0.1PVA has the lowest one (15.2%). Pd(0) specie percentage decreases increasing the PVA amount. In particular, considering the 10_0.3PVA, 10_0.65PVA and 10_1.2PVA samples, 10_0.65PVA sample show the highest value of Pd(0)/Pd(II) (Figure 7-21). We hypothesized that smaller Pd NPs are more active toward the spontaneous passivation.

Table 7-9: Pd(II) and Pd(0) species within the KB series

Sample	Pd (II) (%)	Pd (0) (%)	Pd(0)/Pd(II)
10_0.0PVA	18.5	81.5	4.4
10_0.1PVA	15.2	84.8	5.6
10_0.3PVA	26.9	72.1	2.7
10_0.65PVA	23.1	76.9	3.3
10_1.2PVA	32.2	67.8	2.1

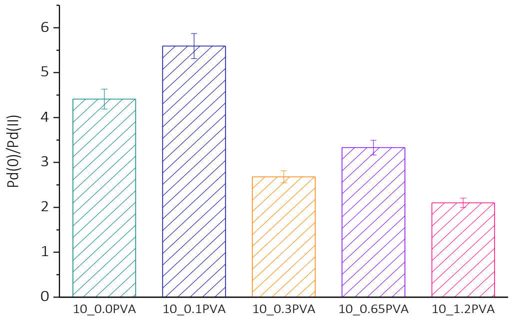

Figure 7-21: Pd(0)/Pd(II) ratio of KB series

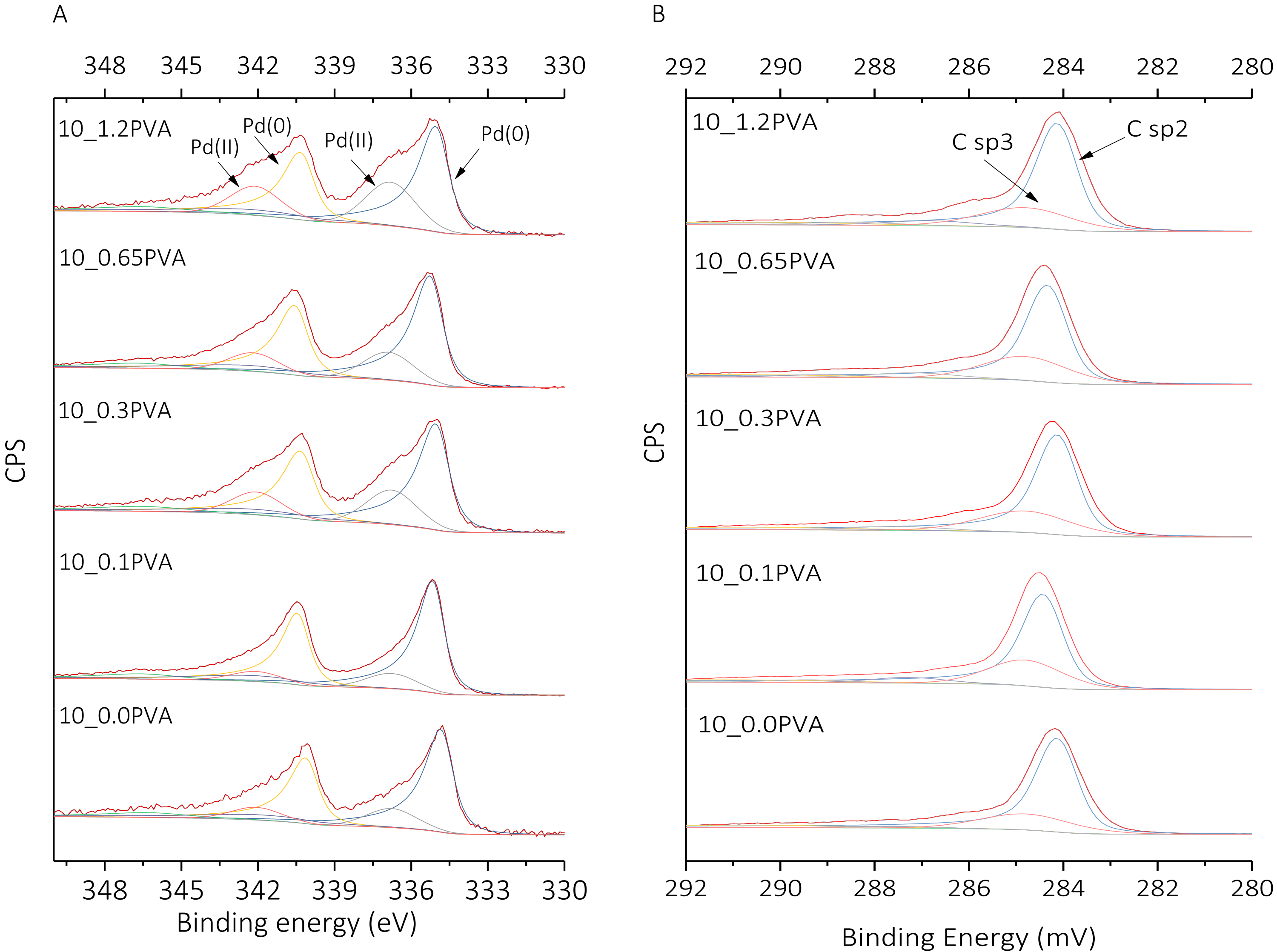

Figure 7-22: Pd (A) and C (B) deconvolution for the different KB samples

7.3.3 Hydrogenation reaction in glass reactor

Hydrogenation reactions were performed in the glass reactor using the following operating conditions:

- temperature: 50 °C;
- stirring: 1200 rpm;
- substrate (*t,t*-ma and Na-muc): 1.42E-02 M;
- volume: 100 ml;
- H_2 pressure: 1.2 bar;
- Pd/substrate= 1/200 (mol_{Pd}/mol_{sub});
- reaction time: 0-90 min.

Substrate conversion and intermediates and products selectivity were evaluated by UV-Vis and GC analysis, respectively. The hydrogenation reactions were performed using Na-Muc and *t,t*-MA to study the effect of the substrate on the catalytic activity. The results of the study are reported in the following paragraphs.

7.3.3.1 *t,t*-MA hydrogenation

Using the same reaction conditions *t,t*-MA was hydrogenated using the catalysts synthesized with the same activated carbon support but varying the PVA/met ratio from 0.0 to 1.2 (wt/wt). *t,t*-MA conversion reaches 100% only after 20 minutes of reaction, except for KB 0.65 and 1.2 PVA (Figure 7-22 A). Contrarywise, AdA yield is affected by the amount of PVA: KB 0.1 and 0.3 PVA samples show the same trend, while for low reaction time KB 0.0 and 1.2 PVA catalysts has the highest value of AdA yield (Figure 7-23 B). All the considered catalysts have an initial activity comparable with the one obtained Pd/AC 5% commercial catalyst (≈0.2 s^{-1}) (Figure 7-24 A).

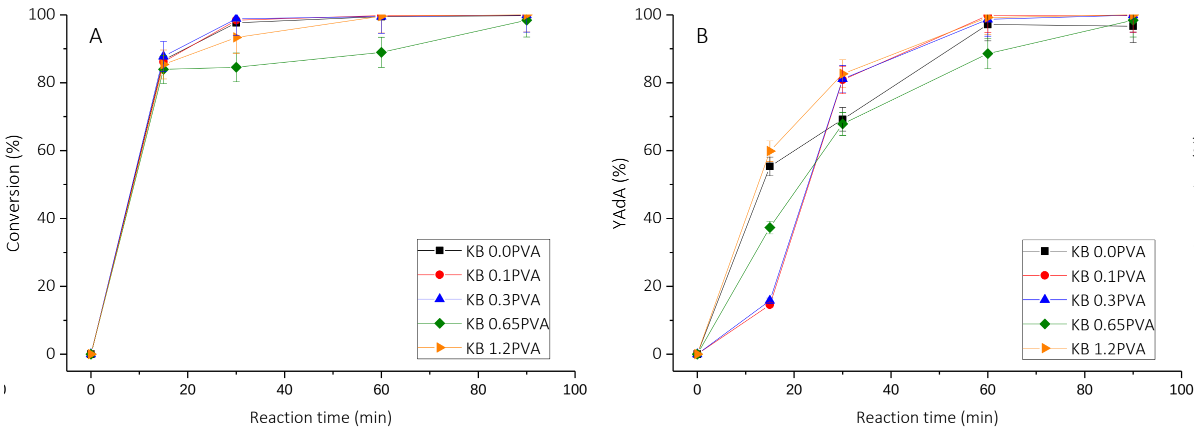

Figure 7-23: conversion (A) and AdA yield (B) during t,t-MA hydrogentation with KB series catalysts

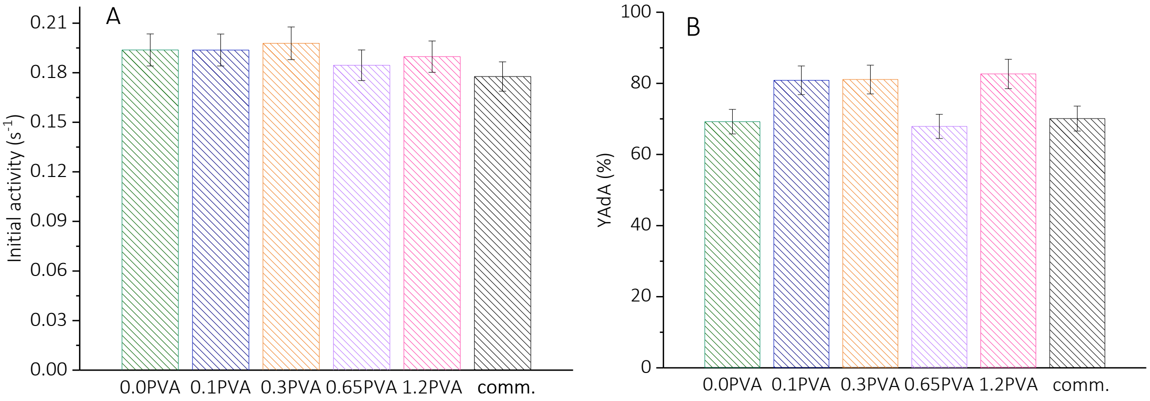

Figure 7-24: initial activity (A) and AdA yield after 30 min of reaction

Comparing the YAdA at 30 min obtained using KB series catalysts with the result obtained with commercial Pd/AC5% we can see that 0.1PVA, 0.3PVA and 1.2PVA have a yield (81%) higher than the commercial catalyst (71%) (Figure 7-24 B).

7.3.3.2 Used catalyst characterization

Pd/AC 1% KB 10_0.65PVA was filtered from the reactant solution after 15 and 90 minutes of reaction. The survey spectrum of used catalyst after **15 min** of reaction shows the presence of C 1s (282.58 eV), Pd 3d (337.54 eV) and O 1s (532.86 eV) species (Table 7-10). Pd 3d peak is very trivial to analyse for further deconvolution, in fact the recovered catalyst was light grey, which means that some adipic acid and intermediates species were covering the surface of the catalyst.

Table 7-10: binding energy of the species after 15 min of reaction

Specie	Binding energy (eV)	Area	Norm Area	Group %
C 1s	284.58	2643	916.0	69.3
Pd 3d	337.54	201	4.48	0.3
O 1s	532.86	2883	400.9	30.4

Considering the deconvolution of C specie (Figure 7-25), 5 different C groups were found in the sample: C sp2 (284.636 eV), C sp3 (285.754 eV), C-O (286.886 eV), C=O (289.187 eV) and C pi (290.798 eV). Csp2 specie is the 47.3% of the total C present on the catalyst surface, therefore we can hypothesize that a lot of reagents and intermediates are adsorbed on the surface of the catalyst (Table 7-11).

Table 7-11: composition of C specie after 15 min of reaction with t,t-MA

Specie	Peak ID	Binding energy (eV)	Area	Atom (%)
C sp2	Pk01	284.636	39712	47.3
C sp3	Pk02	285.754	15020	17.9
C-O	Pk03	286.886	11548	13.7
C=O	Pk04	289.187	14093	16.8
C pi	Pk05	290.798	3655	4.3

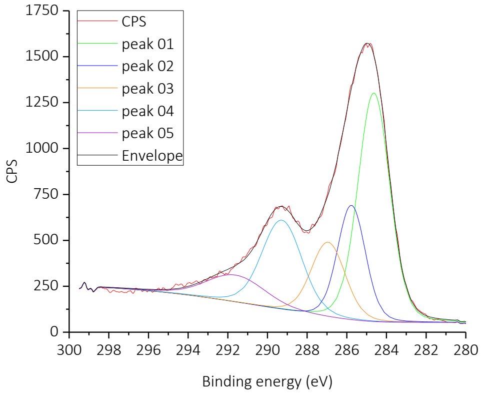

Figure 7-25: deconvolution of C species after 15 min

At **90 minutes** of reaction C 1s, Pd 3d and O 1s signals were clearly detected in the range between 280 and 600 eV. From the evaluation of the area of the different species, C element was detected as the major specie (84.1%). In this case atom percentage of Pd is not negligible (1.2%), therefore during the reaction *t,t*-MA and the intermediates has been desorbed on the catalyst surface.

Table 7-12: species detected from the survey spectrum on KB 0.65 sample after 90 min of reaction

Specie	Binding energy (eV)	Area	Norm Area	Atom (%)
C 1s	284.63	9706	1739.3	84.1
Pd 3d	335.976	2213	25.5	1.2
O 1s	532.851	4231	304.3	14.7

Considering the C species, 5 different carbon groups were detected (Figure 7-26): C sp2 (284.607 eV), C sp3 (285.871 eV), C-O (287.559 eV), C=O (289.334 eV) and c pi (291.223 eV) (Table 7-12).
C=O percentage (5.1%) in the used catalyst at 90 minutes of reaction is slower than the ones at 15 minutes (16.8%). The reducing reaction environment helps not only the reduction of but also the reduction of carboxylic group of the activated carbon (Table 7-13). The amount of C sp 3 specie increases from 17.9% to 21.5% due to the reduction previously mentioned.

Table 7-13: results of the C deconvolution of KB 0.65PVA after 90 minutes of reaction

Specie	Peak ID	Binding energy (eV)	Area	Atom (%)
C sp2	Pk01	284.607	53591	59.2
C sp3	Pk02	285.871	19479	21.5
C-O	Pk03	287.599	9358	10.3
C=O	Pk04	289.334	4694	5.1
C pi	Pk05	291.223	3416	3.8

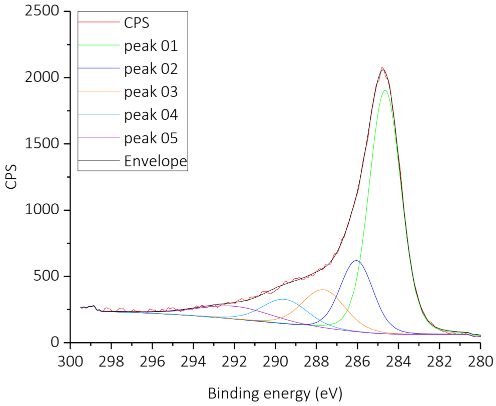

Figure 7-26: deconvolution of C specie after 90 min

The sample collected at 90 minutes of reaction has both Pd(0) (335.895eV and 341.167 eV) and Pd(II) (337.660 eV and 343.237 eV) surface species (Figure 7-27). The main specie is the metal Pd (73.4%) and the ratio between Pd(0) and Pd(II) is equal to 2.8 (Table 7-14).

Table 7-14: results of Pd deconvolution of KB 0.65PVA after 90 minutes of reaction

Specie	Peak ID	Binding energy (eV)	Area	Atom (%)
Pd(0)	Pk01	335.895	24513	40.5
Pd(II)	Pk02	337.660	9322	15.4
Pd(0)	Pk03	341.167	19923	32.9
Pd(II)	Pk04	343.237	6705	11.2

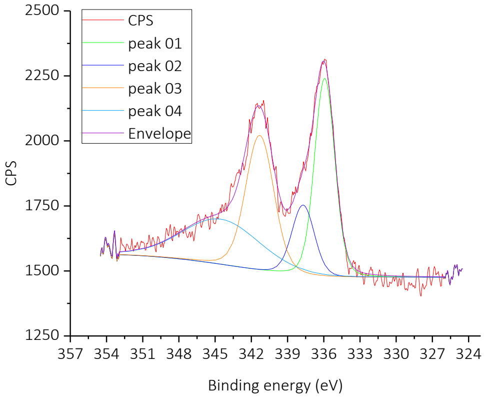

Figure 7-27: Pd deconvolution afte 90 min

Therefore, the Pd NPs supported on the KB activated carbon do not go under a strong reduction process, considering that the fresh catalyst has a Pd(0) total amount of 77% and after 90 minutes it is 71%.

7.3.3.3 Na-Muc hydrogenation

Using the same reaction conditions Na-Muc was hydrogenated using the catalysts synthesized with the same activated carbon support but varying the PVA/met ratio from 0.0 to 1.2 (wt/wt). Na-Muc conversion reaches 100% for all the samples after 1 hour of reaction. For short reaction time (i.e. 10 minutes) the conversion is affected by the amount of PVA, and in particular KB 1.2PVA showed the best performance, as found for *t,t*-MA hydrogenation (Figure 7-28 A). AdA yield is affected by the amount of PVA: KB 0.0 and 0.1 PVA samples show the same trend, while for low reaction time KB 0.3 and 1.2PVA catalysts has the highest value of AdA yield (Figure 7-28 B). All the catalysts show an induction period probably due to the hydrogenation of Na-Muc to the monounsaturated intermediate.

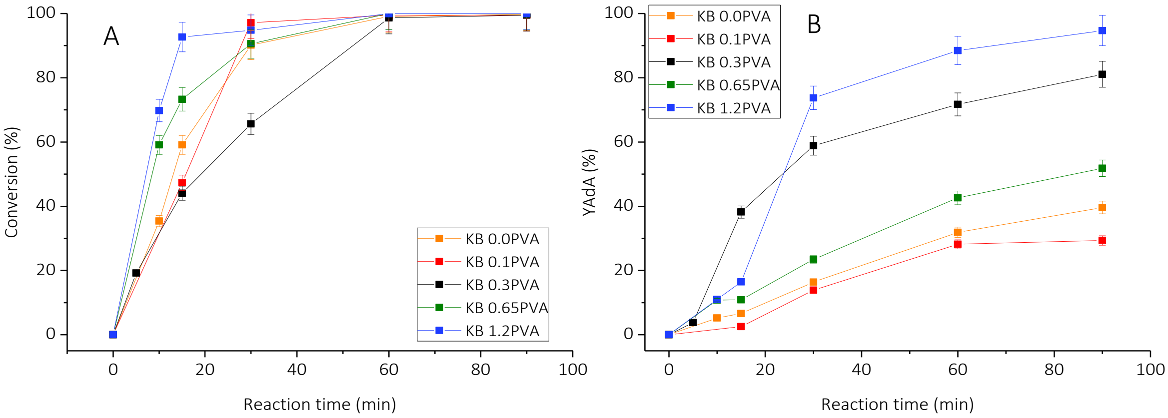

Figure 7-28: conversion (A) and AdA yield (B) during Na-Muc hydrogentation with KB series catalysts

The results about the initial activity of the home-made catalyst are very interesting. The samples KB_0.3PVA and KB_0.1PVA show an initial activity comparable with the one obtained using Pd/A 5% commercial catalyst (0.10 s^{-1}), while all the other home-made catalysts have a higher activity than the commercial one (Figure 7-29 A), while KB 0.3PVA and KB 1.2PVA have the higher AdA yield after 30 min (Figure 7-29 B).

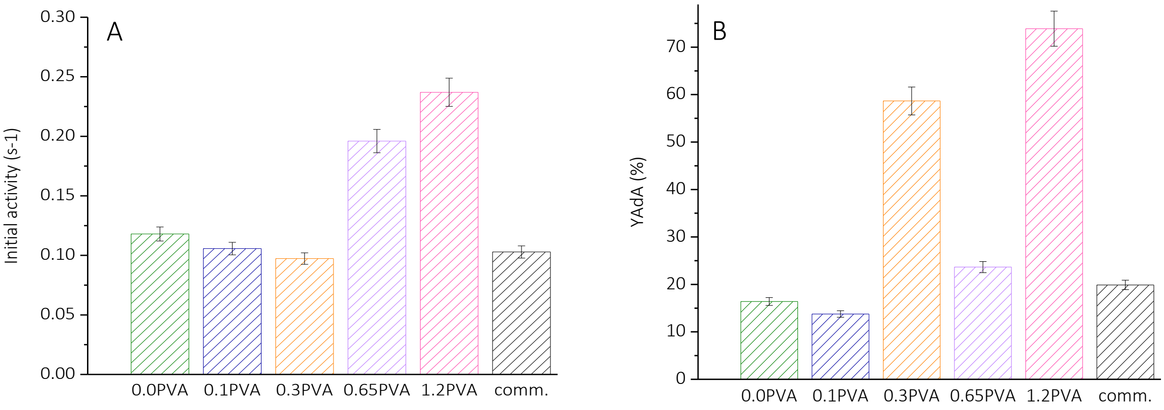

Figure 7-29: initial activity of KB series during Na-Muc hydrogenation and AdA yield at 30 min

7.3.3.4 Used catalyst characterization

The catalyst used for the hydrogenation of Na-Muc was characterized using XPS analysis. Pd/AC 1% KB 10_0.65PVA was filtered from the reactant solution after 30 and 90 minutes of reaction. The survey spectrum shows the presence of C 1s (284. 633 eV), Pd 3d (335.816 eV) and O 1s (532.639 eV) species (Table 7-15). Moreover, Na element was detected due presence of sodium muconate as reaction substrate.

Table 7-15: element detected from a used sample after 30 min of reaction

Specie	Binding energy (eV)	Area	Norm Area	Atom (%)
C 1s	284.633	9480	1698.82	81.1
Pd 3d	335.816	2760	31.79	1.5
Na a	497.089	514	31.04	1.5
O 1s	532.639	4649	334.26	15.9

The deconvolution of C element revealed the presence of different carbon species on the surface of the catalyst. In particular C sp2 specie is the major component (74.1 %) followed by C sp3 (13.8%) (Table 7-16). The high amount of C sp2 specie might be explained considering the adsorption of unsaturated compounds (Na-Muc and intermediates) on the surface of the catalyst. Comparing these results with the % of C=O and C sp2 groups of fresh catalyst our hypothesis was confirmed.

Table 7-16: C species detected from the used sample after 30 min

XPS Line	Peak ID	Binding energy (eV)	Area	Atom (%)
C sp2	Pk01	284.598	70359	74.1
C sp3	Pk02	286.328	13115	13.8
C-O	Pk03	288.012	8465	8.9
C=O	Pk04	289.954	3033	3.2

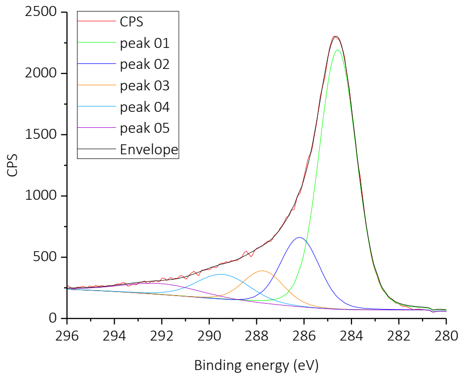

Figure 7-30: deconvolution of C specie after 30 min

Pd deconvolution shows the presence of both Pd(0) (335.568 eV and 340.828 eV) and Pd(II) (337.522 eV and 342.711 eV) specie with a higher amount of Pd(0) (Figure 7-31). The ratio between Pd(0) and Pd(II), after 30 minutes of reaction is equal to 5.1 (Table 7-17).

Table 7-17: Pd species detected after 30 min

Specie	Peak ID	Binding energy (eV)	Area	Atom (%)
Pd(0)	Pk01	335.568	43844	49.5
Pd(II)	Pk02	337.522	8604	9.7
Pd(0)	Pk03	340.828	30346	34.2
Pd(II)	Pk04	342.711	5807	6.6

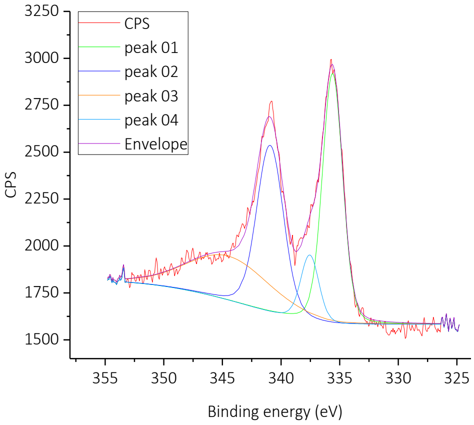

Figure 7-31: Pd deconvolution after 30 min

The composition of the catalyst collected at the end of the reaction (**90 min**) did not show any changes in the composition: Pd, C, O and Na element were detected during the analysis (Table 7-18).

Table 7-18: element detected from a used sample after 90 min of reaction

Specie	Binding energy (eV)	Area	Norm Area	Atom (%)
C 1s	284.649	6572	1177.72	80.7
Pd 3d	335.848	1953	22.49	1.5
Na a	496.517	369	22.28	1.5
O 1s	532.338	3293	236.71	16.3

The deconvolution of C element (Figure 7-32) revealed the presence of different C species on the surface of the catalyst. The percentage of C sp2 group is 7% less than the one evaluated after 30 minutes of reaction while the C sp3 amount increased (Table 7-19). This behavior could be explained considering that the during the hydrogenation reaction double bonds (C sp 2) are converted to single bonds (C sp3).

Table 7-19: C species detected from the used sample after 90 min

XPS Line	Peak ID	Binding energy (eV)	Area	Area (%)
C sp2	Pk01	284.575	49117	67.2
C sp3	Pk02	286.225	13435	18.4
C-O	Pk03	287.798	5621	7.7
C=O	Pk04	289.264	3072	4.2
C pi	Pk05	290.985	1823	2.5

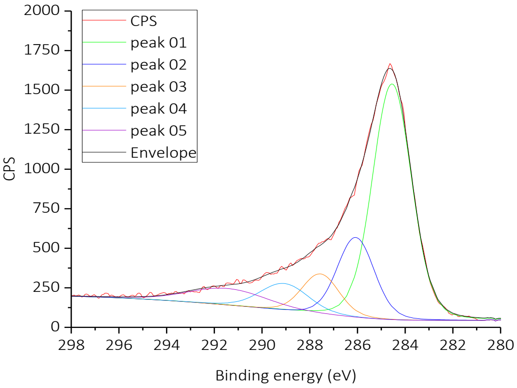

Figure 7-32: C deconvolution after 90 min

Pd deconvolution (Figure 7-33) shows the presence of both Pd(0) and Pd(II) specie with a higher amount of Pd(0). The ratio between Pd(0) and Pd(II), after 90 minutes of reaction is equal to 2.71.

Table 7-20: Pd species detected after 30 min

Specie	Peak ID	Binding energy (eV)	Area	Area (%)
Pd(0)	Pk01	335.627	30848	43.3
Pd(II)	Pk02	337.421	10549	14.8
Pd(0)	Pk03	340.826	21237	29.8
Pd(II)	Pk04	342.47	8609	12.1

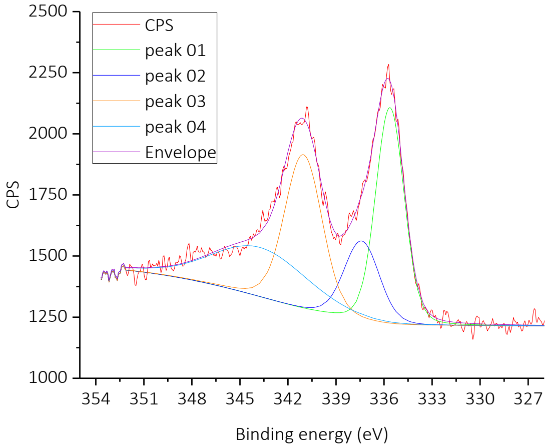

Figure 7-33: Pd deconvolution after 30 min

Considering the Pd(0)/Pd(II) at different reaction times Pd(II) is reduced to Pd(0) during the first moments of the reaction, while after 90 min the composition return to be similar to the first one.

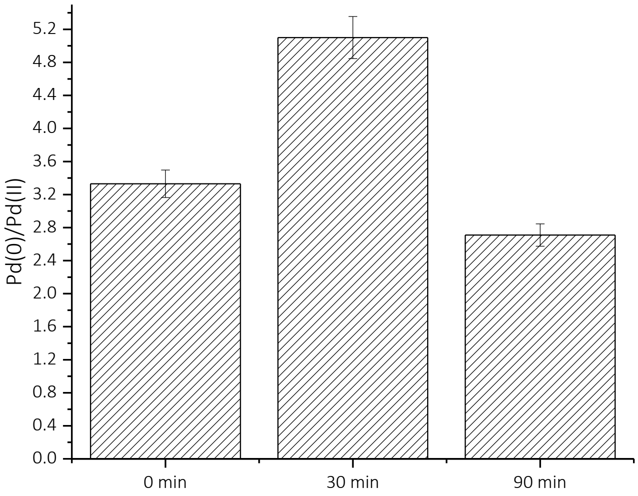

Figure 7-34: variation of Pd(0)/Pd(II) ratio at different reaction times

Conclusion

Na-Muc and *t,t*-MA were hydrogenated using catalyst prepared by sol-immobilization method. Pd NPs were immobilized on three different activated carbon supports. KB Darco 100 mesh activated carbon showed the best results in term of AdA yield, both during *t,t*-MA and Na-Muc conversion. Its best behavior is probably due to the high surface area which help the adsorption and desorption process and the low NPs dimension that are more active.

Therefore 5 catalysts were prepared varying the amount of stabilizer and keeping constant the KB Darco activated carbon support and changing the amount of stabilizer (PVA). The catalysts had the same surface area, while the Pd NP had different dimensions. Using the optimal amount of PVA (0.65 mL) the NPs had an average size of 2.7 nm, although using higher of lower amount of PVA the diameter of the Pd NPs is higher. Low amount of stabilizer is not able to stabilize the NPs during their formation, while high amount of PVA can interfere in the immobilization process.

t,t-MA and Na-Muc were hydrogenated and we obtained good results. *t,t*-MA hydrogenation quickly occurs and the initial activity of the all home-made catalysts is equal to the commercial Pd/AC 5% catalyst. The samples 10_0.0PVA and 10_0.65PVA showed an AdA yield equal to the commercial catalyst after 30 min of reaction, while all the other home-made catalysts are better than the commercial one.

Na-Muc hydrogenation reaction is slower than t,t-MA reduction. 10_0.0PVA, 10_0.65PVA and 10_1.2PVA presented higher activity than commercial Pd/AC 5% catalyst and they have more capability to produce AdA. This behavior could be explained considering the different surface area of the supports: KB activated carbon has a surface area that is twice respect to the commercial Pd/AC 5%.

In all the cases Pd(0) and Pd(II) species are presented on the catalyst surface and Pd(II) is reduced to metal Pd during the reaction, increasing the catalyst activity.

These interesting results opened the possibility to optimize the design of this catalyst and to understand the key catalyst feature for this kind of reaction.

Bibliography

1. Zha, J. & Roggendorf, H. Sol-gel science, the physics and chemistry of sol-gel processing, Ed. by C. J. Brinker and G. W. Scherer, Academic Press, Boston 1990, xiv, 908 pp., bound?ISBN 0-12-134970-5. *Adv. Mater.* **3,** 522–522 (1991).
2. Sharada, S. *et al.* Synthesis of palladium nanoparticles using continuous flow microreactor. *Colloids Surfaces A Physicochem. Eng. Asp.* **498,** 297–304 (2016).
3. Jia, C.-J. & Schuth, F. Colloidal metal nanoparticles as a component of designed catalyst. *Phys. Chem. Chem. Phys.* **13,** 2457–2487 (2011).
4. Ismadji, S. & Bhatia, S. K. Characterization of activated carbons using liquid phase adsorption. *Carbon N. Y.* **39,** 1237–1250 (2001).
5. Chen, X. *et al. Non-covalently modified graphene supported ultrafine nanoparticles of palladium for hydrogen gas sensing*. *RSC ADVANCES* **3,** (2013).
6. Sanchez, F. *et al.* Hydrogen Generation from Additive-Free Formic Acid Decomposition Under Mild Conditions by Pd/C: Experimental and DFT Studies. *Top. Catal.* **61,** 254–266 (2018).

Chapter 8

Life cycle impact assessment analysis (LCIA) and economic feasibility study

This chapter describes the life cycle impact assessment of the industrial process for the production of adipic acid. Two different processes were considered: the conventional oil-based process and the bio-based process. The traditional petrochemical process involves the oxidation of the KA-oil mixture while the bio-based one the production of muconic acid starting from wood biomass and its further hydrogenation to adipic acid. The comparison had been possible thanks to a deep study performed in collaboration with Politecnico di Milano (Alessandro Rosengart et al. *Process Synthesis for the Production of Sustainable Adipic acid,* Biotechnology and Biofuels*,* under review). We designed and optimized the industrial process for the production of bio-adipic acid evaluating the materials and the energy required for the process. This is obviously a preliminary study because no real industrial values and process was taken into account for the bio-process description, but we decided to perform the study placing in the worst operating conditions. Therefore, the values of the impact might change with further detailed studies.

8.1 Overview about LCIA study of adipic acid

There are several studies for the production of AdA starting from renewable sources, in particular from lignin biomass.[1–4] Lignocellulosic biomass is a versatile renewable resource for the production of sustainable chemicals and materials; in fact polysaccharides are the first interest fraction for selective conversion processes obtain from biomass.[5] Xie at al. summed up all the different routes to obtain of an important chemical intermediate in the production of bio-AdA such as muconic acid (MA). MA is a high value-added bio-product produced by biotechnological pathway with different modified and unmodified bacteria strains.[2] Mizuno et.al produced 44.1 g/L of MA in 48 h using *Arthrobacter sp.* and benzoate as feedstock [6], while in 2012 van Duuren et al. used P. *Putida mutant* strain BM014 in a fed-batch reactor feeding benzoate as substrate. They obtained 32.4 g/L of MA with a molar yield of 100%.[7] Vardon et al. in a recent work proposed the downstream process for the MA recovery from the fermentation broth with a purity >98% using active carbon treatment, crystallization in acidic environment and further purification with ethanol.[8] The so produced and purified MA can be converted to AdA in water in mild operating condition[9] or in ethanol[8] obtaining in both cases high conversion (>99%) and selectivity (>99%). Considering that bio-AdA process technology is still at an early development stage (TRL 1-4), it is important to keep updated the environmental results in terms of MA productivity and AdA production. Up to now, only two studies are present in literature. Van Duuren et al. performed a limited LCA study of bio-AdA production at the early stage[7], therefore not considering the new MA recovery strategies and AdA production and purification.[8,10] Furthermore, Aryapratama and Janssen [11] performed a prospective life cycle assessment of bio-based AdA production from forest residues but without passing through MA production. The results of this study show the benefit of the bio-based AdA on the eutrophication, photochemical ozone creation and global warming but on the other side, it has a high impact on acidification.

Rosengart et al. proposed a detailed economical and feasibility study for the production of AdA from glucose via MA pathway: mass balance and energy demand for each unit process are available and they allow the exact evaluation of the amount of chemicals required for the obtainment of AdA and the required energy for each step.[12] The aim is to compare the environmental impact of the synthetic process of AdA starting from non-renewable sources and wood biomass. Generally, this approach is performed for the comparison of new industrial processes (bio-derived AdA) with the consolidated one (oil-derived AdA); this way called “at early stage” helps researchers to verify the environmental sustainability of an innovative chemical process.[13]

8.2 LCIA study: methods and system boundaries definition

8.2.1 Method

The AdA production process from oil and from renewable sources was considered defining the system boundaries reported in System boundaries definition paragraph. The assessment was performed using SimaPro (version 8.4.0) an LCA software that uses a wide set of dedicated libraries. Among these, the Ecoinvent3 database (version 2.2) was adopted while ReCiPe 2016 H (version 1.08) was selected to cover eighteen impact categories. The functional unit in both cases is 1 kg of AdA produced at plant.

8.2.2 System boundaries

The system boundaries used for the LCA of the both processes are reported in Figure 8-1.

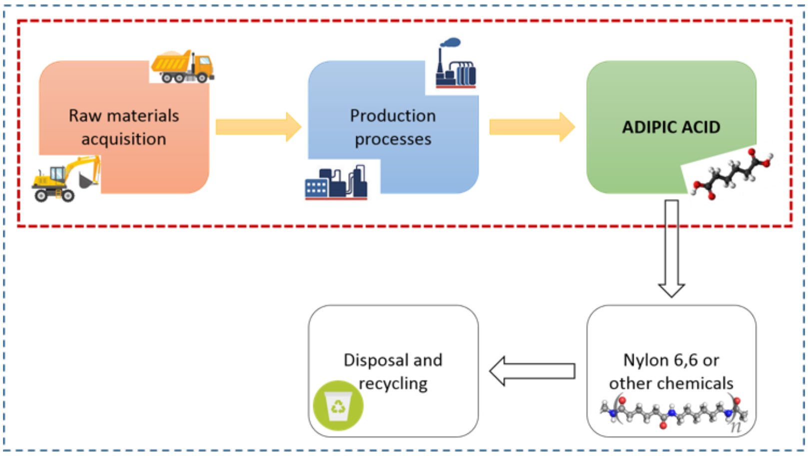

Figure 8-1: system boundaries

A cradle-to-gate study was performed considering the raw materials acquisition and all the production processes required converting them into AdA. The purpose is to evaluate the environmental impact of the processes involved in the production of AdA without considering its transformation to nylon or other chemicals because it is exactly the same route. For the same reason disposal and recycling of the derived AdA chemicals has been neglected. The geographical area selected for the study is the rest of the World, reported in the software with the shortcut <RoW>. In order to operate with the largest number of data present in SimaPro and to avoid limiting the location of the two industrial processes to a single country in the world, global SimaPro data was chosen. Therefore, adopted entries were represented with the shortcut <GLO> or <RoW> and they represent activities which are considered to be an average valid for all countries in the world. It was used a Unit process version with an allocation Default dataset.

8.3 Adipic acid from oil

Oil derived AdA was present in SimaPro database as Adipic acid {RoW}| production | Alloc Def, U; the flow sheet of the whole plant is reported in Figure 8-2.

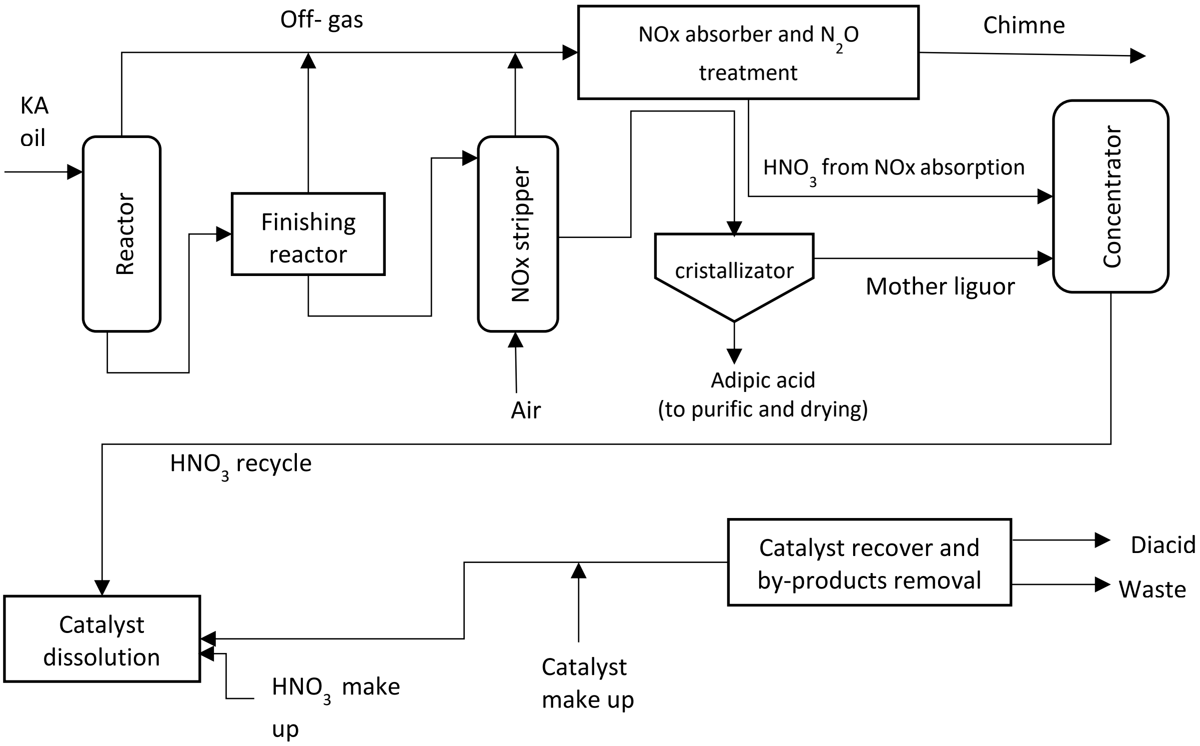

Figure 8-2: industrial process for the production of oil-based AdA

The reactions involved in the production of AdA are reported in Figure 8-3.

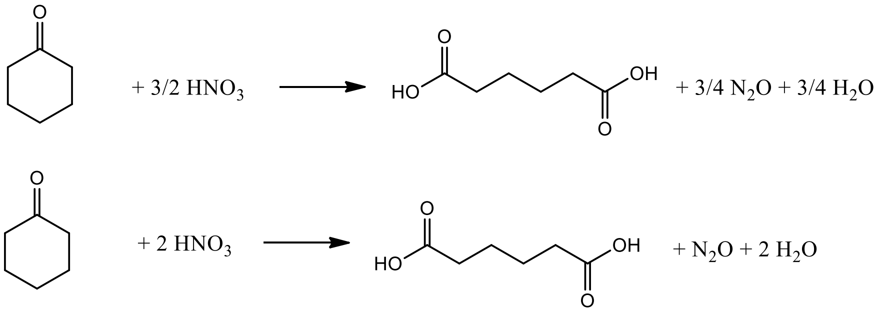

Figure 8-3: reactions involved for the production of AdA from oil

The oxidation of the cyclohexanol-cyclohexanone mixture (KA oil) is carried out using nitric acid (60%) in excess (at least seven times higher than the stoichiometric molar ratio) in the presence of a homogeneous catalysts (Cu(II) and ammonium metavanadate); the temperature is low (50-80 °C), since the reaction that occurs at atmospheric pressure is exothermic.[14] The data reported in the database were modified accordingly to new technologies that are able to reduce NO_x from 90 to 99%.[15,16] Since the most innovative technologies allow an abatement of N_2O of 90-99%[17], an average value of 95% has been taken into account for the real emissions calculation. Moreover, in the database no by-products were present, while in literature glutaric and succinic acid synthesis are always present in AdA plant as by-products. The yield in AdA is normally 92% and for glutaric and succinic acid 2% of yield for both the compounds was considered; as a consequence, the yield in CO_2 is 4%. The final data are reported in Table 8-1. By-products allocation was also considered and set to 96.4% for AdA, 1.7% for succinic acid and 1.9% for glutaric acid. In this LCI since the catalyst is an ancillary product, it is considered negligible compared to the rest of the inputs/outputs. Inputs and outputs (water, chemical factory, heat and electricity) were supposed to be the same of the original process presents in SimaPro database. Since the traditional petrochemical process for the synthesis of AdA is produced by industry from more than 20 years, no uncertainties were considered.

8.3.1 N_2O evaluation

A total conversion of cyclohexanol occurs: 60% is converted giving N_2O since this pathway is more favourable, while the remaining 40% is converted following the other path, releasing NO which is fully recycled to give HNO_3. These percentages have been assumed in the LCA study, but they strongly depend on the operative condition, such as temperature, pressure, kind of reactor, amount of catalyst and so on). 1 mole of cyclohexanol reacts with 2 moles of nitric acid to give 1 mole of AdA.

The amount of nitric acid, necessary for the process, can be calculated with the following relation, taking into account that it is used as solution 50% w/w:

$$m_{HNO_3} = m_{cyclohexanol} \cdot MW_{cyclohexanol} \cdot 2_{(stoichometric\ coefficient)} \cdot MW_{HNO_3} \cdot 0.6 \cdot 2_{(solution\ 50\%\ w/w)} \quad \text{(Eq. 8-1)}$$

N_2O theoretical emissions are calculated from the stoichiometric reaction, so:

$$m_{N2O} = mol_{HNO_3} \cdot MW_{N2O} \cdot \frac{1}{2_{(stoichiometric\ coefficient)}} \quad \text{(Eq. 8-2)}$$

8.3.2 Glutaric and succinic acid evaluation

Nowadays glutaric and succinic acid are recovered by industries and sold (generally as a mixture), so they are taken into account in the allocation of the process.

The actual amount of succinic acid (SAc) produced by the process is the following:

$$m_{SAc} = m_{cyclohexanol} \cdot MW_{cyclohexanol} \cdot yield \cdot MW_{SAc} \quad \text{(Eq. 8-3)}$$

For the glutaric acid (GAc) the same calculation has been performed:

$$m_{GAc} = m_{cyclohexanol} \cdot MW_{cyclohexanol} \cdot yield \cdot MW_{GAc} \qquad \text{(Eq.8-4)}$$

The production of SAc involves a loss of two carbon atoms/molecules as CO_2, while GAc is produced through the loss of only one carbon atom/molecule as CO_2.

In order to close the mass balance of carbon atoms of cyclohexanol, the remaining moles of reactant are transformed into CO_2. The sum of the three quantities of CO_2 are added as air emission (carbon dioxide, fossil). The system allocations are calculated for the three products exiting: AdA, SAc and GAc.

Table 8-1: amount of chemicals for MA production

Product	Amount
Cyclohexanol	0.749 kg
HNO_3 50% wt/wt	1.13 kg
Succinic acid	0.0177 kg
Glutaric acid	0.0198 kg
CO_2 total (air emission)	0.0987 kg
Theoretical N_2O emissions	0.198 kg
Real N_2O emission	0.00988 kg
Allocation:	
Adipic acid	964%
Succinic acid	1.70%
Glutaric acid	1.9%

8.4 Bio-derived adipic acid

8.4.1 Glucose production from maize starch

The presence of the production process of glucose starting from maize starch allowed to simplify and correctly evaluate the environmental impact of this complicated enzymatic process. The “Glucose production from maize starch_APOS,U” has been selected as base case process and it involves the cultivation of maize starch, the enzymatic hydrolysis of maize to glucose considering all the products necessary for the cultivation (i.e. fertilizer, water, land…) and the chemical factory (i.e. land occupation, construction materials, steam production unit, water cooling supplying, electricity…). Dunn et al.[18] studied the environmental impact and the energy consumption and emission associated to the enzymatic hydrolysis process of starch. The reaction involves in the enzymatic hydrolysis of starch is:

$(C_6H_{10}O_5) + nH_2O \rightarrow nC_6H_{12}O_6$

8.4.2 Muconic acid hydrogenation to bio-adipic acid

The glucose obtained is further processed for the synthesis of *cis,cis*-MA. Despite the presence of pilot plant production of bio-AdA from MA, no industrial mass balance or flow sheet process are available for the completely synthetic process. As mentioned at the beginning of the chapter, Rosengart developed a detailed economic and feasibility study for the production of bio-AdA via MA hydrogenation. An evaluation of mass and energy balance was reported allowing the possibility to perform a concrete environmental impact analysis which considers all the units operations requires for the conversion of glucose into MA and the subsequent AdA production and purification. The whole process is schematically reported in Figure 8-4 while the detailed one is reported in Figure 8-5.

8.4.2.1 Fermentation of glucose to *c,c*-MA

Glucose is converted into *cis,cis*-MA using a fermenter in which all the operating parameters must be carefully controlled and monitored due to the sensitiveness of the system about temperature and pH variations.

The reaction that occurs in the fermenter is:

$$7\,glucose + \frac{51}{2}O_2 \rightarrow 3c,cMA + 33H_2O + 24CO_2$$

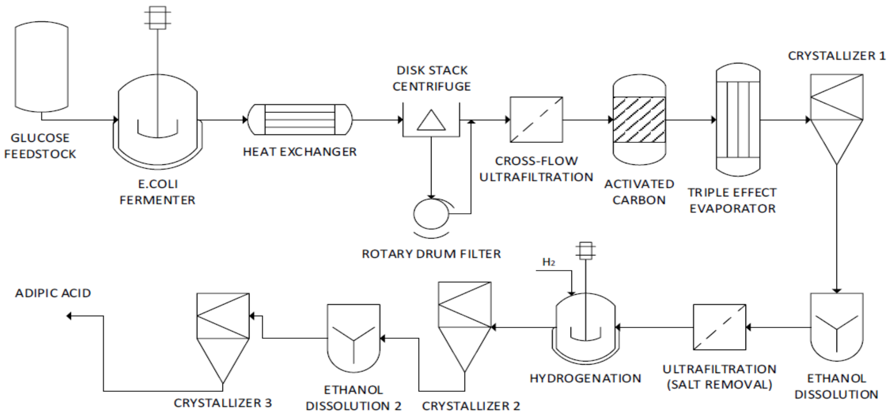

Figure 8-4: block diagram for the production of and purification of AdA

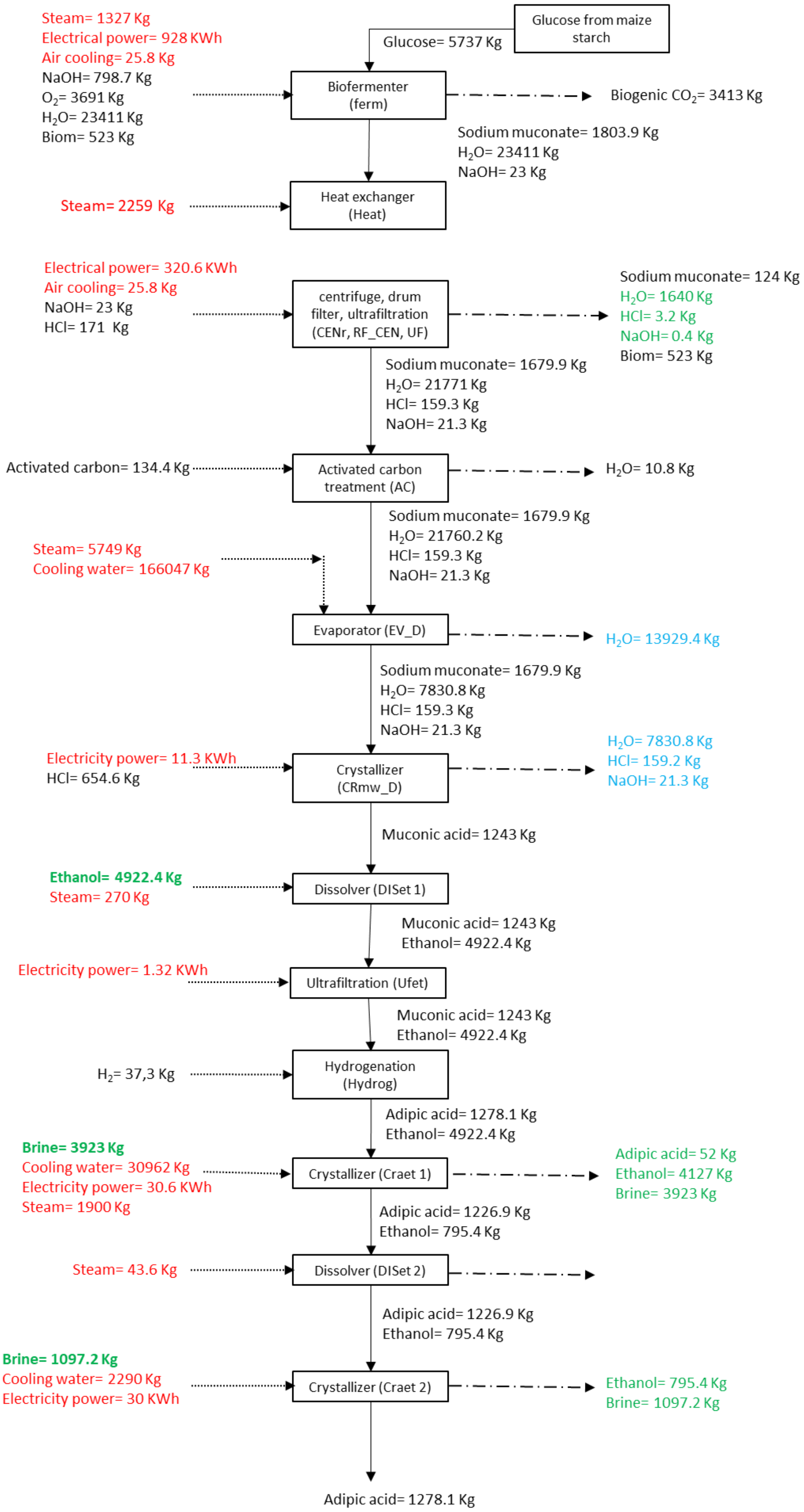

Figure 8-5: detailed flow sheet for the production of bio-AdA (red: utilities, green: directly recycles, blue: recycles with the use of other unit operation or waste water treatment)

The higher amount of water and CO_2 produced during the fermentation requires a big fermenter and all the utilities for the maintenance of the temperature are strictly correlated to the dimension of the unit. In this case a system of parallel reactors is assumed, each of 1000 m^3 (e.g. diameter 4 m, height 60 m, aspect ratio 15). For common biotechnology applications this volume is remarkable (100 m^3 is already considered “big”), however low added value fermentations are normally carried out in very large-scale systems, as biogas or ethanol anaerobic fermentations. Big aerated fermenters with the same scale assumed in this work have been successfully employed for succinic acid fermentations.[19]

8.4.2.2 Biomass deactivation (heat exchanger)

This step contains a single interval, representing a heat exchanger, which brings the raw fermentation broth at 80 °C. The thermal treatment on the fermentation broth has three different effects. The first is the deactivation of the bacteria. Increasing the temperature to 80 °C induces the pasteurization of the fermentation broth, preventing any pathogenic risk. The second is the coagulation of the proteic material present in the fermentation broth, which can be later removed via filtration.[20] The third effect is to promote the spontaneous isomerization of *cis,cis*-muconate salts to *cis,trans*-muconate, as reported in the equation:[21]

$$ccMA \rightarrow ctMA$$

The reaction is complete at 60 °C for 1.25 hours at pH 4, therefore HCl was used to acidify the environment.

8.4.2.3 Bacteria removal (CENr, RF_CEN and UF)

After the deactivation the broth is processed to eliminate the biomass (i.e. all the solids product). Thanks to three different steps: centrifuge (CENr), drum filter (RF_CEN) and ultrafiltration (UF). These unit operations require a lot of energy and steam due to the high amount of products.

8.4.2.4 Activated carbon treatment (AC)

The purification of a clarified broth using granular activated carbon (GAC) in packed beds or slurry reactors is often addressed as “decolorization treatment”. These removed impurities are a class of diverse compounds covering aminoacids, polyphenols, and cell debris. In spite of their variety, the impurities are removed thanks to the non-selective adsorption on the activated carbon internal surface. Decolorization steps for high scale applications are quite similar for all the bio-processes: the process specification applied for succinic acid or lactic acid can be transferred to the case of muconic acid. In a moving bed column, the amount of muconic acid loss is negligible: the small amount of spent carbon is rinsed with fresh water (returned to the main flux) and the adsorbed muconic acid is not relevant as shown by Vardon et al[22]. The consumption of utilities for this unit is negligible (all the operating costs are implicitly carried by the regenerated carbon purchase).

8.4.2.5 Concentration (EV_D) and water separation (CRmw_D)

After the activated carbon treatment the so obtained muconic acid must be concentrated and separated from water. The design specification of the evaporators was taken from Couper et al.[23] using the indication of a thermal economy of 2.4 kg of water evaporated per kg of steam in a triple effect configuration. The thermal stability of the products and the use of high pressure steam ensure a temperature difference of 20 °C in each exchanger (in spite of the possible ebullioscopic rise), avoiding more expensive vacuum systems. After the concentration *cis,cis*-sodium muconate is therefore converted to *c,c*-MA using HCl. This step is one of the most important because the impurities still present in the stream must be completed eliminated. The required purity of muconic acid usable for the hydrogenation to AdA and the further nylon production is very high (>99.98%). Therefore, muconic acid obtained after this step is 97%.

8.4.2.6 Dissolver (DISet 1)

The crystals of muconic acid recovered may contain co-crystals of other inorganic salts. Interval DISet 1assumes the dissolution of the intermediate crystals in ethanol, as suggested in the lab-procedure of Vardon et al.[22] Further studies could identify other alternative solvents for this step. The interval DISet 1 represents a coil jacketed stirred tank, to provide a 30 min residence time at 75 °C to ensure the dissolution of the crystallized muconic acid in ethanol.[23]

8.4.2.7 Ultrafiltration (UFet)

Following Vardon et al.[23] lab-scale procedure, a step of ultrafiltration after the ethanol dissolution is necessary to remove the mineral crystals co-precipitated with muconic acid. The only reference for muconic acid solubility in ethanol is the correlation of *cis,cis*-muconic acid of Scelfo et al.[24] These data are worth as a preliminary estimate. An average flow of 960 $l/h/m^2$ at 4 bar transmembrane pressure is assumed to size the module.

8.4.2.8 Hydrogenation reactor (Hydrog.)

For the hydrogenation in ethanol, the Pd/C catalyst performance of Vardon et al.[22,25] are modelled: Hydrog. assumes the reactant concentration coming from the upstream dissolution step. All the intervals assume the application of a system of agitated jacketed reactors in parallel, with a volume of 10 m^3 and a shape factor H/D of 4, to ensure the longer contact time between the gas and the liquid phase.

8.4.2.9 Final purification steps

All the final purification steps involve a double step of crystallization and dissolution These last steps of crystallization (interval CRaet2) allows the recovery of pure adipic acid. It is possible to see that the superstructure is generated to include at least two crystallization steps for each possible configuration (on muconic acid or adipic acid). This is an important difference from the flowsheets proposed previously, assuming the recovery of 99.96% pure adipic acid (polymer grade) in a single step of crystallization[26,7]. A single crystallization step is unlikely even for the oil-derived process, which operates with more clean substrates.[27] This final interval comprises a double cooler exchanger (cooling water utility and brine), a draft tube crystallizer and a solid bowl centrifuge for the crystals harvest. A complete product recovery is assumed (purge is negligible).

8.4.3 ReCiPe 2016, method used for environmental impact evaluation

LCA calculations were performed using the ReCiPe 2016 method (version 1.1) to evaluate the different impacts in the production of AdA from oil and from renewable resources and elaborating/comparing the results. In particular, 18 impact categories were considered and analysed in detail, trying to highlight the differences between the two production processes. Moreover, thanks to the use of the software SimaPro it is possible to understand which sub-processes, constituting the global process, have a greater numerical impact value. In case the original method only reported a characterisation value for one specific sub compartment, this value is taken as the characterisation value for all sub compartments in this compartment. The characterisation values of the sub compartments "fresh water" under water, "high population density" under air and "industrial soil" under soil were chosen as factor for the sub compartment "unspecified". Please mind that the factors in Global warming differ from the 100a time horizon in IPCC 2013 because climate-carbon feedback for non-CO_2 green-house gasses (GHGs) is included. For further details see the method's documentation.

8.5 Results and discussion

8.5.1 ReCiPe midpoint (H) results

Due to the early stage study of the bio-process the discussion of the results wants to be a critic about the bottle neck of this new process. All the results about the 18 impact voices will be shown and discussed. To simplify the discussion and to establish which unit operations must be improved and optimized, a step by step analysis was performed. In particular, all the figures describe the results obtained for each impact voices for the oil-derived AdA and bio-AdA production process. Regarding the bio-AdA process the chosen impact voice was divided for each unit operation.

8.5.1.1 Global warming

The voice “Global warming” expresses the change in global temperature caused by greenhouse gasses produced by human activity; the reference unit used to measure this category is kg CO_2 equivalent. The raise of global temperature can cause desertification, spread of disease, rising of the level of sea, and climatic disturbance. The climate change is one of the major environmental effects of economic productivity, and one of the most difficult to handle because of its broad scale. Therefore, during LCA study, this category is the most important and the CO_2 eq. released by the new process should be as low as possible. The global warming of bio-AdA production is lower than the oil-based one (Figure 8-6). We must consider that using ReCiPe method the biogenic CO_2 is not considered in the calculation due to its biological derivation. Despite the final value of global warming is not so different (blue and green bar), we can observe that the step where there is the highest increment of CO_2 is the crystallization of sodium muconate to muconic acid. Performing a detailed analysis on this crystallization step we found that the increment of kg CO_2 eq. is due to the waste water treatment used for slightly inorganic and organic contaminated water. Therefore, the introduction of recycle able to separate the flow of water and NaCl (such as an evaporator) could decrease the impact of this unit operation, positively affected the final result. Introducing the evaporation unit and deleting the waste water treatment the CO_2 eq. decreases at 11, underlying the importance of the recycling process within an industrial process.

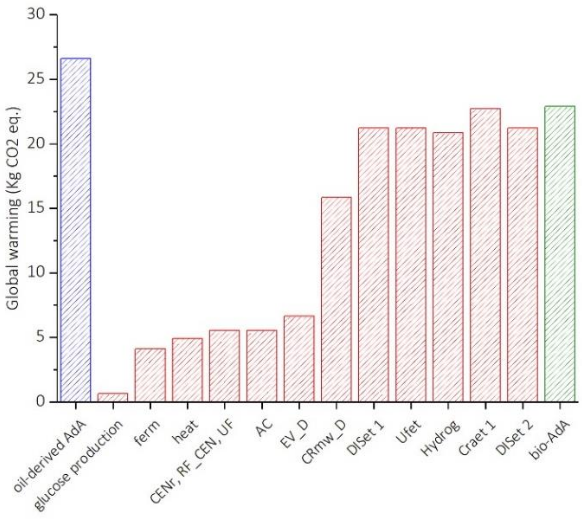

Figure 8-6: global warming

8.5.1.2 Human carcinogenic and non-carcinogenic toxicity

The human toxicity potential is based on both the potential dose of a compound and its inherent toxicity. This index reflects the potential harm of a unit of chemical released into the environment. The considered chemicals are arsenic, sodium dichromate, hydrogen fluoride that mainly derive from electricity production and fossil sources. These compounds are potentially dangerous to human through inhalation, ingestion, and even contact. The unit is expressed as kg of 1,4-dichlorobenzene equivalent (1,2-DB). Although in this case the CRmw_D step increases both the human carcinogenic and non-carcinogenic toxicity the amount of the carcinogenic toxicity is one hundred time lower than the non-carcinogenic one (Figure 8-7).

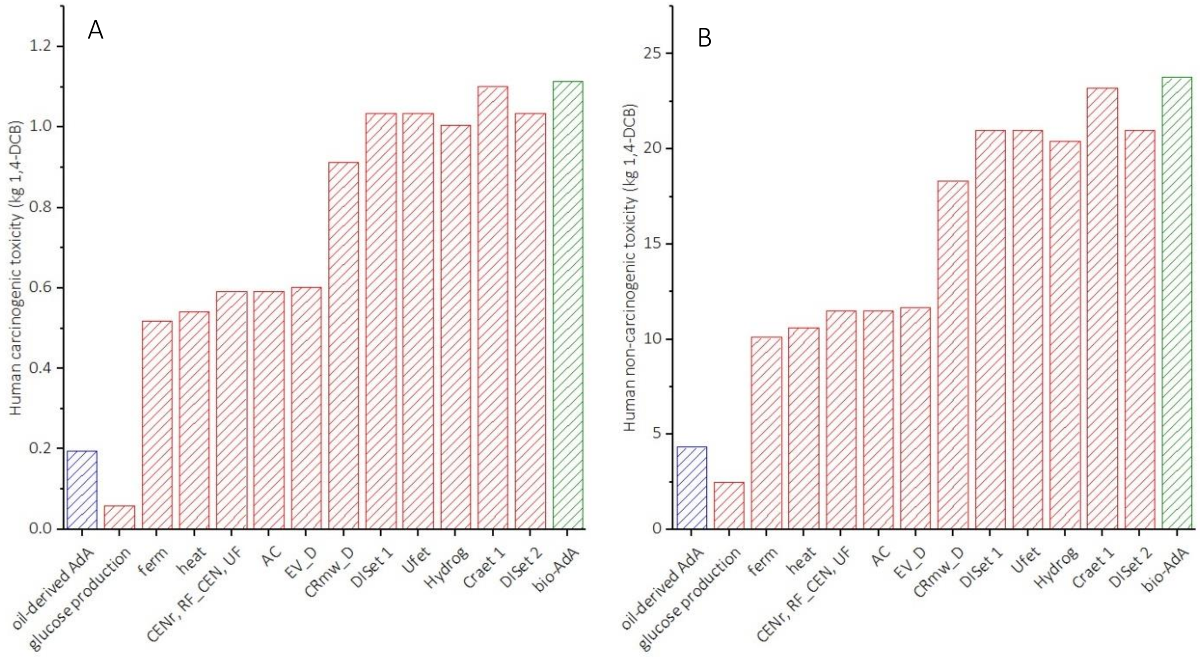

Figure 8-7: human carcinogenic (A) and non-carcinogenic (B) toxicity

8.5.1.3 Land use and water consumption

The study is based on the UNEP/SETAC land use assessment framework and focuses on occupation impacts, i.e. the use of land. The damage is expressed as "potentially disappeared fraction of species" (PDF) per m^2 or m^2 a (square metre of land per year).

Impact on the land due to agriculture, anthropogenic settlement and resource extraction are the main voices involved in the evaluation. Obviously, the land use of the bio process is much more high due to the cultivation of maize and the space occupied by the fermenter (3 fermenters in series). Regarding the water consumption, the new bio-process shows negative value, which means that with the water recycle occurring in the evaporator and in the first crystallizer it is possible to decrease a lot the whole water consumption of the process. Optimizing all the operating unit and performing other possible water recycling (i.e. cooling water and steam recovery) we could abate the water consumption to ≈0 (Figure 8-8).

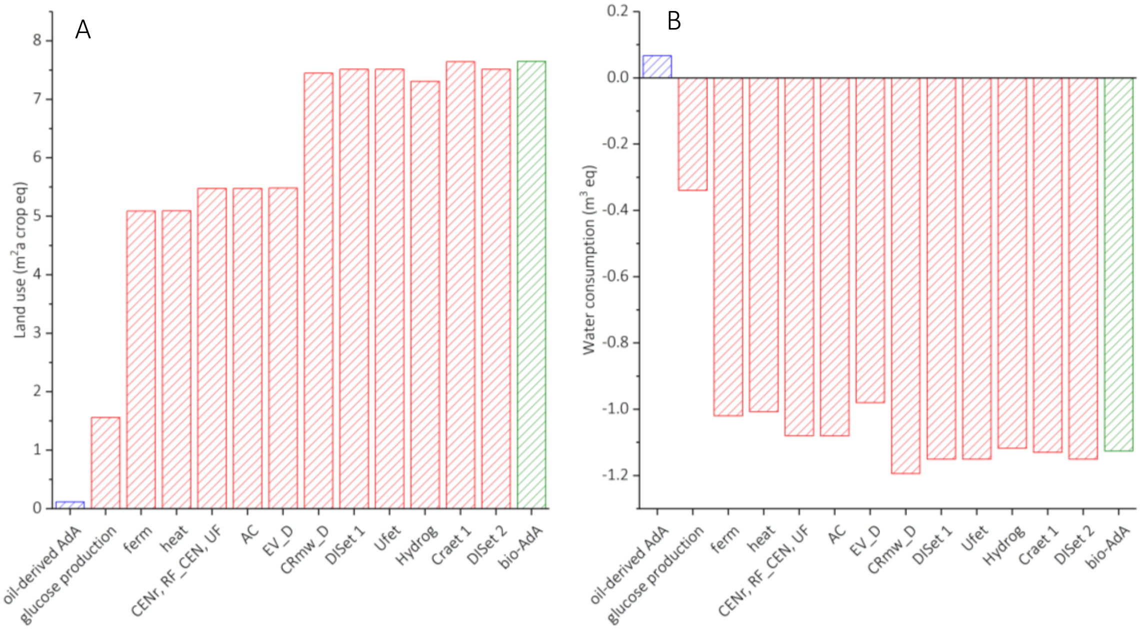

Figure 8-8: land use (A) and water consumption (B)

8.5.1.4 Abiotic resource scarcity

This impact category is referred to the consumption of non-biological resources such as fossil fuels, minerals, metals, water… The value of the abiotic resource consumption of a substance (e.g. lignite or coal) is a measure of the scarcity of a substance. That means it depends on the amount of resources and the extraction rate. It is formed by the amount of resources that are depleted and measured in antimony equivalents in some models or water consumption (in m^3), kg of mineral depletion and MJ of fossil fuels. Considering the mineral resource scarcity (expressed in kg of Cu eq.) the oil-derived process has a value of 0.2 while the bio one 0.075 (Figure 8-9). Studying all the different voices the maize starch production is the process that has the highest score. The use of land, fertilizer and water increase a lot the environmental impact about the mineral resources, while the score of fossil resource mainly derived from ethylene production used during the transportation. We must keep in mind that the bio-process starts from waste wood. Therefore, no cultivation is needed for the production so these impact voices could be decreased considering the use of waste wood.

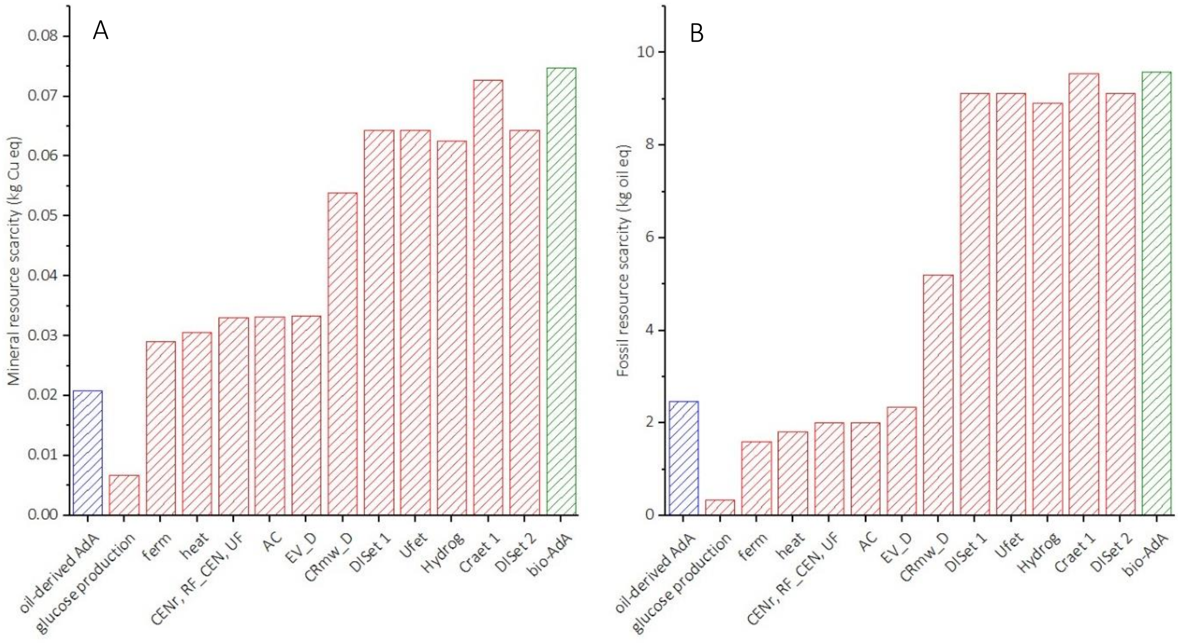

Figure 8-9: mineral (A) and fossil (B) scarcity

8.5.1.5 Terrestrial, mineral and freshwater ecotoxicity

Environmental toxicity is measured as three separate impact categories which examine freshwater, marine and land. The emission of some substances, such as heavy metals, can have impacts on the ecosystem. Assessment of toxicity has been based on maximum tolerable concentrations in water for ecosystems. This provides a method for describing fate, exposure and the effects of toxic substances on the environment. Characterisation factors are expressed using the reference unit, kg 1,4-dichlorobenzene equivalent (1,4-DB), and are measured separately for impacts of toxic substances on fresh water aquatic, marine and terrestrial ecosystem.

Evaluating the impact of these three voices the main step involved in the terrestrial, freshwater and marine ecotoxicity is the evaporator (EV_D) and the crystallizer. In particular terrestrial ecotoxicity mainly derives from the land cultivation, while the marine and freshwater ecotoxicity comes from the sulfidic tailing treatment used for the waste water treatment (Figure 8-10).

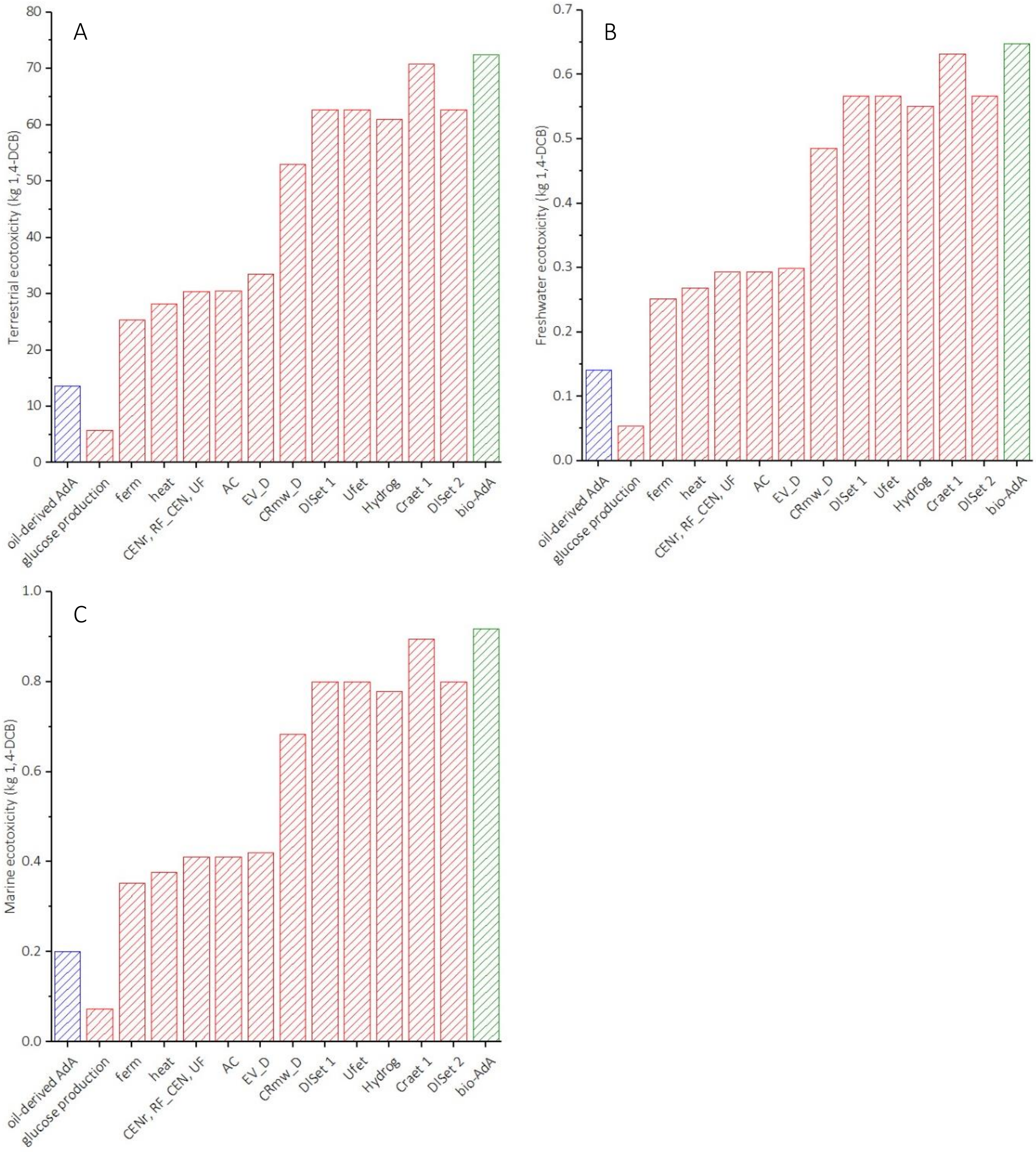

Figure 8-10: terrestrial (A), freshwater (B), and marine (C) ecotoxicity

8.5.1.6 Ionizing radiation, fine particulate matter formation and terrestrial acidification

Ionising radiation is an impact category in LCA related to the damage to ecosystem and human health that is linked to the emissions of radionuclides through a product or building life cycle. In the building area, they can be linked to the use of nuclear power in an electricity mix.

The category considers the radiation types α-, β-, γ-rays and neutrons. The characterization model considers the emissions and calculation of their radiation behaviour and burden based on detailed nuclear-physical knowledge. The unit the impact is given is kg of Cobalt-60 (Co-60 eq.) a radioactive isotope. Considering the Figure A the main steps of the bio-process that release the higher amount of Co-60 eq. are the fermentation step and the evaporator EV_D (Figure 8-11 A). In both cases the ionizing radiation increment is associated to the waste water treatment, in particular the tailing from the uranium milling.

Particulate Matter (PM) is a complex mixture of extremely small particles. Particle pollution can be made up of several components, including acids (such as nitrates and sulphates), organic chemicals, metals, and soil or dust particles. A multitude of health problems, especially of the respiratory tract, are linked to particle pollution. PM is measured in PM2.5 equivalents, i.e. particles with a size of 2.5 µm. Also in this case the two steps in which the amount of PM 2.5 increases are the bio-fermenter and evaporator EV_D (Figure 8-11 B). The PM derives from the sulfuric acid production used for the synthesis of ethanol and from the whole production process of maize starch.

Acidic gases such as sulphur dioxide (SO_2) react with water in the atmosphere to form “acid rain”, a process known as acid deposition. When this rain falls, often a considerable distance from the original source of the gas, it causes ecosystem impairment of varying degree, depending upon the nature of the landscape ecosystems. Gases that cause acid deposition include ammonia (NH_3), nitrogen oxides (NOx) and sulphur oxides (SOx). Acidification potential is expressed using the reference unit, kg SO_2 equivalent. The model does not account for regional differences in terms of which areas are more or less susceptible to acidification. It accounts only for acidification caused by SO_2 and NOx. This includes acidification due to fertiliser use. The two process that release the higher amount of SO_2 are the fermenter and the evaporator, in particular heat production from coal and land cultivation release the 90% of SO_2 of the whole bio-process (Figure 8-11 C).

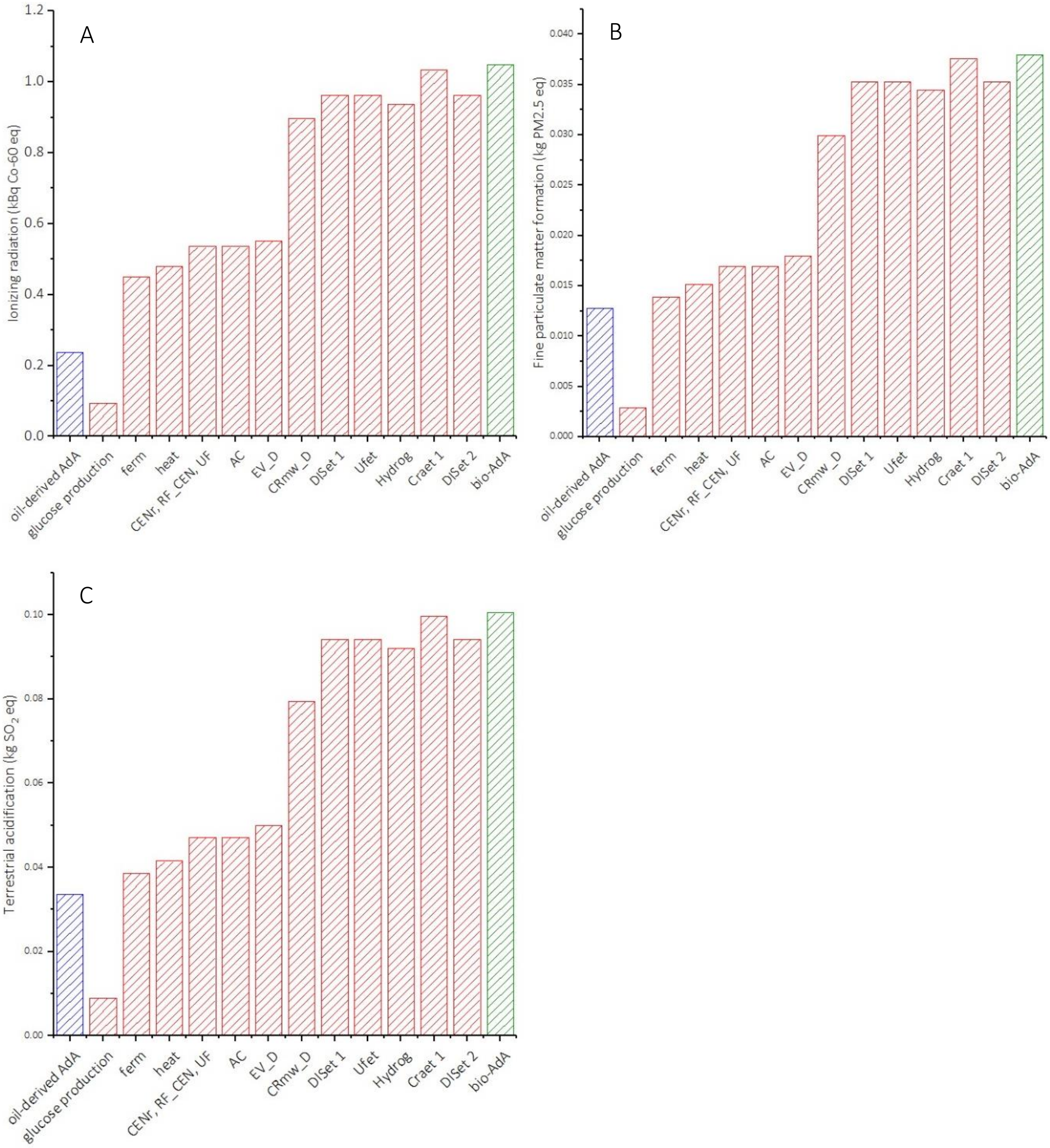

Figure 8-11: ionizing radiation (A), fine particulate matter (B) and terrestrial acidification (C)

8.5.1.7 Freshwater and marine eutrophication

Eutrophication is the build-up of a concentration of chemical nutrients in an ecosystem which leads to abnormal algal productivity. This causes excessive plant growth like algae in rivers which causes severe reductions in water quality and animal populations. Emissions of ammonia, nitrates, nitrogen oxides and phosphorous to air or water have an impact on eutrophication. Indirect and direct impacts of fertiliser are included in the method. The unit used to express freshwater and marine eutrophication are kg P eq. and kg N eq., respectively. Even in this last evaluation the fermenter, the evaporator EV_D and the crystallizer are the key steps of the eutrophication (Figure 8-12). In particular, the release of excessive chemical nutrients derives from the treatment of spoil from lignite mining (in surface landfill), sulfidic tailing and hard coal mining. All these voices derive from waste treatment and the production of maize starch.

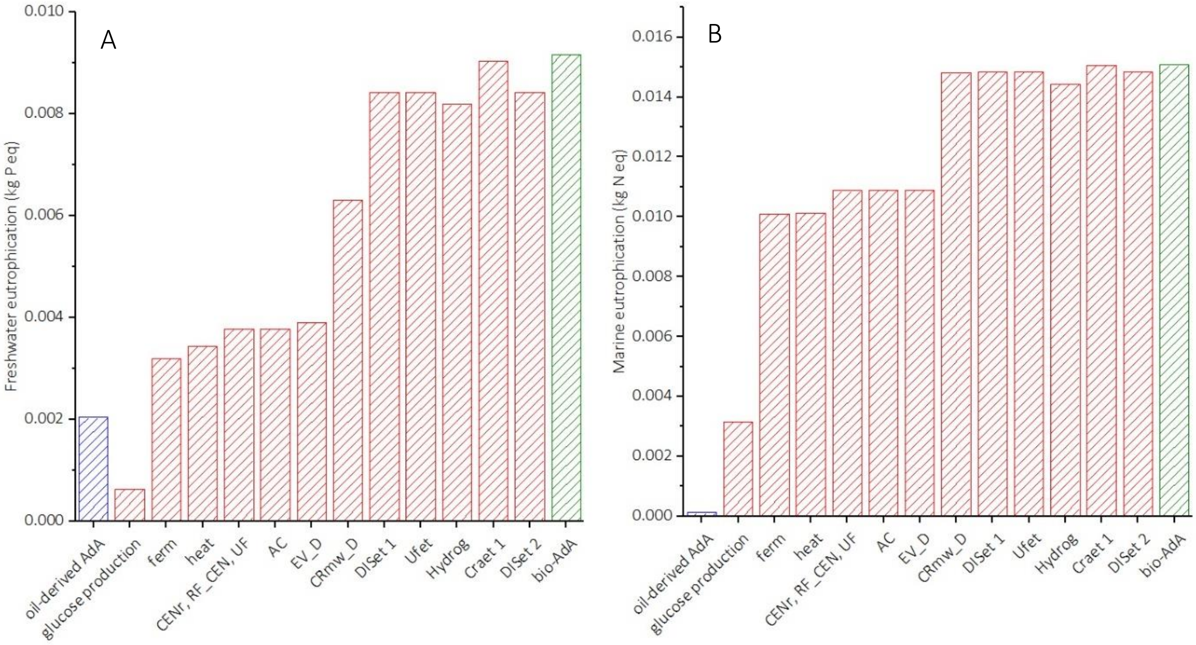

Figure 8-12: freshwater (A) and marine (B) eutrophication

8.6 How to decrease the environmental impact?

The results previously discussed revealed that the new bio-process for the production of bio-AdA releases lower amount of CO_2 respect to the traditional petrochemical process, Observing the other 17 impact categories the results might be discouraging. However, if we carefully analyse the processes from which the environmental impact derives, we note that it mainly derives from the production of starch and from the disposal processes used to treat the waste originating from this process and from the water treatment. For this reason, a preliminary LCA using wood waste for the production of glucose was considered, trying to eliminate the environmental impact of the land cultivation and maize starch production. No recycling of cooling water and steam was considered therefore, we placed the process in the worst conditions. Only ethanol and brine recycle were introduced due to the simplicity of their recovery. To overcome the lack of data about the hydrolysis of waste wood and glucose production from wood hydrolysis literature data were considered as reported in the following paragraphs.

8.6.1 Waste wood hydrolysis and sugar fermentation

Wood may be a source of glucose and other sugars due to the presence of polysaccharides chains. Its average composition is: 15-25% lignin, 23-32% hemicellulose and 38-50% cellulose.[28] The cellulose and hemicellulose can be hydrolysed to sugars that are microbially fermented into various products, such as glucose.[29] Glucose in cellulose is joined in a structure that is more difficult to depolymerize than the other conventional sources of glucose like starch. Diluted acids (1% sulphuric acid) can be used at high temperature (220 °C) to achieve yields of around 50-60%. The presence of water is necessary for the obtainment of sugar monomers.[30] After the hydrolysis, the glucose produced is separated and neutralized. The remaining sulphuric acid is recycled. The glucose obtained from hydrolysis, at a suitable value of pH, is fed to bacteria and *cis,cis*-sodium muconate is obtained from glucose fermentation. Efforts were made by many researchers to obtain a bacterial strain that is able to achieve the maximum possible productivity. According to Weber et al.[31], the final recombinant *E. Coli* strain produced 36.8 g/L of *cis,cis*-MA (as sodium salt), with a yield of 22% (mol/mol) within 48 h of culturing under fed-batch fermenter conditions.(Figure 8-13)

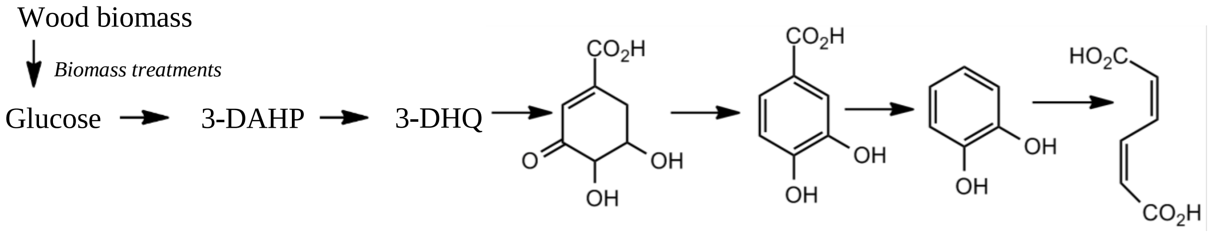

Figure 8-13: reaction pathway from wood biomass to cis,cis-MA

Due to the peculiarity of the process, no related routes were available in SimaPro database but comparable way to convert biomass into chemicals was found. In particular, bio-ethanol production from wood was selected because it considers bio-mass treatment and fermentation processes. The process modified in SimaPro database was: Ethanol, without water, in 95% solution state, from fermentation {RoW}| ethanol production from wood | Alloc Def, U. In this process, ethanol is produced by dilute acid pre-hydrolysis and simultaneous saccharification and co-fermentation of lignocellulosic biomass. Process heat and power supply is ensured by the combustion of unconverted solids such as lignin. The dataset includes the transport of wood from the forest to the distillery, and the processing of wood to hydrated ethanol (95%) and electricity. Dehydration to anhydrous ethanol is not included. The muconic acid production requires a fermenter similar to the one used for ethanol, in fact the same apparatus and the same temperature/pressure conditions are assumed for the two fermentations processes. Moreover, bacteria used for the production of sodium muconate were supposed to have the same environmental impact than the ones used in the production of bio-ethanol and the types of emissions are considered the same as the reference ethanol fermentation. The main difference is that the fermenter requires a different amount of wood and has a different amount of emissions and sulfuric acid concentration. Considering all these differences and accordingly with literature data,[32-34] the different chemicals and materials required for the production of 1 Kg of MA were evaluated and the results are reported in Table 8-2. At the end of the process, a dry solid is obtained.

8.6.2 Muconic acid production

The functional unit is 1 kg of muconic acid.

A yield of 22% mol/mol is obtained starting from a water solution of glucose.

The glucose mass is calculated using Eq.8-5:

$$m_{glucose} = \frac{m_{MA}}{MW_{MA}} \cdot \frac{1}{yield} \cdot MW_{glucose} \qquad \text{(Eq.8-5)}$$

Glucose is produced by cellulose and hemicellulose hydrolysis process, so an increase of weight of 10% occurs due to the addition of a molecule of water.

The composition of wood is assumed to be:[35]

- 50% cellulose, completely made up by glucose polymer;
- 30% hemicelluloses: its composition depends on the species of the considered plant;
- a composition of 33% of glucose, 33% of xylose and 34% of other sugars has been considered;
- 19% lignin;
- 1% ashes according to Sjostrom.[36]

An average hydrolysis yield of cellulose under acid condition of 55% was considered, while for the hemicelluloses of 85% (under the same conditions).

Since for muconic acid synthesis only glucose is used, the actual quantity of useful wood is calculated:

$$\begin{gathered} 5.2382\ kg_{glucose\ as\ polymer} = x \cdot (0.5 \cdot 5 + 0.3 \cdot 0.85 \cdot 0.333) \\ x = 14.554\ kg_{dry\ wood} \end{gathered} \qquad \text{(Eq.8-6)}$$

The mass of wet wood was calculated supposing that the humidity content is about 12% at 20 °C with a relative humidity of 65%. This is an average value, but the water content strongly varies according to the specific zone considered.[34] The final volume of softwood included in the process input is calculated taking into account a wood average density of 0.70 kg/L (considering humidity content of 12%).[34]

Among the inputs, woodchips are calculated considering that they make up the 0.551% of the total wood present, as suggested by the original ethanol fermentation process.

The other inputs and outputs are calculated making a proportion between the wood used in the two processes (supposition: inputs/outputs quantity are linearly correlated to the amount of wood used). The sulfuric acid added to the process is equal to the amount lost by neutralization during products separation (0.218 kg). The other sulfuric acid is supposed to be recycled in the process.

In order to neutralize this amount of sulfuric acid, quicklime is used. The reaction involved is:[37]

$$CaO\text{ (quicklime)} + H_2O + H_2SO_4 \rightarrow CaSO_4\text{ (gypsium)} + 2H_2O$$

Both the amount of used quicklime (input) and produced gypsium (output) are calculated.

The ashes (output) constitutes on average 1% of the dry wood in mass.[32]

A significant voice both in input and in output is water. At the end of the process, a solution of 36.8 g/l of sodium muconate is obtained. Water evaporation is necessary to obtain a dry solid. Nevertheless, water emissions both in water and in air strongly depend on recycle technology present. For this reason, only a part of this water is present in the emissions. Once more a direct proportion between water emissions and total soft wood is considered.

In order to evaluate the emission of CO_2, a mass balance on carbon has been done.

Wood generally contains an average amount of 50%w/w carbon, with respect to dried product.[38]

The carbon contained in wood (softwood and woodchip) is transformed into muconic acid and carbon dioxide biogenic. The mass balance on carbon can be written as:

$$C_{tot\ wood} = \left(m_{wood\ chip} + m_{soft\ wood}\right) \cdot 0.5 = C_{MA} + C_{bioCO_2} \qquad \text{(Eq.8-7)}$$

From the bass balance, the carbon from biogenic carbon dioxide and then the total mass of CO_2 emitted are calculated.

Table 8-2: chemicals and materials for 1 kg of muconic acid

Product	Amount (kg)
Glucose	5.760
Glucose as polymer	5.240
Dry wood	14.55
Wet wood	16.54
Residual softwood	23.65
Woodchips	0.091
Sulfuric acid	0.218
Quicklime	0.125
Gypsium	0.302
Ashes	0.145
Evaporated water	27.20
Biogenic CO_2	24.99

8.6.3 Results

Bio-AdA produced from waste wood shows better results than the bio-AdA from starch in all the impact categories and in most of them the results are comparable with the oil-based production process (Table 8-3).

In particular the global warming decreases from 22.9 to 13.6 kg CO_2, terrestrial acidification from 1.00E-1 to 4.15E-02 kg SO_2 eq. and human carcinogenic toxicity from 1.11 to 0.36 kg 1,4-DCB (Figure 8-14). Therefore, using waste wood as glucose sources makes the environmental impact favourable and a further optimization of the bio-process and the introduction of recycles will lead to better and better results.

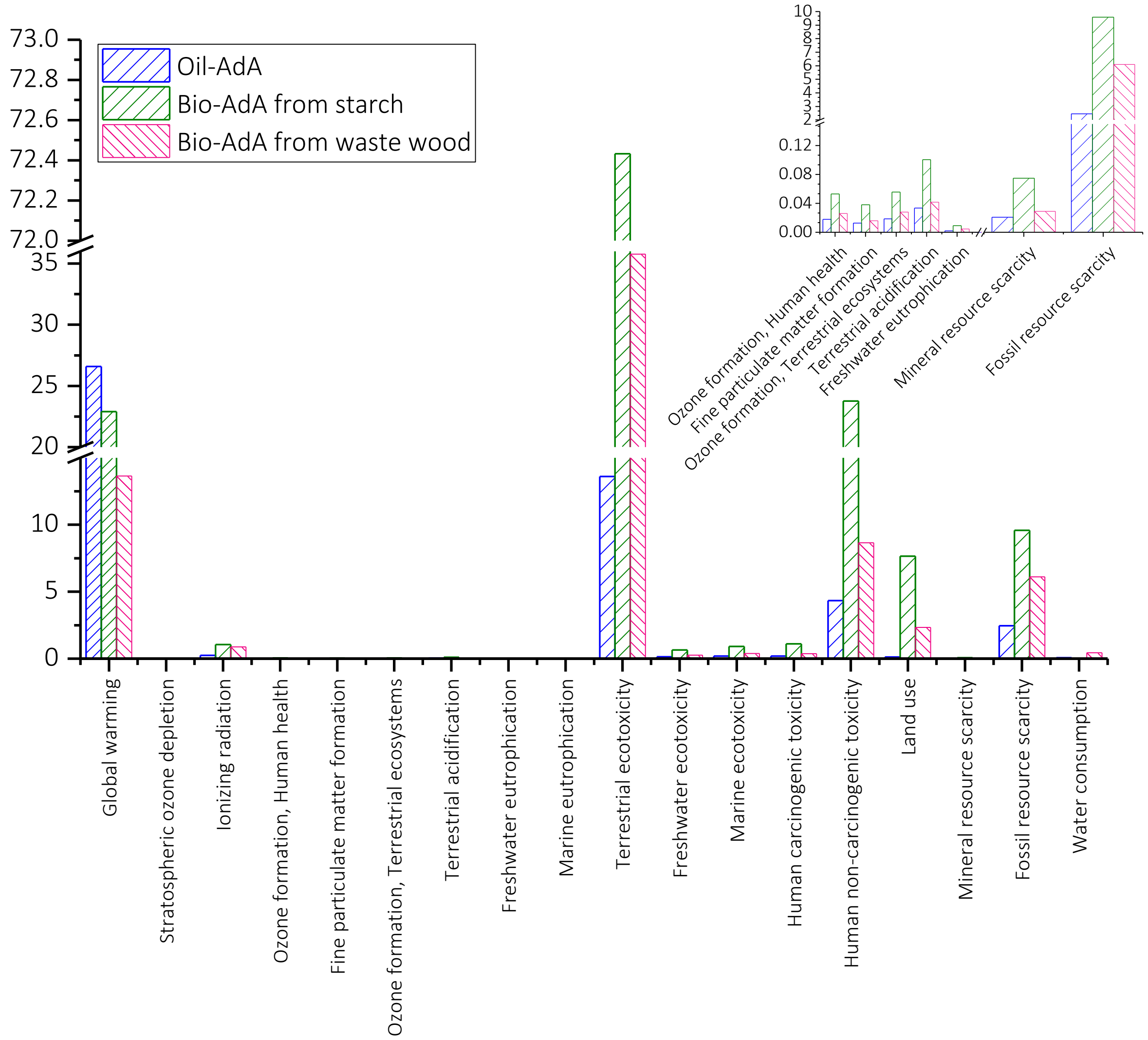

Figure 8-14: LCA results comparison among oil derived AdA, Bio-AdA from starch and bio-AdA from waste wood

Table 8-3: LCA results comparison among oil derived AdA, Bio-AdA from starch and bio-AdA from waste wood

Impact category	Unit	Oil-AdA	Bio-AdA from starch	Bio-AdA from waste wood
Global warming	kg CO_2eq	2.66E+01	2.29E+01	1.36E+01
Stratospheric ozone depletion	kg CFC11 eq	7.26E-04	7.39E-06	8.43E-06
Ionizing radiation	kBq Co-60 eq	2.38E-01	1.05E+00	8.75E-01
Ozone formation, Human health	kg NOx eq	1.79E-02	5.31E-02	2.61E-02
Fine particulate matter formation	kg PM2.5 eq	1.28E-02	3.79E-02	1.60E-02
Ozone formation, Terrestrial ecosystems	kg NOx eq	1.86E-02	5.55E-02	2.81E-02
Terrestrial acidification	kg SO_2 eq	3.36E-02	1.00E-01	4.15E-02
Freshwater eutrophication	kg P eq	2.04E-03	9.16E-03	4.66E-03
Marine eutrophication	kg N eq	1.26E-04	1.51E-02	3.45E-04
Terrestrial ecotoxicity	kg 1,4-DCB	1.36E+01	7.24E+01	3.58E+01
Freshwater ecotoxicity	kg 1,4-DCB	1.41E-01	6.48E-01	2.65E-01
Marine ecotoxicity	kg 1,4-DCB	2.00E-01	9.17E-01	3.82E-01
Human carcinogenic toxicity	kg 1,4-DCB	1.95E-01	1.11E+00	3.60E-01
Human non-carcinogenic toxicity	kg 1,4-DCB	4.33E+00	2.38E+01	8.66E+00
Land use	m^2 a crop eq	1.16E-01	7.65E+00	2.33E+00
Mineral resource scarcity	kg Cu eq	2.08E-02	7.48E-02	2.90E-02
Fossil resource scarcity	kg oil eq	2.46E+00	9.58E+00	6.10E+00
Water consumption	m^3	6.69E-02	-1.13E+00	4.46E-01

8.7 LCA study conclusions

The environmental impact of AdA production process from oil and renewable sources have been compared. Detailed analysis of the results revealed the advantages and weaknesses of the innovative bio-process. ReCiPe method was adopted for the evaluation of 18 environmental impact categories. The results show that the traditional petrochemical process has a lower environmental impact in all the categories except for the global warming. Firstly, industrial process for the production of glucose from starch was considered and the results were largely affected by the cultivation, the production of maize starch and all the respective waste treatments. Since the purpose is to produce glucose from waste wood, a second study was performed starting from the hydrolysis of wood and its further conversion to glucose. In this case the study started from the production process of bio-ethanol since no hydrolysis plant is present in the software. Moreover, an average wood humidity was considered using literature data for the yield of the process. Despite these limitations, the results obtained without considering cooling water recycle and steam production from the process water were extremely different from the first study. The global warming decreases from 22.9 to 13.6 Kg CO_2 eq. that is the half of the value obtained from the oil-derived process. All the results can be further improved introducing recycles of chemicals and water, which will lead to a process capable of quasi-self-sustaining from energy demand point of view and the purification products demand.

Since the data used in this work derive from early-stage and lab-scale investigations, using non-optimized data, the estimates can be further refined, as soon as new insights are provided by the ongoing R&D.

8.9 Economic feasibility analysis

Thanks to the collaboration with Politecnico di Milano a sustainability economic analysis was performed. The cost information can be retrieved from industrial quotes and estimates, from general market overviews,[39] or using equipment cost correlations[40,41] and utilities cost correlations.[42]

The "best processing route" was selected according to its ability to generate profit, since industrial innovation is determined first by economic drivers. Environmental impacts assessment and process optimization will be performed on the optimal route, during stage 2 and 3 of process design as they need a detailed process simulation to be meaningful.[43] The objective function implemented considers the annual incomes, deriving from the product sales, and the annual expenditures, related to capital investment and to the operating costs (utilities and consumables). The sum of these contributions is one formulation of the process economic potential[44] and is a first indication of the profitability of the process, providing also an order-of-magnitude estimate of the production cost. When the sum is equal or greater than zero, the breakeven point is reached, and the process can be considered economically feasible. As for the capital cost annuity estimation, an investment duration of 10 years and a MARR (minimum attractive rate of return) of 7% is considered.[45] Since the most updated available market analysis were referred to 2014, this year was chosen as reference. Table 8-4 summarizes the main 2014 pricing information included in the problem.

Table 8-4: chemicals and utilities cost

Chemicals	Price	Notes
Glucose	0.428 $/kg	[39]
Sodium Benzoate	1.774 $/kg	ICIS*
Adipic Acid	1.600 $/kg	[40]
Hydrogen (gas)	3.615 $/kg	Electrolysis, 50kWh/kg
Utilities**		
Electric power	0.0723 $/kWh	US energy mix base
High pressure steam	0.0168 $/kg	8 bar steam, 170 °C
Low pressure steam	0.0160 $/kg	2 bar steam, 120 °C
Cooling water	2.09E-05 $/kg	River water, 15 °C
Compressed air	0.07157 $/kg	Compresses air

*The price refers to the oil derived feedstock. No commercial plants of renewable sodium benzoate are available yet.

** The utilities cost estimates were derived from Ulrich & Vasudevan.[35]

When performing conceptual estimation, the accuracy is around 30%:[45] enough to quantify the potential of the bio adipic acid biorefinery and rank the many processing alternatives. The base case scenario and the results are reported in the following paragraphs. All the cots are based on the chemicals and utilities reported in Figure 8-5.

8.9.1 Base case scenario

The base case solution considered a plant for 10000 metric ton/year of adipic acid, located in North America, with an annual productivity of 8150 h. This scenario was identified in the results as SC_1.

8.9.1.1 Scenario with variation of AdA price

The following values from 2014 were considered, based on different locations: 1.60 $/kg for North America (lower bound), 1.94 $/kg and 2.28 $/kg (intermediate values), and 2.61 $/kg for South America (upper bound). Note that the high price for South America is due to the anti-dumping resolution approved by the government of Brazil in December 2013.[46] These four price values are identified with the letters a, b, c, d respectively and are combined with the other scenarios (e.g. SC_1_a, SC_1_b …).

8.9.1.2 Scenario with variation of glucose price

The price of glucose from 2014, varies with location too, which was considered through different values: 0.428 $/kg for North America, 0.210 $/kg in South America (Brazil). The price of 0.428 $/kg was considered in the base case scenario.

8.9.1.3 Scenario with variation of plant size

To get closer to the recommended size for a commodity chemical biorefinery, a capacity of 200000 ton/year, corresponding to 20-fold the base case size, was considered as well.[47] This scenario was identified as “SC_3”: this size is comparable to a medium sized plant for petrochemical-derived adipic acid. The base-case scenario is sufficiently small to not consider raw-material supply chain. Existing bio-gas plants distributed in rural areas have similar order of magnitude of feedstock requirement, either from first or second generation biomass.[48] The 200000 ton/year plant would require instead around 950 kton/year of glucose, which is equivalent to a large scale sugarcane mill in Brazil or a sawmill in US, assuming second generation biomass use.[49] The optimal size of the plant according to the local feedstock availability was not covered in this work.

8.9.1.4 Scenario with variation of strain yield and product concentration

More favourable values have been assumed for fermentation yield and product concentration. This was done to determine which of these has the biggest impact on the solution and then should be targeted by future research. In the results, SC_4 assumes a higher product concentration (+30%), SC_5 a higher bioconversion selectivity, SC_6 the combination of both higher selectivity and concentration.

8.9.2 Sustainability analysis

The calculated economic potential can be used to provide a first estimate of the bio-derived adipic acid production costs, assessing the level of maturity of the technology and the feasibility of the plant. Under the conditions of the base-case scenario (SC_1 in Table 8-5), the optimal flowsheet is economically feasible for a price of adipic acid of 3.60 $/kg. This value is more than double the reference price of adipic acid in North America. Still, different market scenarios confirm the potential of industrialization.

Table 8-5: results of the economical feasibility using different scenarios

		Profit on sales ($/kg AdA)			
SC_1	Base case	-2.00	-1.66	-1.32	-0.99
SC_2	Sugar price (0.210 $/kg)*	-1.00	-0.67	-0.33	0.00
SC_3	Scale up (200kton/year AdA)	-0.93	-0.59	-0.25	0.08
SC_4	Concentration (+30%)	-0.75	-0.41	-0.07	0.26
SC_5	Selectivity (93%)	-0.76	-0.42	-0.08	0.25
SC_6	Selectivity (93%)+conc.	-0.51	-0.17	0.17	0.50
	AdA selling price ($/kg)	a 1.6	b 1.94	c 2.28	d 2.61

Not feasible -20% to -5% -5% to 0% breakeven/profit

*This sugar price applies also to the following scenarios

For a benzoic acid-based process, on the other hand, the economic performances would be always worse, requiring a selling price higher than 5.00 $/kg for the base case, and unacceptable price values even in the most optimistic scenarios. As a general indication, the current benzoic acid route is not as good as the glucose one for the industrial scale-up. Regarding the glucose-based process, the multi-scenario analysis reported in Table 8-5 considers the price of glucose for a plant located in Brazil (SC_2). In this case, when adipic acid is sold at 2.28 $/kg (SC_2_c), the estimated loss is within the uncertainty of the cost estimates and profitability is reached at 2.61 $/kg (SC_2_d), which is the actual

Brazilian selling price of 2014 given the protectionist measures. Therefore, the process for sustainable adipic acid production becomes economically feasible under Brazil's market conditions, assuming no improvements in the current technology. The development of new technologies to achieve cheaper glucose from second generation biorefineries could eventually allow extension to other countries. Considering the solutions for the plant size (SC_3 series), it is observed that an increase of the plant production up to 20-fold that of the reference does not affect the result significantly: the plant feasibility maintains its dependency on external incentives. Interestingly, with an assumed improved upstream performance (increased fermentation yield and product concentration), profitability could be reached for prices of adipic acid lower than the 2.00 $/kg threshold (SC_6_b, c, d).

8.9.3 Cost distribution and process bottleneck analysis

Finally, the overall capital cost is estimated to be 15.2 M$ for the base-case plant, the annualized amount of which corresponds only to 6% of the production costs. The largest contributions to the capital expenditures come from centrifuges (32%) and crystallizers (31%), which are the most complex pieces of equipment in the process layout.

Table 8-6: impact of utilities, chemicals and capital on the production cost of bio-AdA from glucose

Utilities	
Electric power	76.8%
Steam high pressure	17.4%
Steam low pressure	5.1%
Cooling water	0.6%
compressed air	0.3%

Chemicals	
Growth support	30.4%
NaOH	19.4%
HCl	24.02%
H_2	16.3%
Activated carbon	9.8%
Others	0.1%

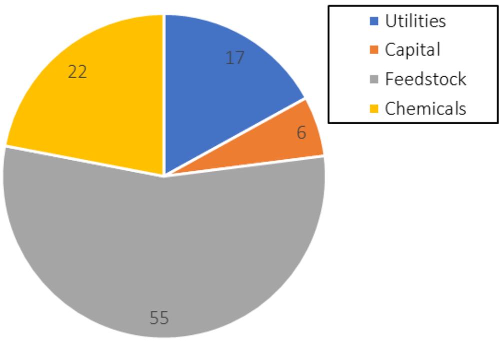

Capital	
Total	12.5M$
Fermenter	10.1%
Heat exchanger	0.4%
Centrifugue	33.1%
Ultrafiltration 1	7.2%
Activated carbon	0.8%
Evaporator	
Cristalization (water)	12.1%
Dissolution 1	1.0%
Ultrafiltration 2	0.6%
Hydrogenation	9.2%
Crystalization (EtOH) 1	10.6%
Dissolution 2	1.0%
Crystalization (EtOH) 2	8.4%

8.10 Conclusion about the economic feasibility of the bio-process

This work applied a systematic methodology for early-stage process synthesis and design to obtain a sustainable process design for the production of bio-derived AdA. A large number of reported technologies associated with bio-conversions and downstream separation operations were employed in the model of the process superstructure formulation. This included also the best and most updated information about bio-catalytic and chemical conversions, related to the transformation of renewable feedstocks to adipic acid. The main insights on the sustainable process design for adipic acid are: the preference to the glucose feedstock (*E. coli* fermentation) instead of the benzoic acid feedstock (*P. putida* fermentation); the need to reduce the product losses during the downstream purification; and the advantages of converting the intermediate product (*cis,cis*-muconic acid) hydrogenation in an organic solvent (ethanol). The economic analysis in different scenarios confirmed that a bio-adipic acid production is affected by the availability of cheap feedstock. In this specific case, the adipic acid process can be profitable if it is located in Brazil, using first generation glucose at a price not higher than 0.21$/kg. Finally, since the data used in this work are derived from early-stage and lab-scale investigations, the estimates can be further refined, as soon as new insights are provided by the ongoing R&D. The indications on the current technological bottlenecks, the main assumptions done while defining the superstructure and the sensitivity analysis are useful to indicate the priority aspects to be further investigated. Moreover, the lack of data did not allow to perform the economic analysis within the European market, but due to the increment of the price of oil, the bio-route could be competitive in a few years. Moreover, due to the instability price of AdA in Europe and the continuous increment of incentives bio-AdA could find in a few years a piece of market.

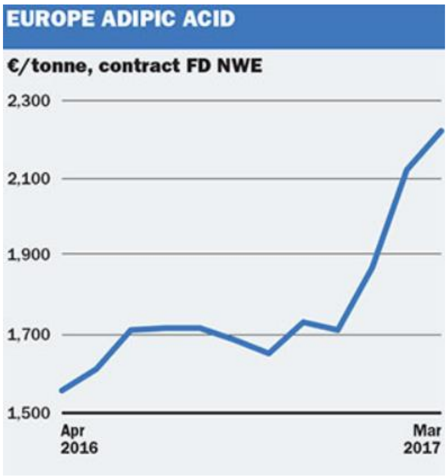

* https://www.icis.com/resources/news/2017/03/30/10093195/chemical-profile-europe-adipic-acid/

List of symbols

AdA: adipic acid

3-DAHP: 3-Deoxy-D-arabino-heptulosonic acid 7-phosphate

DHQ: 3-dehydroquinate

LCI: Life Cycle Inventory

MA: muconic acid

ILCD: International Reference Life Cycle Data System

IPCC: Intergovernmental Panel on Climate Change

Bibliography

1. Vardon, D. R. *et al.* Adipic acid production from lignin. *Energy Environ. Sci.* **8,** 617–628 (2015).
2. Xie, N.-Z., Liang, H., Huang, R.-B. & Xu, P. Biotechnological production of muconic acid: current status and future prospects. *Biotechnol. Adv.* **32,** 615–622 (2014).
3. Wu, C. M. *et al.* Microbial synthesis of cis,cis-muconic acid from benzoate by Sphingobacterium sp. mutants. *Biochem. Eng. J.* **29,** 35–40 (2006).
4. Bart, J. C. J. & Cavallaro, S. Transiting from adipic acid to bioadipic acid. Part II. Biosynthetic pathways. *Ind. Eng. Chem. Res.* **54,** 567–576 (2015).
5. Zakzeski, J., Bruijnincx, P. C., Jongerius, A. L. & Weckhuysen, B. M. The catalytic valorization of lignin for the production of renewable chemicals. *Chem. Rev.* **10,** (2010).
6. Mizuno, S., Yoshikaw, N., Seki, M., Mikawa, T. & Imada, Y. *Microbial production of cis,cis-muconic acid from benzoic acid*. *Appl. Microbiol. Biotechnol* **28,** (1988).
7. van Duuren, J. B. J. H. *et al.* Generation of a catR deficient mutant of P. putida KT2440 that produces cis, cis-muconate from benzoate at high rate and yield. *J. Biotechnol.* **156,** 163–172 (2011).
8. Vardon, D. R. *et al.* cis,cis-Muconic acid: separation and catalysis to bio-adipic acid for nylon-6,6 polymerization. *Green Chem.* **18,** 3397–3413 (2016).
9. Capelli, S. *et al.* Bio-adipic acid production by catalysed hydrogenation of muconic acid in mild operating conditions. *Appl. Catal. B Environ.* **218,** 220–229 (2017).
10. Vardon, D. R. *et al.* Adipic acid production from lignin. *Energy Environ. Sci.* **8,** 617–628 (2015).
11. Janssen, M., Aryapratama, R. & Tillman, A.-M. *Prospective life cycle assessment of adipic acid production from forest residue*. (2016). doi:10.13140/RG.2.2.36490.47049
12. Rosengart, A. *et al.* Process synthesis for bio-adipic acid 1 production via muconic acid route. *Biotechnol. Biofuels, Under review*
13. Cespi, D. *et al.* A simplified early stage assessment of process intensification: glycidol as a value-added product from epichlorohydrin industry wastes. *Green Chem.* **18,** 4559–4570 (2016).
14. Castellan, A., Bart, J. C. J. & Cavallaro, S. Industrial production and use of adipic acid. *Catal. Today* **9,** 237–254 (1991).
15. Shimizu, A., Tanaka, K. & Fujimori, M. Abatement technologies for N2O emissions in the adipic acid industry. *Chemosph. - Glob. Chang. Sci.* **2,** 425–434 (2000).
16. Lee, S.-J., Ryu, I.-S., Kim, B.-M. & Moon, S.-H. A review of the current application of N2O emission reduction in CDM projects. *Int. J. Greenh. Gas Control* **5,** 167–176 (2011).
17. Reimer, R. A., Slaten, C. S., Seapan, M., Lower, M. W. & Tomlinson, P. E. Abatement of N2O emissions produced in the adipic acid industry. *Environ. Prog.* **13,** 134–137 (1994).
18. Dunn, J. B., Mueller, S., Wang, M. & Han, J. Energy consumption and greenhouse gas emissions from enzyme and yeast manufacture for corn and cellulosic ethanol production. *Biotechnol. Lett.* **34,** 2259–2263 (2012).
19. Lubben, M. No Title https://www.bio.org/sites/default/files/WorldCongress/Marcel Lubben.pdf (accessed Oct 25, 2017).
20. Van De Graaf, M. J.; Vallianpoer, F.; Fiey, G.; Delattre, L.; Schulten, E. A. M. US20120238722A1
21. Babi, D. K.; Holtbruegge, J.; Lutze, P.; Gorak, A.; Woodley, J. M.; Gani, R. Comput. Chem. Eng. **81**, 218 (2015).
22. Vardon, D. R.; Rorrer, N. A.; Salvachúa, D.; Settle, A. E.; Johnson, C. W.; Menart, M. J.; Cleveland, N. S.;

Ciesielski, P. N.; Steirer, K. X.; Dorgan, J. R.; Beckham, G. T. *Green Chem.* ***18*** (11), 3397 (2016).

23. Couper, J. R.; Penney, W. R.; Fair, J. R. *Chemical Process Equipment: Selection and Design*; Elsevier Science (2012).

24. Scelfo, S.; Pirone, R.; Russo, N. Thermodynamics of cis,cis-muconic acid solubility in various polar solvents at low temperature range. *J. Mol. Liq.* **222** (Supplement C), 823-827 (2016).

25. Vardon, D. R.; Franden, M. A.; Johnson, C. W.; Karp, E. M.; Guarnieri, M. T.; Linger, J. G.; Salm, M. J.; Strathmann, T. J.; Beckham, G. T. Adipic acid production from lignin. *Energy Environ. Sci.* **8** (2), 617-628 (2015).

26. Matthiesen, J. E.; Suástegui, M.; Wu, Y.; Viswanathan, M.; Qu, Y.; Cao, M.; Rodriguez-Quiroz, N.; Okerlund, A.; Kraus, G.; Raman, D. R.; Shao, Z.; Tessonnier, Electrochemical Conversion of Biologically Produced Muconic Acid: Key Considerations for Scale-Up and Corresponding Technoeconomic AnalysisJ.-P. *ACS Sustain. Chem. Eng.* **4** (12), 7098-7109 (2016).

27. Castellan, A.; Bart, J. C. J.; Cavallaro, S. Industrial production and use of adipic acid. *Catal. Today* **9** (3), 237-254 (1991).

28. Anderson, A. B. THE COMPOSITION AND STRUCTURE OF WOOD '. *J. Chem. Educ.* **35,** 487–492 (1958).

29. Onda, A., Ochi, T. & Yanagisawa, K. Selective hydrolysis of cellulose into glucose over solid acid catalysts. *Green Chem.* **10,** 1033–1037 (2008).

30. Kennedy, J. F. & Alanís, R. M. No Title. *Carbohydr. Polym.* **62,** 301 (2005).

31. Weber, C. *et al.* Biosynthesis of cis,cis-Muconic Acid and Its Aromatic Precursors, Catechol and Protocatechuic Acid, from Renewable Feedstocks by Saccharomyces cerevisiae. *Appl Env. Microbiol* **78,** 8421–8430 (2012).

32. Misra, M. K., Ragland, K. W. & Baker, A. J. Wood ash composition as a function of furnace temperature. *Biomass and Bioenergy* **4,** 103–116 (1993).

33. SJÖSTRÖM, E. Chapter 10 - WOOD-BASED CHEMICALS AND PULPING BY-PRODUCTS BT - Wood Chemistry (Second Edition). in 225–248 (Academic Press, 1993). doi:https://doi.org/10.1016/B978-0-08-092589-9.50014-0

34. Bonamini, G. & Noferi, M. Umidità del legno strutturale. Problemi e soluzioni. *L'edilizia* **134,** 72–77 (2004).

35. Anderson, A. B. The composition and structure of wood. *J. Chem. Educ.* **35,** 487 (1958).

36. Sjöström, E. Chapter 1 - THE STRUCTURE OF WOOD BT - Wood Chemistry (Second Edition). in 1–20 (Academic Press, 1993). doi:https://doi.org/10.1016/B978-0-08-092589-9.50005-X.

37. National Lime association. Acid Neutralization with Lime for Environmental Control and Manufacturing Processes. Vol. 213 (1995).

38. Sjöström, E. Chapter 9 - CELLULOSE DERIVATIVES BT - Wood Chemistry (Second Edition). in 204–224 (Academic Press, 1993). doi:https://doi.org/10.1016/B978-0-08-092589-9.50013-9

39. Green, D. W. & Perry, R. H. *Perry's Chemical Engineers' Handbook*. (McGraw-Hill: New York, Chicago, San Francisco, Lisbon, London, Madrid, Mexico City, Milan, New Delhi, San Juan, Seoul, Singapore, Sydney, Toronto, 2007).

40. Couper, J. R., Penney, W. R. & Fair, J. R. *Chemical Process Equipment*. (Elsevier, 2012).

41. Turton, R., Bailie, R. C., Whiting, W. B. & Shaeiwitz, J. A. *Analysis, Synthesis and Design of Chemical Processes*. (Pearson Education, 2008).

42. Ulrich, G. D. & Vasudevan, P. T. How to Estimate Utility Costs. *Chem. Eng.* **113,** 66–69 (2006).

43. Babi, D. K. *et al.* Sustainable process synthesis–intensification. *Comput. Chem. Eng.* **81,** 218–244 (2015).

44. Douglas, J. M. A hierarchical decision procedure for process synthesis. *AIChE J.* **31,** 353–362 (2018).

45. Biegler, L. T., Grossmann, I. E. & Westerberg, A. W. *Systematic methods of chemical process design*. (Upper Saddle River, N.J. : Prentice Hall PTR, 1997).

46. Godinho, M. D. *Secretaria de Comercio exterior: Circular n75 de 13 Dezembro 2013*. (2015).

47. Wright, M. & Brown, R. C. Establishing the optimal sizes of different kinds of biorefineries. *Biofuels, Bioprod. Biorefining* **1,** 191–200 (2007).

48. Walla, C. & Schneeberger, W. The optimal size for biogas plants. *Biomass and Bioenergy* **32,** 551–557 (2008).

49. Neves, M. F., Trombin, V. G. & Consoli, M. A. Measurement of Sugar Cane Chain in Brazil. *Int. Food Agribus. Manag. Rev.* **13,** 37–54 (2010).

General conclusion and future perspective

The Doctoral project presented in this Thesis addresses the feasibility study of a novel bioprocess for the production of a drop-in commodity chemical, adipic acid. The topic belongs to the general framework of renovation of the traditional oil-based industry toward a sustainable manufacturing, as required by the most recent European Union policies. Bio adipic acid production process has been chosen because it is characterized by a very early stage development. The lack of kinetic data and operating parameters optimization, as well as economic feasibility had attracted our interest. The peculiarity of this project is its interdisciplinarity: biotechnologists, chemists and engineers are invited to collaborate to achieve good results and make wider the knowledge about bio adipic acid production at scale industry.

This study follows the classical steps to achieve robust and reasonable results: a critic literature analysis was performed with the purpose to establish the weak points of the new technology and those not yet investigated. We decided to focus our attention on the kinetic study and operating parameters optimization, since no studies were found in literature. The possibility to evaluate the kinetic constants and activation energies opened the opportunity to start computational work about the feasibility of this reaction at industrial scale, allowing to estimate the production costs and the environmental impact. Finally, a great attention toward catalyst tuning helped to design a series of catalysts (using green process) which have higher activity respect to commercial materials.

i. A new analytical method was developed able to correctly evaluate the conversion of the substrate and the selectivity of the product and reaction intermediates. The most important goal to achieve was the evaluation and chromatographic separation of *cis/trans* isomers and compounds which differ only for one double bond. UV-Vis analysis allowed the calculation of conversion, while GC/FID or TCD analysis valuated the selectivity.

ii. A first operating parameters optimization was completed with noble metal commercial catalyst (metal loading 5%) in water. Pt and Pd supported on activated carbon were used and with Pt catalyst a pre-activation step was performed before starting the reaction. The reaction was performed in a stainless-steel autoclave for pressure from 2 to 6 bar, while for 1 bar of hydrogen a bigger glass reactor was designed. In the optimum condition Pt/AC 5% is able to fully convert sodium muconate in adipic acid. Pd/AC 5% catalyst was then chosen for further studies due to its lower cost and the possibility to avoid catalyst pre-treatment. The hydrogenation reaction provided good results at low hydrogen pressure (1.2 bar) and low temperature (50 °C). Used and fresh catalyst was characterized in collaboration with Cardiff Catalysis Institute and some significant changes of the catalyst surface have been observed. In particular, during the reaction, Pd(II) is reduced to Pd(0) increasing the activity of the catalyst.

iii. After the collection of the first experimental data, in collaboration with Politecnico di Milano, a kinetic model was designed, and the regression of the kinetic parameters was performed. The *cis/trans* isomerization does not occur on the muconate, while the monounsaturated intermediates are preferably in their *trans* configuration. The estimation of kinetic constants, activation energies open the opportunity to model a hypothetic industrial reactor.

iv. Due to the good results obtained with Pd catalysts, a series of home-made catalysts was prepared with 1% of metal loading. Metal NPs were prepared using a bottom-up approach and sol-immobilization method allowed the deposition of Pd NPs on activated carbon support. Hydrogenation reactions occurred on sodium muconate and *t,t*-muconic acid revealed that some of the home-made catalyst had an initial activity equal or higher than the Pd/AC 5% commercial catalyst. This open the opportunity to tune and optimize the synthesis of a durable catalyst with optimum surface properties.

v. Finally, an environmental impact analysis was performed comparing the new bio adipic acid production process with the traditional one. The results are comforting because the bio process has a total global warming lower than to the more than optimized petrochemical process. Economic analysis showed the possibility to produce bio adipic acid with a price that is a little more expensive than the actual cost of oil based one. Further deeper studies will allow to establish if the purposed technology can fully compete with adipic acid produced by non-renewable sources.

The work is not finished and opens the possibility to further interesting researches.

i. In particular one of the first task is to optimize the bacteria strain (*E. Coli* or other strains) to increase the production of muconic acid. *The research group of Prof. Luca Brambilla of Università di Milano Bicocca, interested in our topic, started the exploration of this difficult issue and they are obtaining interesting results, but the work is only at the beginning.*

ii. One of the main worry is the use of gaseous hydrogen as reduction agent. Although the new technologies for hydrogen production are more and more sustainable, the use of this gas is object of severe protocols. To make the process safer, researchers are exploring new ways for *in-situ* hydrogen production. One of the most interesting topic is the hydrogen transfer catalysis. In particular conditions, a solvent (called donor), is able to offer a proton to an acceptor species. Hydrogen transfer catalysis occurs in presence of a metal that could be a homogeneous complex, or transition metal catalysts (Mn, Mo, Co, W…). The pro of this reaction is the exclusion of gaseous hydrogen within the plant, but on the other hand hydrogen transfer catalysis occurs with the consumption of the donor solvent and at higher temperature and pressure respect to the classic hydrogenation. Therefore, further studies will carry out to establish the optimum reaction and product purification conditions as well as the life of the catalyst. *Molybdenum and tungsten oxides were tested during the research project, but the results are far from to be competitive with the reactions that use gaseous hydrogen.*

iii. The development of new technologies and unit operations more and more specific will allow to minimize the use of utilities hypothetically exploiting all the resources within the company. Bio-based adipic acid process is the ideal field for one of the first circular industrial plants, capable to auto- maintain itself. Therefore, other studies about the possibility to recycle chemicals and energy will allow to make the process greener and more competitive on the market, maybe support from some international incentives.

Due to rising price of crude oil and the impact adipic acid has on the environment, the world is shifting towards the use of bio-based adipic acid. Apart from providing a clean solution, bio-based adipic acid is also economically viable against its synthetic counterpart.

Bio-based adipic acid market is expected to register significant growth on account of increasing demand for production of industrial chemicals through sustainable means. The market is still in nascent stages with companies focused R&D to develop manufacturing capabilities to produce bio-based adipic acid on an industrial scale. Development of bio-based adipic acid as a substitute for conventional adipic acid is expected to impact the latter’s demand in the market. Key factors influencing the shift from adipic acid produced through crude oil could be attributed to growing concerns regarding environmental impact and high feedstock prices of petrochemical based products. Stringent regulations by Food and Drug Administration (FDA) regarding nitrogen dioxide emissions from adipic acid are expected to act favorably for bio-based adipic acid market. The demand for bio-based adipic acid in medical and food applications is expected to grow over the forecast period owing to the above stated regulatory scenario.

High investment and R&D costs associated with the production of bio-based adipic acid are expected to pose challenges to the market participants.

For all these reasons the work done can be a useful starting point for the design of a sustainable and competitive adipic acid production, but a lot of attempts must still be made to increase the possibility to switch oil-based chemicals to bio-based ones.

Acknowledgements

I want to thank my supervisor Prof. Carlo Pirola and my co-supervisor Prof. Laura Prati for gave me the opportunity to work in their lab on a very interesting project. I want also to thank Alberto Villa for all the help during my last year of PhD, I learnt a lot about catalyst characterization an synthesis. Finally, I want to thank Prof. Nikolaos Dimitratos who gave me the opportunity to work at Cardiff Catalysis Institute for 5 months; I found an expert in characterization and catalyst synthesis, a lover of Italy and Italian food (tiramisù) and a very English drinker.

Now it is time to switch the language to allow to my parents and friends to read the acknowledgements.

Partendo dal mio gruppo di ricerca vorrei innanzitutto ringraziare i tesisti e i tirocinanti che si sono intervallati e hanno lavorato e ottenuto risultati impensabili. Senza di voi questa tesi sarebbe incompleta. Quindi ringrazio Luca, Emilio (il mio portafortuna), Ivan, Giulia, Michela, Marco, Gabri (ricorderò per sempre la faccia di Riikka), Leila e Mavi. Non posso di certo non ricordare anche tutti i tirocinanti e tesisti che sono passati in questi tre anni dal gruppo capanno, siete tanti, tantissimi e ognuno di voi avrà sempre un posto speciale nei miei ricordi: Pacia e i suoi/nostri asfalti, Basha con mille progetti (o forse nemmeno uno), Cipo in lotta continua con il sistema, Leila la fortunata del gruppo, Emy il lavoratore instancabile, Nafi la nostra fotografa ufficiale, Dalma dall'anima oramai canadese, Vale e la sua vita australiana, wikiPese e le sue continue polemiche, Gabri che non saprà mai com'è il sapore di una lasagna o del cioccolato, Ale e Cri i due opposti sotto la stessa cappa, Fede il mago del GC, Marco convertito da fotocatalista a impiantista, il Mammo produttore di aria arricchita, Fede Sacco il mago del GC, Pigozzi sparito nel nulla, Jack che ha trovato la sua strada ad Amsterdam, Sansone amante delle auto d'epoca, Richi Motta e i suoi mille disastri, Siro e Curdo con cui avrò piacere di lavorare in futuro e la mia bresciana preferita Vane con i viaggi della speranza. Mi scuso se dovessi aver dimenticato qualcuno, ma siete davvero in tanti.

Un ringraziamento importante va anche ai miei compagni di avventure e disavventure Fede, Alberto, e Marta, come dimenticarsi Benedetta, senza di te questa tesi non esisterebbe.

Ma se questa è stata la mia famiglia UNIMI, non posso dimenticare di ringraziare anche gli ingegneri (ma ricordatevi che ci sarà sempre un infiltrato) POLIMI. Ringrazio davvero di cuore Alessandro per avermi aiutato e per aver collaborato a questo progetto, senza il tuo prezioso aiuto e qualche parola veneta questa tesi sarebbe un groviera. Come dimenticare Anisolo, grazie per il sostegno che mi hai

sempre dato, ne abbiamo passate tante, forse troppe, ma ricorda che non sei stato assunto per fare la guida turistica!

Un ringraziamento al gruppo di Cardiff, e siccome tra italiani, spagnoli e messicani ci si capisce posso scrivere i ringraziamenti in italiano. Grazie a Marti, compagna di laboratorio e di avventure, di cinema e di dolci; un grazie particolare ai coinquilini più diversi che io conosca Luca e Max, ora non avete più scuse per cucinare sempre le stesse cose; un grazie particolare a Davide che mi ha seguito e tramandato le sue conoscenze. Un grazie anche ad Anna, Giulia e Grazia, le anime femminili e chiacchierone di questo grande gruppo; grazie a Keiko e Guillermo e infine al grandissimo Ricardo, il messicano, ma un po' americano, che vorrebbe diventare italiano. Infine un grazie a Matteo, il ragazzo più orgoglioso di essere trentino mai incontrato in vita mia (come potrò scordarmi la scena dell’aeroporto) e a Stefano, mio futuri collega, che gentilmente mi ha ospitato i miei primi due giorni rendendo il mio arrivo a Cardiff meno traumatico.

Un ringraziamento speciale va ai miei genitori e alle mie sorelle, agli zii e nonni che hanno accettato questa mia scelta e mi hanno aiutata in questi 3 lunghi anni; un ringraziamento particolare a Fulvio, compagno di vita e di avventure, sempre in grado di stupirmi e di essere presente in ogni momento. Grazie anche ad Anna ed Armando che mi hanno sfamato e tenuto al fresco in questa torrida estate di scrittura.

Un ringraziamento anche a Riccardo ed Elena, il reverendo Davide, Alberto, Paolo, Samu Franci e la piccola Cate per tutte le risate e la spensieratezza che ci unisce durante le nostre serate.

Per ultimo, ma non in ordine di importanza, un grazie ai Carminis, che sanno sempre regalarmi grandi emozioni e che mi trasportano in un’altra dimensione facendomi scordare gli imprevisti e le difficoltà della settimana.